

Submerged Floating Tunnels

The Design of the End Joint



Laura Bakker

MSc Hydraulic Engineering – Hydraulic Structures

February 2019



This master thesis is established in collaboration with TEC company and their support is hereby highly appreciated.



Copyright © department of Hydraulic Engineering at the TU Delft. All rights reserved.

Illustration front page: www.vegvesen.no NPRA/Vianova/Baezeni

Submerged Floating Tunnels

The Design of the End Joint

Laura Bakker

Master of Science in Civil Engineering

Hydraulic Engineering – Hydraulic Structures and Flood Risk

Graduation Committee

Prof.dr.ir Jonkman, S.N.	TU Delft – Section Hydraulic Engineering
Ir. Reinders, K.J.	TU Delft – Section Hydraulic Engineering
Ir. 't Hart, M.	RHDHV – Section Transport & Planning
Dr. ir. van Dalen, K.N.	TU Delft – Section Dynamics of Structures

Delft University of Technology
February 2019

Summary

The Submerged Floating Tunnel (SFT), also called an Archimedes Bridge, is a state of the art solution for crossing deep and large waters. The concept of a SFT has been around for many decades. From just a sketch back in the late 1800s till full worked out designs the last couple of years. However, none has still been build up till today.

A general literature study showed a number of 'blank spots' which still need to be researched before building the first ever "test" submerged floating tunnel. The most interesting research topic has been chosen from these blank spots: the connection between the SFT and the shore. The main question of this study is: What type of end joint is recommended for a submerged floating tunnel?

A location has been chosen to limit the number of variable parameters. Setting a location gives a better understanding of force distributions in the end joint only depending on variables related to tunnel elements and not to the surroundings itself. The location will be one of the fjords in Norway on auto route E39: the Bjørnafjord, for which studies have been performed on a submerged floating tunnel concept.

The SFT design in the Bjørnafjord has been modelled in the FEM program, SCientific Applications engineer (SCIA). The purpose of the model is to assess, on a more global scale, how the design of the end joint and the tunnel structure are influenced by several parameters. The essential parameters of the design are all present in the model while the model remains easy to manipulate. Only the static loading is considered for the tunnel structure and the model is validated using rules of thumb and basic physics laws.

A comparison is made in between the FEM-model results and the analytical approach which uses differential equations to describe the force distributions and displacements of the tunnel structure. Both the analytical and numerical approach result in the same order of values for the displacements of the tunnel structure. The difference in values found between SCIA calculations and analytical calculation, is due to the assumptions made for the models not being similar.

A parameter study has been performed to get a better understanding of the forces working in the tunnel structure and the end joint. 3 Significant parameters are selected and studied using the SCIA program and tunnel model. The effect of the spring stiffness k_u of the supports (i.e. tethers or pontoons) is investigated as well as the parameters k_ϕ (segment connections) and SC (end joint or shore connection).

The support spring stiffness k_u has a relatively large influence on the tunnel structure. The Norwegians in designing the Bjørnafjord tunnel have found the optimal solution regarding the stiffness of the support system.

The connection spring stiffness k_ϕ has a relatively small influence compared to the two other parameters and hardly influences the moments in the end joint. A low connection spring stiffness has a negative effect on the moment distribution of the tunnel structure. The segment connections therefore need to be fixed connections.

The type of end joint SC has a relatively large influence on the tunnel structure. The types of end joint applicable in a SFT have in common that they either have no degrees of freedom or have rotational freedom. Not limiting the rotational degree of freedom in the end joint proves to be favourable for the moment M_y at the end joint, but the moment in the tunnel structure itself doubles. Rotational freedom of the end joint allowing rotations during static loading will create physical challenges.

Multiple aspects influence the design of the tunnel structure and the end joint connection. It can be concluded from the research that multiple types of end joints may be suitable in the Submerged Floating Tunnel structure. The most obvious and easy solution is the fixed end joint. Also two proposals have been made for flexible end joint solutions, which have potential and should be taken into consideration during the design process. To remain physically practical, the ranges of the degrees of freedom of motion need to be limited. The fixed end joint however appears to be most recommendable in view of ease of construction and expected maintenance.

Preface

From a young age, tunnels have always been interesting for me. The large hand carved and bored tunnels in the Alps as well as the immersed tunnels in my direct surroundings fascinated me. The ingenuity of such large hydraulic structures influenced the choice for further education. Even during the university years, with other interesting subjects brought in the spotlight, the love for tunnels did not disappear. Therefore, when the opportunity came by, it took me less than a second electing the submerged floating tunnel as my graduation subject. So, the choice was easy, especially because it is an innovating new concept already triggering my creative brain.

This research is done as a graduation thesis for the Master of Science in Hydraulic Engineering at the faculty of Civil Engineering at the Delft University of Technology. This research is performed in cooperation with Tunnel Engineering Consultants (TEC).

Many thanks to my thesis committee for their support and advice throughout my thesis. Thank you, Marcel and Kristina for your continuous support as your input helped give perspective and direction to my thesis. In addition, I would like to thank Ir. Wilfred R. Molenaar for suggesting the thesis topic and connecting me with TEC. Last, I would like to thank my family and close friends for supporting me during my years as a student.

Laura Bakker,
January 2019

Table of Contents

Summary	i
Preface	iii
1. Introduction.....	1
1.1. Background	1
1.2. Problem definition	3
1.3. Research questions	4
1.4. Methodology.....	4
1.5. Scope.....	5
2. General literature study	7
2.1. Systems	7
2.2. Tunnel tube structure	7
2.3. Loading.....	7
2.4. Other	7
2.5. Conclusion.....	7
3. Design location - Bjørnafjord.....	9
3.1. Situation and proposed layout.....	9
3.1.1. Pontoon variant	12
3.1.2. Tether variant.....	14
3.2. Boundary conditions	15
4. FEM Modelling	17
4.1. Introduction	17
4.2. Basic model.....	17
4.2.1. Spring stiffness of the supports.....	19
4.3. Load cases	21
4.3.1. Permanent nett force.....	21
4.3.2. Current	23
4.3.3. Waves.....	26
4.3.4. Overview load case values	28
4.4. Load combinations	29
4.5. Results.....	30
4.6. Design checks	31
4.6.1. Service Limit State	31
4.6.2. Ultimate Limit State	33
4.7. Conclusion.....	35
5. Analytical approach	37
5.1. Differential equation.....	37
5.2. Results.....	38
5.3. Conclusion.....	40
6. Parameter study	41

6.1.	Methodology.....	41
6.2.	Supports stiffness – ku	43
6.2.1.	SCIA Results.....	43
6.2.2.	Physical limitations.....	48
6.2.3.	Conclusion.....	48
6.3.	Secondary connections – $k\phi$	49
6.3.1.	SCIA Results.....	54
6.3.2.	Physical limitations.....	58
6.3.3.	Conclusion.....	59
6.4.	End joint – SC	60
6.4.1.	SCIA Results.....	62
6.4.2.	Physical limitations.....	66
6.4.3.	Conclusion.....	69
6.5.	Conclusion.....	70
7.	Conceptual Design of the End Joint.....	71
7.1.	Variants.....	71
7.1.1.	Fixed end joint.....	71
7.1.2.	Partially free end joint.....	73
7.1.3.	Delayed fixed end joint.....	78
7.2.	Conclusion.....	79
8.	Conclusion.....	81
9.	Recommendations.....	83
	References.....	85
	List of Figures.....	87
	List of Tables.....	89

Appendixes

Appendix A – General literature study

Appendix B – SCIA basic model results

Appendix C – IdeaStatica cross-section capacity

Appendix D – Gina-profile properties

1. Introduction

This master thesis focusses on the design of the End Joint for the Submerged Floating Tunnel (SFT). The first SFT still needs to be constructed but Norway and China are taking the lead in developing the SFT. As the most data was available from Norway, the Bjørnafjord SFT project was chosen for research.

In this chapter, the current situation is described and the problem definition is stated. The research objective and research questions of this study are presented followed by the approach to achieve this objective as well as the structure of the remainder of this report.

1.1. Background

The Submerged Floating Tunnel (SFT), also called an Archimedes Bridge, is a state of the art solution for crossing deep and large waters. The concept of a SFT has been around for many decades. From just a sketch back in the late 1800s till full worked out designs the last couple of years. However, none has still been build up till today.

The SFT is a tunnel structure which pierces through a water body under the water surface level. Because the buoyancy-weight-ratio is slightly larger or smaller than one, the tunnel tends to float. The position of the tunnel is not fixed by a soil body, but the structure is secured at the shore junctions and/or tethers along the tunnel length.

The main difference of the SFT compared to the conventional tunnels is its position in the water: instead of being located on or under the bed, it passes right through the water. Figure 1 nicely illustrates these differences. The SFT is a desirable solution for locations which are, due to extreme circumstances, difficult to cross using present solutions. The main extreme circumstance which prevents the use of present day solutions is a large water depth. Very large water depths and wide waters, like in the Norwegian fjords, result in tunnels with very long vertical alignments or bridges with a very large span.

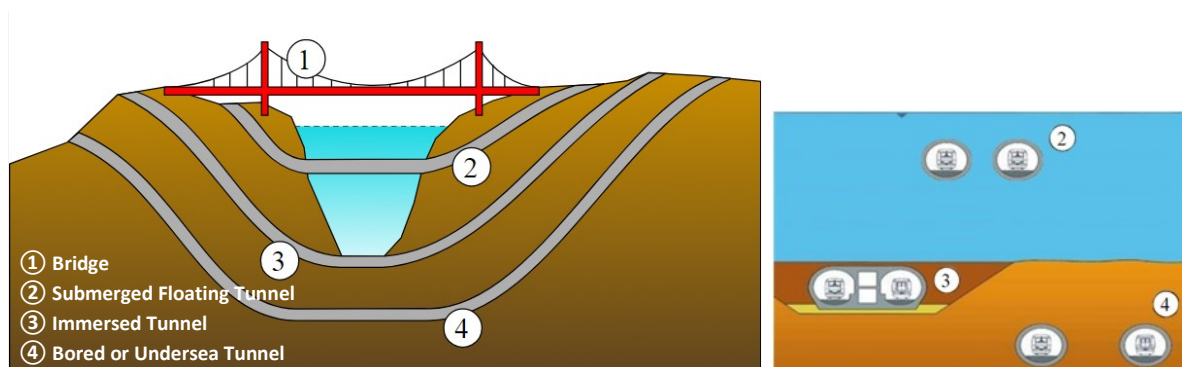


Figure 1 - Continuous methods to cross a water body¹

¹ Modified illustration: https://en.wikipedia.org/wiki/Submerged_floating_tunnel#/media/File:Bridge_types.svg
<https://pt.slideshare.net/Sagnik1/submerged-tunnel-ppt/4?smtNoRedir=1>

The SFT can have different types of support structures. Which type is applied mainly depends on the buoyancy to weight ratio. There are many possibilities and combinations. Four main types however can be distinguished: free floating, pontoons suspended, tension legs or columns.

A comparison of the main forms of the submerged floating tunnels has been performed [1]: comparing aspects such as main forms, different layouts and anchorage materials using the Delphi method. Each concept will be elaborated on and the scope of application of the different support systems will be considered.

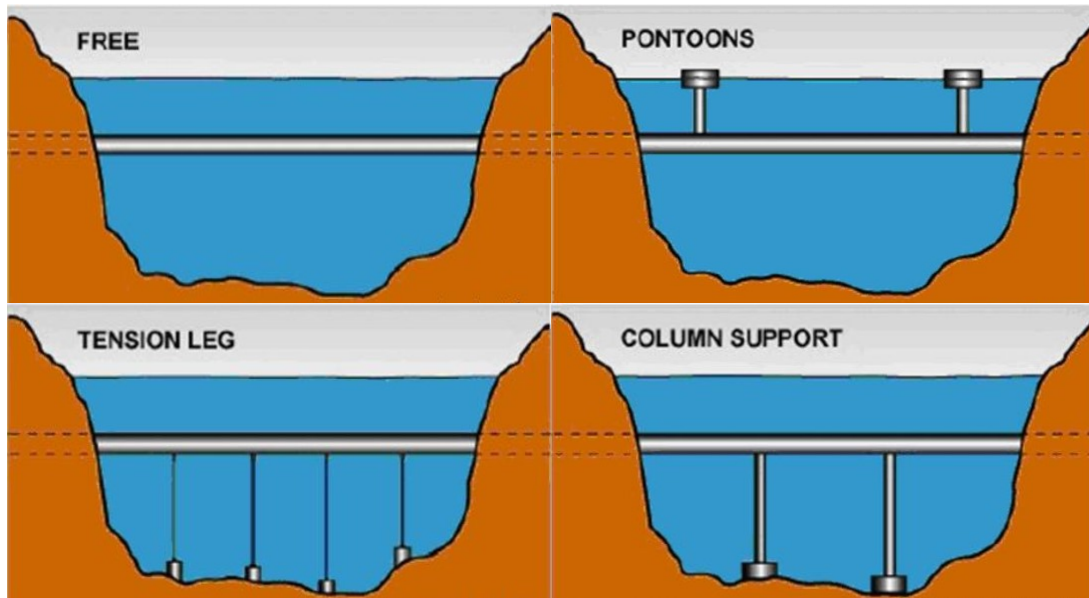


Figure 2 - Type of SFT support[2]

FREE	<p>When the buoyancy-weight-ratio is close to unity and only in case of small spans, the SFT can have a free support. It is an ideal design shape for it needs no complicated support structures. The tunnel is therefore only anchored at the shore ends. The length limitation is of structural origin; the maximum moments and shear forces allowed in the cross-section which are caused by the distribution of the loads, are largely influenced by the length of the span.</p> <p><u>Scope of application:</u> very short distances in the order of several 100 meters.</p>
PONTOONS	<p>The pontoon supported SFT seems one of the best options available, for it is independent of the water depth. The pontoons can support fishery and tourism such as overwater facilities. This alternative however is very sensitive to wind, waves and currents as well as the possibility of collision with ships and floating ice.</p> <p>The dynamic response and displacements must be looked into with caution, because the pontoons, in view of the vertical cables, can only offer the tunnel vertical restraint.</p> <p><u>Scope of application:</u> gentle, non-wave inland rivers, lakes and non-ice region.</p>
TENSION LEG	<p>There are several variants within the tether anchoring as support system for the SFT. The possibilities are endless; from different configurations of tether anchoring to the sea bed, till basically suspended bridges turned upside down.</p> <p>The optimal solution for tether configuration often depends on the project location. The tunnel is not depending on the water depth and slightly from the underwater soil conditions. The structure is not being effected by waves or floating ice and does not hinder navigation.</p> <p>The current however has quite an effect on the tunnel: fatigue damage occurred in the cables by the effect of vortex-induced vibration and wear easily befalls at the upper and the lower ends of joints.</p> <p><u>Scope of application:</u> widespread use in various ocean environments.</p>
COLUMNS	<p>The SFT supported by columns is literally an underwater bridge. It has a simple shape which can be substantiated with the mature knowledge of bridge structures. The column support system is limited to shallow waters because the columns cannot become too large.</p>

The construction of the columns as well as the maintenance of them under water is costly. Also, the construction has high demands of the soil conditions.

Scope of application: shallow waters, short tunnel lengths.

Each type of support has its advantages, disadvantages and scope of application. Which support system will be the best alternative needs to be considered carefully at each specific location. Beforehand it may be concluded that the tether type of the submerged floating tunnel has distinct advantages in the complicated marine environment and wide application in the ocean engineering [1].

Worldwide, the concept of a submerged floating tunnel has been known for decades. The first to put forward the concept of the submerged floating tunnel was Grant in 1966.

Design and construction technologies develop with tremendous speed in present day with new materials and the aid of more powerful computers.

One can go higher, larger and further in more special and elegant ways. This also holds for the hydraulic engineering section. The question therefore rises as to why the SFT never has been constructed before, because the SFT structure could prove to be beneficial for future road projects.

A general literature study has been performed to investigate which aspects need further research and development, to be able to build a prototype of the SFT allowing real time measurements. Abundant research has been done regarding the hydrodynamic and seismic response of the tunnel structure. Other aspects and parts however have been investigated only on a superficial scale; multiple alternative layouts are considered but arguments for certain preferences are not presented, few alternatives for the structural design of the tunnel segments are looked into, the need for appropriate end joints is frequently mentioned but not explored and researches regarding safety and risk assessment, durability, renewability and cost evaluation have been performed only on a very basic level.

A summary of the general literature study can be found in Chapter 2.

Though multiple aspects regarding the submerged floating tunnel need further research, a lot of essential components of the structure have been looked into. Decades of dreaming and research: the finish line is almost there. The focus now lies more on the details and construction phase, to get closer to making the submerged floating tunnel into a reality.

From the aspects found during the literature study, one aspect caught my attention: the design of the end joint of the Submerged Floating Tunnel. As many elements have already been considered, I favoured to put my energy into the subject connecting the pieces of the puzzle to get the SFT a step closer to completion.

The end joint, connecting the floating tunnel to the shore, is both a beginning and an end piece which allows others to enter the tunnel to design or inspect their component.

1.2. Problem definition

As mentioned before, there are still knowledge 'blank spots' regarding the SFT and possibilities to fill one.

One of the "loose ends" is the shore end joints of the SFT which will be the focus of this research.

The exact position and design of the tunnel end connections basically depends on the location, because each location comes with different conditions. For example, an area prone to seismic activity results in other load conditions than a quiet enclosed bay. The surroundings and the choice of support system of the SFT influences aspects such as the shape of the cross-section, length of the spans and the type of inter segment connections.

The combinations of these variables produce large range of forces in the end joints. Just one simple universal solution is therefore probably not applicable.

The end joints have to be able to support the allowed displacements, rotations and forces induced by the loads on the tunnel. The joint must not collapse and still remain waterproof under such forces and deformations; the structural integrity must be maintained.

Details in respect to range and direction of the forces and displacements are not yet known. A better understanding of the range of forces in the end joint will help in creating a proper design.

1.3. Research questions

The background information and problem definition have led to the following research objective;

“The main design criteria of a SFT end joint are like any tunnel end joint, it must be able to withstand loads and deformations whilst maintaining water tightness and structural integrity.

The aim of this study is to design an end joint which is suitable for the specific circumstances surrounding a SFT.”

From this research objective, a main research question and several sub questions were formulated.

Main question

“What type of end joint is recommended for a submerged floating tunnel?”

Sub questions

- Which load cases need to be taken into account?
- Which variable parameters are taken into account?
- What is the influence of these parameters on the end joint and on the total structure?
- Which load transfers does the end joint have to absorb?
- Which connections are already available for the end joint?
- How to maintain the joint's water tightness?

1.4. Methodology

The aim of this research is to draft a report describing the design strategy of an end joint in a SFT.

At first a general literature study is performed to obtain a better understanding of this new state of the art solution in tunnel engineering. From this study, a research topic has been chosen from the ‘blank spots’ found: the design of the end joint for a submerged floating tunnel.

The summary of the general literature study can be found in Chapter 2 and the full study is added in Appendix A.

In the literature study, a small side step will be made to explore existing solution of joints and connections.

Perusal of the available knowledge on immersed tunnels, previous papers on submerged floating tunnels and different industrial branches, will give an overview of possibly existing solutions. Existing solutions need to be validated to be applicable for submerged floating tunnels.

In Chapter 3, the design location is looked at in order to determine the relevant values and dimensions. The selection of a design location limits the number of variables, allowing to research the influence of more important parameters on the tunnel structure and the shore end joint.

With the use of numerical computer programs and analytical ‘rules of thumb’, the force distribution, displacements and other structural values are determined, validated and compared.

In Chapter 4, the basic FEM-model is constructed and the results validated.

A comparison is made in Chapter 5 between the FEM-model results and the analytical approach which uses differential equations to describe the force distributions and displacements of the tunnel structure.

After the FEM-model is verified, a parameter study is performed in Chapter 6. The results of this study will give an overview of the influences of several parameters on the design aspects of the tunnel and the end joint structure.

In Chapter 7 the knowledge gained will be used to create a conceptual design of the end joint for submerged floating tunnels.

Finally, conclusions and recommendations can be found in Chapter 8 and 9.

1.5. Scope

The most powerful solution would be to design an end joint adaptable to, or valid for all SFT designs. Due to the limited time available for the research however, it is necessary to narrow the options by setting some restrictions.

One of the restrictions is the reduction of the number of variable parameters by choosing a location. Current, wave and seismic loads are defined by the surroundings of the location. The basic design of the SFT itself also needs to be determined; cross-section, support layout, buoyancy weight ratio, materials and tunnel trace to name a few. A large portion of these variables are set by choosing a design location.

In this case, the Bjørnafjord in Norway is selected as the design location mainly because a tender design already has been made for this location and thus a lot of the required information is available.

To abridge the scope of the master thesis, the free and column supported SFT systems are no longer considered as a solution to the objective of the SFT: crossing deep and/or large water bodies.

Finally, the level of detail during structure calculations was limited. The possibility exists to calculate with the most detailed models and determine results till the last bolt or weld. Such a level of detail is not of importance, as only certain parameters are relevant to the design of the end joint.

2. General literature study

An extensive literature study was performed and documented in a separate literature report, to obtain a general understanding of the construction of SFT, the methods of construction, their application and the limitations of the presently available designs. The full report can be found in appendix A. The inquiries' findings are summarised in the following paragraphs.

2.1. Systems

At first glance, multiple alternatives are presented, from free spans to suspension bridges turned upside down. However, many researchers restrict themselves to anchoring using simple tension piles or floating pontoons. Arguments for these preferences are not presented and/or have not been found. Only a basic comparison was made between the alternatives [1], see also Figure 2, suggesting the tether variants as the most likely winner.

2.2. Tunnel tube structure

The same arises for the structural design of the tunnel segments; few alternatives are explored. Some research has been done regarding axial forces in a concrete tunnel lining, the influence of cable configuration on the stress state of the SFT [3][4], the use of different shell materials regarding water tightness and corrosion protection [5]. Only two papers have been found with respect to the layout of the cross-section; a comparison is made between a rectangular and a tubular cross-section[6] and a comparison between a octagon and an elliptical cross-section[7].

There is a mention of the need for appropriate joints [2], but only a small note has been made on the possibility of a spherical hinge and a mechanical device [8]. Another option given is the use of known technologies from immersed tunnels, but without validation. The same holds for tunnel installations as well as the overall construction methods for SFT.

2.3. Loading

The load cases of the tunnel structure have been considered on many aspects. The coefficients induced by currents and waves have been investigated and a 2D numerical wave-current tank has been developed, agreeing with experimental data [9]. Research also has been done on the effect of a detachable escape device on the flow and wave loads [10].

Research is done on the dynamic response due to hydraulic loads and the fluid-structure interaction [11]. The structural shape indicated with the BWR is a critical parameter that influences the response of the SFT structure [12]. Considering the hydrodynamics, both currents [13–15] and wave [16,17] vortex induced vibrations have been widely accounted for. Extended research has been done on seismic response such as the individual P-wave [18,19], random excitation and multi-support excitation [20].

Dynamic response and forces have been determined in the tethers [21] as well as for the SFT itself. Dynamic response on traffic moving loads [22] and accidental loads [23] have only been explored lightly.

2.4. Other

There have been some researches regarding durability, renewability and safety. Topics which have been encountered are: fire [24], corrosion [25], fatigue [26] and the life cycle of the structure[27]. Research on these topics can be extended, in view of the basic aspects being considered only.

Risk assessment has been lightly investigated. Identifying potential risks and impact factors and developing a risk index system [28]. Researches state that the risks can be minimized to the lowest level [29]. A single research is done regarding the calibration of the design codes for SFT [30].

Only one study has been found on the cost evaluation comparing traditional water crossings and the SFT [31]. In the current design stage, costs are not that relevant in determining whether a SFT is chosen as a valuable alternative.

2.5. Conclusion

The general literature study showed a number of above mentioned 'blank spots'. The most interesting research topic has been chosen from these blank spots: the shore end joints of the SFT. With this subject, the designer would like to contribute to the development of the SFT in a creative way and hopefully contributing to the process of building the first ever SFT. Specification of the research topic will be addressed in the next chapter.

3. Design location - Bjørnafjord

A location is chosen to limit the number of variable parameters. Setting a location also gives a better understanding of force distributions in the end joint only depending on variables related to tunnel elements and not to the surroundings itself. The location will be one of the fjords in Norway on auto route E39: the Bjørnafjord, for which studies have been performed on a submerged floating tunnel concept.

A detailed design study has been made by a partnership of three companies: consulting engineers Reinertsen, Dr. techn. Olav Olsen and Norconsult [32] [33]. The assessment study is commissioned by the Norwegian Public Road Administration Region West as objective that the SFT can be regarded as a safe, robust and viable option in the governmental regional plan for the E39. This resulted in design reports which are the most detailed and complete regarding available designs on the SFT structure. The access to the large amount of information therefore makes the Bjørnafjord SFT design a suitable location and structure to define boundaries and restrict the number of variable parameters.

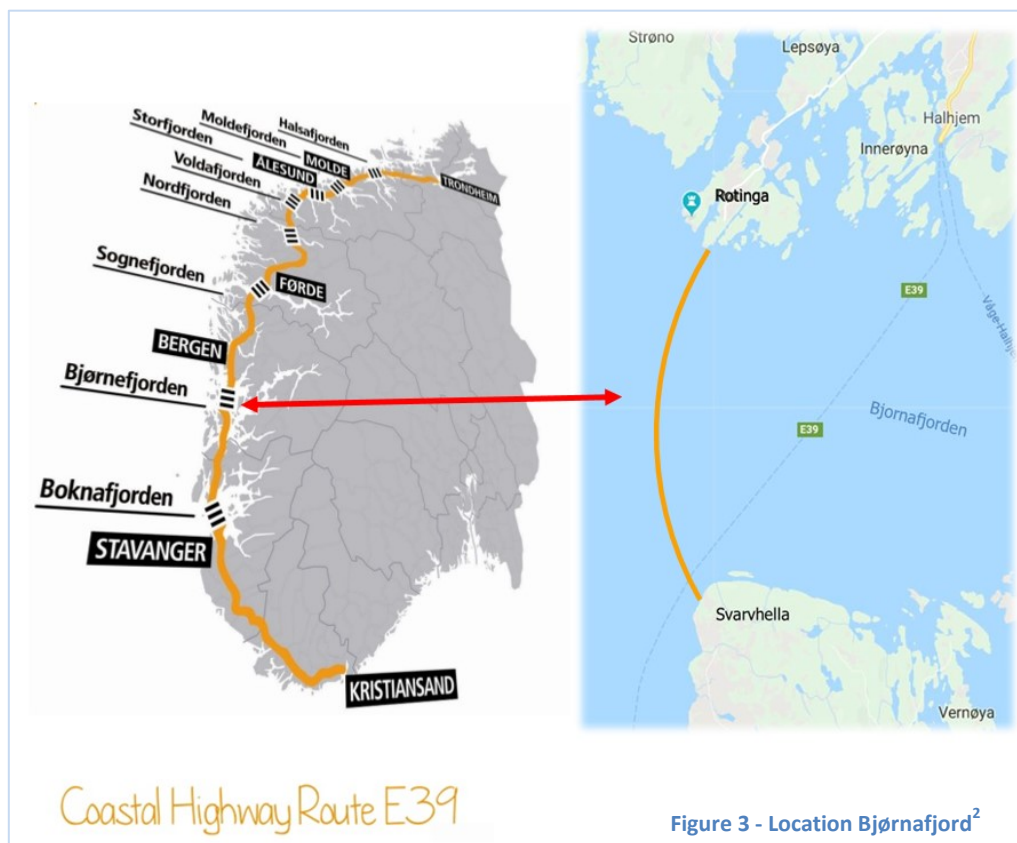
This chapter gives a summary of these reports; the information is mainly focused on the data which is relevant for this thesis. To avert an overflowing amount of same reference notations, hereby it is stated that information in this chapter is gathered from these reports or stated otherwise.

3.1. Situation and proposed layout

The Bjørnafjord is located near the middle Westcoast of Norway. The Bjørnafjord crossing is part of the new South to North connection route E39. This new route will decrease the traveling time with several hours and is therefore a very saleable project. Different solutions were considered on multiple locations along route E39, to hopefully gain the most suitable propositions to attract future consumers and possibly decrease the size and costs of the total project (in 2016 it was estimated for 35.7 billion Euros).

For the Bjørnafjord this resulted in the option between a (floating) bridge and a SFT instead of a ferry. As mentioned before, only the SFT solution will be investigated in this more in depth going research on the end joint of the SFT.

The SFT will be located between Svarvhella and Røtinga, close to the original ferry line along the old E39.



² www.vegvesen.no/_attachment/2044354/binary/1289211?fast_title=An+overview+-+The+E39+Coastal+Highway+Route.pdf

There are two variants considered for this specific fixed crossing; a SFT anchored to pontoons on the sea surface and a SFT anchored to the seabed by tethers. Apart from the different solutions for vertical mooring, the two variants share common concept characteristics regarding to the alignment, horizontal stabilization, tube configuration and abutments.

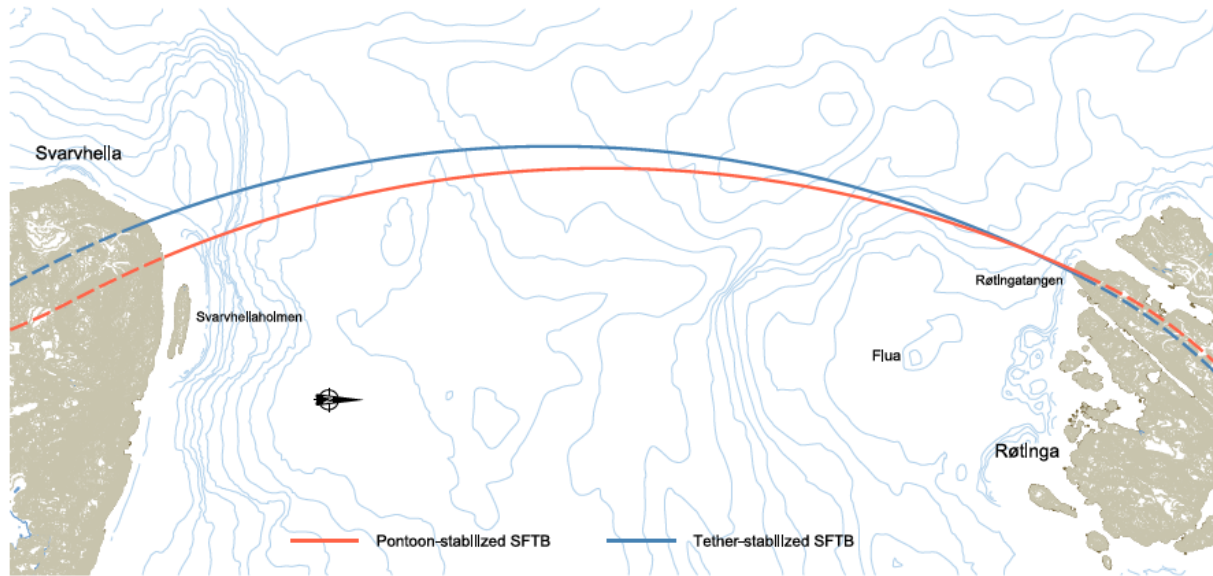


Figure 4 - General crossing alignments [33]

Though resulting in a larger tunnel length, the arc shape has been selected by the engineers for reasons of its flexibility to thermal expansion, favourable roadway layout, consistency with the approach tunnel alignments as well as horizontal stabilization. The constant curvature of the arc with a radius R_H of 6400 m has been adopted because of its simplicity for design, layout and construction. The shift in alignment for the pontoon and tether is due to different requirements of the support application. Very steep slopes are not favourable for the tether anchorage. The pontoon however needs the very steep slope close to a large shallow shore to accommodate enough clearance for the navigation channel.

The top of the SFT is located at 30 m below water level. Studies have shown that lowering the SFT has a positive effect on hydrodynamic response, because the excitation from especially wind generated sea is considerably reduced from 20 to 30 m water depth. Both the access hard rock tunnels have a longitudinal gradient of 3.5-5%. The vertical alignment of the SFT itself is zero.

The structure consists of two coupled concrete road tubes. The twin cylindrical tube configuration with a centre distance between the tubes of 40 m, has been selected by the engineers based on a comparative study on structural behaviour and efficiency of alternative section shapes and distances. The most distinct advantage of the cylindrical section is seen in the hydrodynamic performance due to significantly less added mass, but this shape also has an effective weight/displacement ratio and high resistance towards concentrated loading. The centre distance of the tubes is determined such to prevent in line VIV-response of the structure.

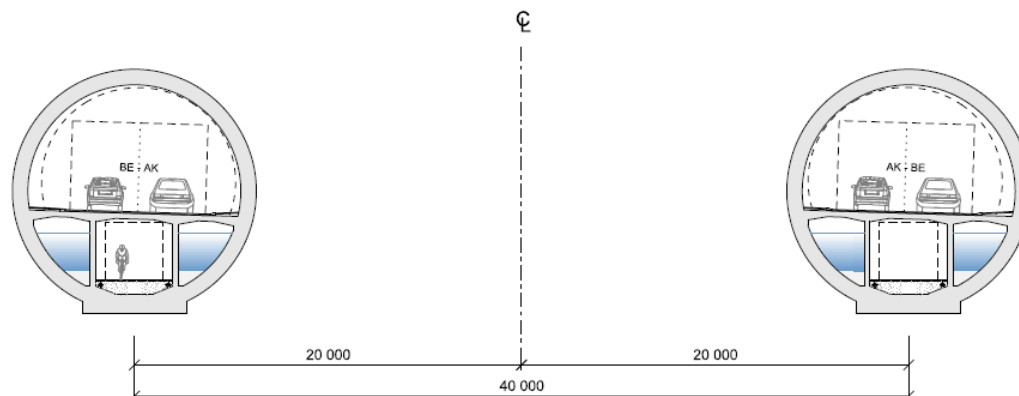


Figure 5 - General SFT configuration [33]

There are two typical cross-sections of the main tube, determined by the size of the standard tunnel profile. A general profile and a lay-by profile, with the latter creating a space for passing or stopping of vehicles during emergency situations. The cross-sectional properties are given in Table 1, as well as an illustration of the typical cross-sections.

Profile			General T9,5	Lay-by T12,5
Outer diameter	OD	m	12.6	15.0
Cross-sectional area	A_c	m^2	37.3	46.7
Outer area	A_o	m^2	125.7	177.9
Vertical offset COG	z	m	0.55	0.76
Moment of inertia	I_{yy}	m^4	574	1002
Moment of inertia	I_{zz}	m^4	592	1059

Table 1 - Cross-sectional properties of the main tube [33]

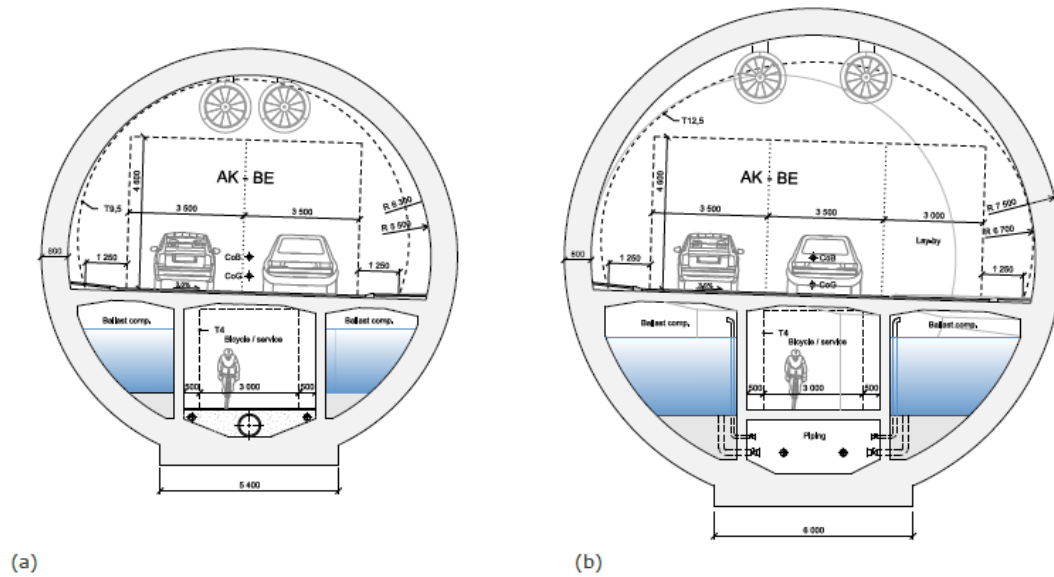


Figure 6 - Cross-section for (a) the general T9.5 profile and (b) the T12.5 lay-by profile [33]

The profiles are connected by an asymmetric cone, keeping the two main lanes aligned. This results in an eccentricity within the cross-section core, the offset will cause tensile stresses only under axial tension and on the opposite side of the lay-by. According to the technical report, the local bending stresses at the unstiffened tubular-cone junction is estimated to be marginal compared to the stresses from global actions (2-3 %) and therefore will not be considered in the thesis.

The main traffic tubes are coupled by cross tubes at each support and are rigidly connected with the tubes. The cross tubes fulfil both structural functions as well as accommodating space for technical installations and escape ways. The main tubes also have additional horizontal bracing along the full length of the tubes, with pre-stressed concrete braces in the shape of a dog bone.

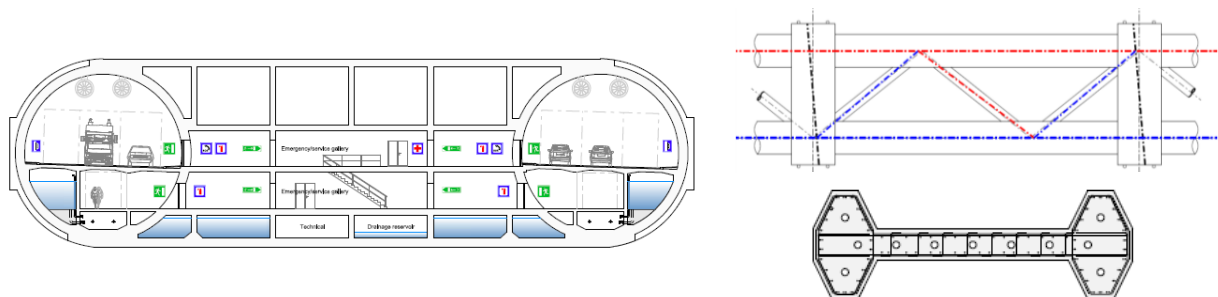


Figure 7 - Typical cross tube and horizontal bracing configuration with dog bone [33]

The abutment restraint of the SFT consists of a large gravity based concrete box caissons, founded on a prepared bedrock base. The caisson is ballasted with solid ballast (iron ore) after final placement, to ensure adequate stability and fixed end support for the SFT. The same caisson arrangement is used for both tether- and pontoon-stabilized SFTB concept.

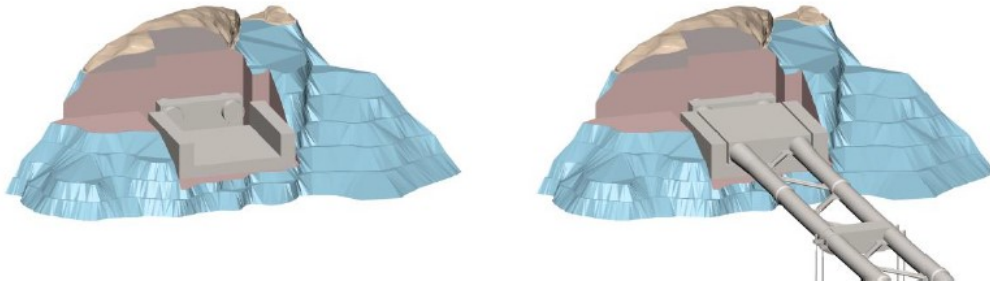


Figure 8 - Landfall arrangement prior to installation and in operation [33]

Table 2 shows the basic properties used in the SFT design, such as concrete and steel class.

Properties		Value		
Concrete	B45 = C35/45	Compressive strength	f_{cm}	43 N/mm ²
		Tensile strength	f_{ct}	3.2 N/mm ²
		Young's modulus	E	34100 N/mm ²
		Yield strength	f_{yk}	500 N/mm ²
Steel	B500NC	Yield strength	f_{yk}	500 N/mm ²
		Young's modulus	E	210000 N/mm ²

Table 2 - Basic material properties

3.1.1. Pontoon variant

The SFT anchored by pontoons has the advantage of being independent of the water depth. It however has to be able to interact with ships as the pontoons restrict free passage. The horizontal alignment and spacing of the pontoons is illustrated below. The pontoons have a general spacing of approximately 200m, with larger spans of almost 400m at both ends to allow ships to pass.

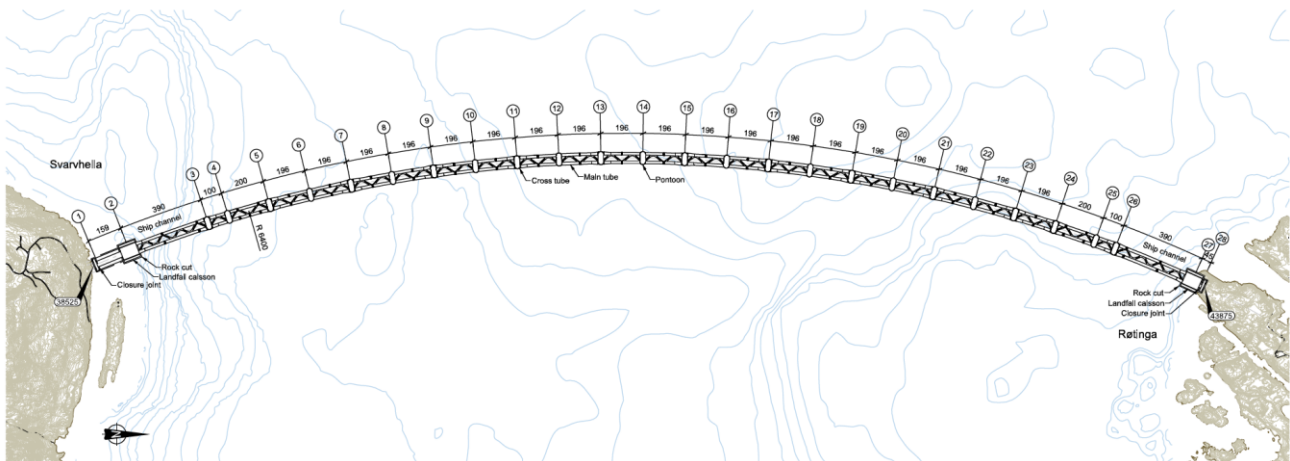


Figure 9 - Plan view of the pontoon-stabilized SFT [33]

Due to the larger end spans necessary for the navigation channels, the general tube cross sections have undergone some redesigning to increase the stiffness. Increasing solely the outer diameter of the concrete tube was not an option, because this would result in an outer diameter of 20m. Therefore, a double steel shell tube with concrete ballast filling is chosen which matches the increased bending stiffness of the concrete tube.

The pontoons which act as supports in this variant and consist of concrete caissons, connected by steel trusses to the SFT. They have a combined shape of a rectangular and cylinder to reduce the forces from ship impact and to mitigate roll behaviour from wave loading. The multiple compartments in the pontoon result in a two-compartment damage stability. The main dimensions of the pontoon and truss system are illustrated below.

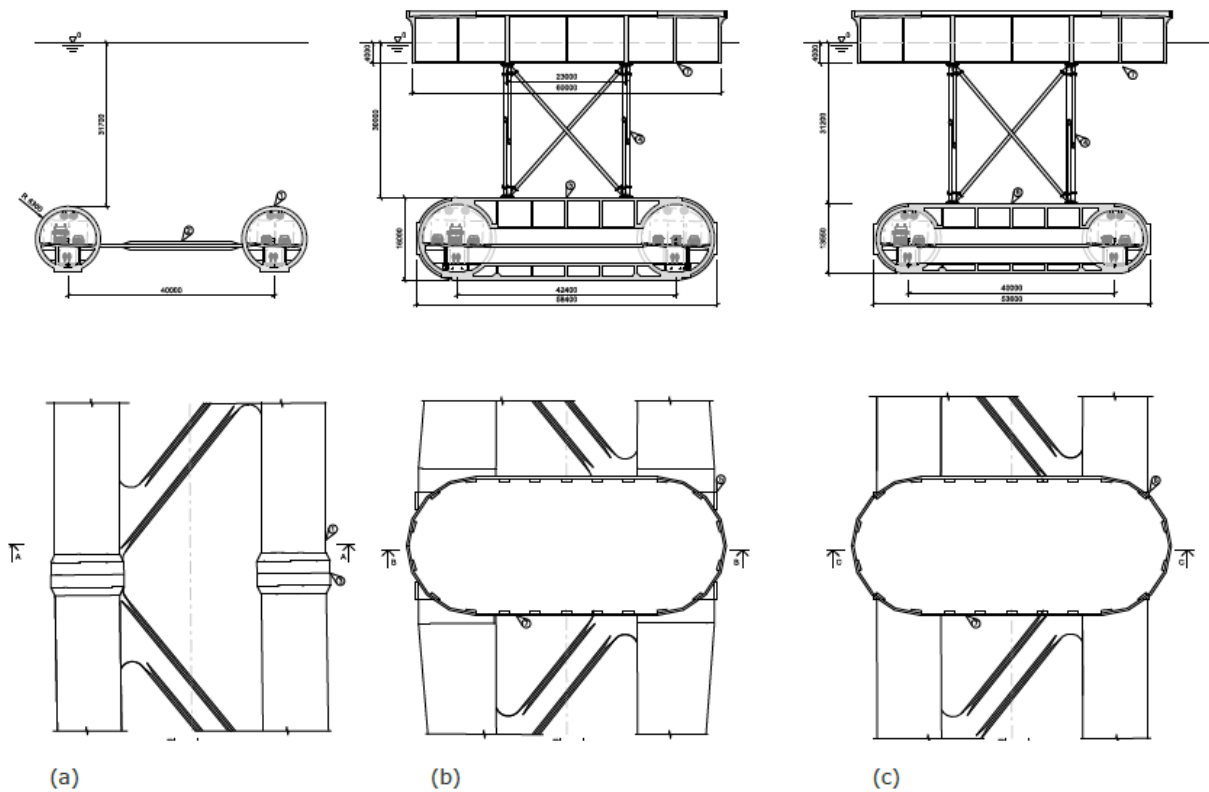


Figure 10 - Typical sections at (a) mid-span and (b) (c) at support with and without lay-by [33]

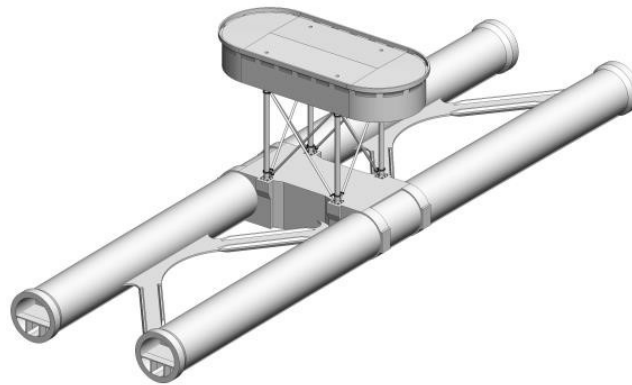


Figure 11- Typical pontoon support elements [33]

Properties			Value
Draft	d	m	4.0
Length	LOA	m	60
Breath	B	m	25
Water plane area	A_{wpa}	m^2	1366
Moment of inertia	$I_{wpa,xx}$	m^2	349974
Moment of inertia	$I_{wpa,yy}$	m^2	64748

Table 3- Pontoon characteristics [33]

3.1.2. Tether variant

The advantage of the tether variant is that it gives no restrictions to the navigation channels. Large depths however could result in more complex tether designs or hard to construct anchorage systems. The variation of the tether spacing, in the range from 150 – 300 m, revealed that a general distance of 200 m between the moorings gave a reasonable compromise between the static and dynamic response in the main tubes.

The supporting mooring tethers have a general spacing distance of 200m, with 4 tethers at each mooring group: 2 at both sides. The tethers are moored individually by means of rock anchors connected to the outer side of each tube. The stabilization of the tube bridge in horizontal plane is maintained by the arched tubes, because the mooring concept contributes marginally to the bridge lateral stiffness due to the lengths of the tethers in deep water.



Figure 12 - Plan view of the tether-stabilized SFT [33]

The cross-section for the main tubes is the same as for the pontoon variant. Here however, no local strengthening is required at the ends because the end spans are smaller. Properties of the cross-sections can be found in previous paragraphs. The figure below illustrates the bed level of the fjord along the crossing and the length of the tethers.

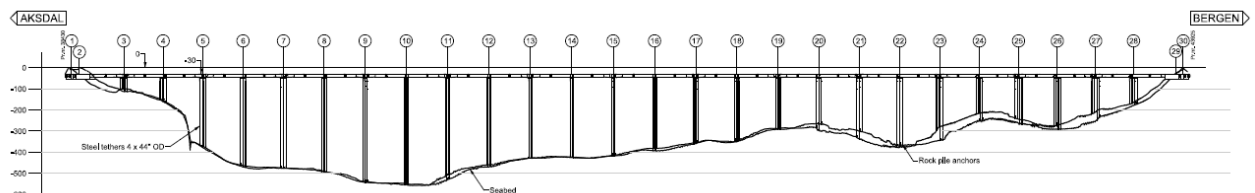


Figure 13 - Elevation of the tether-stabilized SFT [33]

The tether assembly is based on already available systems. The tether assembly consist of a top connector, the tether string and a bottom connector and has a quasi-neutral buoyancy.

Properties		Value	
No. of tethers	n		4
Tether outer diameter	R	mm	1118
Wall thickness	t	mm	38
Cross-sectional area	A	m ²	0.129
Tether resistance	F _{t,Rd}	MN	27

Table 4- Characteristics of the tether mooring [33]

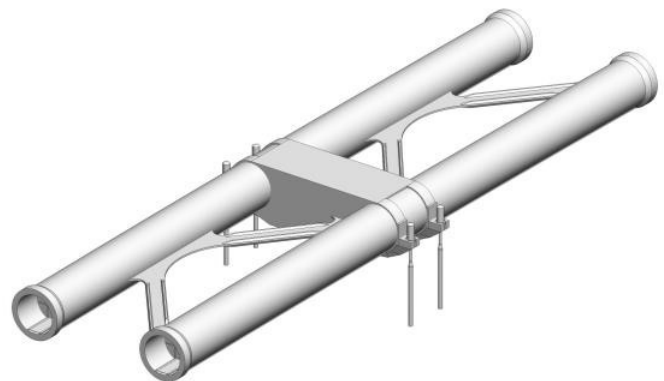


Figure 14 - Typical tether support elements [33]

Compared to the pontoon alternative, the cross tubes are basically the same but differ in overall size. The larger size is necessary to create excess buoyancy for keeping the tethers in tension under the most severe conditions. Rather than distributing the excess buoyancy on the main tubes, the buoyancy required to prevent slacking is lumped at the cross tubes to avoid unnecessary loading of the main tubes. The main dimensions of the mooring support are illustrated below.

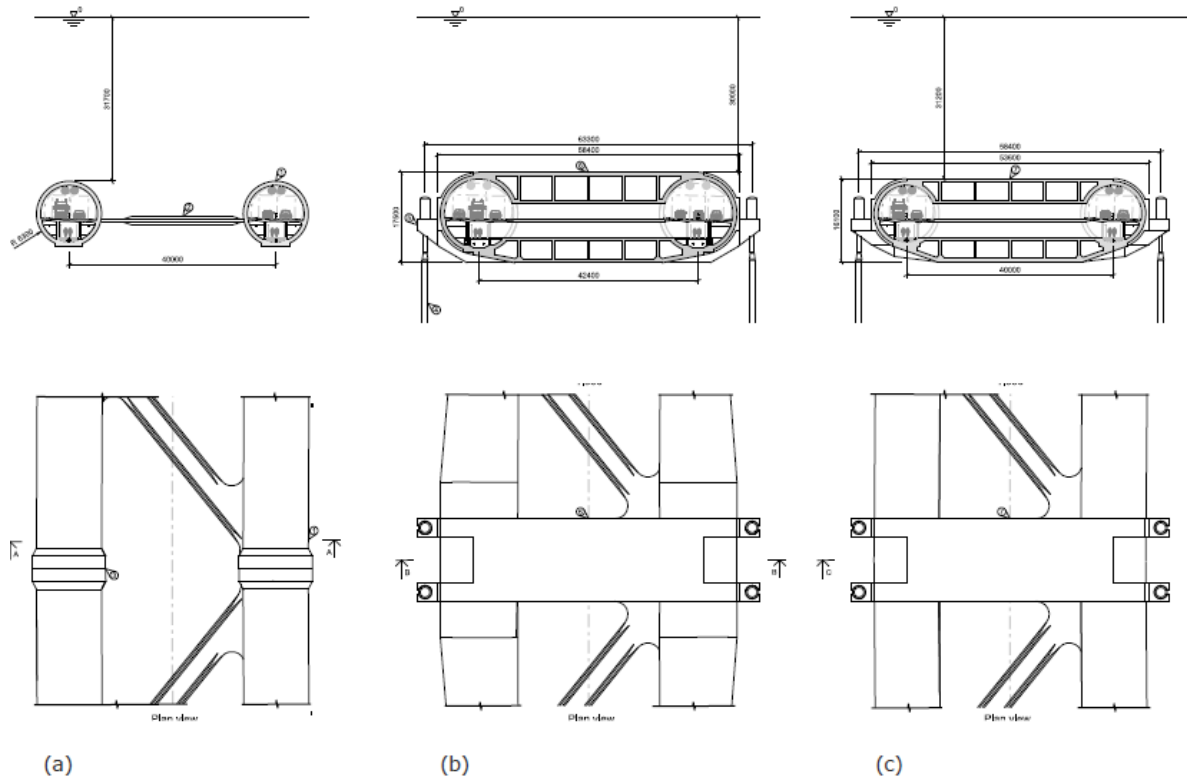


Figure 15 - Typical sections at (a) mid-span and (b) (c) at support with and without lay-by [33]

3.2. Boundary conditions

The location and layout of the Bjørnafjord results in boundary conditions depicted by its characteristic surroundings, such as currents, wave loads, water depths and soil conditions.

Bathymetry and soil conditions

The Bjørnafjord has water depths down to about 500 to 600 m. On both sides of the crossing, there are steep underwater slopes down from the shoreline to the middle part of the fjord. These slopes are assumed to have protruding rock segments. The near-shore areas are characterized by undulating surface, covered by limited soil. The middle part is covered by varying types of sediments, described as moraine, mixed deposits and clay.

Environment

Water levels

In the Bjørnafjord there is tidal movement as well as river discharges. This causes variation in sea water density due to the constant mixing of salt and fresh water. Mean Sea Level (MSL) is at 0.9 m above Lowest Astronomical Tide (LAT). After corrections for relation to the MSL and fresh and seawater density, the following values for the water levels are used in the analyses;

- High water level: +1.43 m MSL
- Low water level: -1.21 m MSL

Current

According to the numerical simulation that has been performed by the engineering team, the current is found to be strongest in the middle of the fjord. The predicted omnidirectional extreme current speeds are shown in the table below.

Depth	10 year	100 years
Surface	1.13 m/s	1.33 m/s
30 m	0.46 m/s	0.54 m/s

Table 5 - Extreme current velocity for given return period [33]

For calculation simplicity however, the worst-case scenario is assumed instead of calculating all load cases of the omnidirectional current. It is assumed that the current flows in the two main directions perpendicular to the tunnel arch during rising and falling tide. The latter causes two extreme situations and with a third situation, the eddy currents during slack tide, they cover the worst-case scenarios.

Waves

For wind sea, the NPRA has specified a significant wave height $H_{s,100y} = 3.0$ m with period range of $4 < T_p < 6$ s (for both crossings). The sea state characteristics (H_s , T_p , direction) should be considered constant along the SFT. In the table below 330 degrees corresponds with an angle of attack perpendicular to the SFT.

Return period	Scaling from 100 y	H_s (m)	$T_{p,min}$ (s)	$T_{p,max}$ (s)	γ (-)	Spread n	Dir (deg)
1 y	0.67	2.0	4.0	6.0	2 - 4	5 - 10	330°
10 y	0.81	2.4	4.0	6.0	2 - 4	5 - 10	330°
100 y	1.00	3.0	4.0	6.0	2 - 4	5 - 10	330°
1000 y	1.19	3.6	4.0	6.0	2 - 4	5 - 10	330°
10000 y	1.29	3.9	4.0	6.0	2 - 4	5 - 10	330°

Table 6 - Highest significant wave height values [33]

Swell sea state in the fjord is determined by transferring offshore wave conditions to the tunnel location by applying a numerical wave model. The significant wave height and corresponding wave directions for primary swell for given return periods are shown in the table below.

Return period	Scaling from 100 y	H_s (m)	$T_{p,range}$ (s)
1 y	0.63	0.19	12 - 16
10 y	0.81	0.24	12 - 16
100 y	1.00	0.30	12 - 16
1000 y	1.16	0.36	12 - 16
10000 y	1.31	0.39	12 - 16

Table 7 - Primary swell peak values [33]

The bathymetry and environmental boundary conditions will be used when constructing the SCIA model.

4. FEM Modelling

Modelling is used to represent the structure in which the level of detail can vary a lot. To reduce the amount of calculations, thus reducing the computer power necessary to do such calculations, basic models are often used. Basic models will quickly produce the understanding of how the structure behaves. Following the test run with basic models, detailed models can be useful to get more accurate values if required. In this Chapter, the basic model is setup in the FEM program, SCIENTIFIC Applications engineer (SCIA) and validated using rules of thumb and basic physics laws.

4.1. Introduction

A computer model of the SFT is made using the FEM computer program SCIA which is an integrated software package to analyse and design different structures composed of multiple materials. Thanks to its flexible operation, SCIA offers a solution for nearly every type of construction, from simple day-to-day tasks to complex and challenging projects. The program uses the "finite element method" for the calculations.

The model of the SFT is not created in full detail because that is not relevant at this stage of design. The purpose of the model is to see on a more global scale what the influence is of several parameters on the design of the end joint and the tunnel structure itself. These effects will be researched and elaborated on in the Chapter 6.

To remain close to the design made for the Bjørnafjord tunnel in Norway, the basic dimensions such as the layout, cross-sections and supports are determined and incorporated in the model. Design checks are performed in the Service Limit State (SLS) and Ultimate Limit State (ULS).

The correct modelling of the tunnel in SCIA is verified with analytical differential equations for a beam in bending in Chapter 5.

4.2. Basic model

The tunnel will be modelled as a simple double beam on multiple supports, with cross-connections and horizontal bracings. The beam is a hollow tube with the outer diameter equal to the original design. The wall thickness is chosen such that the moment of inertia is the same as for the final cross-section. This resulted in a larger wall thickness, but the weight value per meter length is smaller than that of the original design. The latter has been corrected by increasing the forces due to gravity on the structure.

The same method is used for the cross tubes and dog bone horizontal bracing. The tables below show the parameter values of the main tube of the tunnel model in SCIA.

Parameter	Symbol	Unit	Original	Model	Ratio (model/original)
Outer diameter	OD	m	12.6	12.6	1.00
Wall thickness	t	m	0.800	0.946	1.18
Cross-sectional area	A_c	m ²	37.3	34.6	0.93
Outer area	A_o	m ²	125.7	125.7	1.00
Moment of inertia	I_{zz}	m ⁴	592	592	1.00
Tunnel length between grid 2 and 29	L	M	5373	5373	1.00

Table 8 - Cross-section values of the main tube as SCIA model

Parameter	Symbol	Unit	Value
Tunnel length between grid 2 and 29	L	m	5373
Concrete strength C35/45	f_{cd} f_{ctd}	N/mm ² N/mm ²	30 1.47
Young's modulus	E_c	MPa	34100
Concrete density	ρ_c	kg/m ³	2400
Material factor concrete	γ_c	-	1.5

Table 9 - Material values of the SFT

The supports at the landfall caissons (grid 2 and 29) are considered to be of a fixed constraint type, because the original design comprises the caissons to be encased and therefore free displacements are prevented. The outer supports (grid 1 and 30) are modelled as hinges, with rotational freedom in all directions. The remaining supports consist of springs.

The representative spring stiffness, for the tethers and the pontoons, has been determined by using Hooks law and assuming only elastic deformation of the tethers and pontoons, see chapter 4.2.1. The positions of the supports need to be considered, as they differ between the pontoon and tether variant relative to the tube axis.

On closer inspection, the model for the tether and pontoon variant do not differ much from each other. To correctly represent the pontoon mechanism, a combination of a normal and moment spring is applied at the supports. The system therefore remains the same and the only difference occurs at the supports. The changing stiffness of the supports will be considered during the parameter study in the next chapter. Consequently, only one main model will be considered and the pontoon variant will not be elaborated separately.

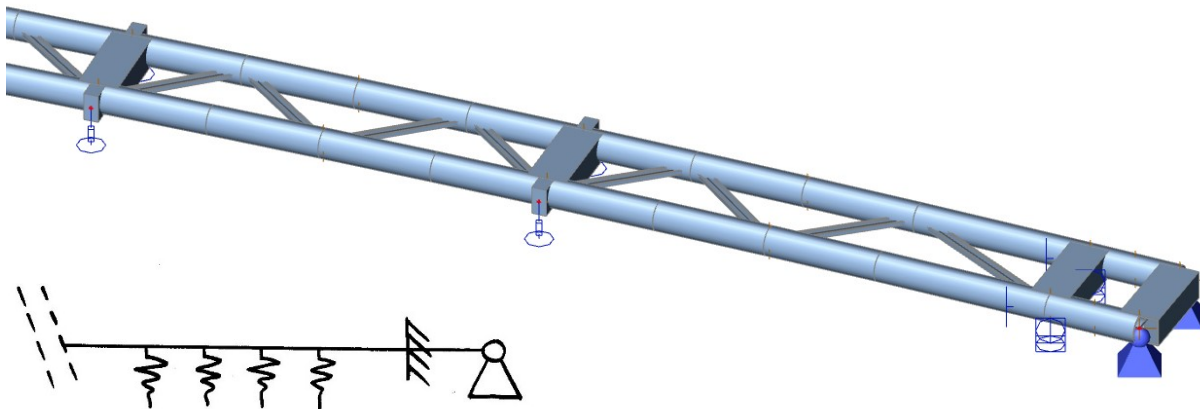


Figure 16 – SCIA basic model of the SFT

The coordinate system used in SCIA is illustrated in Figure 17

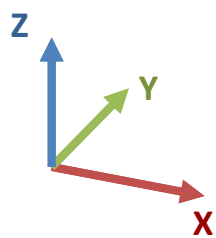


Figure 17 - Coordinate system SCIA

4.2.1. Spring stiffness of the supports

The representative spring stiffness of the supports are determined using Hook's law, the Young's Modulus, and the summation rules for springs.

Hook's law $F = k \cdot u$

Youngs modulus $E = \frac{\sigma}{\varepsilon}$

Parallel springs $k = k_1 + k_2 + \dots$

Serie springs $k = \frac{1}{\frac{1}{k_1} + \frac{1}{k_2} + \dots}$

With;

F Force applied on the spring [N]

k Spring stiffness [N/m]

u Displacement of the spring [m]

E Youngs modulus [N/mm² = MPa]

σ Stress [N/mm²]

ε Strain (proportional deformation) [-]

Tethers

The *tethers* are made of steel tubes and have different lengths. Therefore, they have a different spring stiffness and these different stiffness's can be calculated with the formula derived below:

$$E = \frac{\sigma}{\varepsilon} = \frac{F/A}{\Delta l/l_0} = \frac{F \cdot l_0}{\Delta l \cdot A} = k \cdot \frac{l_0}{A} \quad \rightarrow \quad k_{tether} = E \cdot \frac{A}{l_0} \quad \text{with, } A = \pi(R^2 - r^2)$$

With;

l_0 Original length [m]

Δl Elongation [m]

A Surface area [mm²]

Bearing in mind that k_{tether} as calculated with the above equation equals the spring stiffness of a single tether. For the total spring stiffness of one support, the tether spring stiffness needs to be multiplied by two.

As the tether lengths differ along the tunnel, because l_0 is different at each support, the spring stiffness of the supports has values in the following range;

$$0.98 \cdot 10^7 \text{ N/m} < k_{support} < 5.42 \cdot 10^8 \text{ N/m}$$

$$\text{with, } k_{support,mean} = 1.83 \cdot 10^8 \text{ N/m}$$

Note: the tether variant has a shift in position relative to the tunnel axis where the support is secured. The shift has no influence on M_z and M_y , but it does cause a torsion in the system. For more detailed design phases the latter should be considered in the calculations.

Pontoons

The spring stiffness of the pontoon supports will be determined to obtain the order of magnitude of the spring stiffness. As stated before, there will not be a separate model for both the tether and pontoon design. The order of magnitude of the spring stiffness however will give insight in the relative difference between the support stiffness between the tethers and pontoons, when performing the parameter study.

The *pontoon* support consists of two parts; the concrete pontoon and the steel truss. The main dimensions of the pontoon are illustrated in Figure 18. The water plane area of the pontoon is equal to $A_{pontoon} = 1366 \text{ m}^2$.

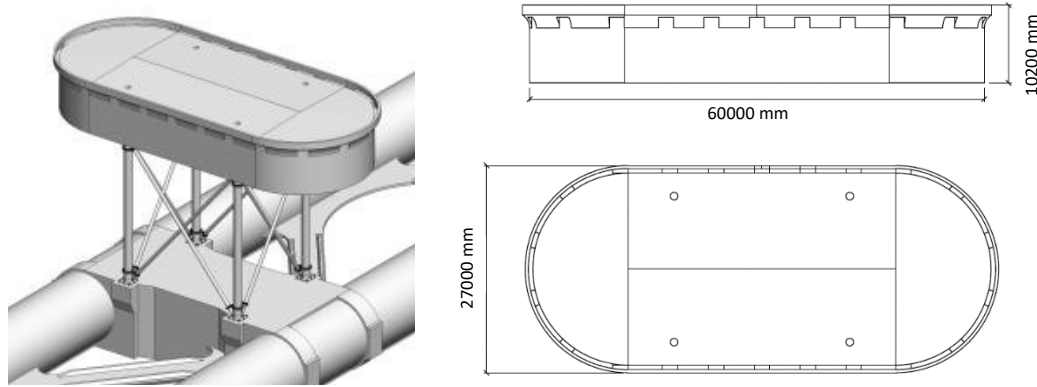


Figure 18 - Pontoon dimensions [33]

The spring stiffness of the concrete pontoon can be calculated using Archimedes law. It is assumed that the 4-meter draft of the pontoon is due to the weight of the pontoon itself. An increase of downward force on the pontoon is equal to an increase in draft (Δh), shown as formula;

$$\Delta F = \Delta h \cdot A_{pontoon} \cdot \rho_{water} \cdot g \quad \rightarrow \quad k_{concrete\ pontoon} = A_{pontoon} \cdot \rho_{water} \cdot g$$

With the $A_{pontoon} = 1366 \text{ m}^2$ and $\rho_{water,mean} = 1023 \text{ kg/m}^3$ results in a spring stiffness of the concrete part equal to;

$$k_{concrete\ pontoon} = 1.37 \cdot 10^7 \text{ N/m}$$

The spring stiffness of the truss is determined using the parallel spring relation formula. That way, the individual stiffness of the braces and columns of the truss can be combined into a single spring stiffness. The below illustration indicates the symbols and angles used in the formulas.

$$l_{0,brace} = \sqrt{23^2 + 30^2} \approx 37.8 \text{ m}$$

for small rotations holds: $\angle \varphi \approx \angle \varphi + \angle \alpha$

$$\text{thus, } u_b = \frac{u_c}{\sin(\varphi)}$$

$$F = 4 \cdot (F_{column} + 2F_{brace})$$

$$F = 4 \cdot ((k_c \cdot u_c) + 2(k_b \cdot u_b))$$

$$F = 4 \cdot \left(\left(k_c + 2 \frac{k_b}{\sin(\varphi)} \right) \cdot u_c \right)$$

Note that the multiplication of 2 in the brace section is because two braces are connected to one column. Likewise, there are four sets of columns with braces to create the total truss system.

$$\rightarrow k_{truss} = 4 \cdot \left(k_c + 2 \frac{k_b}{\sin(\varphi)} \right)$$

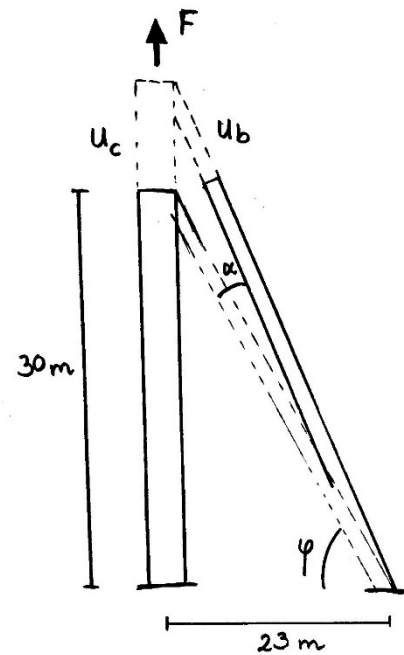


Figure 19 - Truss stiffness parameters

The spring stiffness of the column (k_c) and braces (k_b) can be calculated using the mechanical property of steel; the Young's modulus equal to 210.000 N/mm^2 .

$$k_i = E \cdot \frac{A_i}{l_{0,i}}$$

Filling in all the values into the formulas, will result in the following spring stiffness of the truss:

$$k_{truss} = 6.18 \cdot 10^9 \text{ N/m}$$

The spring stiffness of the trusses is small relative to the spring stiffness of the pontoon. Using the calculation rules for summation of springs, it can be shown that the contribution of the trusses to the total spring stiffness of the pontoon support can be negligible.

$$k_{pontoon\ total} = \frac{1}{\frac{1}{k_{pontoon}} + \frac{1}{k_{truss}}} = 1.37 \cdot 10^7 \frac{\text{N}}{\text{m}}$$

Compared to the tether system, the spring stiffness determined for the pontoon shows to be about one order of magnitude lower vertical stiffness. The vertical stiffness from the pontoons is less than 10 % of the tether stiffness. The smaller vertical stiffness can lead to resonance issues for the pontoon variant due to wave loading.

Another aspect which would need to be considered is tilting sideways of the pontoon. This mechanism would result in a moment spring and thus an additional spring stiffness at the support. As stated before however, only one model will be used and therefore several values for the spring stiffness will be considered during the parameter study.

4.3. Load cases

There are multiple loads acting on the tunnel. Permanent, variable as well as accidental loads can be distinguished. It is not possible to take into account all occurring loads due to the scope of this research. Only the basic static loads are therefore considered. Apart from the individual loads, load combinations are also determined in paragraph 4.4 Load combinations.

The four basic forces acting on the tunnel are; gravity, buoyancy, current and waves. The gravity and buoyancy forces are combined into one resulting force. The fjord is connected and located close to the sea, it is therefore assumed that the current is mainly caused by the tide and has two main directions. Due to the location and the size of the fjord, a wave climate is present.

4.3.1. Permanent nett force

On the structure, there are two permanent forces present; the gravity force working downwards and the buoyancy force working upwards. Gravity and buoyancy forces are combined into one force on the system: nett buoyancy. For first indication the commonly used amount of nett buoyancy of 6% working upwards on the structure is considered. The amount of nett buoyancy is taken relative to the amount of displaced water.

$$q_{6\%} = 0.06 \cdot \rho_{w,mean} \cdot g \cdot (\pi \cdot R^2)$$

$$q_{6\%} = 0.06 \cdot 1023 \cdot 9,81 \cdot (\pi \cdot 6.3^2) = 75.1 \text{ kN/m}$$

The structure wants to start floating but is retained by the tethers. This floatation is due to the fact that the buoyancy force is always kept larger than the gravity working on the structure, to prevent slack of the tethers. The structure between two supports acts as a beam on fixed supports. The overall tunnel structure acts as a beam on fixed supports as well, with the sinusoidal shape caused by the spring supports (tethers) restricting movement in z-direction. The moment line also clearly shows that the structure acts the same as a beam on multiple supports.

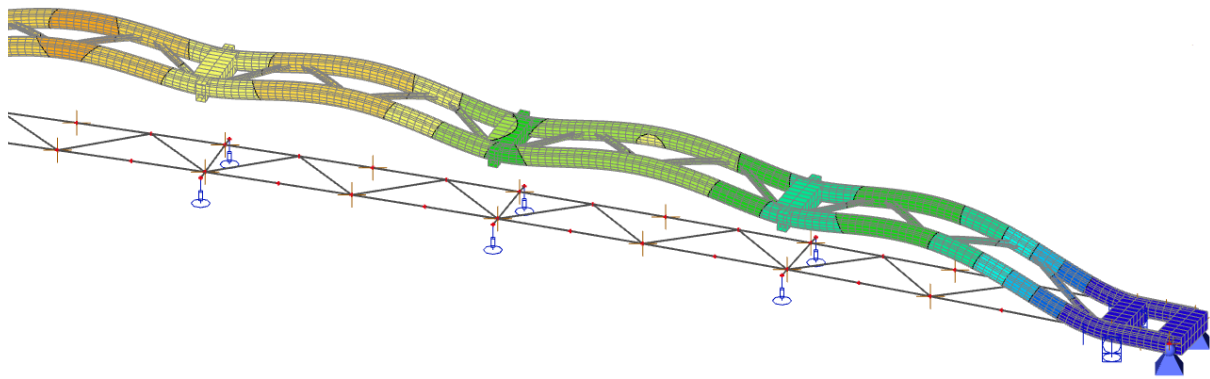


Figure 20 – Displacement due to nett buoyancy force

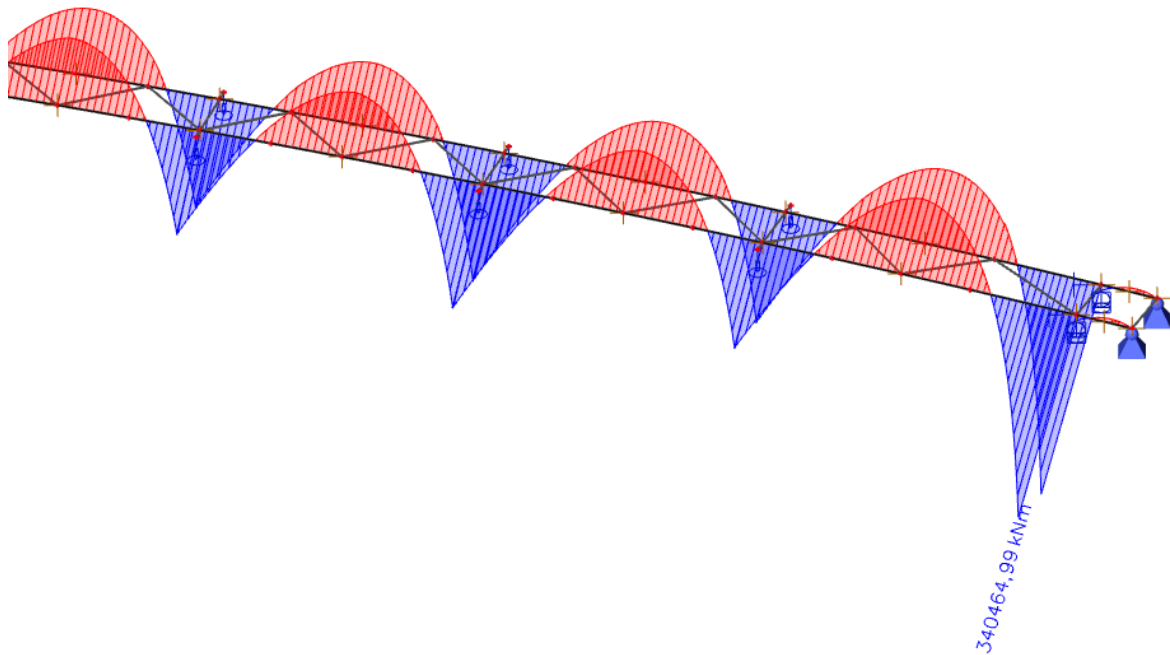


Figure 21 - Moments in y-direction due to nett buoyancy force (SLS)

The normal force working in the cross-section of the system is very small and almost zero. In the original design, there however are pre-stressing elements present which provide an axial pressure force in the cross-section. The pre-stressing has no influence on the moment line or the displacements itself, but it may have influence on the cross-section capacity. Pre-stressing forces increase the cross-section capacity and will be further elaborated on during the design checks in paragraph 4.6.

4.3.2. Current

The tunnel is located in a fjord, perpendicular to the main current directions. This means that during rising and falling tide, the current force is directed perpendicular to the middle section of the tunnel. Because the arch of the tunnel is very small (relative to the length of the tunnel, the eccentricity is small), it is assumed that the current hits the tunnel perpendicular everywhere. In reality, the current velocity will reduce on the bank sides of the tunnel. There is no information available on the current velocity profile and therefore a more conservative approach is taken. It is assumed that the current velocity will be the same everywhere along the entire tunnel length.

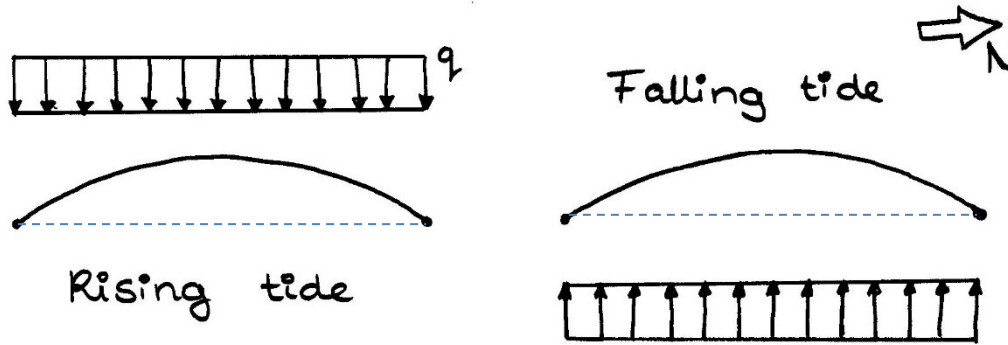


Figure 22 - Falling and rising tidal current directions, top view

The force acting on the tunnel caused by the current can be determined using the following formula [34]:

$$q_{current} = C_w \cdot \frac{1}{2} \rho u^2 \cdot D$$

With:

- C_w drag coefficient [-]
- u current velocity [m/s]
- D diameter of the object perpendicular to the current direction [m]

The drag coefficient is largely dependent on the shape of the structure and the flow around the structure, which are expressed in the Reynolds number:

$$Re = \frac{u \cdot D}{\nu}$$

With:

- ν kinematic viscosity [= $10^{-6} \text{ m}^2/\text{s}$]

Determining the Reynolds number and with the logarithmic plot of the drag coefficient as a function of the Reynolds number, results in the following values:

$$Re = 6.8 \cdot 10^6 \quad \rightarrow C_w \approx 0.9$$

Finally, the current force can be calculated using $u = 0.54 \text{ m/s}$ and $D = 12.6 \text{ m}$:

$$q_{current} = 1.695 \text{ kN/m}$$

Falling tide

The current is unfavourable for the tunnel structure and goes from East to West, pushing against the inside of the arch. The displacement of the structure causes the arch to increase and pulls the structure apart. This will result in a tension force in the cross-section, lowering the total pre-stressing force. The latter will cause a decrease in cross-sectional capacity. It also need to be checked whether there is enough pre-stressing force left to preserve the water tightness of the seals.

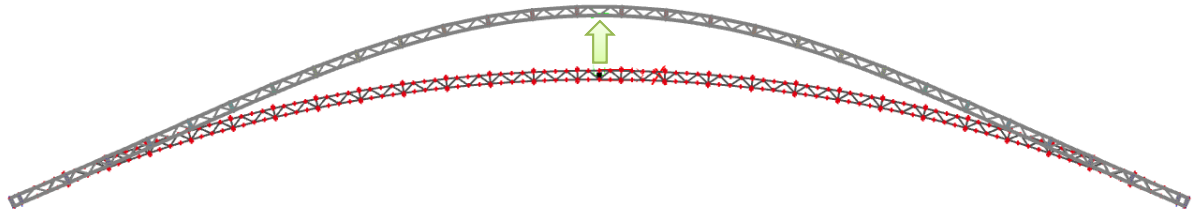


Figure 23 - Displacement profile caused by the falling tide, top view

The moments in y-direction and z-direction are in the same order of magnitude. The cross-section has a rotation symmetry shape. Therefore, the moments in both directions can be combined as vectors using the Pythagoras theorem. This will increase the total moment in the cross-section approximately with 50%.

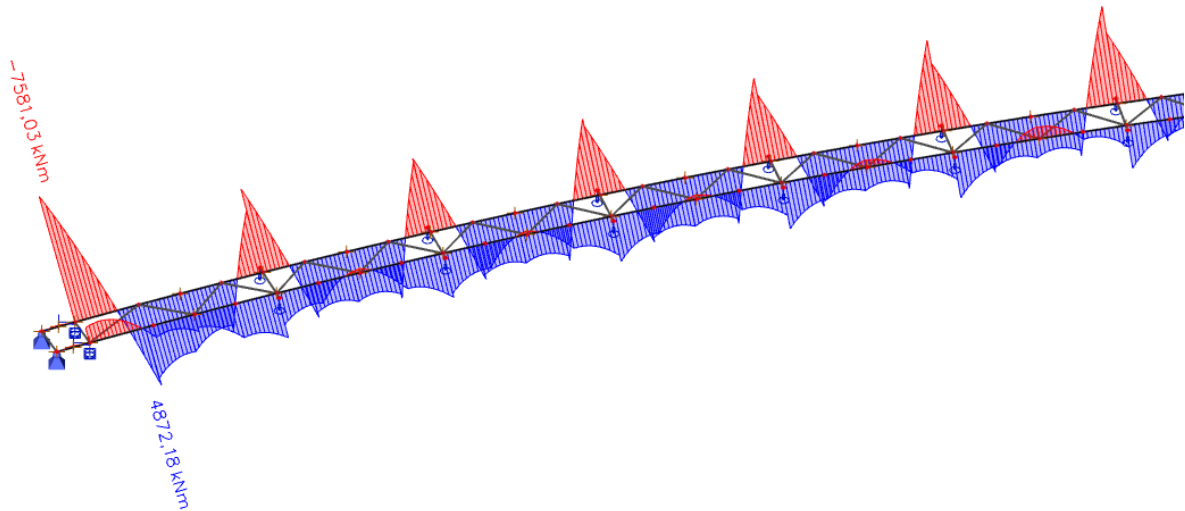


Figure 24 - Moments in y-direction due to falling tide current (SLS)

Rising tide

In the case of rising tide, the load is favourable for the tunnel structure. The current flows from West to East, pushing against the outside of the arch. The loading will result in an additional normal force in the cross-section, which is preferable for the water tightness of the seals. Caution has to be taken not to overload the cross-section by normal force, exceeding the material strength.

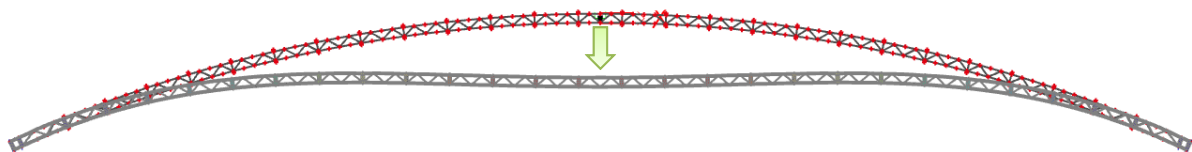


Figure 25 – Displacement profile caused by the rising tide, top view

The moments in y-direction and z-direction are in the same order of magnitude as for the falling tide current. The cross-section has a rotation symmetry shape. Therefore, the moments in both directions can be combined as vectors using the Pythagoras theorem. This will increase the total moment in the cross-section approximately with 50%

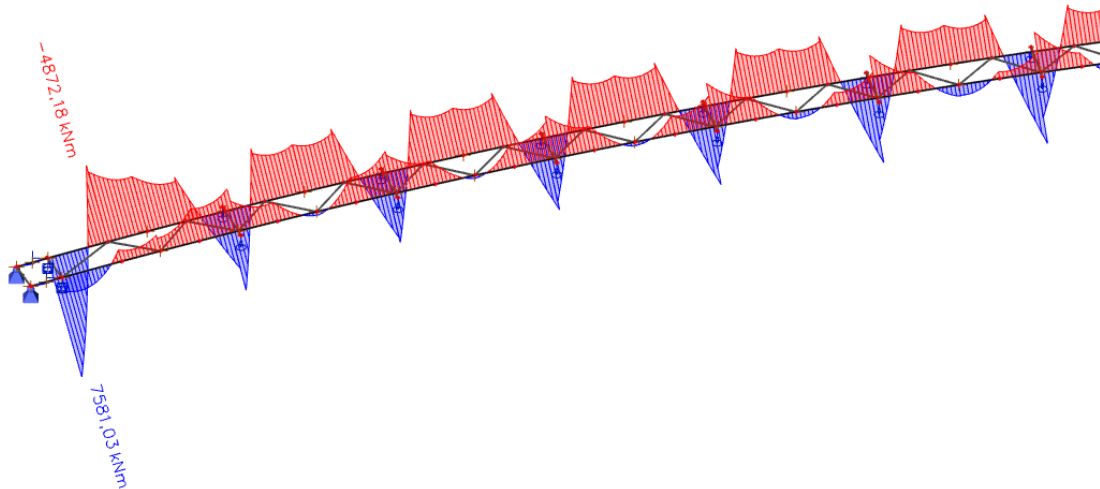


Figure 26 – Moments in y-direction due to rising tide current (SLS)

Slack tide

Apart from the rising and falling tidal currents, there is another scenario which needs to be considered. The change of tidal direction almost never runs smoothly, causing eddy currents which are smaller than the main tidal currents, but could be unfavourable for the structure.

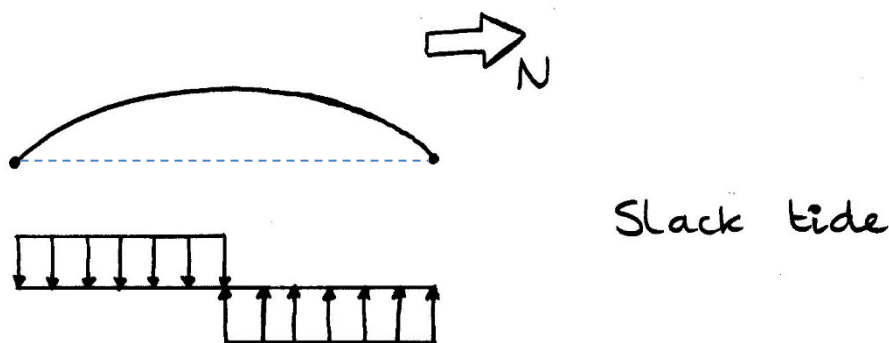


Figure 27 - Loading of the tunnel structure during slack tide, top view

Assuming that the magnitude of the slack tide current is about 25% of the main tidal current, it will give the following value:

$$q_{\text{slack}} = 0.25 \cdot q_{\text{current}} = 0.424 \text{ kN/m}$$

The forces caused by the current during slack tide cause a shifting of the whole tunnel structure and it basically gets pulled apart. The loading results in very large normal forces in the tubes, which could be problematic for the water tightness of the water seals.

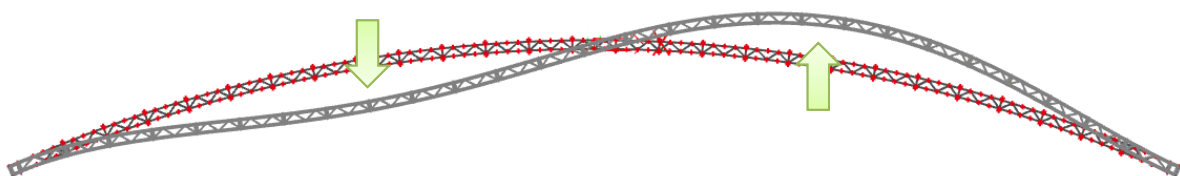


Figure 28 - Displacement of the tunnel structure due to current during slack tide, top view

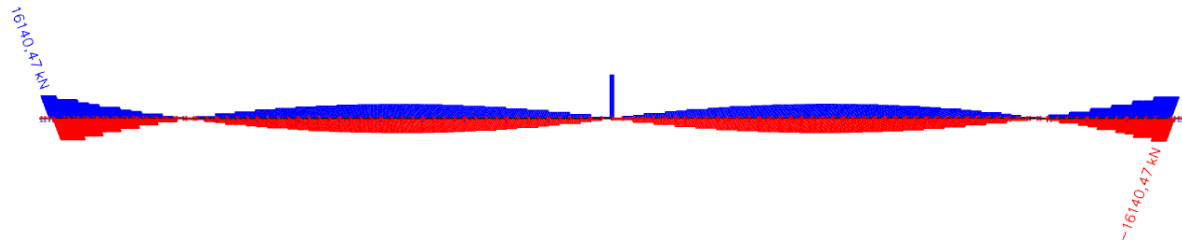


Figure 29 - Normal forces resulting from slack tide (SLS), side view

The moments due to slack tidal currents along the tunnel length are quite large compared to the moments caused by the falling and rising tidal currents. Combining the moments from y-direction and z-direction will result in a moment in the cross-section which is approximately four times larger than the total moment during falling or rising tide.

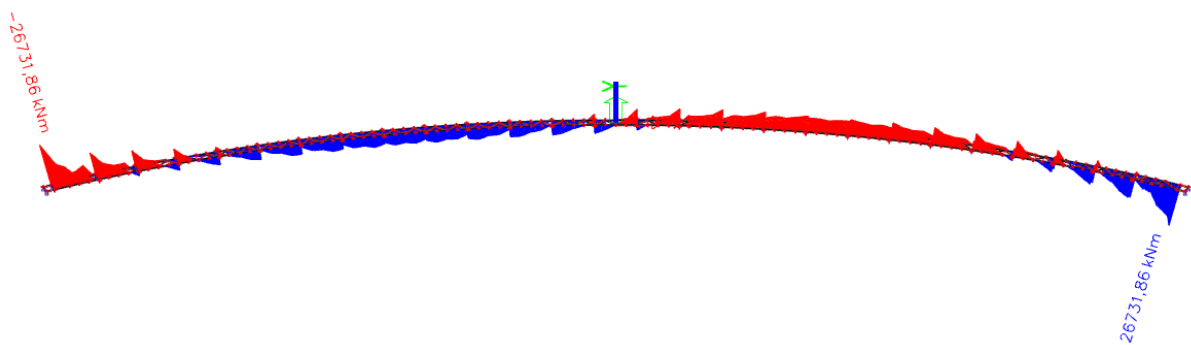


Figure 30 - Moments in y-direction due to slack tide current (SLS)

4.3.3. Waves

Wave loads are mostly of interest whilst researching the dynamic responses of a structure. A small step however is made on the static load of the waves on the tunnel tube structure. Lowering the tunnel has a positive effect on wave loading as the wave load decrease by increasing water depths. Figure 31 shows that wind generated waves are negligible because the tunnel is located well below the water surface level at 30 meters. Swell waves on the other hand still influence the tunnel, as the ratio plot from the study illustrates: at 30m depth below water level, 50% of the swell wave load remains.

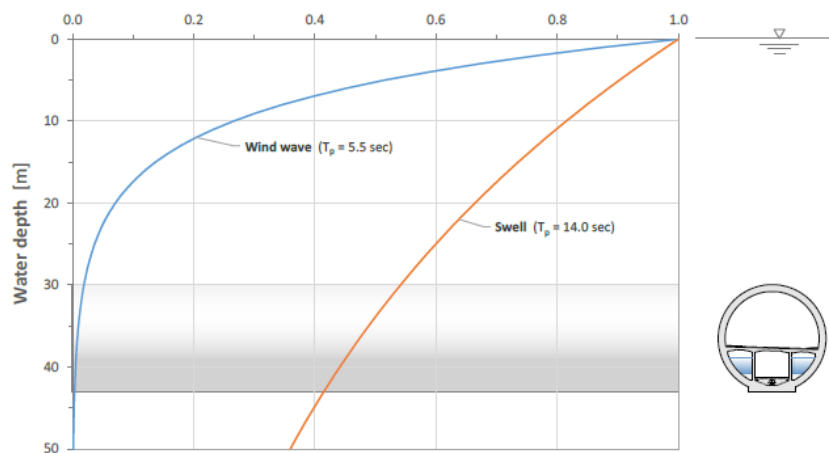


Figure 31 – Penetration of wave loads (normalized) with water depth [33]

The swell wave present in the fjord with a return period of 100 years is quite small, because it has a wave height and wave period of (see paragraph 3.2);

$$H_{100y} = 0.30 \text{ m}, \quad T_p = 14 \text{ s}$$

The wave load on the structure can be determined with the same formula as for the tidal currents. First, however the maximum horizontal and vertical components of the orbital velocity of the water particles need to be determined. The wave theory equations for deep water [34] can be used, because the water depth ($h \approx 350 \text{ m}$) to wave length ($L \approx 300$) ratio is larger than 0.5.

$$\text{horizontal velocity } u = \frac{\pi H}{T} \cdot e^{\left(\frac{2\pi}{L}z\right)} \cdot \cos(\theta)$$

$$\text{vertical velocity } w = \frac{\pi H}{T} \cdot e^{\left(\frac{2\pi}{L}z\right)} \cdot \sin(\theta)$$

With;

H wave height

T wave period

z co-ordinate of the considered depth relative to the average water surface

θ combination of the angular frequency and wave number ($\theta = \omega t - kx$)

For the horizontal velocity, the maximum occurs when θ is equal to 0 and for the vertical velocity the maximum occurs when θ is equal to π . With the wave height and wave period mentioned above, $z = 30 \text{ m}$ and a wave length of;

$$L = \frac{gT^2}{2\pi} \approx 300 \text{ m}$$

The maximum particle velocities will be:

$$u = w = 0.036 \text{ m/s}$$

The wave load on the structure than becomes:

$$q_{wave,u} = q_{wave,w} = C_w \cdot \frac{1}{2} \rho u^2 \cdot D = 7.48 \text{ N/m}$$

The wave load is less than one percentage relative to the current load and therefore, when considering only the static loads, the wave load can be neglected.

4.3.4. Overview load case values

An overview is given of the maximum moments, shear forces and normal forces present in the tube cross-section for the individual load cases. In Table 10, only the maximum values are presented and indicated in bold print. Multiple values per load cases are given because the maxima of several force values do not occur on the same location along the tunnel. The beam number is given which indicates the location along the tunnel. Tube with the largest arch has beam numbers B1-B110 from South to North and the other tube has beam numbers B111-B220 from South to North. Indication of these beam numbers and there location along the tunnel is illustrated in Figure 32. The extended quantity of all the values along the tunnel is given in Appendix B.

SLS	Member	Mx	My	Mz	Vy	Vz	N
Permanent load	Start B112	-10111	299759	-279460	6394	-6858	0
	End B109	-10034	340464	-317410	-6834	7331	0
Current	Falling tide	Start B2	0	-7581	-8131	131	122
		Start B3	0	4872	5226	218	203
		Middle B213	0	-247	-264	-11	-10
	Rising tide	Start B2	0	7581	8131	-131	-122
		Start B3	0	-4872	-5226	-218	-203
		Middle B213	0	247	264	11	10
	Slack tide	Start B2	0	-26731	-28674	312	291
		Start B3	0	5277	5660	290	270
							-16141

Table 10 – Force values of the load cases in kN and kNm

SLS	Ux	Uy	Uz	Utotal
Permanent load	0	-145	155	212
Current	Falling tide	1	90	84
	Rising tide	-1	-90	-84
	Slack tide	34	185	172
				255

Table 11 – Maximum displacement values of the load cases in mm

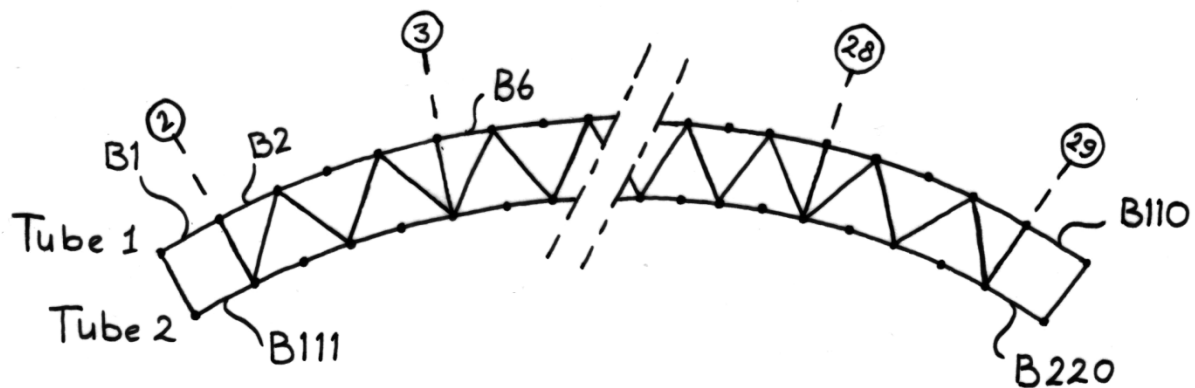


Figure 32 - SCIA model beam identification

4.4. Load combinations

The load combinations consist of a combination of design values of the permanent and variable loads. Both characteristic and reduced characteristic loads are combined for the ULS or SLS. The reduced characteristic loads refer to permanent loads which are added to the permanent loads in a reduced amount due to favourable working. Structures must be sufficiently reliable during their service life. They must withstand the most unfavourable combination of loads that can act simultaneously. In formula form:

$$\begin{aligned} \text{ULS:} \quad & \gamma_G \cdot G_k + \gamma_{Q:1} \cdot Q_1 + \sum (\gamma_{Q:i} \cdot \Psi_i \cdot Q_i) = E_d \\ \text{SLS:} \quad & G_k + Q_1 + \sum (\Psi_i \cdot Q_i) \end{aligned}$$

With;

E_d	Ultimate limit state load
γ_G	partial factor for permanent loads
G_k	total permanent loads
$\gamma_{Q:i}$	partial factor for variable loads
Q_1	value of the leading variable load
Ψ_i	factor for combination of variable load i with the leading variable load
Q_i	value of variable load i

An overview of the load factors is given below.

	Permanent loads unfavourable	favourable	Variable loads leading	other
Load factor γ	1.2	0.9	1.5	1.5

Table 12 - Load factors

Another factor which needs to be considered is the robustness of the structure. This is measured with the consequence classes, defined in the NEN Eurocode as; the ability of a structure to withstand events without being damaged to an extent disproportionate to the original cause. A large traffic structure such as a the SFT belongs to class CC3: having a high consequence for loss of human life or economical, social or environmental consequences are very great.

To take the consequence class into account, the applicable load factors have to be multiplied by K_{FI} .

$$K_{FI,CC3} = 1.1$$

In this case the permanent load consists of the nett buoyancy force; a summation of the buoyancy and gravity based forces. The variable loads comprise the three types of currents. The load combinations considered and the corresponding load factors used are stated in the table below.

	Load combination	Permanent load	Falling tide	Current Rising tide	Rotary tide
SLS	1	1.0	1.0	-	-
	2	1.0	-	1.0	-
	3	1.0	-	-	1.0
ULS	4	1.32	1.65	-	-
	5	1.32	-	1.65	-
	6	1.32	-	-	1.65

Table 13 - Load combinations

The requirement states that the resistance forces need to be larger than the load forces to maintain a stable structure.

$$R_d > E_d$$

The latter is often rewritten as a unity check. The structure is stable when the unity check is smaller than one.

$$\text{unity check} = \frac{E_d}{R_d} < 1$$

4.5. Results

Calculations are performed in SCIA for several load combinations in SLS and ULS. In Table 14 and Table 15 the forces present in the structure are stated, in SLS and ULS respectively. The bold printed values are maxima occurring along the total length of structure. The extended quantity of values is given in appendix B.

Member	css	dx [m]	Case	N [kN]	Vy [kN]	Vz [kN]	Mx [kNm]	My [kNm]	Mz [kNm]
B109	CS1 - Tube	0,000	CO3/4	-16140,47	-2602,36	3372,86	-10034,85	-53277,74	60248,99
B2	CS1 - Tube	76,488	CO3/4	16140,47	2999,02	-2635,38	9965,12	-77620,40	61785,24
B109	CS1 - Tube	76,488	CO1/1	10110,76	-6965,87	7208,73	-10034,85	332883,94	-325541,63
B2	CS1 - Tube	0,000	CO3/4	16127,43	6962,99	-6843,73	9965,12	284897,92	-319200,90
B2	CS1 - Tube	0,000	CO2/3	-10110,76	6520,02	-7256,71	9965,12	319210,78	-282395,71
B109	CS1 - Tube	76,488	CO3/4	-16127,43	-6522,90	7621,70	-10034,85	367196,80	-288736,45
B112	CS1 - Tube	0,000	CO1/1	12401,49	6373,90	-6877,72	-10111,34	298866,34	-280418,56
B2	CS1 - Tube	0,000	CO1/1	10110,76	6782,48	-7012,02	9965,12	304048,74	-298659,07
B114	CS1 - Tube	0,000	CO3/4	-12470,15	-372,20	505,96	-4458,05	-131414,09	111208,07
B3	CS1 - Tube	44,466	CO1/1	10034,07	-16,32	20,90	6741,17	-120846,51	119595,02

Table 14 - SLS values

Member	css	dx [m]	Case	N [kN]	Vy [kN]	Vz [kN]	Mx [kNm]	My [kNm]	Mz [kNm]
B109	CS1 - Tube	0,000	CO6/8	-26631,77	-3339,41	4541,40	-13246,00	-68585,37	81396,40
B2	CS1 - Tube	76,488	CO6/8	26631,78	4054,42	-3389,48	13153,96	-104200,18	79688,78
B109	CS1 - Tube	76,488	CO4/5	16682,76	-9238,25	9475,15	-13246,00	436905,06	-432398,40
B2	CS1 - Tube	0,000	CO6/8	26610,26	9294,03	-8937,82	13153,96	367243,74	-430807,46
B2	CS1 - Tube	0,000	CO5/7	-16682,76	8563,13	-9619,23	13153,96	423860,00	-370078,91
B109	CS1 - Tube	76,488	CO6/8	-26610,26	-8507,35	10156,55	-13246,00	493521,31	-371669,86
B112	CS1 - Tube	0,000	CO4/5	20462,46	8406,82	-9084,86	-13346,97	394208,90	-370468,61
B2	CS1 - Tube	0,000	CO4/5	16682,76	8996,18	-9215,50	13153,96	398842,59	-396913,41
B114	CS1 - Tube	0,000	CO6/8	-20575,74	-473,74	684,24	-5884,63	-175327,70	144798,38
B217	CS1 - Tube	49,095	CO6/8	20575,74	403,81	-257,05	5885,06	-151322,34	159732,16

Table 15 - ULS values

The cross-section is rotational symmetric and therefore the total moment can easily be determined. The total moment is calculated using Pythagoras theorem and the maximum moment M_i with the corresponding moments.

$$M_{total} = \sqrt{M_x^2 + M_y^2 + M_z^2}$$

The maximum total moment occurs for the load combination of the permanent load and slack tide, for as well as the SLS and ULS calculations, at beam B109. Beam B109 is the tunnel section located just before the fixed restraint at grid 29.

$$M_{Ed-total,SLS} = 467 \text{ MN}$$

$$M_{Ed-total,ULS} = 618 \text{ MN}$$

The displacements, rotations and the total displacement in SLS and ULS are presented as well in Table 16 and Table 17.

Name	dx [m]	Fibre	Case	u _x [mm]	u _y [mm]	u _z [mm]	φ _x [mrad]	φ _y [mrad]	φ _z [mrad]	U _{total} [mm]
B112	0,000	1	CO1/1	0,0	0,0	0,0	0,0	0,0	0,0	0,0
B32	4,940	10	CO3/2	32,3	-329,5	-17,2	-0,1	0,0	0,0	331,5

Table 16 - Displacements in SLS

Name	dx [m]	Fibre	Case	u _x [mm]	u _y [mm]	u _z [mm]	φ _x [mrad]	φ _y [mrad]	φ _z [mrad]	U _{total} [mm]
B112	0,000	1	CO4/1	0,0	0,0	0,0	0,0	0,0	0,0	0,0
B32	9,881	11	CO6/2	53,1	-495,8	-80,0	-0,1	0,1	0,0	505,0

Table 17 - Displacements in ULS

4.6. Design checks

Several model and design checks are performed to see whether the model is functioning correctly and the structure is safe conform the standards.

4.6.1. Service Limit State

Displacements

The maximum displacement occurring for SLS load combinations is equal to 332 mm. According to NEN-EN 1990 Basis of structural design (A2.4.5.2.3), the comfort regulations prescribe a maximum displacement equal to:

$$w < \frac{L}{600} = \frac{\pm 5300}{600} = 8.83 \text{ m}$$

A more important aspect, rather than the total displacement itself, would be the inclination of the road caused by the displacement. Heavy vehicles lose too much speed going upwards when the road gradient becomes too large. Road inclinations between 2% and 5%, given that a truck has a speed reduction of 30 km/h, the slope must not be larger than 1200m till only 450m for slopes of 5%. [35]

Vertical arches are another aspect to take into account. Small vertical arches in a road could be uncomfortable for the road users as it obstructs the view of the road users. These arches need to be carefully considered as well.

The maximum displacement of 332 mm occurs over the running length of 600m of which the gradient can be calculated, is equal to:

$$\tan^{-1}(0.332/\pm 600) \approx 0^\circ$$

There is a barely noticeable gradient in the tunnel due to the displacements caused by the load combinations. Additional measurements are not necessary.

The same comfort requirement is taken to verify a single tunnel segment with l being the distance between two supports. The length l is equal to 197m and results in a maximum allowed displacement of:

$$w_{max} = 0.0017 \cdot l$$

$$w_{max} = 0.328 \text{ m}$$

The individual displacement of a beam section between two supports are small, in range of 20 to 60 mm, and thus the requirement holds. The maximum displacement of the entire tunnel as a single beam does not even exceed the regulations considering a single tunnel segment.

Cross-section capacity

A basic method to determine cross-section capacity is done by checking whether both top and bottom stress requirements are met. The stresses are caused by the moment and axial force loading on the cross-section.

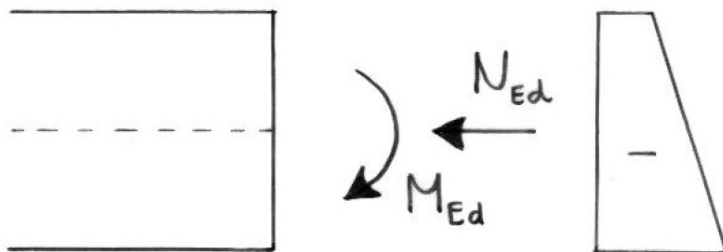


Figure 33 - Stress-diagram cross-section

The formula for top and bottom fibre becomes[36];

$$\sigma_{outer \text{ fibre}} = \frac{M_{Ed}}{W} + \frac{N_{Ed}}{A}$$

With,

W	section modulus [m ³]	$W = \frac{I}{z} = \frac{\pi(D^2-d^2)/64}{0.5D} = \frac{\pi(D^2-d^2)}{32D} = 94 \text{ m}^3$
A	surface area of the cross-section [m ²]	$A = \pi(R^2 - r^2) = 29.6 \text{ m}^2$

Only the surface area of the concrete ring is taken into account for the strength calculations, equal to 29.6 m². Doing so is conservative, but easier during the initial phase of design and leaves the internal design of the tunnel free.

The maximum moment and normal force in SLS are repeated for convenience;

$$M_{Ed} = 467 \text{ MNm}$$

$$N_{Ed} = -280 \text{ MN}$$

The structure is situated in a marine environment and therefore crack formation in the concrete is not desirable. In case of a conservative approach, there must be no tensile forces present in the cross-section to prevent any cracks forming in the concrete.

$$\begin{aligned} \sigma_{top} &< 0 & \sigma_{top} &= \frac{M_{Ed}}{W} + \frac{N_{Ed}}{A} \\ & & \rightarrow M_{Rd} &= -\frac{N_{Ed}}{A} \cdot W \\ M_{Rd} &= 889 \text{ MNm} \end{aligned}$$

At the bottom fibre, the opposite is of importance. The material strength of the concrete must not be exceeded to prevent failure. Concrete class C35/45 has a compressive strength equal to [36];

$$f_{cd} = \frac{f_{ck}}{\gamma_c} = \frac{35}{1.5} = 23 \text{ N/mm}^2$$

With,

f_{cd}	the design compressive strenght of concrete [N/mm ²]
f_{ck}	the cubic compressive strenght of concrete [N/mm ²]
γ_c	material factor of concrete [-]

$$\begin{aligned} \sigma_{bottom} &= \frac{M_{Ed}}{W} + \frac{N_{Ed}}{A} < f_{cd} \\ &\rightarrow M_{Rd} = \left(f_{cd} - \frac{N_{Ed}}{A}\right) \cdot W \\ M_{Rd} &= 1.273 \text{ MNm} \end{aligned}$$

It can be concluded that the cross-section capacity for the crack formation is governing, because the calculations above show that the smallest moment causing failure is due to crack formations. The cross-section capacity is sufficient for the acting bending moment on the structure because the unity check is smaller than one.

$$\text{unity check} = \frac{M_{Ed}}{M_{Rd}} = \frac{467}{889} = 0.53$$

4.6.2. Ultimate Limit State

Cross-section capacity

Again, the basic method for determining the cross-section capacity is applied. The cross-section capacity remains the same, as the cross-section itself does not change.

$$M_{Rd} = 889 \text{ MNm}$$

In this case however, the full load combinations with load factors are used when calculating the maximum moment in the cross-section.

$$M_{Ed-total,ULS} = 618 \text{ MNm}$$

The cross-section capacity is sufficient to prevent crack formation, for the moment acting on the structure.

$$unity\ check = \frac{M_{Ed}}{M_{Rd}} = \frac{618}{889} = 0.70$$

A more refined method would be to use M-N interaction diagram. The M-N diagram renders the reinforcement required in the cross-section as a function of the relative normal force and relative moment. In several publications, only the M-N diagram for the rectangular cross-section is stated. Using the computer program IdeaStatica, the cross-section capacity can be determined from the calculated M-N diagram of any cross-section with reinforcement.

An iteration process of changing the amount of reinforcement allows to find a fitting cross-section which satisfies for multiple types of safety checks.

The full results of the cross-section capacity calculations in IdeaStatica can be found in appendix C.

The analytical calculations state that the normative check which determines the cross-section capacity is due to stress constraints. The numeric calculations performed with IdeaStatica resulted in the same stress constraints when imposing the normative cross-section capacity.

$$unity\ check_{analytical} = 0.70$$

$$unity\ check_{IdeaStatica} = 0.73$$

The small difference is because IdeaStatica considers the reinforcement elements in the cross-section surface as a material property, while the analytical calculations only take the prestressing force itself into account.

Shear force capacity

To see whether shear force reinforcement is necessary, calculations are performed to determine the shear force capacity of the cross-section without shear force reinforcement. The minimum shear force capacity of the cross-section can be determined with the formulas [36]:

$$V_{Rd,c} = v_{min} \cdot b_w d$$

$$v_{min} = 0.035 k^{3/2} \cdot f_{ck}^{1/2} + k_1 \cdot \sigma_{cp}$$

$$k = 1 + \sqrt{\frac{200}{d}} \leq 2.0$$

$$V_{Rd,c} = \left[0.035 \left(1 + \sqrt{\frac{200}{d}} \right)^{3/2} \cdot f_{ck}^{1/2} + (k_1 \cdot \sigma_{cp}) \right] \cdot b_w d$$

With,

k	size factor with d in mm
b_w	the smallest width of the cross-section [mm]
d	Effective height of the cross-section [mm] $d = h - c - \phi_{link} - 0.5\phi$
k_1	coefficient, with recommended value of 0.15
σ_{cp}	concrete compressive stress at the at centroidal axis due to axial loading or pre-stressing

These formulas are valid for rectangular cross-sections. Computer programs are often used for more complicated cross-sections. An approximation however can be made, by estimating certain parameters. The smallest width of the cross-section would be 1600 mm at half the height. When determining the effective height, commonly only the concrete cover and the thickness of the reinforcement are subtracted from the total height. In this case however, the reinforcement bars are not located at the same distance from the neutral axis and thus a smaller height is used. Taking these considerations into account, the values $d = 12000$ mm and $b_w = 1600$ mm are applied, equal to 65% of the cross-section area, to calculate the minimum shear force capacity of the cross-section.

$$V_{Rd,c} = \left[0.035 \left(1 + \sqrt{\frac{200}{12000}} \right)^{3/2} \cdot 35^{1/2} + (0.15 \cdot 7.5) \right] \cdot 1600 \cdot 12000$$

$$V_{Rd,c} = 26370 \text{ kN}$$

The maximum shear force working on the structure is equal to:

$$V_{Ed-total,SLS} = 13249 \text{ kN}$$

The unity check then results in a sufficient shear force capacity of the cross-section, without using shear force reinforcement.

$$unity \text{ check} = \frac{V_{Ed}}{V_{Rd}} = \frac{13249}{26370} = 0.50$$

According to IdeaStatica, the shear force loading consumes 62 percent of the calculated shear force capacity. The later indicates that the shear force capacity determined in IdeaStatica is lower than the capacity calculated using the analytical formulas.

The shear force capacity in IdeaStatica is lower because IdeaStatica considers the stress changes along the height of the cross-section due to the moments present. The moments lower the pressure stresses and therefore the maximum shear stress calculated are lower as well.

Tethers

The tension forces of the tethers need to be verified. The tethers have a cross-sectional area $A = 0.129 \text{ m}^2$ and a reported resistance force of $F_{t,Rd} = 27 \text{ MN}$ [33].

The same resistance tensile force can be found through the material strength properties of steel grade S235 of which the tethers are fabricated.

$$f_{yd} = \frac{f_{y,k}}{\gamma_s} = \frac{235}{1.15} = 204 \text{ N/mm}^2$$

With,

f_{yd}	design yield strength [N/mm ²]
f_{yk}	yield strength [N/mm ²]
γ_s	material factor of steel $\gamma_s = 1.15$

The resistance force is determined by multiplying the design yield strength with the cross-sectional area of the tethers.

$$F_{t,Rd} = f_{yd} \cdot A = 26.4 \text{ MN}$$

The largest shear force occurs for the load combination of the permanent load and slack tide.

$$F_{Ed-total,ULS} = 13249 \text{ kN}$$

The support on a single tube has two tethers and therefore the resistance force needs to be multiplied by two. The unity check results in an over dimensioning of the tethers.

$$\text{unity check} = \frac{F_{Ed}}{2 \cdot F_{Rd}} = \frac{13249}{52800} = 0.25$$

At first it could be considered to opt for reduction of the number of tethers per support or to lower the strength quality of the tethers. During the load calculations, the static loading however has only been included.

The required strength capacity of the tethers will increase when performing dynamic calculations and considering fatigue issues.

4.7. Conclusion

The model created in SCIA is very suitable to determine the reaction of this structure to static loads. Analytical calculations, the basic formulas and rules of thumb, show that the model produces results within range of expected values. A first estimation of the forces acting on the structure and displacements of structure elements can be safely made.

Simplifications in the model are implemented to ease the amount of calculations the computer program needs to perform. The purpose of the model is to assess, on a more global scale, how the design of the end joint and the tunnel structure are influenced by several parameters.

The essential parameters of the design are all present in the model while the model remains easy to manipulate.

The vertical stiffness from the pontoons is less than 10 % of the tether stiffness. The smaller vertical stiffness can lead to resonance issues for the pontoon variant due to wave loading and needs to be looked at with care in the next design phase.

The design checks which are performed appeared to result in a slight over dimensioning of the structure. In view of certain aspects not yet considered, such as dynamic response, accidental loadings and fatigue, refining the design is not preferable at this stage.

5. Analytical approach

Apart from the numerical calculations done in SCIA, a small step is made to model the tunnel structure as an algebra problem. The algebraic solution is compared to the SCIA model to see how the differential equations relate to the numerical calculations of the SCIA-model. It is also useful to see which method it is preferred during certain phases of the design. Although more complex structures can be determined more accurate using numerical programs, building a computer model and doing large amounts of numerical calculations can be time consuming compared to an analytical approach of the problem.

5.1. Differential equation

The tunnel itself is modelled as a beam on multiple supports, using springs as supports. Determining the differential equations for a beam with separate multiple supports is a complex and time-consuming method. Therefore, the spring supports are spread on the full length of the tunnel, mimicking a beam on elastic foundation.

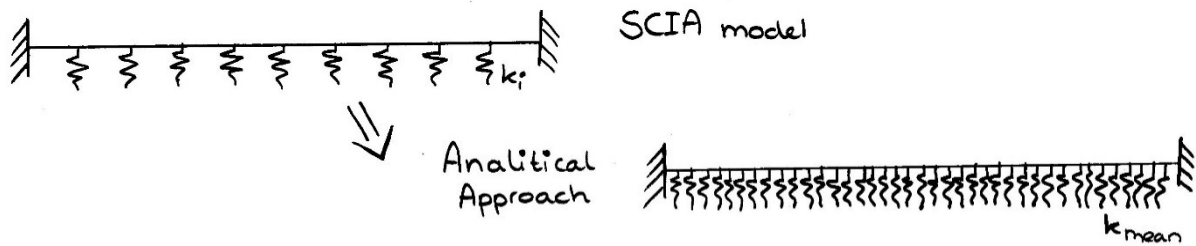


Figure 34 - Analytical model of the tunnel structure

The differential equation for a beam on elastic foundation is:

$$EI \frac{d^4 w}{dx^4} + Kw = q$$

Where;

EI	elasticity modulus times the moment of inertia of the concrete tunnel [kNm ²]
K	spring stiffness [kN/m ²]
w	deflection in z-direction [m]
q	distributed load [kN/m]

To solve this equation, the homogeneous solution is derived as well as the particular solution. Both solutions are added to obtain the general solution.

Homogeneous solution

First, the homogeneous solution to the differential equation has to be determined.

$$EI \frac{d^4 w}{dx^4} + Kw = 0$$

Assume;

$$4\beta^4 = \frac{K}{EI}$$

and fill in gives the reduced differential equation;

$$\frac{d^4 w}{dx^4} + 4\beta^4 w = 0$$

Substitution of $w = e^{rx}$ in the differential equation, determining the results for r and rewriting the solution to eliminate the imaginary parameters, will result in the following displacement function of the homogeneous part;

$$w_h = e^{\beta x}(C_1 \cos \beta x + C_2 \sin \beta x) + e^{-\beta x}(C_3 \cos \beta x + C_4 \sin \beta x)$$

Particular solution

The choice for the particular solution should match the structure of the right side of the nonhomogeneous equation. As the right-hand side of the equation is a single constant, the particular solution therefore becomes a constant as well.

$$w_p = \frac{q}{K}$$

General solution

The general solution to the differential equation is the sum of the homogeneous and particular solution.

$$w = w_h + w_p$$

$$w = e^{\beta x}(C_1 \cos \beta x + C_2 \sin \beta x) + e^{-\beta x}(C_3 \cos \beta x + C_4 \sin \beta x) + \frac{q}{K}$$

The constants C1-C4 can be determined by making use of the boundary conditions at the ends of the beam. The boundary conditions for a beam with fixed supports at both ends are:

For $x = 0$ and $x = L$;

$$w = 0$$

$$\varphi = \frac{dw}{dx} = 0$$

$$EI \frac{d^2 w}{dx^2} = -M$$

$$EI \frac{d^3 w}{dx^3} = -V$$

5.2. Results

The algebra problem is defined as a differential equation with its general solution and boundary conditions. The problem can be solved using the derivatives of the general solution, boundary conditions and parameter values. The derivatives of the general solution are determined using the equations of beam theory and the product rule for differentiation.

$$w = e^{\beta x}(C_1 \cos \beta x + C_2 \sin \beta x) + e^{-\beta x}(C_3 \cos \beta x + C_4 \sin \beta x) + \frac{q}{K}$$

$$\varphi = \frac{dw}{dx} = \beta e^{\beta x}(C_1 \cos \beta x + C_2 \sin \beta x) + e^{\beta x}(-C_1 \beta \sin \beta x + C_2 \beta \cos \beta x) - \beta e^{-\beta x}(C_3 \cos \beta x + C_4 \sin \beta x) + e^{-\beta x}(-C_3 \beta \sin \beta x + C_4 \beta \cos \beta x)$$

$$M = -EI \frac{d^2 w}{dx^2} = -EI[\beta^2 e^{\beta x}(C_1 \cos \beta x + C_2 \sin \beta x) + 2\beta e^{\beta x}(-C_1 \beta \sin \beta x + C_2 \beta \cos \beta x) + e^{\beta x}(-C_1 \beta^2 \cos \beta x - C_2 \beta^2 \sin \beta x) + \beta^2 e^{-\beta x}(C_3 \cos \beta x + C_4 \sin \beta x) - 2\beta e^{-\beta x}(-C_3 \beta \sin \beta x + C_4 \beta \cos \beta x) + e^{-\beta x}(-C_3 \beta^2 \cos \beta x - C_4 \beta^2 \sin \beta x)]$$

$$V = -EI \frac{d^3 w}{dx^3} = -EI[\beta^3 e^{\beta x}(C_1 \cos \beta x + C_2 \sin \beta x) + 3\beta^2 e^{\beta x}(-C_1 \beta \sin \beta x + C_2 \beta \cos \beta x) + 3\beta e^{\beta x}(-C_1 \beta^2 \cos \beta x - C_2 \beta^2 \sin \beta x) + e^{\beta x}(C_1 \beta^3 \sin \beta x - C_2 \beta^3 \cos \beta x) - \beta^3 e^{-\beta x}(C_3 \cos \beta x + C_4 \sin \beta x) + 3\beta^2 e^{-\beta x}(-C_3 \beta \sin \beta x + C_4 \beta \cos \beta x) - 3\beta e^{-\beta x}(-C_3 \beta^2 \cos \beta x - C_4 \beta^2 \sin \beta x) + e^{-\beta x}(-C_3 \beta^3 \sin \beta x + C_4 \beta^3 \cos \beta x)]$$

Filling in parameters and solving the differential equation with the set boundary conditions will give the displacement function for the tunnel structure. The parameter values used are:

$$EI = 34.1 \cdot 10^9 \text{ N/m}^2 \cdot 592 \text{ m}^4 = 20.187 \cdot 10^{12} \text{ kNm}^2$$

$$K = \frac{26 \cdot k_{\text{mean}}}{L - 251} = \frac{26 \cdot 1.83 \cdot 10^8}{5373 - 251} = 930 \frac{\text{kN}}{\text{m}}$$

$$q = q_{6\%} = 75.1 \text{ kN/m}$$

$$\beta = \sqrt[4]{\frac{K}{EI}} = 0.0104$$

Note: An evenly distributed spring stiffness is obtained by reducing the total structure length with 251 meters. This reduction of the length is necessary, because the tunnel segments at the end are longer than in the middle (224 meters compared to 197 meters), which would lead to a lower calculated spring stiffness than present in reality. Now the supported spring stiffness K is equal to the mean spring stiffness $1.83 \cdot 10^8$ divided by a tunnel section of 197 meters.

The displacement function then becomes;

$$w = e^{0.0104x}(7.14 \cdot 10^{-27} \cos(0.0104x) + 7.56 \cdot 10^{-26} \sin(0.0104x)) + e^{-0.0104x}(-0.081 \cos(0.0104x) - 0.081 \sin(0.0104x)) + 0.081$$

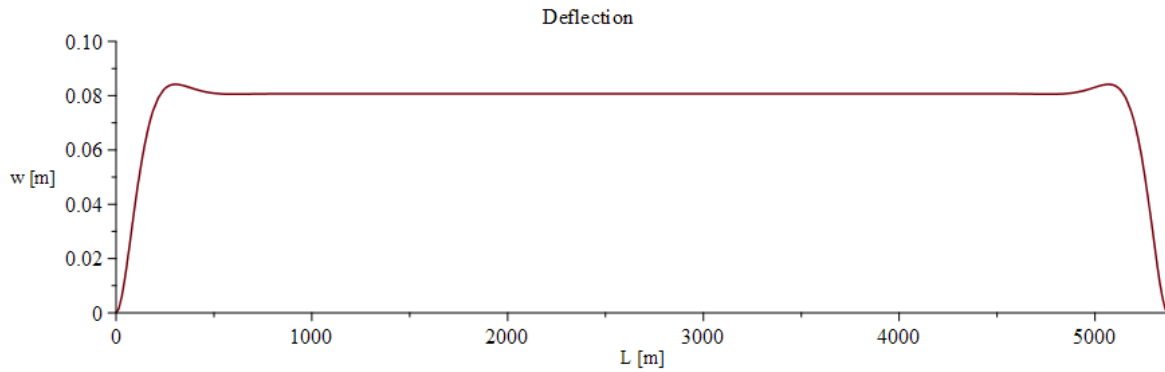


Figure 35 - Deflection along the tunnel length – Analytical approach

The main deflection is approximately 81 mm, with two extreme values of 84.5 mm. These values are lower than the results from SCIA, which has a maximum displacement of 155 mm in z-direction. In the SCIA model however, the exact spring stiffness per tether are implemented. The maximum displacement then occurs at the support where the spring stiffness has the lowest value of $0.985 \cdot 10^8 \text{ N/m}$, which is much smaller than the mean spring stiffness used in the analytical approach; $1.83 \cdot 10^8 \text{ N/m}$. Figure 36 shows a more uneven shape of the deflection of the tunnel structure determined with the SCIA model having individual spring stiffness.

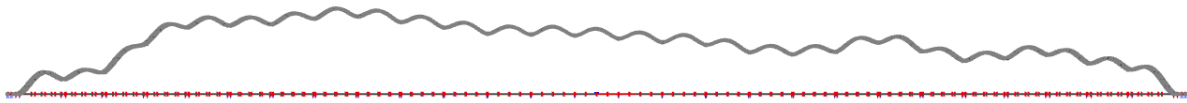


Figure 36 - Deflection along the tunnel length - SCIA model with varying spring stiffness, according to the original design

When implementing the mean value of the spring stiffness used in the analytical approach for all the tethers in the SCIA model, the deflection shape and values of the displacements will be equal to the analytical approach. The sinusoid look of the structure is because the supports are spaced at equal distances and the tunnel structure acts as a beam in bending in between supports. The supports have a displacement of 82 mm (the lowest points in the sinusoid).

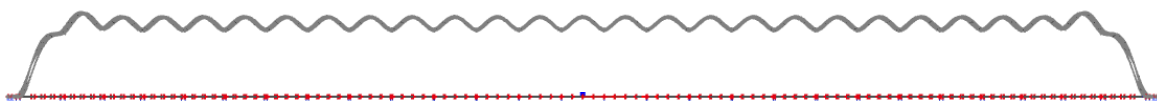
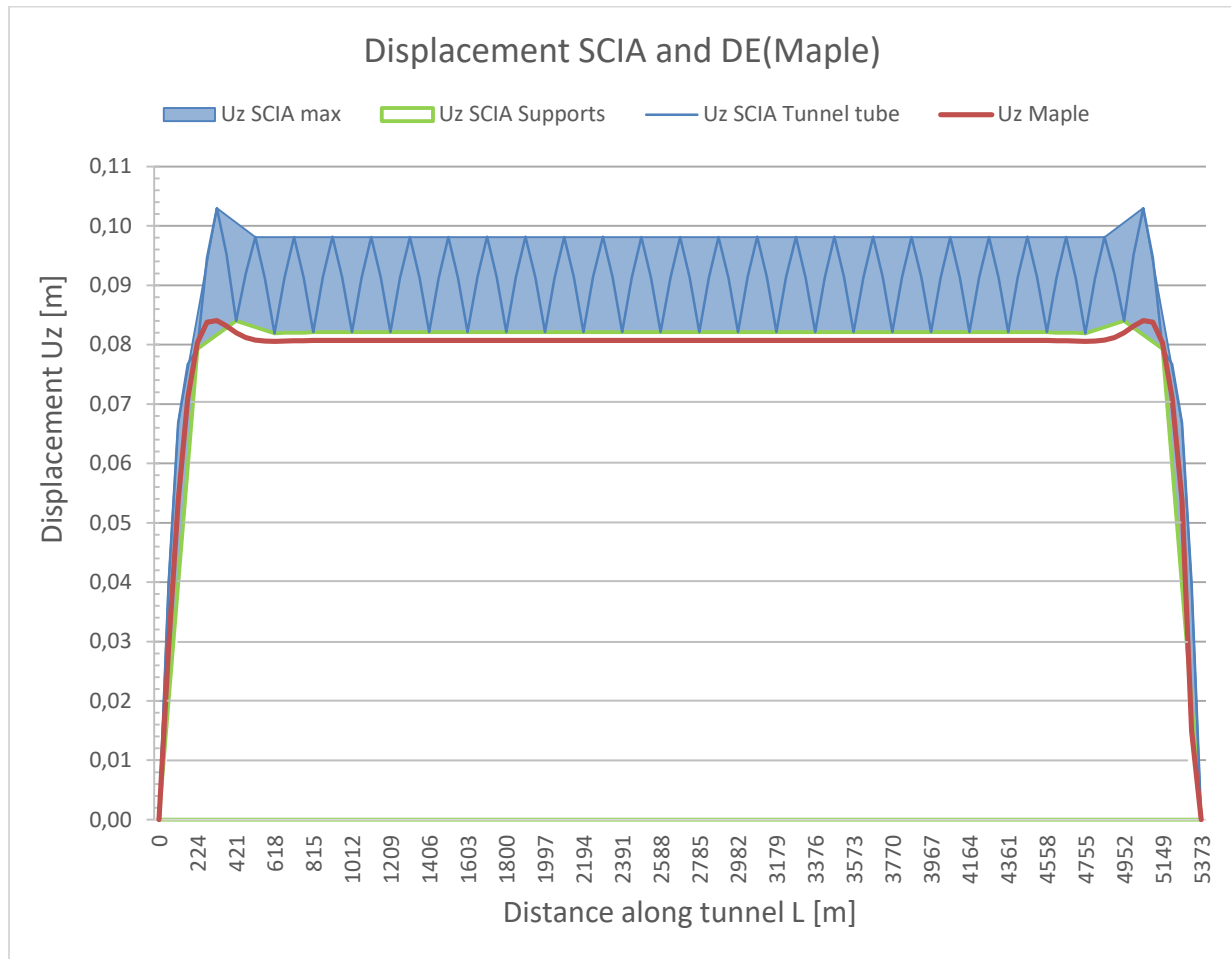


Figure 37 – Deflection along the tunnel length – SCIA model with mean spring stiffness

The slight difference in displacement determined in SCIA and Maple is clearly visible when adding all the displacement shapes in one diagram. A distinction is made between the displacement of the entire tunnel in SCIA and the displacement of only the supports in SCIA as well as the maximum displacement of the tunnel. These three lines define the overall shape of the tunnel displacement which better shows the similarity in displacement shape between SCIA and Maple.



5.3. Conclusion

Both the analytical and numerical approach result in the same order of values for the displacements. The difference in values found between SCIA calculations and analytical calculation, is due to the assumptions made for the models not being similar. If the assumptions and the models for both approaches are identical, both models will produce the same outcome.

The analytical approach gives good insight in magnitude order of the value. The method is faster and easier to use when in need of first estimates for main design parameters. One must be mindful however of the model design assumptions that are made. The magnitude of displacement in the analytical approach can differ greatly from the displacements in the more detailed initial model in SCIA. Displacement deviations occur especially when extreme values of the spring stiffness deviate too much from the mean value of the spring stiffness or large deviations in any nature of design parameter occur. It is advisable to also run the calculations with the maxima and minima values of such parameters, resulting in a bandwidth for the design parameters.

6. Parameter study

Creating a fitting solution for the design of an end joint, or any kind of connecting element, is not an easy task. Going the fast and easy route will probably result in a working system, but it usually does not get you the optimal solution. To create a fitting and optimal design, a better understanding of the forces working in the end joint is required. A possible solution would be to adjust the end joint to the tunnel design from the Bjørnafjord, used in the thesis.

Instead of making a specific design for the Bjørnafjord, it is preferred to see whether it is possible to create an end joint which is applicable under multiple circumstances and within different tunnel designs. Significant parameters are selected and are studied using the SCIA program and tunnel model. The methodology is explained first, after which each individual parameter is studied and elaborated on in separate paragraphs.

6.1. Methodology

The most significant parameters are studied to get a better understanding on how these parameters affect the response of structure, such as force distributions and displacements at the end joint as well as along the tunnel. The parameters which are investigated are stated in the list below.

- k_u – spring stiffness of the supports
- k_φ – segment connections: hinges and variation in moment springs
- SC – type of end joint: free, fixed, combinations of translational and rotational freedoms

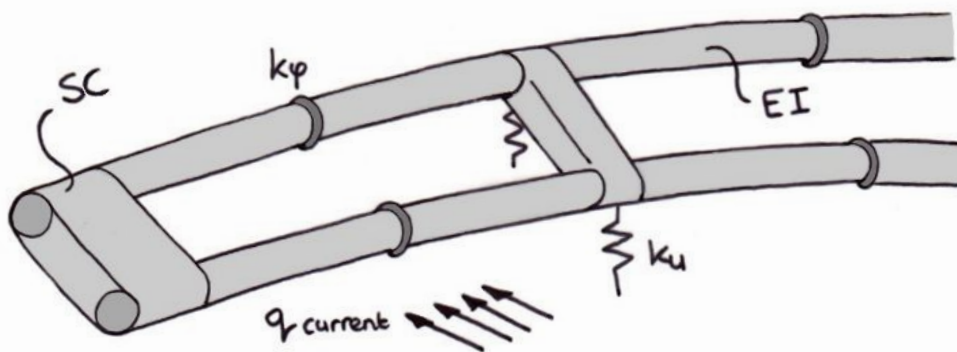


Figure 38 - Overview of variable parameters

The effect of the spring stiffness k_u is investigated by increasing and decreasing the value for the support stiffness. The parameters k_φ (segment connections) and SC (end joint or shore connection) are elaborated in their specific paragraphs.

Other potential parameters to potentially be studied are the different types of loading or the cross-section flexibility. Different types of loading are already included into the parameter study by considering load combinations and classes which have been elaborated in Chapter 4. Cross-section flexibility is a very interesting parameter. Changing the cross-section properties however changes the essential basics of the structure such as the cross-section capacity. Comparing the individual influence of other parameters becomes far too complicated when the basic tunnel cross-section changes. Cross-section flexibility has such a large impact on the structure system that it can be seen as a research topic on its own. Cross-section flexibility is outside the scope of the end joint research.

Elements which are not implemented into the model but will influence the internal force distributions of the structure:

- The larger lay-by sections of the tunnel
The larger diameter of the lay-by lay sections of the tunnel increases the buoyancy and causes a shift of the main axis. This will result in larger force distributions and possible torsion forces.
- Cross tubes
The cross tubes are considered as boxes. These cross tubes however differ in shape, weight and potential buoyancy adaption, depending on whether it is a lay-by crossing or normal crossing.
- Buoyancy-weight-ratio (BWR)
The buoyancy-weight-ratio determines the nett vertical force acting on the structure.

The SCIA program and tunnel model are used to research the significance of the parameters. The parameters mentioned above are considered separately to get an overview of the individual influence they have on the force and displacement distribution along the tunnel. SCIA produces the results in tables which for the ease of accessing the data have been compiled into figures and graphs.

The full effective range is explored in SCIA for each parameter. Full effective range indicates that there are no longer changes in displacements and force distributions when changing the parameter value outside this range. The range may extend beyond the mechanical and physical limits in SLS and ULS. The SCIA program does notify values outside of the physical limitations of the construction.

Real life limitations are considered after the full range of the parameter is determined. Some parameter values entered in the model cannot be realised. For example: the strength and number of tethers at the supports of the tunnel are physically limited which in turn limits the modelled spring stiffness at the supports. Hence, the influence of the parameter on the tunnel structure within the range of reality is determined.

The displacements, moments and shear forces are considered for each parameter. The maximum displacement and the relative displacement between two supports are evaluated in SLS. The maximum moments and shear forces are evaluated in ULS.

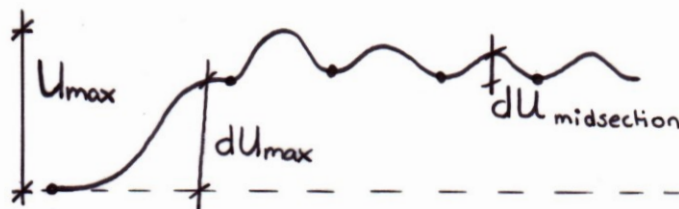


Figure 39 - Types of displacement measurements in the parameter study

Figure 39 - Types of displacement measurements in the parameter study Figure 39 illustrates the displacement measurements which are considered. Three different displacements are considered; the maximum displacement U_{max} , the maximum displacement between two supports overall dU and the maximum displacement between two supports at the middle section $dU_{midsection}$ (between grid 6 and 25). Only the vertical direction will be considered and the transverse direction will be neglected in this parameters study, because of the 2D approach of the tether supports.

$$U_{max} = U_{total,max} = \sqrt{U_x^2 + U_y^2 + U_z^2}$$

The same type of method has been used for the moment and shear forces. The absolute maximum of the moments and shear forces on the total structure are considered as well as the absolute maximum at the middle section (between grid 6 and 25).

The remaining parameters are kept fixed when the influence of an individual parameter is studied. Table 18 gives an overview of the parameter values used during the parameter study. The parameters with the name “variable” are varied in such a manner, that outside the stated range, values such as displacements and moments do not change any longer.

Parameter which is being researched	k_u	k_ϕ	SC
k_u	Variable	∞	Fixed
k_ϕ	$1.83 \cdot 10^2 \text{ MN/m}$	Variable	Fixed
SC	$1.83 \cdot 10^2 \text{ MN/m}$	∞	Variable

Table 18 - Values parameter during each individual parameter study

The parameter study indicates which values of the parameters are desirable for designing the tunnel structure and end joint. The influence of a certain parameter on the tunnel structure and the end joint can be considered, after the full range of an individual parameter has been determined. The results of the parameter study may indicate that certain types of end joints can be ruled out for further evaluation during this research thesis.

6.2. Supports stiffness – k_u

The tunnel design has tethers as support system and these supports are modelled as springs with a certain spring stiffness. The mean spring stiffness determined before in paragraph 4.2.1. is used as a starting point.

$$k_{support,mean} = 1.83 \cdot 10^2 \text{ MN/m}$$

The connection stiffness between the segments is kept at $k_\varphi = \infty$ and the end joint is of the fixed type with no degrees of freedom. The springs stiffness is then investigated by increasing and decreasing the value in the SCIA model, between the values;

$$1.83 \cdot 10^{-5} \text{ MN/m} \leq k_{support} \leq 1.83 \cdot 10^4 \text{ MN/m}$$

6.2.1. SCIA Results

The results of varying the spring stiffness parameter in the SCIA tunnel model are presented. The displacements are evaluated using the SLS Classes results. The moments and shear forces are evaluated using the ULS Classes results.

SLS – 3D Displacements

Displacements due to the force loading under changing support spring stiffness show a distinct shape of the deformation. The shape of the displaced tunnel as well as the moment line for several values of the support spring stiffness is illustrated in Figure 41 (the spring stiffness is given in MN/m).

The deformation of the structure for different support spring stiffness can also be presented in a graph, to show the trend more clearly. The below graph illustrates the deformations in the SLS Classes. The dashed line indicates the mean spring stiffness $k_{support,mean}$.

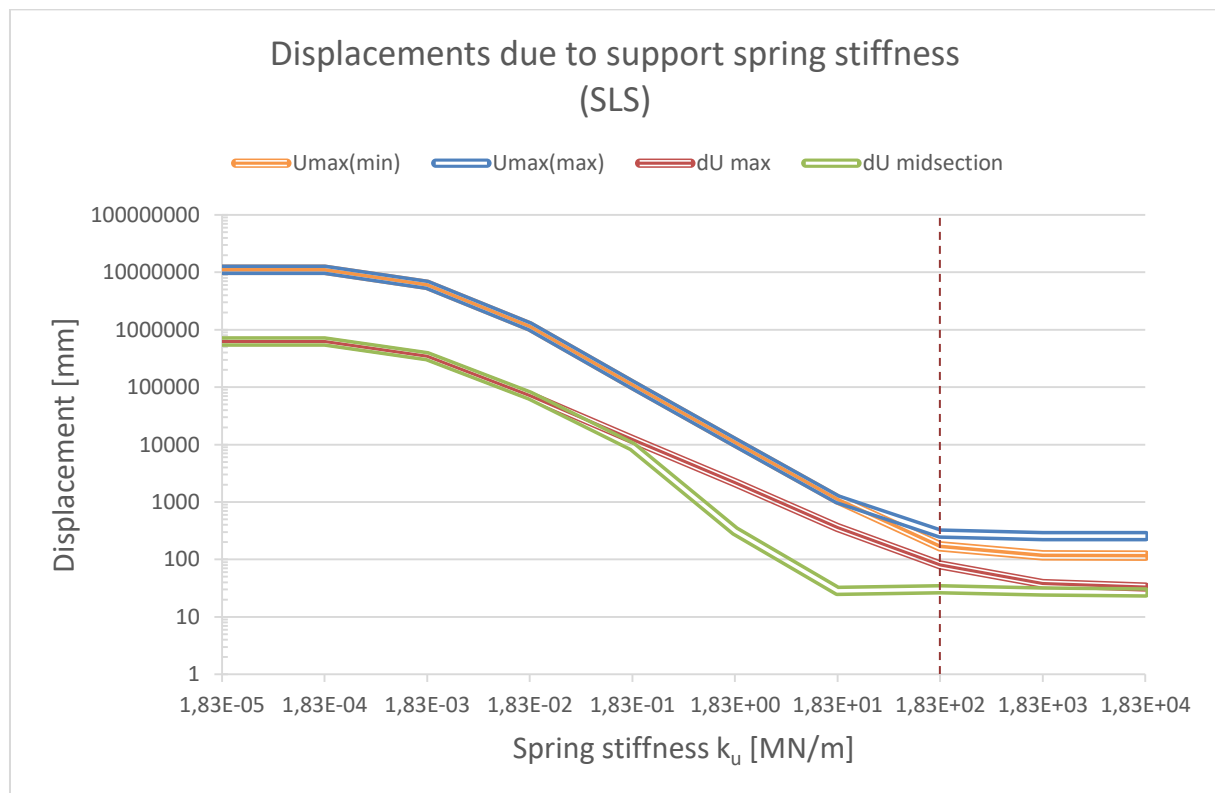


Figure 40 - Displacements due to support spring stiffness

For very small support stiffness, the structure acts as a beam on two supports. The tether supports along the beam do not influence the structure anymore. When the support stiffness becomes very large, the structure reacts like a beam on multiple translation fixed supports.

The relative displacement in the midsection between two supports (green line, dU midsection) reaches its minimum value faster than the total maximum displacement (blue line) and maximum displacement between two supports (red line).

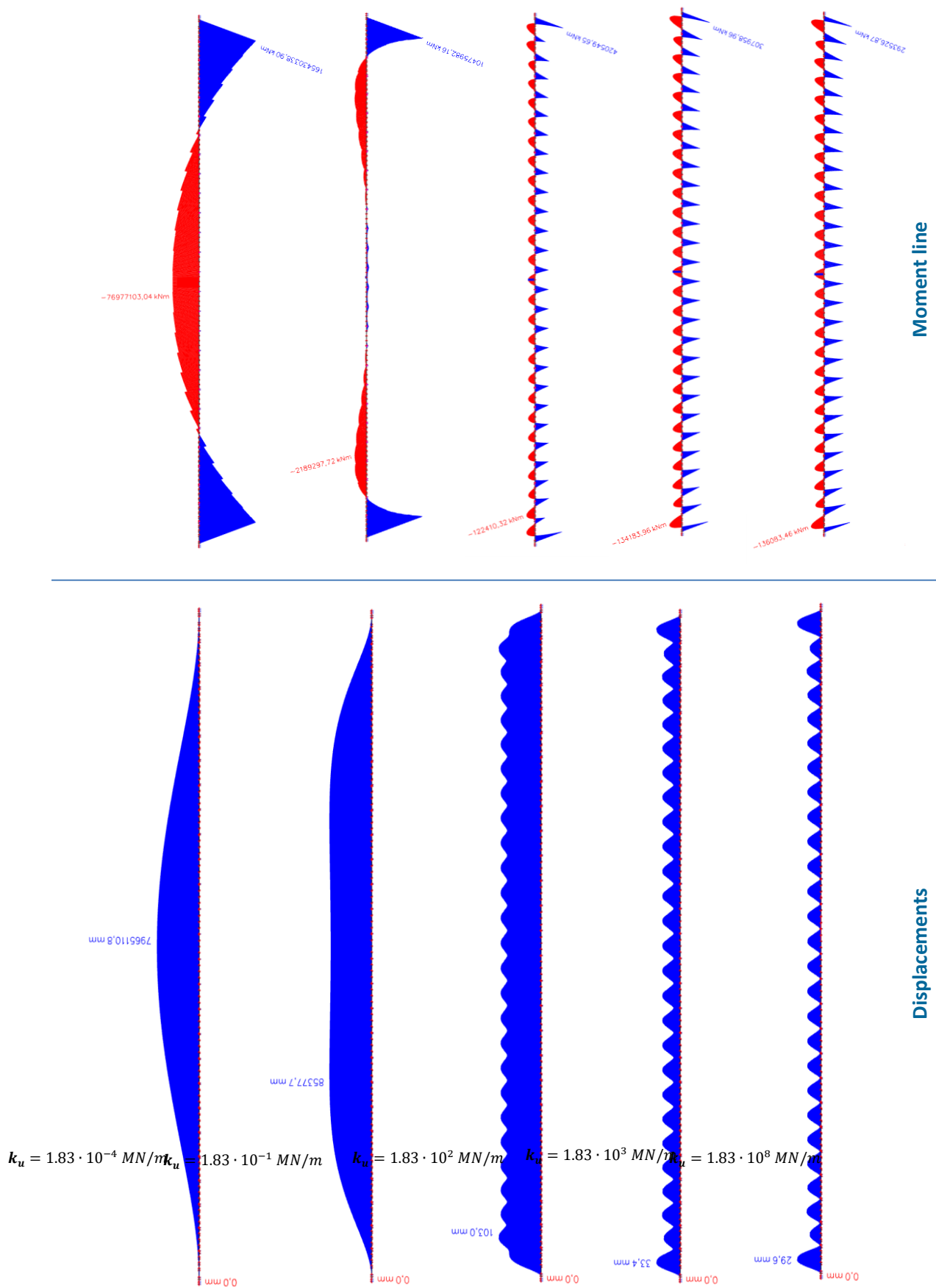


Figure 41 - Displacement shape and moment line due to support spring stiffness

ULS – Moments and shear forces

Moments and shear forces due to the force loading under changing support spring stiffness show distinct trends.

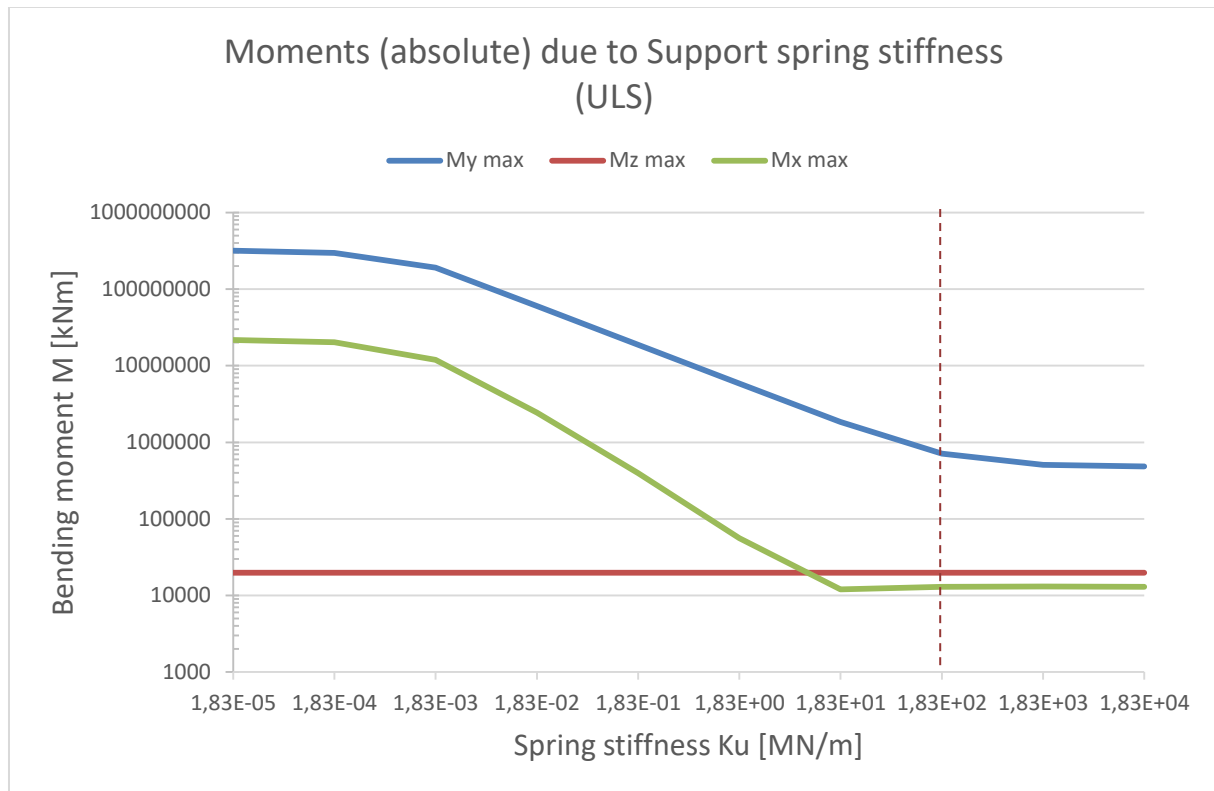


Figure 42 - Moments due to support spring stiffness

The maximum moments decrease with increasing support stiffness, because the tunnel starts acting as a beam on multiple supports instead of a beam on only two end supports. Moments around the z axis do not show any change with increasing or decreasing support stiffness. The M_z being stable can be explained by the fact that the situation does not change in y direction. Only a change in strength or external forces in y-direction would result in a redistribution of the M_z .

The original design has a support spring stiffness $1.83 \cdot 10^2 \text{ MN/m}$. A tenfold more rigid support system could be favourable, because it decreases the M_y moment with 30 percent. Strengthening the supports even further will lead to a minimal decrease of moments in the tunnel structure of five percent. Choosing a much larger support stiffness therefore is not very effective in respect to the moment distribution.

Decreasing the support stiffness is not recommended from a bending moment point of view. While the M_x moment does not change much, the M_y moment will increase with 40 percent.

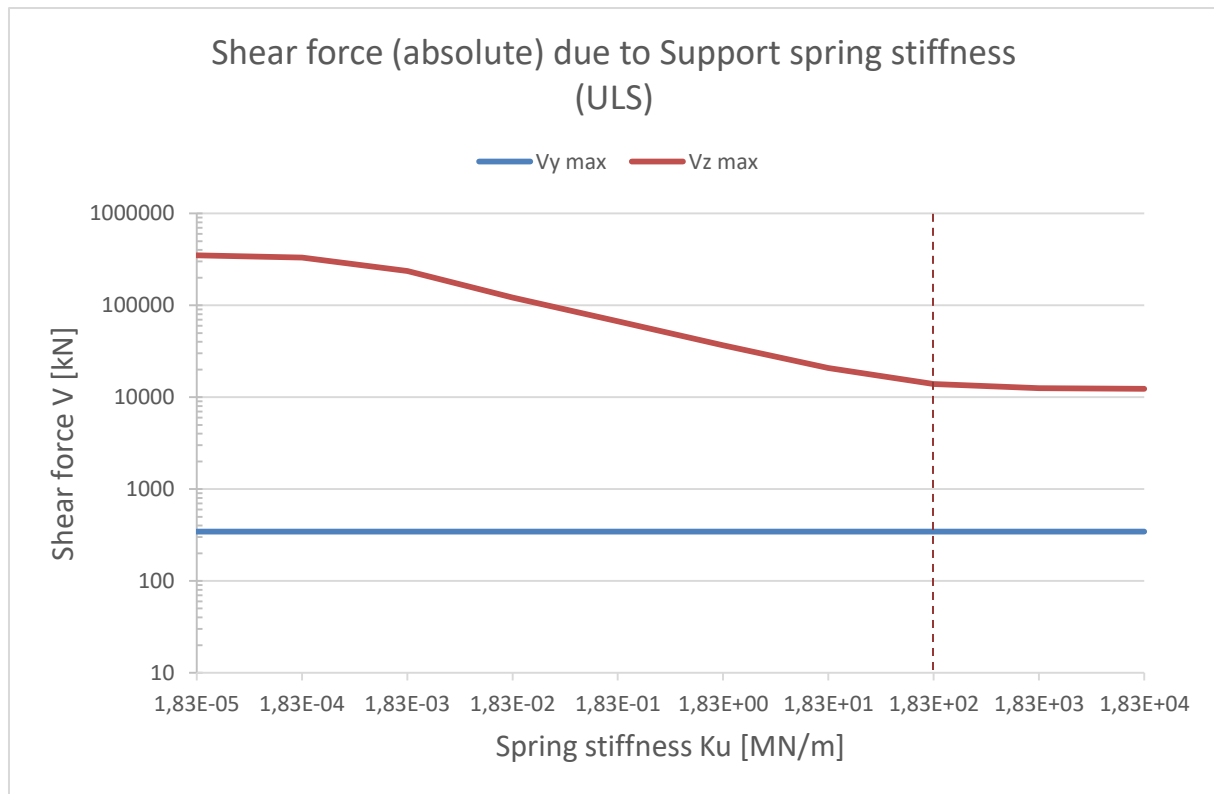


Figure 43 - Shear force due to support spring stiffness

The shear force decreases with increasing support stiffness, equal to the decreasing trend of the moments. The shear force in y-direction stays equal with changing support stiffness because changes in strength or external forces do not occur in y-direction.

The support spring stiffness varies only in z-direction, because of the 2D approach of the support system. The shear force in vertical direction (V_z) therefore is significant when determining the optimal value for the support spring stiffness.

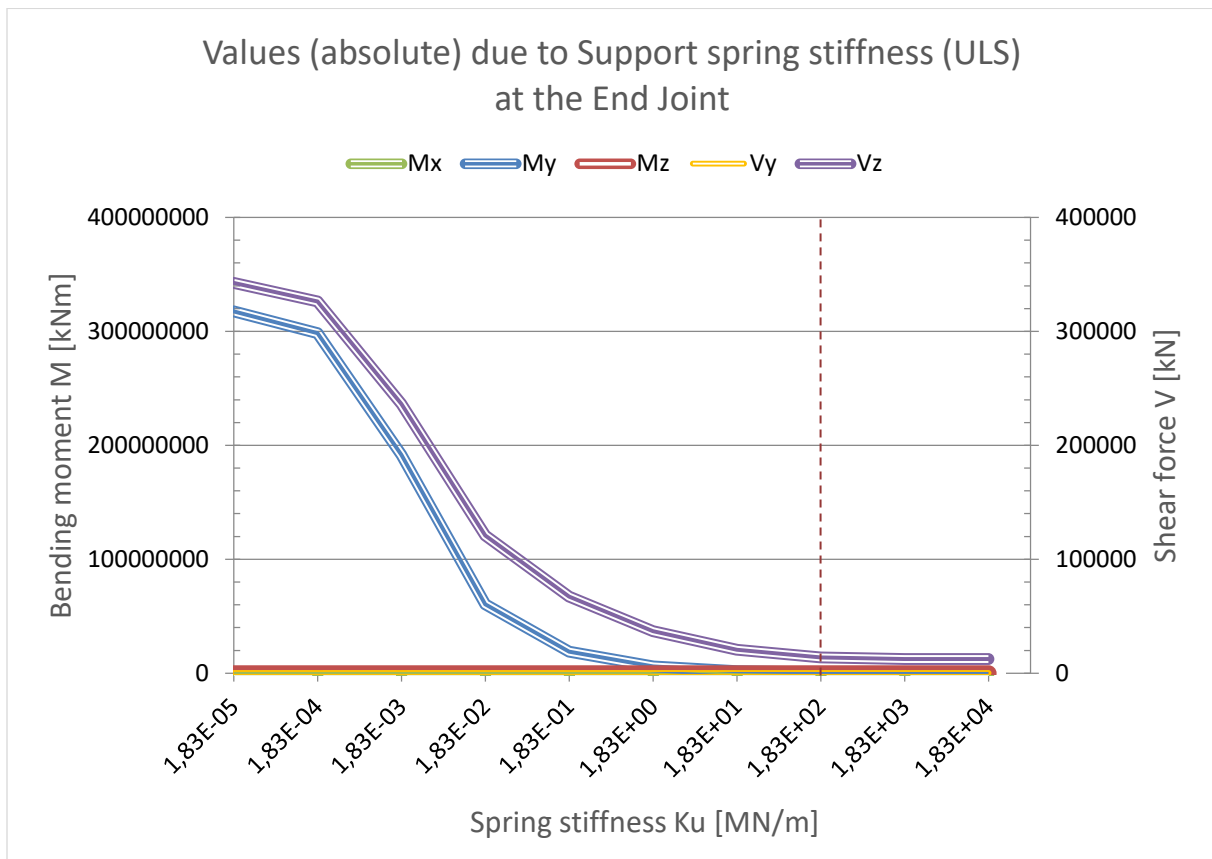


Figure 44 – Moment and shear forces at the end joint due to support spring stiffness

From the above graph goes forward that: the influence of the support spring stiffness governing the amount of moments and shear forces applied by the tunnel structure to the end joint, is negligible when the support spring stiffness is above $1.83 \cdot 10^1 \text{ MN/m}$.

6.2.2. Physical limitations

In the original design, the tether supports consist of two tethers with a mean spring stiffness value of $1.83 \cdot 10^2 \text{ MN/m}$ every 197 meters. It is not possible to keep increasing the number of tethers per support due to the physical limitations of connecting the tethers to the tunnel and the anchors.

Increasing the spring stiffness by a tenfold, only decreases the displacements by 10 percent. An increasing stiffness by a tenfold means that there will be 20 tethers per support.

$$k_u = 1.83 \cdot 10^3 \text{ MN/m} \quad U_z = 0.9 \cdot U_0$$

The displacement of the tunnel increases when lowering the spring stiffness of the supports. A lower spring stiffness can be obtained by for example using less or thinner tethers or lowering the steel quality of the tethers.

$$k_u = 1.83 \cdot 10^1 \text{ MN/m} \quad U_z = 3 \cdot U_0$$

$$k_u = 1.83 \cdot 10^0 \text{ MN/m} \quad U_z = 38 \cdot U_0$$

Increasing or decreasing the spring stiffness further is not relevant, as it either is no longer physically possible or has no positive effect on the displacements.

The cross-section capacity regarding moments and shear forces also limits the value of the support spring stiffness. The calculated strength is mentioned again for convenience (see paragraph 4.6.2).

$$M_{Rd} = 889000 \text{ kNm} \quad V_{Rd} = 26370 \text{ kN}$$

Checking the graphs with cross-section capacity limitations results to the following support spring stiffness boundaries;

$$M_{Rd} \rightarrow k_u \geq 1.83 \cdot 10^2 \text{ MN/m}$$

$$V_{Rd} \rightarrow k_u \geq 1.83 \cdot 10^1 \text{ MN/m}$$

6.2.3. Conclusion

The support spring stiffness does have a significant effect on the displacement and force distribution. The range of reality for the support spring stiffness parameter has been determined by restricting the full parameter range with real life limitations.

$$1.83 \cdot 10^2 \text{ MN/m} < k_u \leq 1.83 \cdot 10^4 \text{ MN/m}$$

The limitation on the parameter range produces a maximum displacement decrease ranging from 10 till 60 percent (with a maximum change in displacement of 42 mm), moments varying up to 32 percent in y-direction and shear forces only varying by 12 percent.

An increase in support spring stiffness based on the static loading is thus only effective and relevant for decreasing the moment in y-direction and decreasing the displacement at the outer most segments of the tunnel (Figure 40; red line, dU).

The Norwegians apparently put a lot of thought into their design [33], because the Bjørnafjord design has the optimal dimensioning regarding the stiffness of the support system. The support stiffness of the tethers in the Bjørnafjord design range from $1.00 \cdot 10^2 \text{ MN/m}$ till $5.42 \cdot 10^2 \text{ MN/m}$ and the mean support stiffness is equal to $1.83 \cdot 10^2 \text{ MN/m}$.

6.3. Secondary connections – k_{φ}

In the original SFT design in the Bjørnafjord, the tunnel elements are bolted together and filled up with concrete. The segment connections are fixed because the tunnel elements cannot rotate or move individually. The connection stiffness for a fixed connection is $k_{\varphi} = \infty$.

In immersed tunnelling, Gina gaskets and Omega seals are used to prevent water seeping into the tunnel due to the external water pressure. The SFT design for the Bjørnafjord is in essence a type of immersed tunnel. In the design report however, no mention is made of such type of seals.

The Gina and Omega combination of seals not only provide sealing for the transfer of the hydrostatic loads but as well as for small displacements between the tunnel segments due to soil settlement, creep of concrete, temperature effects and if required earthquakes. The designs are generally based on the expected tunnel lifetime of 100 years. The Gina gasket is to be manufactured from a blend of SBR and NR rubber [37].

It is interesting to explore whether this multiple functionality of the Gina gasket and Omega seals could be an asset to the total design of the SFT. The Gina-profile is therefore considered as a significant parameter in the research on the end joint of the tunnel.

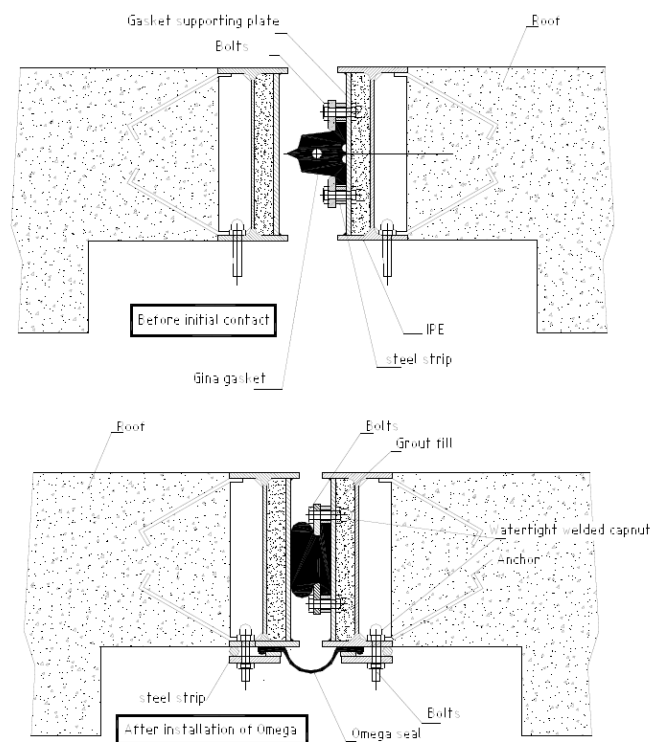


Figure 45 - Gina profile before and after full contact [37]

The Gina-profile is made of a rubber material and acts like a type of spring during compression and relaxation. During initial contact of the two tunnel segments there is a low pulling force present. The water between the bulkheads is pumped out when the Gina-profile has full contact around the total circumference. Due to pressure differential between the bulkheads and the hydrostatic pressure on the outside of the tunnel, the Gina-profile compresses and seals the joint.

Using a standard Gina-profile type, the spring stiffness of the Gina-profile can be determined using the force-compression graph created by the manufacturer. The Gina-profile used is a ETS 180/220 by Trelleborg, see also Appendix D.

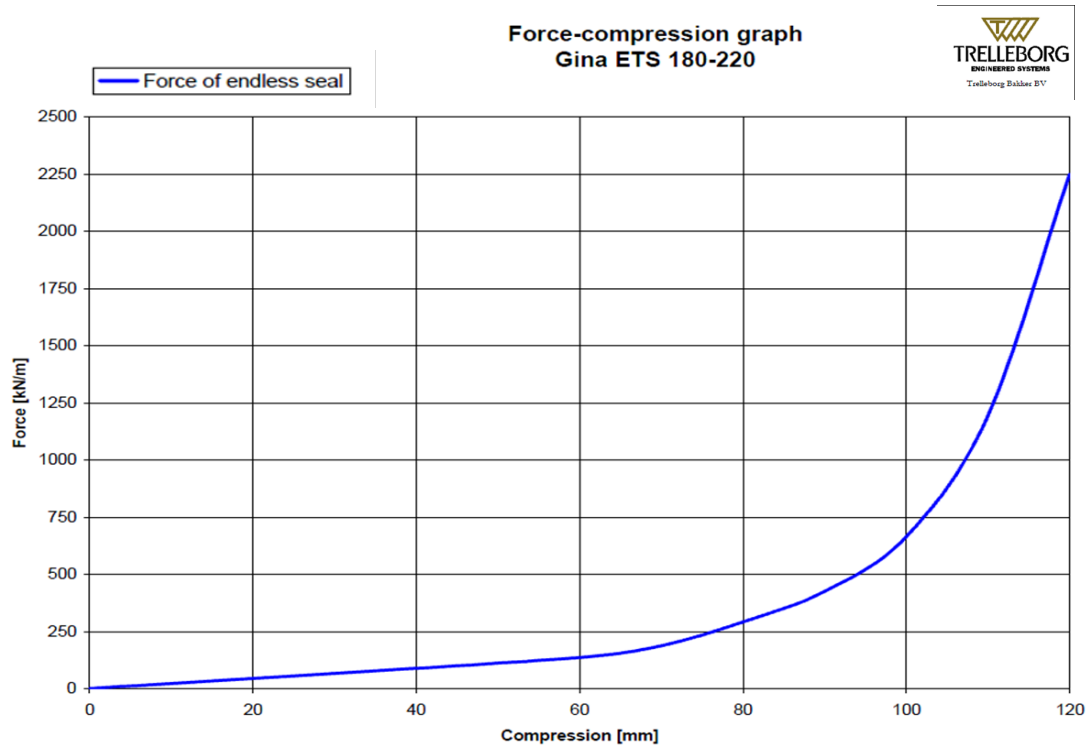


Figure 46 - Force-compression graph Gina-profile ETS 180/220 (Trelleborg) [37]

The graph shows that the spring stiffness is non-linear. The non-linearity is very complex to model and therefore only the representing initial spring stiffness k_0 will be used in the calculations. The graph was simplified by dividing the graph in 3 parts: a very low spring stiffness indicates the relaxation of the Gina-profile, the middle section represents the placements and thus initial compression of the seal (pink dotted line), and the large spring stiffness indicates further compressing of the Gina-profile.

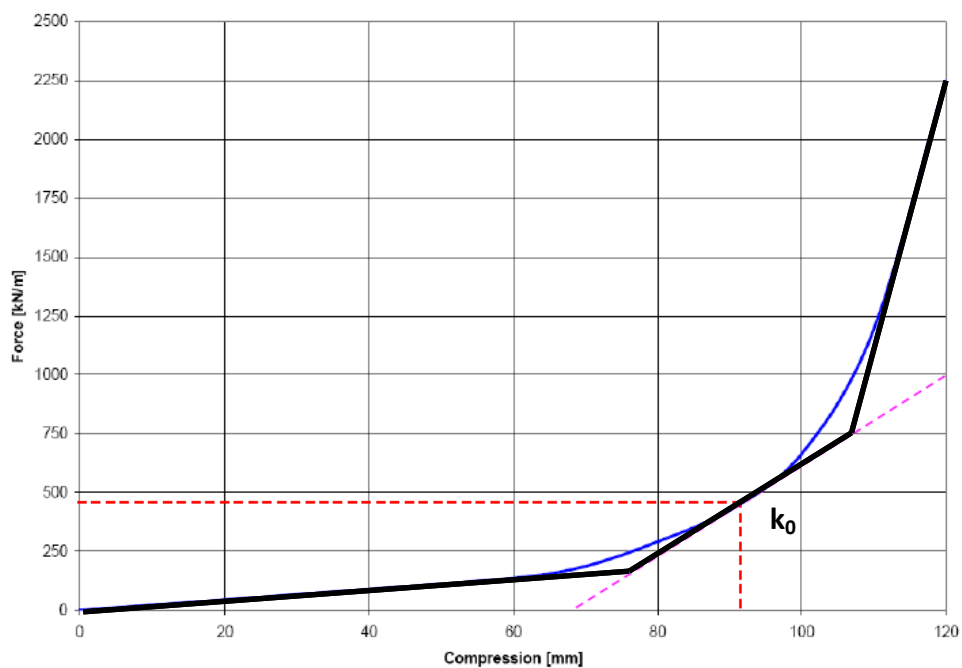


Figure 47 - Simplified Force-compression graph Gina-profile

From the simplified graph, it is derived that the initial force and compression displacement are equal to:

$$F_0 = 460 \text{ kN/m}$$

$$u_0 = 90 \text{ mm}$$

The initial spring stiffness is determined at the initial compression of the Gina-profile. Using the tangent to the force-compression graph at the intersecting red dotted lines, will result in the initial spring stiffness.

$$k_0 = \frac{F_2 - F_1}{u_2 - u_1} = \frac{(900 - 0) \text{ kN/m}}{(120 - 63) \text{ mm}} = 15789 \text{ kN/m/m}$$

Secondly, expressions are determined to calculate the bending moments and forces in the segment joints relative to the displacements and rotations.

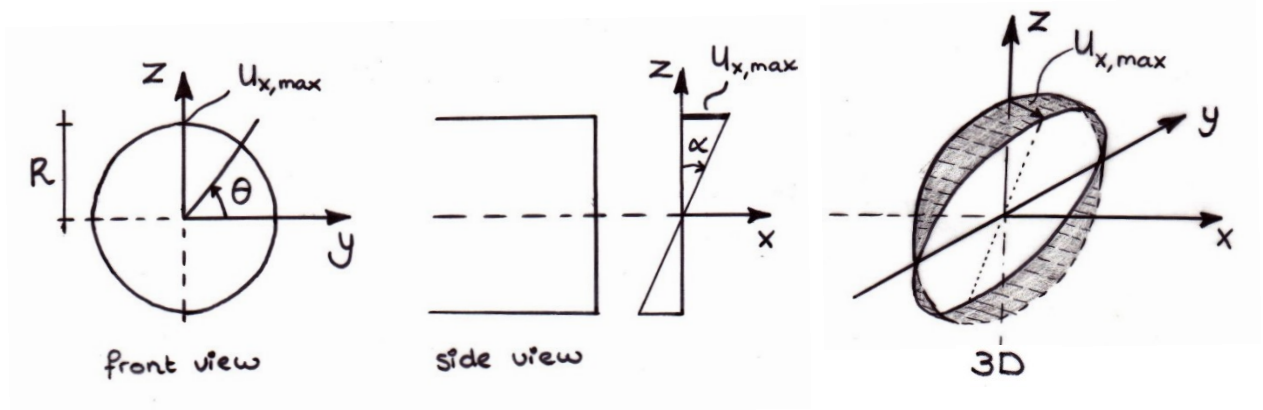


Figure 48 - Units and directions determining Gina-profile stiffness

The illustrations in Figure 48 indicate positive directions and the names of the variables. It is assumed that the segments have a certain displacement due to rotation α of one segment relative to another segment.

$$u_{x,max} = \sin(\alpha) \cdot R$$

$$u_x(\theta, \alpha) = \sin(\theta) \cdot u_{x,max}$$

The shift in normal force and bending moment can be calculated using the following formulas;

$$N(\theta) = k_0 \cdot u_x$$

$$N(\theta) = k_0 \cdot \sin(\theta) \cdot \sin(\alpha) \cdot R$$

$$M(\theta) = N(\theta) \cdot lever$$

$$M(\theta) = k_0 \cdot \sin(\theta) \cdot \sin(\alpha) \cdot R \cdot (\sin(\theta) \cdot R)$$

With, the total value of normal force and/or bending moment consisting the upper half of the cross-section;

$$N_{0.5} = k_0 \cdot \sin(\alpha) \cdot R \cdot \int_0^\pi \sin(\theta) d\theta$$

$$N_{0.5} = k_0 \cdot \sin(\alpha) \cdot R \cdot (-\cos(\theta)) \Big|_0^\pi$$

$$N_{0.5} = k_0 \cdot \sin(\alpha) \cdot R \cdot 2$$

$$N_{0.5} = 64108 \cdot \sin(\alpha)$$

$$M_{0.5} = k_0 \cdot \sin(\alpha) \cdot R^2 \cdot \int_0^\pi \sin(\theta)^2 d\theta$$

$$M_{0.5} = k_0 \cdot \sin(\alpha) \cdot R^2 \cdot \left(\frac{\theta}{2} - \frac{1}{4} \sin(2\theta) \right) \Big|_0^\pi$$

$$M_{0.5} = k_0 \cdot \sin(\alpha) \cdot R^2 \cdot \frac{\pi}{2}$$

$$M_{0.5} = 317211 \cdot \sin(\alpha)$$

Similarly, the values can be determined for the total cross-section;

$$N_{total} = 0$$

$$M_{total} = k_0 \cdot \sin(\alpha) \cdot R^2 \cdot \frac{2\pi}{2} = 634422 \cdot \sin(\alpha)$$

Bearing in mind that values calculated with the formulas above, are only the incremental forces. An initial pressure force is present in the Gina-profile to create the watertight seal. In this case, the initial force is assumed to be;

$$F_0 = 460 \text{ kN/m}$$

$$N_{initial} = F_0 \cdot 2\pi R = 460 \cdot 2\pi \cdot 6.3 = 18 \text{ MN}$$

The rotational stiffness of the Gina-profile can be determined, because the formula for the moment in the Gina-profile has been derived. Basic physics state that;

$$M = k_\varphi \cdot \alpha$$

With the moment equation determined before and assuming small rotations, the rotational stiffness will be equal to:

$$k_\varphi = \frac{M}{\alpha} = \frac{k_0 \cdot \sin(\alpha) \cdot R^2 \cdot \frac{2\pi}{2}}{\alpha}$$

$$k_\varphi = k_0 \cdot \pi R^2$$

$$k_\varphi = 1.969 \cdot 10^3 \text{ MNm/rad}$$

Tension should not occur in the cross-section to prevent water leakage and preferably a small amount of compression should remain to keep a tight seal formed by the Gina-profile. If tension should occur in these joints, couplers can be used to limit the relaxation of the Gina-profile. This method is now mostly used in seismic areas, where extreme cases of “snaking” of the immersed tunnels occur. The use of added couplers allows compression as well as tension between two segments.

Considering no couplers are used and no tension should occur, the relaxation of the Gina-profile is limited. The simplified initial spring stiffness allows for a maximal relaxation of $91 - 69 = 22 \text{ mm}$. Using the formulas above, and the initial spring stiffness (pink dotted line limits);

$$u_{x,max} = \sin(\alpha) \cdot R = 22 \text{ mm}$$

Gives a maximum rotation of;

$$\alpha = 0.00349 \text{ rad} \quad (= 0.20^\circ)$$

A certain amount of compression is maintained, approximately 165 kN/m, on the tension side of the cross-section. This keeps the seal intact so no leakage of water is present when the above mentioned maximum rotation occurs.

The accepted rotation and force values would be considerably higher in case the full compression diagram of the Gina-profile is considered. More relaxation on the tension side of the profile is allowed and a larger force is necessary to arrive at the same rotation angle due to the increase in stiffness of the Gina-profile for compression. The maximum rotation which is acceptable, can be approximated by shifting the rotation axis from the middle of the cross-section to one third of the cross-section height.

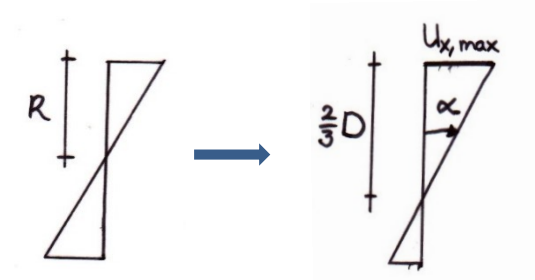


Figure 49 - Shift rotation axis Gina-profile

The displacement range for this particular Gina-profile is between 50 and 120 mm. The maximal relaxation then becomes equal to $91 - 50 = 41 \text{ mm}$. Using the shifted rotation axis;

$$u_{x,max} = \sin(\alpha) \cdot \frac{2}{3}D = 41 \text{ mm}$$

Gives a maximum rotation of;

$$\alpha = 0.00513 \text{ rad} \quad (= 0.29^\circ)$$

6.3.1. SCIA Results

The results of varying the Gina-profile connection spring stiffness parameter in the SCIA tunnel model are presented. The displacements are evaluated using the SLS Classes results. The moments and shear forces are evaluated using the ULS Classes results. For convenience, the calculated connection spring stiffness is mentioned again.

$$k_{\phi} = 1.969 \cdot 10^3 \text{ MNm/rad}$$

The connection stiffness is then investigated by increasing and decreasing the value in the SCIA model, between the values;

$$1.97 \cdot 10^0 \text{ MNm/rad} \leq k_{\phi} \leq 1.97 \cdot 10^8 \text{ MNm/rad}$$

SLS – 3D Displacements

Displacements due to the force loading under changing connection spring stiffness show a distinct shape of the deformation. The shape of the displaced tunnel as well as the moment line for several values of the support spring stiffness is illustrated in Figure 51 (the spring stiffness is given in MNm/rad).

To show the steepness of the trend more clearly, the deformation of the structure for different connection spring stiffness are presented in a graph.

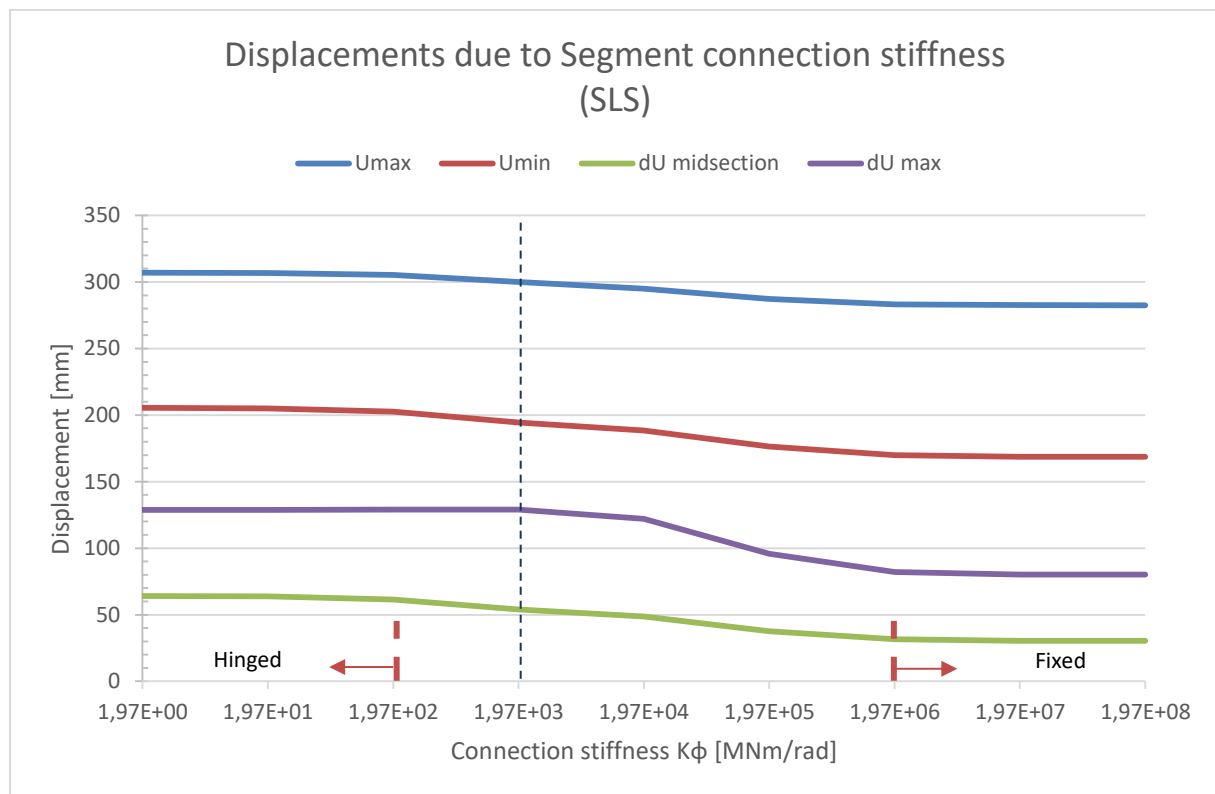


Figure 50 – Displacements due to segment connection stiffness

The maximum displacement and the displacement between two supports in the midsection start to decrease earlier than the maximum displacement between two supports (purple line). This is caused by the maximum moment which occurs between grid 2 and 3 (the fixed support and the first spring support). Although the moment at the fixed support decreases, it decreases relatively slower than the redistribution of moments in the midsection.

The overall effect of the connection stiffness is low, looking at the displacements. The reason that the effect of the connection stiffness is low, is because the largest part of the displacement is a result of the stiffness of the supports. Increasing the connection stiffness from $1.97 \cdot 10^2 \text{ MNm/rad}$ to $1.97 \cdot 10^6 \text{ MNm/rad}$, causes a displacement reduction of approximately 40 percent. Such a large reduction may sound alluring; but 40% only means a displacement decrease in the order of a few centimetres for a beam with a length of 197 meter. The segment connection stiffness is not of large influence on the tunnel structure. The segment connection is considered a joint when a Gina-profile is applied.

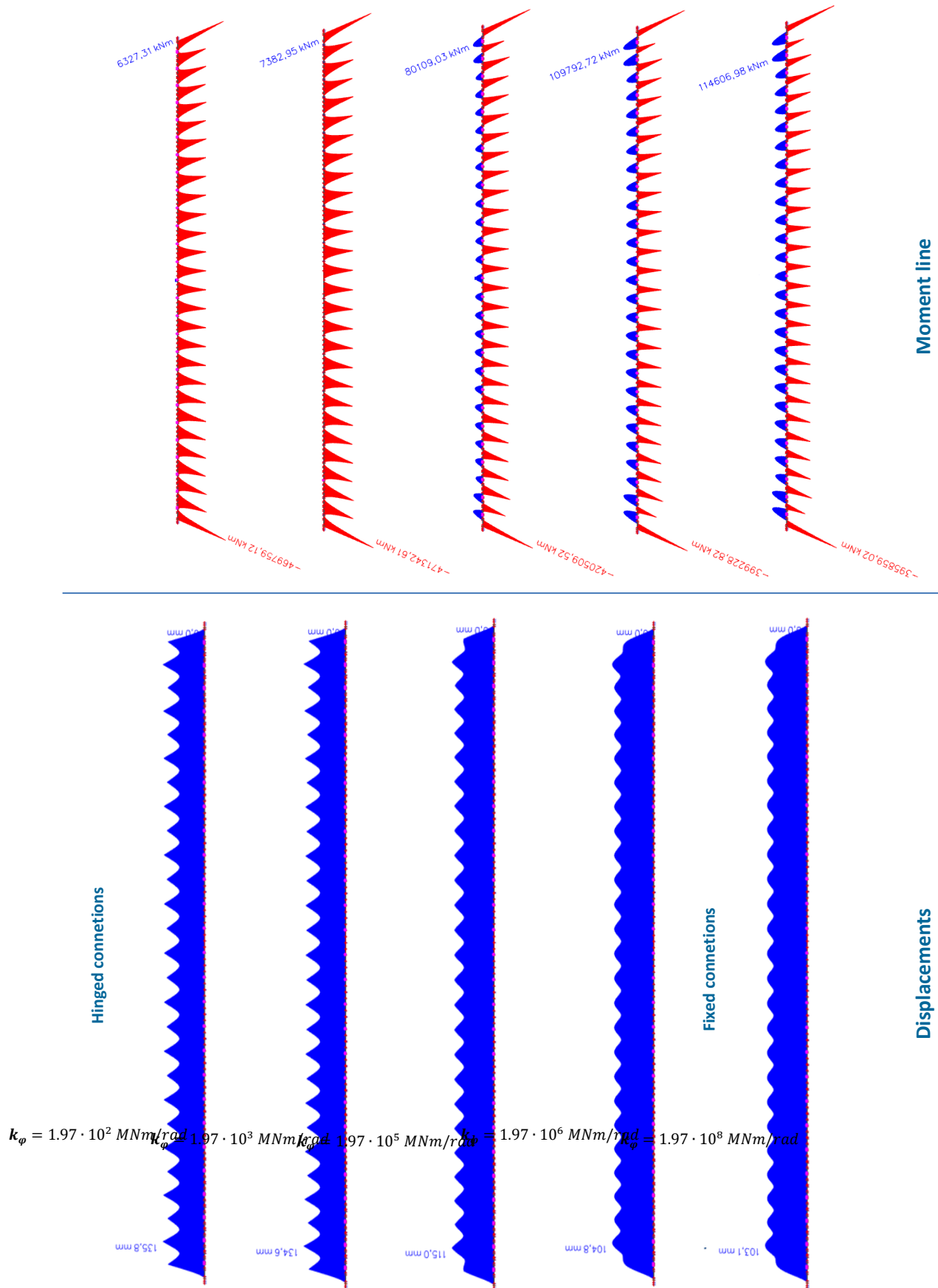


Figure 51 – Displacement shape and moment lines due to connection stiffness

SLS – Rotations

The maximum rotation at the Gina-profile due to force loading under changing connection spring stiffness is stated in the table below.

Connection stiffness K_y [MNm/rad]	Rotation [mrad]		
	Rx	Ry	Rz
1.97 E+00	0.5	1.3	0.4
1.97 E+01	0.5	1.3	0.4
1.97 E+02	0.5	1.3	0.4
1.97 E+03	0.5	1.3	0.4
1.97 E+04	0.4	1.1	0.4
1.97 E+05	0.2	0.7	0.4
1.97 E+06	0.2	0.5	0.4
1.97 E+07	0.1	0.5	0.4
1.97 E+08	0.1	0.5	0.4

Table 19 - Maximum rotations due to connection spring stiffness

Rotation around the z-axis does not change with increasing or decreasing connection stiffness. When the connection stiffness is between 1.97 E+03 and 1.97 E+07, the rotation angle around the x-axis and y-axis decrease with decreasing connection stiffness.

ULS – Moments and shear forces

Moments and shear forces due to the force loading under changing connection spring stiffness show distinct trends.

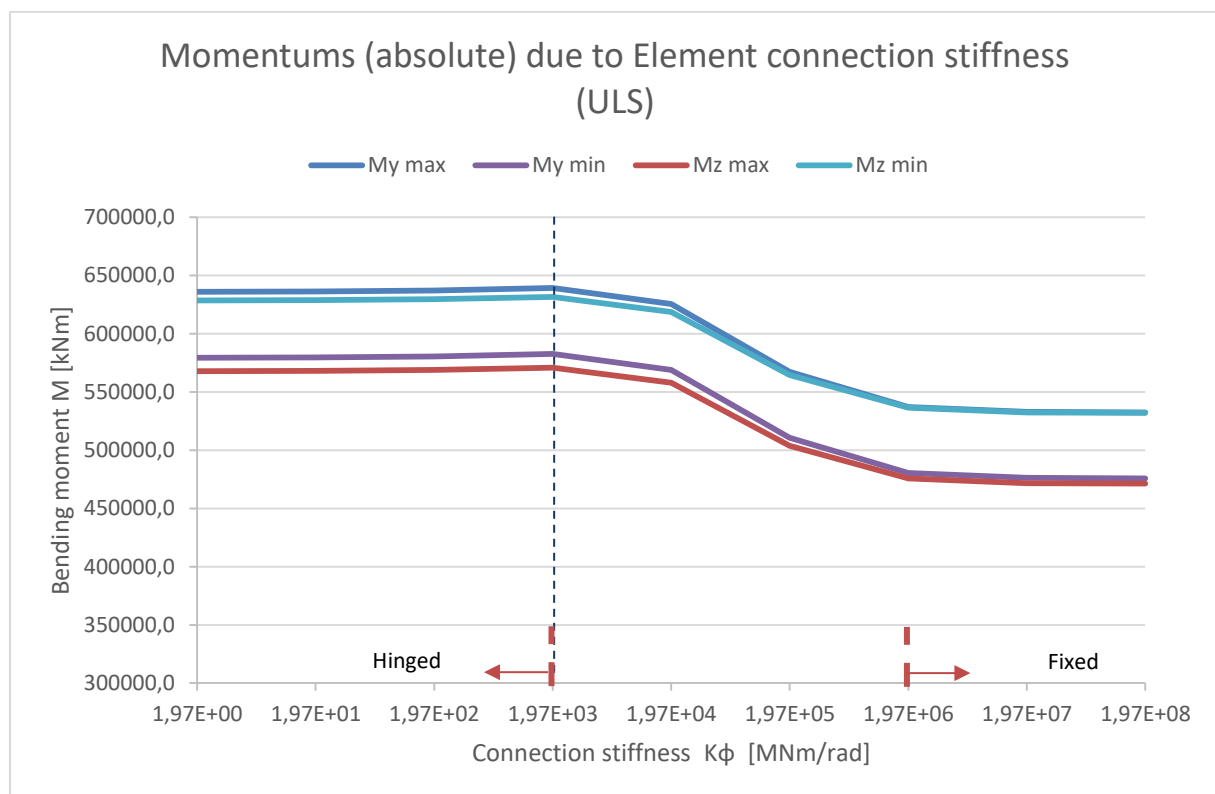


Figure 52 - Moments due to connection stiffness

The moments decrease with increasing connection stiffness as illustrated above. Normally, one would expect the opposite to happen. Hinges are often introduced in a system to relieve the structure by decreasing the moments. This method is used in immersed tunnelling for example, by cutting the expansion joints. Hence, comparing the very small and very large connection stiffness with each other is the same as comparing two different systems, see Figure 53.



Figure 53 - Different systems due to connection stiffness

The moments line seems to shift upward with increasing connection stiffness (see Figure 51). With increasing connection stiffness, the tunnel segments however start to react as a single beam because the connections are attracting more of the load. The larger connection stiffness which approaches a fixed connection, is therefore favourable because the absolute moments are smaller by 20 percent (between a stiffness of $1.97 \text{ E}+03$ and $1.97 \text{ E}+06$.)

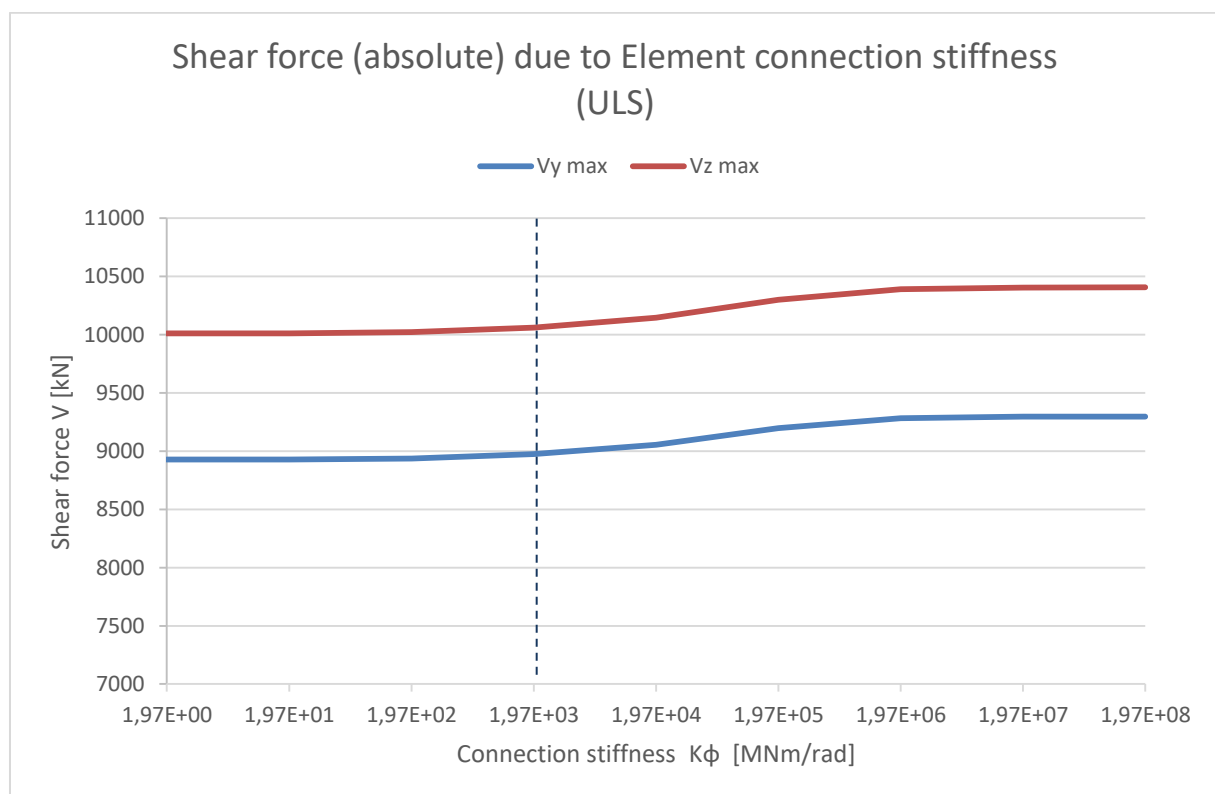


Figure 54 - Shear forces due to connection stiffness

The shear force increases with increasing connection stiffness, while the moment decreases. One would usually expect the shear force to decrease as well. The cause is found in the shape of the moment line itself, rather than the absolute value of the moments.

The shear force is the derivative of the moment. Meaning that the steepness of the moment line determines the value of the shear force. The absolute moment has its maximum for a small connection stiffness. Increasing the connection stiffness results in a smaller moment, but the steepness of the moment line increases. The shear force therefore increases with increasing connection stiffness.

The increase of shear force is however very small. The difference in shear force is approximately four percent between a very weak connection stiffness and a very strong connection stiffness. Changing the connection stiffness in respect to shear forces is therefore not relevant.

6.3.2. Physical limitations

The original design has no Gina-profile in the segment connections or any type of flexible connections. These connections are bolted together and cast in concrete, acting as a fixed beam connection.

Considering a Gina-profile fabricated by Trelleborg, the maximum displacement and rotation between the segments has been determined in paragraph 6.3 and are mentioned here again for convenience.

$$u_{x,max} = 41 \text{ mm} \quad \rightarrow \quad \alpha = 0.00513 \text{ rad} \quad (= 0.29^\circ)$$

Table 19 shows that rotations around the x-axis and z-axis do not exceed the maximum values beyond which water tightness may be compromised. Rotation around the y-axis however limit the applicable range of connection stiffness and results in the following boundaries;

$$1.97 \cdot 10^6 \text{ MN/m} \leq k_\varphi \leq 1.97 \cdot 10^7 \text{ MN/m}$$

The upper boundary is actually equal to infinity, however it is not relevant to increase the connection stiffness that far. A connection stiffness larger than the upper boundary of $1.97 \cdot 10^7 \text{ MN/m}$ will not change the values of the displacements and forces in the tunnel.

The cross-section capacity regarding moments and shear forces can also limit the value of the support spring stiffness. The calculated strength is mentioned again for convenience (see paragraph 4.6.2).

$$M_{Rd} = 889000 \text{ kNm} \quad V_{Rd} = 26370 \text{ kN}$$

Checking the graphs with cross-section capacity limitations give no boundaries regarding the connection stiffness;

$$M_{Rd} \quad \rightarrow \quad k_\varphi \geq 1.97 \cdot 10^0 \text{ MN/m}$$

$$V_{Rd} \quad \rightarrow \quad k_\varphi \geq 1.97 \cdot 10^0 \text{ MN/m}$$

A pre-stressing force is present in the original SFT design and causes a initial pre-stressing force which is much larger than the initial force assumed for the Gina-profile.

$$N_{prestress} = 280 \text{ MN} \quad > \quad N_{initial,Gina} = 18 \text{ MN}$$

The pre-stressing force would result in a distributed force in the Gina-profile equal to;

$$F_{Gina} \approx 7000 \text{ kN/m}$$

The chosen Gina-profile is not adequate to bear such large forces. Even the larger standard profile produced by Trelleborg is not sufficient and a specially produced Gina-profile will be necessary.

The second situation to consider is the normal force in the cross-section caused by the different loads on the tunnel structure. According to the calculations performed in SCIA (see paragraph 4.5), the maximum normal force is;

$$N_{ULS} = 26632 \text{ kN}$$

Which will result in a distributed force in the Gina-profile equal to;

$$F_{Gina} \approx 670 \text{ kN/m}$$

The Gina-profile considered in the parameter study would be fitting, but only if the normal force caused by the loads would be present in the cross-section and not the pre-stressing force as well.

6.3.3. Conclusion

The connection spring stiffness does have an influence on the displacement and force distribution. The range of reality for the connection spring stiffness parameter has been determined by restricting the full parameter range with real life limitations.

$$1.97 \cdot 10^6 \text{ MN/m} < k_{\phi} \leq 1.97 \cdot 10^7 \text{ MN/m}$$

The boundaries are a result of the rotation restrictions to guarantee water tightness of the segment connections. Moments and shear forces do not limit the parameter range.

The original Gina-profile has a connection stiffness equal to $1.97 \cdot 10^3 \text{ MN/m}$, which is outside of the parameter range. A possible solution is to use couplers in combination with the Gina-profile. These couplers limit the relaxation of the Gina-profile. The combination of Gina-profile and couplers guarantee compression while also allowing tension between two segments.

The range of the connection stiffness has very high values and approaches a fixed connection. Using a flexible Gina-profile with connection stiffness far less than required, will not be practical. Adapting the Gina-profile to fit the requirements would render a fixed type coupling which are already at hand.

A change in connection spring stiffness based on the static loading is thus only relevant to allow small rotations between segments. Allowing rotations has the disadvantage of introducing increased moments in this specific tunnel structure.

It can be concluded that the Gina-profile is not applicable in the segment connections when used as the single means of connection and waterproofing. The stiffness of the segment connections has to be very large to which only a fixed type connection suffices.

6.4. End joint – SC

There are many types of end joints possible. The most well-known standard and basic types of joint in mechanics are;

- Fixed
- Translation free (Sliding)
- Rotation free (Hinged)
- Free

End joints purely based on the number of degrees of freedom, will result in a large number of joints to investigate. The following six degrees of freedom can be distinguished; 3 translation freedoms and 3 rotation freedoms.

$$U(x, y, z) \quad \text{and} \quad \varphi(x, y, z)$$

These 6 positions, viewing them as a binary number of 6 digits, result in 64 unique combinations. Some combinations can be eliminated beforehand and therefore it is not necessary to investigating them all.

No torsion (Rx)

Rotation around the x-axis will not be considered because of traffic safety. Rotation around the x-axis would result in irregular humps and bumps in the road, increasing the risk of car drivers losing control over their vehicle.

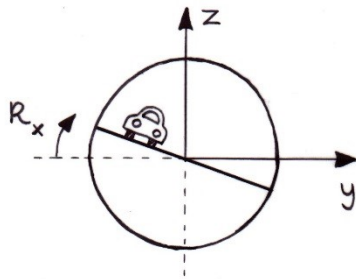


Figure 55 - Traffic safety, rotation around x-axis

Only Ry and Rz simultaneously

External nett forces on the tunnel structure most likely occur simultaneously in xy and xz plane. Rotation around the y-axis and z-axis will therefore not be considered individually.

No lateral displacements (Uy)

The SCIA model is set up with only vertical springs at the supports to represent the tethers. The real mechanism of the tether support however, has a horizontal stiffness component when the tunnel starts to displace, see Figure 56.

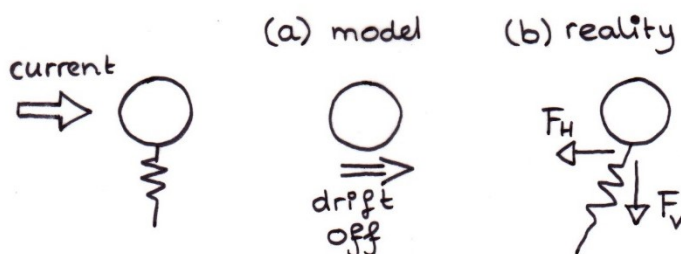


Figure 56 - Mechanism of the tether support

The horizontal stiffness component has not been taken into account in the SCIA tunnel model. Allowing translation in the y-direction (U_y) is not practical, because the SCIA model does not behave correctly according to the real-life situation. The forces working on the structure will lead to extreme values of U_y because there is no contra support or strength to prevent the displacement in y-direction, only the end joint at the other side.

End joints to investigate and freedom restrictions

The three arguments stated before eliminate a lot of combinations, leaving only 9 combinations to investigate.

The table below gives an overview of the 9 combinations which will be considered. The blue shaded box indicates that the degree of freedom is possible. (The light blue shading indicates the rotation around the x-axis and translation in y-direction which will not be considered). Figure 57 indicates the degrees of freedom which will be considered.

Name	U _x	U _y	U _z	R _x	R _y	R _z
Fixed	1					
Rotation free (Hinged)	2					
	3					
	4					
	5					
	6					
	7					
	8					
	9					

Table 20 - Types of end joint connections

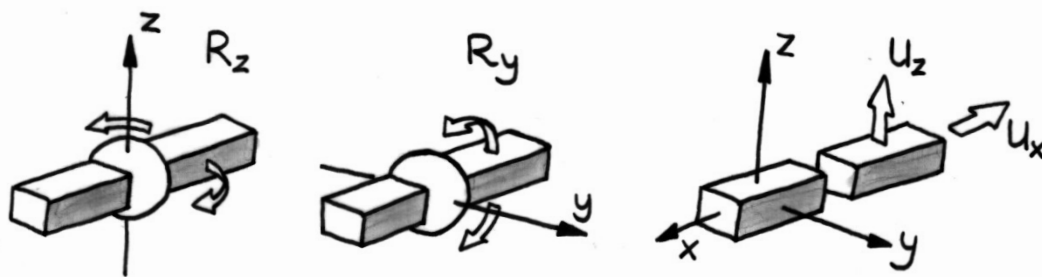


Figure 57 - Degrees of freedom in the end joint

Different types of displacements and rotations are allowed, but they only remain practical till a certain maximum level. For example, a small displacement in x-direction can be accommodated in a sliding mechanism in the tunnel connection but not displacements in the order of 100 meters. Some limits are therefore set for the maximum displacements and rotations.

Here, only some rough first estimations are made to limit the displacements and rotations. In paragraph 6.4.2 more detailed approximations are performed. Displacements limits are based on common sense as well as safety and comfort regulations, like maximum slope percentages.

$$U_x \leq 10 \text{ meter}, \quad U_z \leq 1 \text{ meter}, \quad R_y \leq 10^\circ, \quad R_z \leq 4.5^\circ$$

Coordinate system

The whole tunnel model was turned, in order to line up the local coordinate system to the global coordinate system. SCIA then produces results relative to the local coordinate system. The x-axis of the tunnel end joint is now lined up with the global x-axis. This way, SCIA results are easier to interpret. U_x is now translation in the end joint x-axis only.

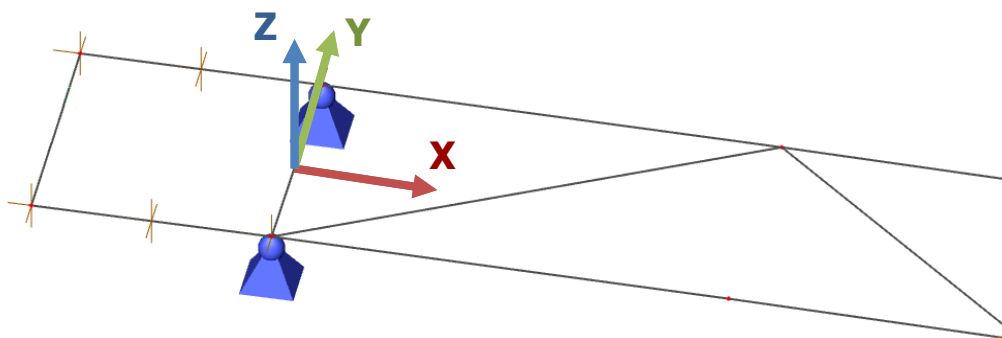


Figure 58 - Local axis system end joint

6.4.1. SCIA Results

The tunnel design of the Bjørnafjord has a fixed end joint. The fixed end joint as well as the remaining 8 types of end connections will be investigated. The displacements, rotations, forces and moments are all measured in the middle of the end joint, located at the supports in the SCIA model as illustrated in Figure 58.

SLS – Displacements and rotations

Displacements and rotations are presented in the bar diagram below and are a result of the different combinations of degrees of freedom assigned to each end joint type.

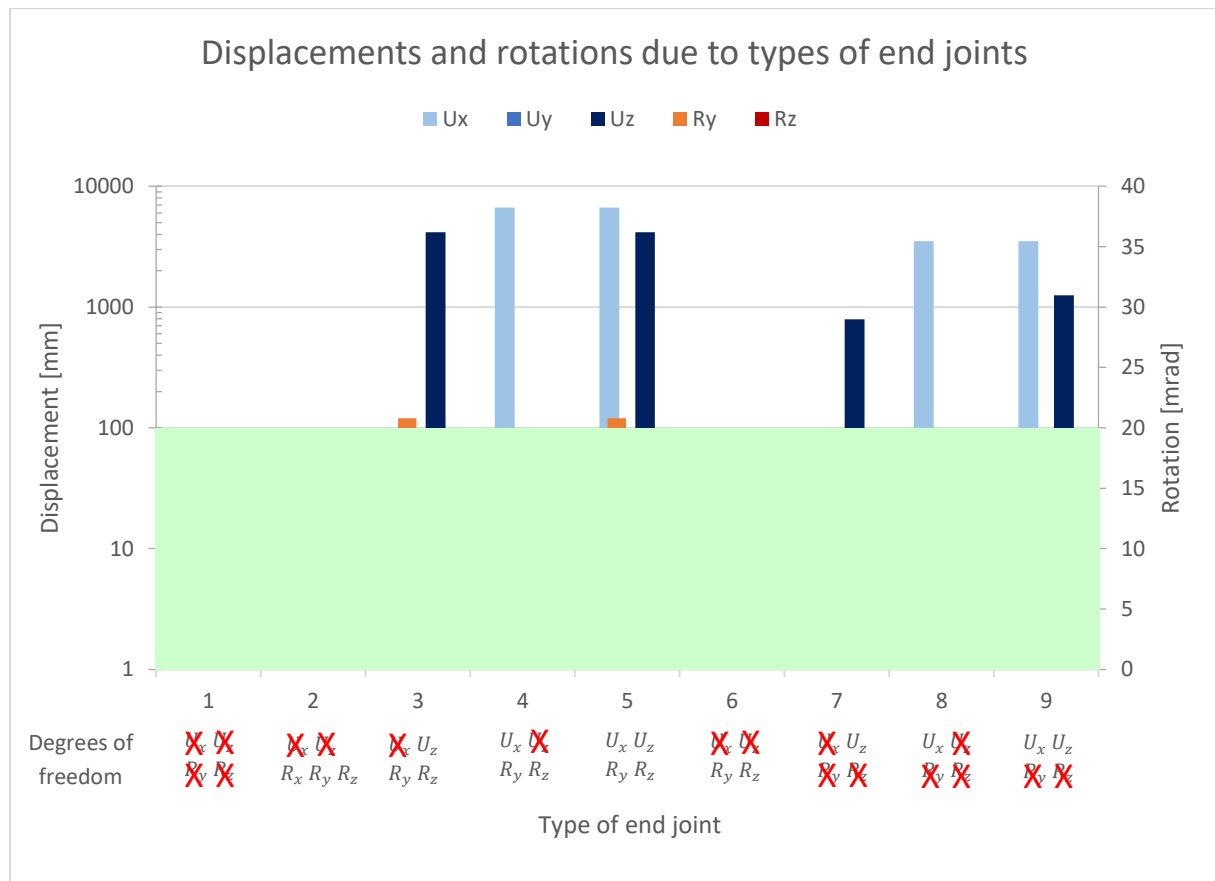


Figure 59 - Displacements and rotations different types of end joints

From the diagram graph above it is clearly visible which end joints result in the largest displacements and rotations. End joint number 3 till 5 and 7 till 9 are most interesting in respect to displacements and their physical challenges. These joints have a horizontal (U_x) and vertical displacements (U_z) which are very large. The displacements are in the range of several meters. The end joints number 3, 5 and 9 will probably not be considered as useful solutions because the displacement U_z of the end joint is larger than 1 meter. The 1 meter limitation of the displacement U_z has been determined in the previous paragraph.

The logarithmic scale for the displacement is chosen to show more clearly the different values between joints number 1, 2, 6 and 7. On a linear scale the small differences are not visible in the graph. The green shaded area indicates displacements and rotations which are relatively small and considered possible to integrate into the end joint design.

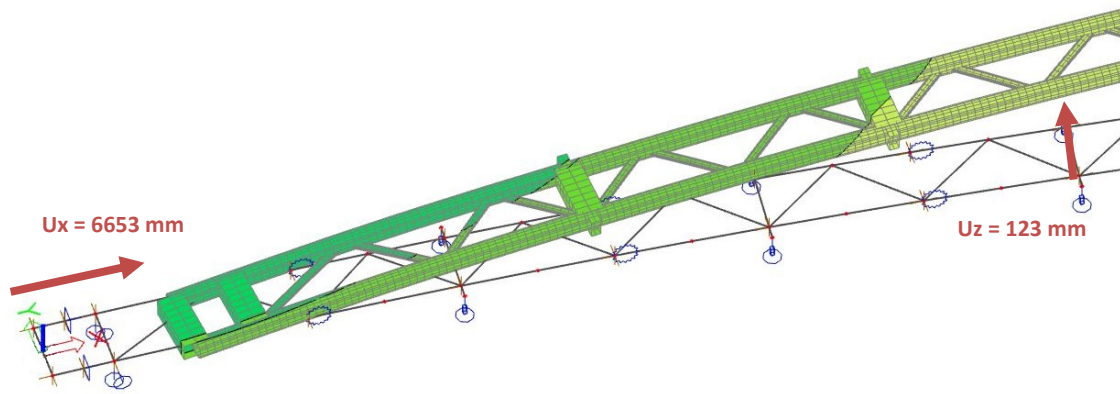


Figure 60 - 3D displacement of the end joint with free translation in x-direction (nr 4)

End joint 4 has translational freedom in x-direction and both rotational freedoms. The large displacement in x-direction is clearly visible in the 3D displacement illustration. The tunnel structure cannot transfer moments at the end joint because there is rotational freedom in the end joint.

The fixed end joint (joint number 1) has no degrees of freedom contrary to end joint number 4. The sinusoidal shape of the displacement is also present in the displacement of the end joint number 4 and actually for every type of end joint. The main shape of the displaced structure does not change because the main parameters of the structure do not change, only the type of support at one shore connection changes. Changing the end joint only effects the displacements and rotations for a small section at the shore side of the tunnel: approximately up to the third tether support.

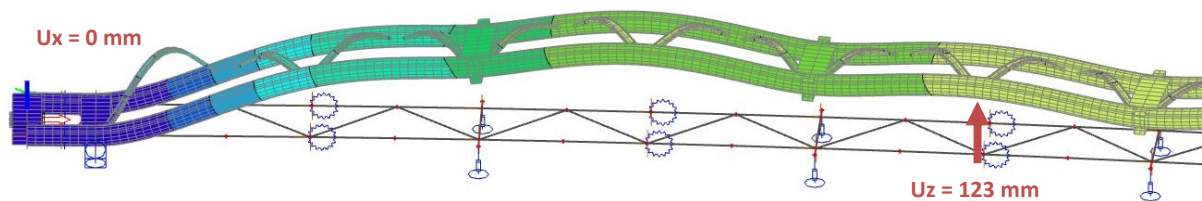


Figure 61 - 3D displacement of the Fixed end joint (nr 1)

ULS – Moments and shear forces

Moments and shear forces due to the force loading under changing end joints are presented together in the bar diagram below.

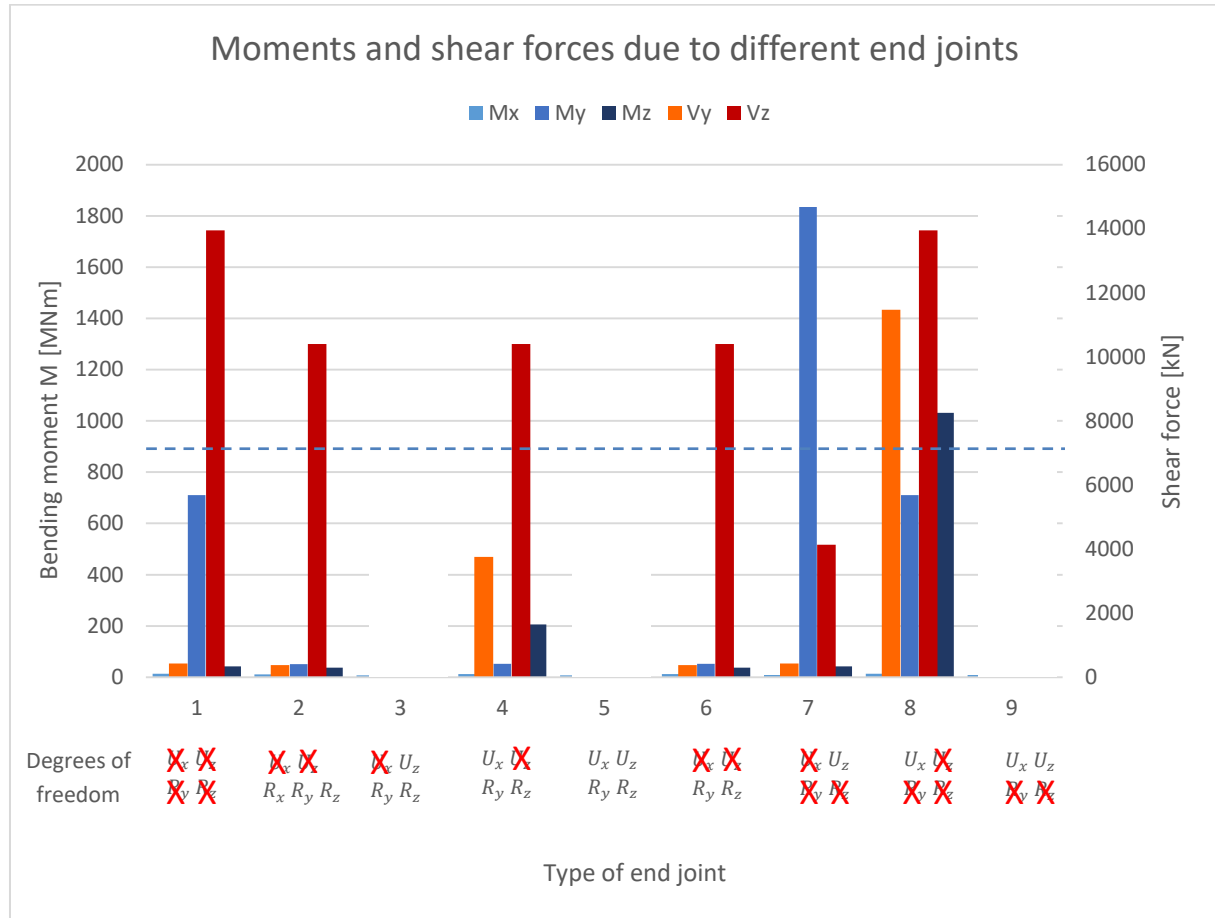


Figure 62 - Moments and shear forces due to different types of end joint

From the diagram graph above, it can be observed that end joint 2 till 6 clearly have two degrees of freedom of rotation because the moments are small. To the contrary, end joints 1 and 7 till 9 show that limitation of rotation freedom creates larger moments. The blue dotted horizontal line indicates the cross-section moment capacity. The maximum cross-section shear force capacity of 26,370 kN is not reached.

The cross-section capacity limitations result that the end joints 7 till 9 will not be considered as suitable solutions because these end joints cause moments larger than the construction capacity. The end joints number 3, 5 and 9 are of a lighter colour because these end joints were already considered not suitable due to the large displacements U_z they invoke.

The shear force V_y (orange) and bending moment M_z (dark blue) are not relevant in this parameter study, because of the 2D approach of the tether supports in the SCIA model. The horizontal stiffness component has not been taken into account in the SCIA model, causing distortions of the model results in lateral directions.

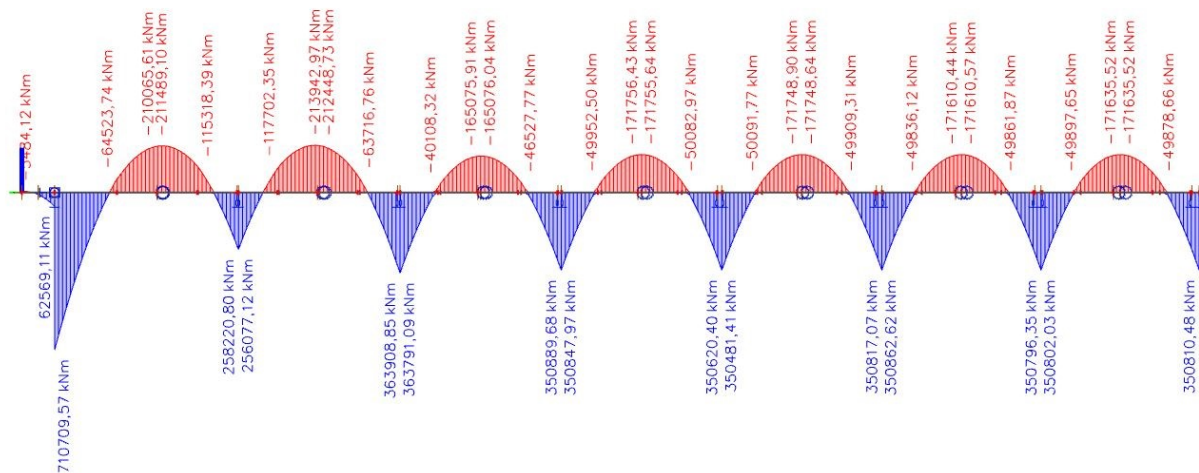


Figure 63 - Moment line M_y of the Fixed end joint (nr 1)

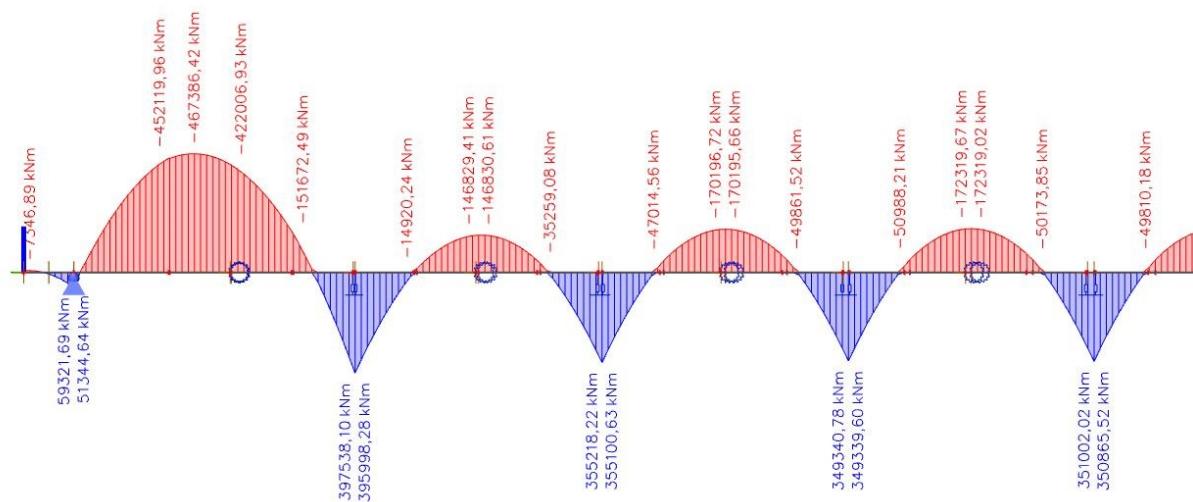


Figure 64 - Moment line M_y of the Hinged end joint (nr 2) and end joint nr 4

Inserting end joint 4 in the tunnel structure doubles the negative moment, but the positive moment present in the end joint decreases drastically to only 10%.

The type of end joint influences the M_y moment until approximately the third tether support, the remaining part of the tunnel structure is not influenced. The latter holds when comparing all the different types of end joint.

6.4.2. Physical limitations

The original design of the Bjørnafjord SFT has a fixed end joint. Multiple types of end joints have been investigated. Real life limitations however have to be considered.

Cross-section capacity

The cross-section capacity regarding moments and shear forces limits the type of end joint which are applicable. The calculated strength is mentioned again for convenience (see paragraph 4.6.2).

$$M_{Rd} = 889000 \text{ kNm} \quad V_{Rd} = 26370 \text{ kN}$$

Checking the graphs with cross-section capacity limitations result that the end joints 7 till 9 are not suitable because these end joints cause moments larger than the construction capacity.

Displacements

Very large displacements and rotations are not feasible in any type of end joint. Realistic estimations of the maximum displacements and rotations are done using road construction recommendations.

The maximum displacement in x-direction is lower than 10 meters. A displacement in longitudinal direction of 10 meters seems to be quite large, but consideration must be made to the idea that the displacement can be distributed over several sections. The end joint system does not have to consist of one single mechanism. Secondly, at the beginning of paragraph 6.4 it was stated that the horizontal stiffness component has not been taken into account in the SCIA tunnel model. The actual displacement in x-direction will be much smaller than determined with the current SCIA model. Therefore, none of the end joint are excluded based on longitudinal displacement.

The maximum displacement in z-direction is more than 4 meters, which is too large to be transferred at the end joint. The minimum distance necessary to overcome the height difference caused by the U_z displacement is calculated.

Three types of minimum distance L are considered: minimum raw slope length L_{min} , minimum connecting arch length L_{arches} and minimum comfort length $L_{comfort}$, see Figure 65.

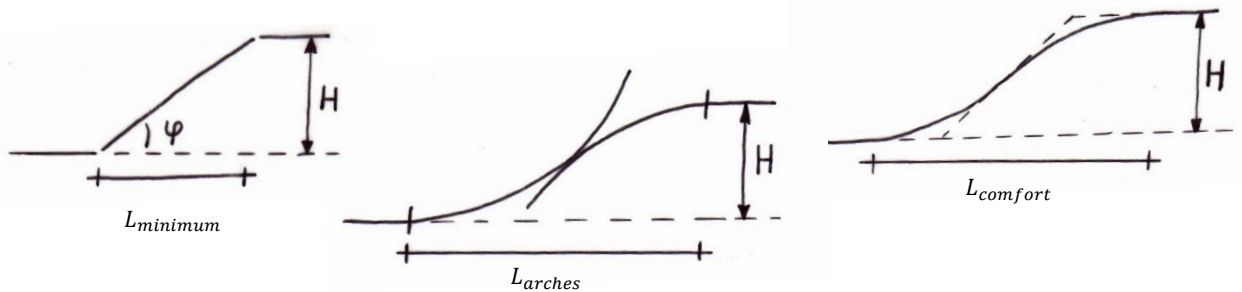


Figure 65 – Minimum distance to overcome height difference

The minimum comfort length is used when the steepness of the slope at the inflection point of the arches is larger than which is acceptable. If the slope steepness is too large after determining the minimum arch length, both arches are pulled apart and an additional slope section is added to decrease the slope steepness, resulting in the minimum comfort length. The minimum comfort length therefore is either equal to or larger than the minimum arch length. The largest of both lengths needs to be taken.

The minimum length for two connecting arches and the maximum slope at the inflection point can be calculated with the following formulas;

$$L_{arches} = \sqrt{2H \cdot \Sigma R}$$

$$i = 200 \cdot \frac{H}{L_{arches}}$$

With,

H	the height difference [m]
ΣR	summation of hollow and convex arch radius [m]
i	slope steepness [%]

Table 21 gives an overview of the required minimum raw slope length and the minimum connecting arch length associated with various displacements, assuming that the angle of inclination of the road can range between 0 and 4.5 percent. The radius of the hollow and convex arch depends on the design speed of the road and the minimum unobstructed view. The hollow arch radius depends on the design speed of the road and comfort criteria.

$$R_{convex,100km/h} = 8300 \text{ m}, \quad R_{convex,80km/h} = 5000 \text{ m}, \quad R_{convex,50km/h} = 1100 \text{ m}$$

$$R_{hollow,100km/h} = 850 \text{ m}, \quad R_{hollow,80km/h} = 500 \text{ m}, \quad R_{hollow,50km/h} = 200 \text{ m}$$

H [m]	L_{min} [m] 1 – 4.5%	100 km/h		80 km/h		50 km/h	
		L_{arches} [m]	i [%]	L_{arches} [m]	i [%]	L_{arches} [m]	i [%]
0.1	2 - 10	43	0.5	33	0.6	16	1.3
0.5	11 - 50	96	1.0	74	1.4	36	2.8
1.0	22 - 100	135	1.5	105	1.9	51	3.9

Table 21 - Slope lengths necessary regarding displacements U_z

From Table 21 it clearly shows that none of the calculated slope angles exceed the maximum angle of 4.5 percent. The minimum connecting arch lengths are however relatively large. A displacement U_z of more than 0.5 meter therefore is not practical, even when considering dividing the displacement in sections. The connecting arches require such large lengths that it becomes nearly impossible to even consider a practical solution. The displacement of 0.5 meter demands a minimum connecting arch slope length of more than 50 meters. Larger displacements will increase the required slope length to reconnect the road and these larger lengths are considered impractical. The maximum displacement U_z of 0.5 meters excludes end joints 3, 5, 7, and 9 as viable solutions.

Rotations

Besides the displacements, the maximum rotations need to be considered as well. At first approximation, the maximum rotation R_y is set to 4,5 percent, comparable to the maximum slope for highway traffic roads. The rotation R_y needs to be limited even further when considering the length of the connecting arch or plate between the two tunnel segments. The arch length or length of the plate can be calculated with the following formula;

$$L_{plate} = 2\pi \cdot R_{hollow} \cdot \frac{\theta}{360^\circ}$$

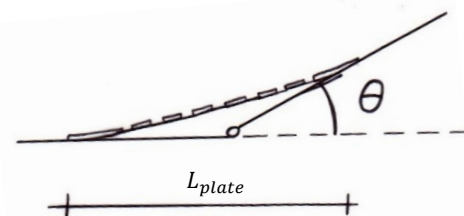


Figure 66 - Hollow arch length with rotation R_y

A rotation of 1.15 degrees (2% slope or 20 mrad rotation) results in a large plate length of 17 meters, assuming a design speed of 100 km/h. Lowering the design speed to 80 km/h, lowers the length of the plate to 10 meters, which is still quite large. The smaller rotations R_y which occur for some of the types of end joint result in more favourable values of the plate length. A rotation R_y of 2 mrad (0.11 degree angle or 0.2% slope) and a design speed of 100 km/h results in a more practical length of the plate equal to 1.6 meters. End joints 3 and 5 have a rotation R_y larger than 20 mrad and are therefore excluded as viable solutions.

End joints 4 and 5 are the only ones which have a rotation R_z which are equal to 9 mrad (0.52 degrees). Common sense concludes that such small rotations are acceptable in a flexible end joint. It is valuable to determine however what the limiting rotation of the tunnel structure is. Safety regulations for roads state that a certain unobstructed view is required for the road users. A design speed of 100 km/h results in a free line of sight equal to 185 meters. Using the line of sight requirement, the maximum rotation can be determined.

The minimal inner horizontal arch due to the required unobstructed view is determined with the following formula;

$$R_H = \frac{z^2}{8(a+2)}$$

6.4.3. Conclusion

The type on end joint has a large influence on the displacements, rotations and force distributions of the tunnel. Real life limitations and construction capacity reduce the number of viable solutions.

The types of end joint remaining are; 1, 2, 4 and 6. Their properties are stated again in Table 22. The blue shaded area indicates the degrees of freedom which are allowed in the end joint. The values of the displacements [mm], rotations [mrad], moments [kNm] and shear forces [kN] are rounded off because the variation of these values is of importance and not the exact value. The end joints have in common that they either have no degrees of freedom or have rotational freedom. End joint 4 has additional displacement freedom in longitudinal direction of the tunnel.

Name	U _x	U _y	U _z	R _x	R _y	R _z	M _x	M _y	M _z	V _y	V _z
1	2	9	80	0.1	0.5	0.1	13000	710700	42100	400	14000
2	0	0	0	0	1.7	0	10700	51300	37800	400	10400
4	6700	0	0	0	1.7	9.2	12300	52100	205400	3800	10400
6	0	0	0	0	1.7	0	12300	52100	37800	400	10400

Table 22 – Valuable types of End joints

The longitudinal displacement occurring at end joint 4 is quite large; 6.7 meters. The end joint has not been excluded because at the beginning of paragraph 6.4 it was stated that the horizontal stiffness component has not been taken into account in the SCIA tunnel model. The actual displacement in x-direction will be much smaller than determined with the current SCIA model. A smaller displacement U_x can be considered when creating a conceptual design for end joint 4.

The moment M_y decreases to a small 10 percent of the original value when allowing rotational freedom in the end joint, especially when rotation around the y-axis (R_y) is possible. The influence of the end joint on the moment M_x is not worth mentioning because it is relatively small. The moment M_z does increase significantly when allowing translation in longitudinal direction. The largest part of increased moment M_z is however caused due to the imperfection in the SCIA model, comparable to the large longitudinal displacement U_x .

Adding rotational freedom in the end joint decreases the moment M_y drastically and can therefore be favorable regarding the strength requirements of the end joint. Some distance from the end joint however, the moment in the tunnel structure itself doubles. The rotations create physical challenges as well and careful considerations need to be made regarding the choice of the end joint.

6.5. Conclusion

All three parameters do influence the tunnel structure when considering the full parameter range. After restricting the full parameter range with physical limitations, the effects on the tunnel structure however become very small.

The support spring stiffness k_u has a relatively large influence on the tunnel structure. The support spring stiffness however has a limited influence on the tunnel structure, when considering the range value restricted by physical limitations. The influence of the support spring stiffness governing the amount of moments and shear forces applied by the tunnel structure to the end joint, is negligible when the support spring stiffness is above $1.83 \cdot 10^1 \text{ MN/m}$.

The Norwegians apparently put a lot of thought into their design, because Bjørnafjord tunnel has the optimal solution regarding the stiffness of the support system. An increase in support spring stiffness by a tenfold and based on the static loading, is only effective and relevant for decreasing the moment in y-direction by 30% and decreasing the displacement at the outer most segments of the tunnel.

The connection spring stiffness k_ϕ has a relatively small influence compared to the two other parameters and mainly has influence on the moments in the tunnel structure. The effect of the connection stiffness is low regarding displacements. The influence of the connection stiffness on the end joint is negligible. The assumed Gina-profile with a stiffness of $1.97 \cdot 10^3 \text{ MN/m}$ is outside the parameter range. Using a flexible Gina-profile by itself with a connection stiffness far less than required, will not be practical. Adapting the Gina-profile to fit the requirements would render a fixed-like coupling which are already at hand.

The type of end joint **SC** has a relatively large influence on the tunnel structure. The remaining types of end joints are numbers 1, 2, 4 and 6. The end joints have in common that they either have no degrees of freedom or have rotational freedom. Adding rotational freedom in the end joint decreases the moment M_y drastically (to 10%) and therefore can be favourable in respect to the strength requirements of the end joint. Some distance from the end joint however, the moment in the tunnel structure itself doubles. The largest part of the apparent increased moment M_z and the longitudinal displacement U_x is caused due to an imperfection in the SCIA model: the horizontal stiffness component has not been taken into account in the SCIA tunnel model.

The lack of horizontal stiffness in the SCIA model distorts the research of different types of end joints, but it does not significantly influence the other two parameter studies (k_u and k_ϕ). The support spring stiffness and the connection stiffness influence the vertical stiffness and only marginally influence the horizontal stiffness.

7. Conceptual Design of the End Joint

A conceptual design of the end joints will be created in this chapter, to accommodate the displacements, rotations, forces and bending moments found during the parameter study. These first designs are focused on tackling the basic principles and creating a probable solution. Detailed mechanical solutions will not be considered.

The parameter study gives a good overview of the influence of the three different parameters on the tunnel structure. The influence of the support spring stiffness and connection stiffness on the end joints are negligible and are therefore not considered any further regarding the conceptual design of the end joint.

Variants are considered based on the different types of end joint which are applicable in the tunnel structure of the Bjørnafjord. Each variant must provide a watertight connection and needs to be able to transfer the forces in the end joint.

7.1. Variants

Multiple types of end joints are applicable in the Bjørnafjord design. End joint 1 is equal to the end joint applied in the Bjørnafjord. The fixed end joint is a plausible variant as found during the parameter study.

Three other concepts of the end joints have evolved from the parameter study. End joints 2, 4 and 6 however are almost the same, because they mostly have the same degrees of freedom. End joint 4 has an additional degree of freedom compared to end joints 2 and 6. A concept design of end joint 4 will envelope the design of the other two end joints.

A third variant will be considered as well. The end joint will be a combination of the fixed and partial free end joint. In this variant, the initial deformations and translations can take place after which the end joint will be fixated.

Variant	Type of End joint	Degrees of freedom
Variant 1	number 1: Fixed end joint	None
Variant 2	number 4: Partially free end joint	Ux, Ry, Rz
Variant 3	Combination	restricted Ux, Ry, Rz

Figure 68 - Variants of the end joint

7.1.1. Fixed end joint

The fixed end joint is a connection without any degrees of freedom. This type of end joint is applied in the Bjørnafjord SFT design. The end joint of the Bjørnafjord SFT consists of three parts; the abutment restraint, the transition to the hard rock tunnel and the end box of the SFT itself (see Figure 69).

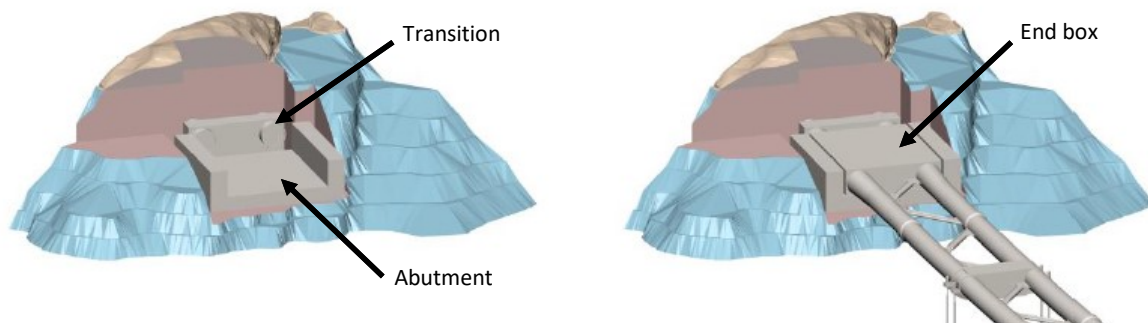


Figure 69 - Landfall arrangement prior to installation and in operation [33]

The abutment restraint of the SFT consist of a large gravity based concrete box caissons, founded on a prepared bedrock base. The support caisson is set down directly on a levelled bedrock base and under base grouted with concrete to ensure bonding between the caisson and the bedrock. The support caisson is ballasted with solid ballast (iron ore) after final placement, to ensure adequate stability and fixed end support for the SFT [33].

The transition of the SFT to the hard rock tunnel is also constructed with a caisson and filled with solid ballast.

The end anchorage of the tube bridge is constituted by a box-shaped cellular structure connecting the two main tubes. The transition element is in contrast practically unloaded and will be ballasted permanently with water.

In the Bjørnafjord design of the end joint, it is conservatively assumed that the restraint is provided by on-bottom weight (i.e. gravity) and base friction only. At the time the design was made, limited information about the bedrock geology was available. Installation of rock anchors, shear dowels and activation of lateral hard rock support are potential measures that can be utilized in further optimization [33].

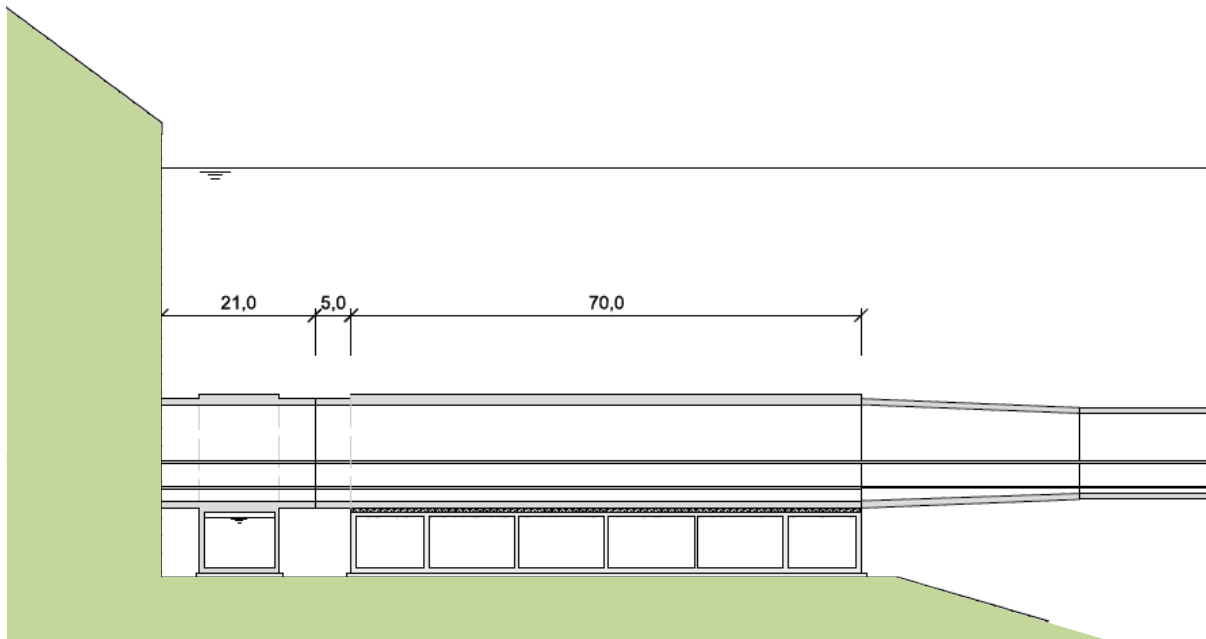


Figure 70 - Cross-section side view fixed end joint [33]

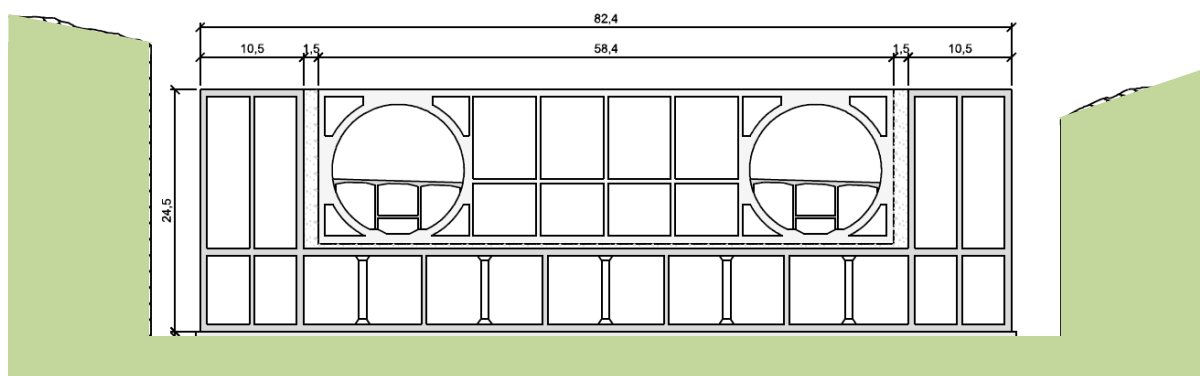


Figure 71 - Cross-sections front view fixed end joint [33]

7.1.2. Partially free end joint

Variant 2 will consist of an end joint with rotation and translation freedom. End joint 4 is taken as an example, because this end joint has the largest amount of degrees of freedom, enveloping the other types of end joints (end joints 2 and 6).

Previously it was mentioned that the SCIA model has a lack of horizontal stiffness. The latter probably causes the very large displacement U_x equal to 6.7 meters. It is considered that the 6.7 meters is an initial displacement and that the remaining continuing movement in the end joint only consist a small fraction of the total displacement.

The displacement is caused by the nett force which is a result of the self-weight of the tunnel and the displaced water volume. The variance of the self-weight is assumed to be 5% and the variance of water is 2% due to the density differences between salt and fresh water. A conservative approach is taken by assuming a displacement of 10% of the initial displacement. A remaining displacement U_x between 0.5 and 1 meter is considered in this variant.

Variant 2 also has rotational freedom; rotation around the z-axis R_z and rotation around the y-axis R_y . The rotations in end joint 4 are very small, smaller than one degree. The static loading results in a rotation R_y of 2 mrad (equal to an angle of 0.11 degrees or a 0.2% slope) and a rotation R_z of 9.2 mrad (equal to an angle of 0.5 degrees).

These small rotations can probably be compensated by special expansion junctions. The small rotation R_y for example can be accommodated by an expansion joint such as cantilever joints (finger joint), see Figure 72.

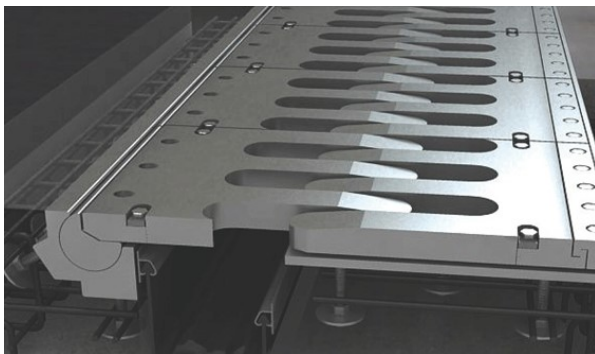


Figure 72 - Cantilever finger joint³

The rotation R_z is a more challenging degree of freedom regarding reconnecting the road. The rotation R_z has a maximum value of 8 degrees due to physical limitations, which has been determined in paragraph 6.4.2. A practical solution could be a seismic joint with a lamella system, such as the MAURER Swivel-Joist Expansion Joint [38] [39]. These type of expansion joints are especially designed to withstand large displacements in any direction.



Figure 73 - Seismic lamella joint [38]

³ http://www.joostdevree.nl/bouwkunde2/jpgv/voegovergang_staal_51_vingervoeg_earthquake_resistant_expansion_www_ilwontec_com.jpg

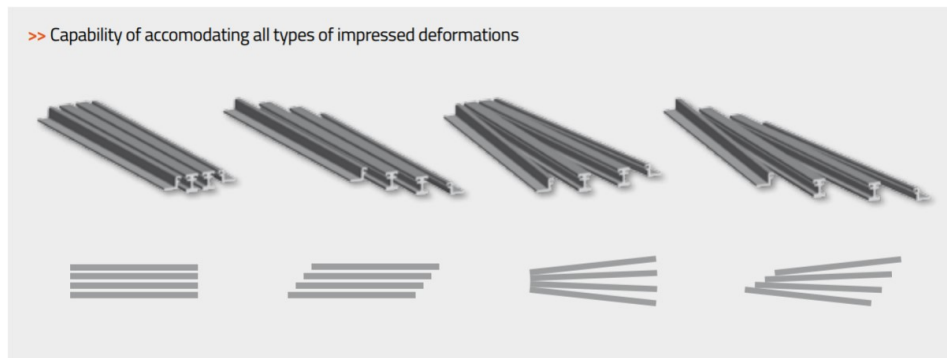


Figure 74 - Deformation capabilities [38]

Concept design

The above mentioned practical solutions considers the degrees of freedom as separate sections. Additional research is necessary to determine whether combining multiple degrees of freedom in a single joint or to keep these degrees of freedom separate influences factors such as construction costs, failure probabilities and maintenance.

An optional flexible end joint could be to continue developing a seismic expansion joint and adapting it to the specific requirements of the SFT. The seismic expansion joint appears to be a promising candidate as it already can accommodate some extreme situations.

Another possibility to design the end joint is to combine systems from different engineering sections, such as multiple expansion joints placed in series, the connection plates between train wagons, the water seals from immersed tunnelling and the synthetic flexible connection of the body work on an articulated bus. Examples of a water tight connection is sketched in Figure 75. On the left side is a combination of the omega seal from immersed tunnelling and a seal inspired by the articulated bus. On the right side is omega seal combined with a concept of a sliding outer seal secured on one side by some type of magnet. The double omega seal allows for larger displacements.

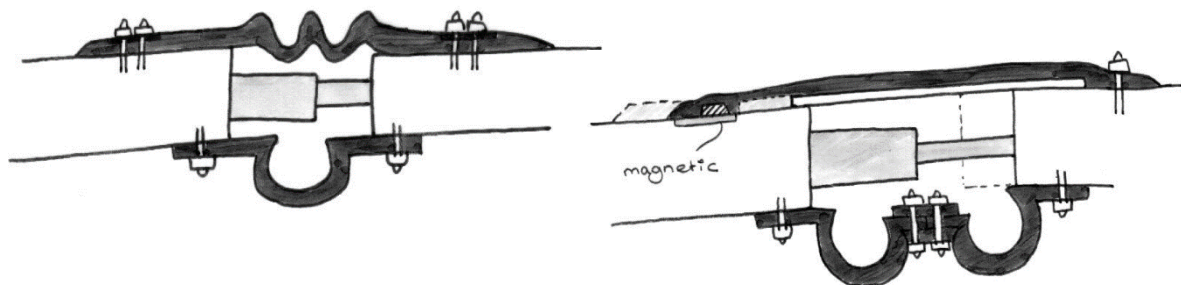


Figure 75 - Examples water tight connection

Forces and moments need to be transferred in the end joint as well. The initial idea is to use hydraulic rams on the full cross-section ring to transfer the forces and keep the joint flexible. A single hydraulic ram cannot endure/bear moments. The moments can probably be compensated when the full ring of hydraulic rams acts as a single system and has an active control system. The active control system increases and decreases the fluid pressure in the jacks. The different forces in each ram together create a resulting moment in the end joint.

Three sketches illustrate the conceptual design of the end joint. Two for the rotations (Figure 77) and one for the displacement in longitudinal direction (Figure 78). The degrees of freedom were individually illustrated to ease the several options relating water tightness and road connection available. Both designs can be combined if the hydraulic rams have enough strength to bear the forces and moments in the end joint. Additional attachment points need to be added if the strength of the rams is insufficient. Displacements and rotations in the sketches are exaggerated to clearly see what happens.

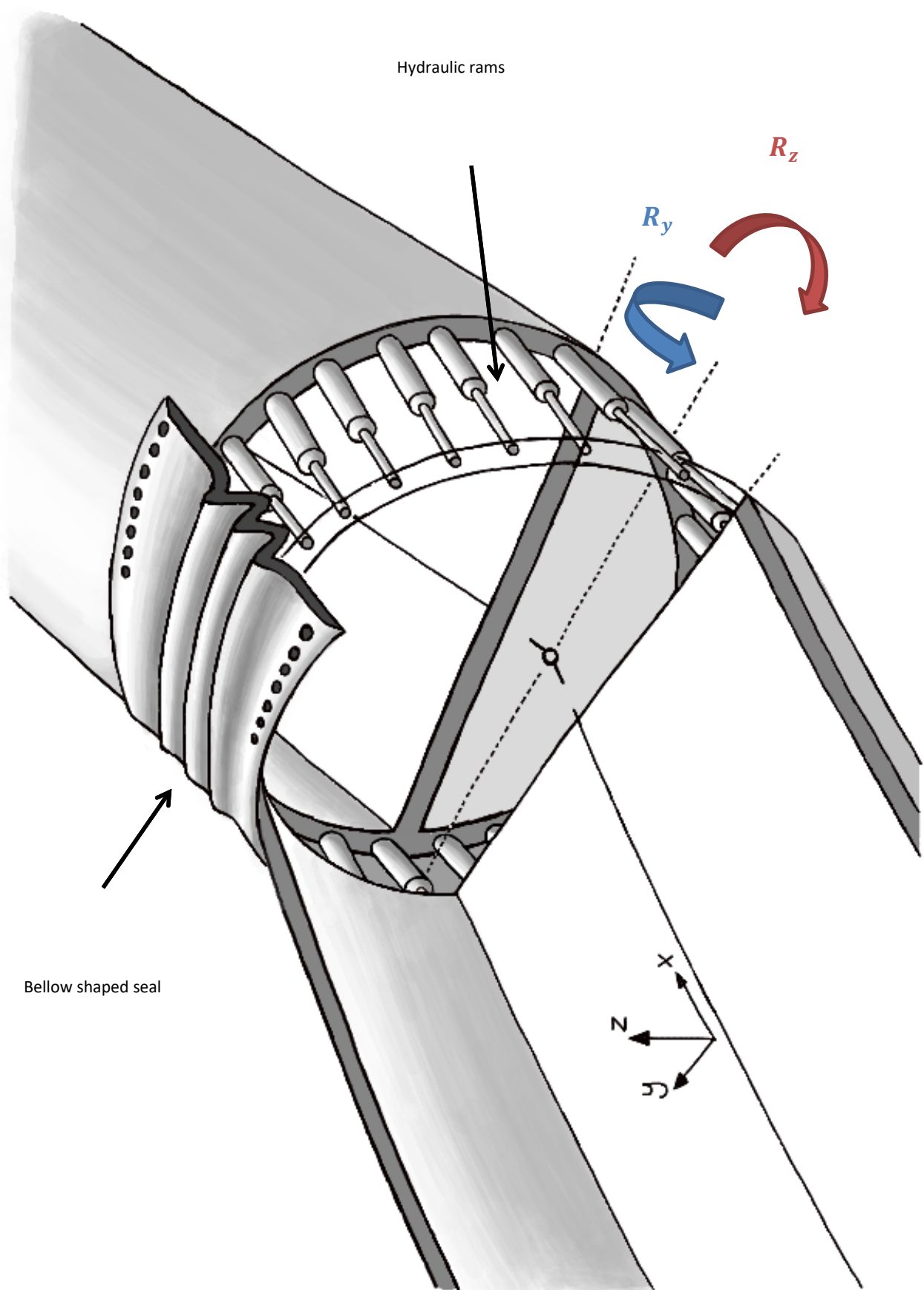


Figure 76 - Concept design for rotations

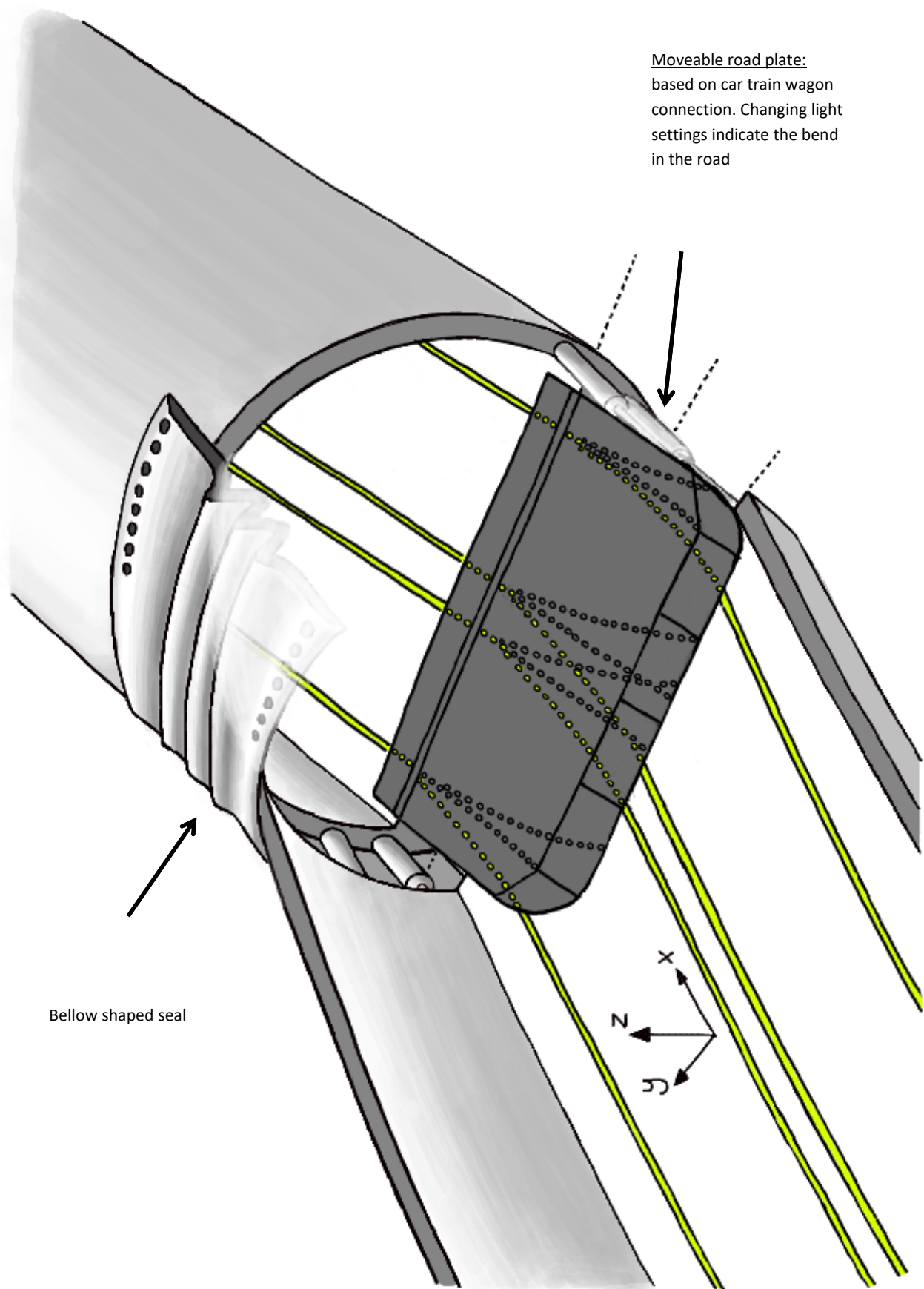


Figure 77 - Concept design for rotations

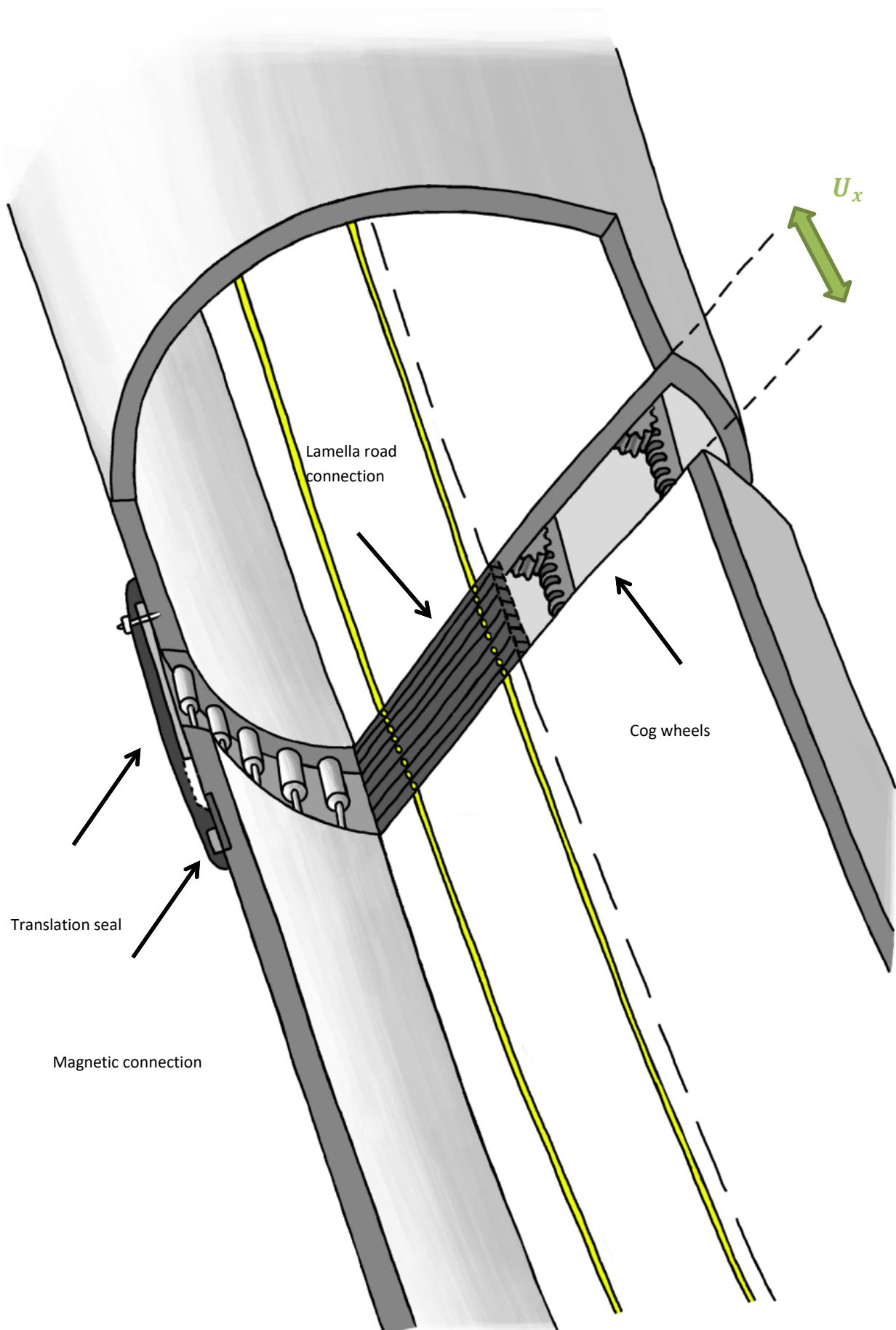


Figure 78 - Concept design for longitudinal displacement

7.1.3. Delayed fixed end joint

A combination of the two previous variants is considered; not fully fixed but also not entirely free either. The initial translations and rotations can take place, after which the end joint will be fixated.

This type of end joint especially becomes interesting when the end joint needs to accommodate the variable part of the total deformations, not the total initial deformations. There is no need for extreme expansion joints and complex elements, because the large initial deformations do not have to be compensated in these expansion joints.

Concept design

The delayed fixed end joint consists of two elements; the permanent flexibility with a small range in deformations and a segment which accommodates the temporary initial deformations.

The permanent flexibility can be accommodated with the existing expansion joints and roadway expansion joints (as mentioned in paragraph 7.1.2).

An abutment caisson which is larger than the actual interlocking end section of the tunnel could arrange the needed space for the initial deformation to take place. When the initial settlements have taken place, the gaps can be filled with stabilised ballast materials (i.e. concrete, grout).

Another possibility to accommodate the initial deformations could be by using a telescopic joint, like a thermal expansion joint, part of pipeline systems or the longitudinal adaptable connection as is applied in the Unkapani project (see Appendix A, paragraph 9.2 and 9.3). The telescopic joint may be guided by guide rails which could later on be used to limit longitudinal displacement. The disadvantage of the telescopic joint is that only the longitudinal displacement can be accommodated.

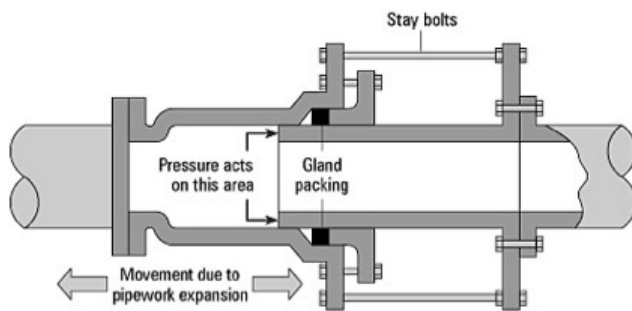


Figure 79 - Telescopic expansion joint⁴

⁴ <http://www.sunnysteel.com/images/What-different-varieties-of-expansion-joints-are-there.jpg>

7.2. Conclusion

Multiple types of end joints may be suitable in the Submerged Floating Tunnel structure, not just a single type of end joint. The most obvious and easy solution is the fixed end joint which has no movable or technically complicated elements with the resulting higher cost of maintenance. The fixed end joint is recommended, provided that the remaining set of parameters is carefully selected to keep moments and shear forces in the end joint within acceptable ranges.

The 'partially free' end joint as well as the 'delayed fixed' end joint however do have potential and should be taken into consideration during the design process. The range of the degrees of freedom of motion need to be limited for the end joint to remain physically practical.

In chapter 6 it was initially assumed that displacements in axial direction of the tunnel up till 10 meters would be acceptable in the end joint. It will however not be practical to accommodate large displacement U_x from 2 till 10 meters in a single end joint. Linking multiple end joints may be considered to compensate larger displacements.

The flexibility of the end joint has to be limited for practical and constructive reasons. It is advised that within a single end joint, the degrees of freedom are limited to the following values;

$$U_x \leq 2 \text{ meter}$$

$$U_z \leq 0.1 \text{ meter}$$

$$R_y \leq 5^\circ$$

$$R_z \leq 1^\circ$$

8. Conclusion

The aim of this research thesis is to design an end joint which is suitable for the specific circumstances surrounding a Submerged Floating Tunnel. Multiple aspects influence the design of the tunnel structure and the end joint connection. It can be concluded from the research that multiple types of end joints may be suitable in the Submerged Floating Tunnel structure. The fixed end joint appears to be most recommendable in view of ease of construction and expected lowest cost of maintenance.

The SFT design in the Bjørnafjord in Norway has been considered and modelled in the FEM computer program SCIA. Only the static loading is considered for the tunnel structure. The current, due to tides, and the waves were modelled as a distributed static load along the tunnel. The wave force is negligible because it only has a relatively small influence due to the depth of the tunnel of more than 30 m. The load combination of the nett vertical force (i.e. the buoyancy force minus the tunnel weight) and the horizontal current during slack tide is governing.

The most significant parameters have been studied regarding their influence on the tunnel structure and the end joint.

- The support spring stiffness k_u (i.e. the stiffness of the tethers or pontoon supports) has a relatively large influence on the tunnel structure. The support spring stiffness however has a limited influence on the tunnel structure, when considering the range restricted by physical limitations. The Norwegians in designing the Bjørnafjord tunnel have found the optimal solution regarding the stiffness of the support system.
- The connection spring stiffness k_ϕ (i.e. the type of connection between the different tube sections) has a relatively small influence compared to the two other parameters and hardly influences the moments in the end joint. In the Bjørnafjord SFT structure, the low connection spring stiffness has a negative effect on the moment distribution. The segment connections therefore need to be fixed connections.
- The type of end joint **SC** has a relatively large influence on the tunnel structure. The types of end joint applicable in a SFT have in common that they either have no degrees of freedom or have rotational freedom. Not limiting the rotational degree of freedom in the end joint proves to be favourable for the moment M_y at the end joint, but the moment in the tunnel structure itself doubles. Rotational freedom of the end joint allowing rotations during static loading will create physical challenges.

The lack of horizontal stiffness in the SCIA model distorts the research of different types of end joints, but it does not significantly influence the other two parameter studies (k_u and k_ϕ). The support spring stiffness and the connection stiffness influence the vertical stiffness and only marginally influence the horizontal stiffness.

The conceptual designs of the end joint have potential. Either large forces or deformations have to be transferred in the end joint. The most obvious and easy solution is the fixed end joint, which also has been designed in the Bjørnafjord. This research showed that existing flexible connecting elements from other fields of engineering may be incorporated into the end joint design. Some proposals have been made for flexible end joint solutions. The ‘partially free’ end joint as well as the ‘delayed fixed’ end joint have potential and should be taken into consideration during the design process. To remain physically practical, the ranges of the degrees of freedom of motion need to be limited.

Finalising the study, the following conclusions were drawn to the research questions:

Main question

“What type of end joint is recommended for a submerged floating tunnel?”

This research shows that multiple types of end joints may be suitable in the Submerged Floating Tunnel structure, not just a single type of end joint. The most obvious and easy solution is the fixed end joint which has no movable or technically complicated elements with the resulting higher cost of maintenance. The ‘partially free’ end joint as well as the ‘delayed fixed’ end joint however do have potential and should be taken into consideration during the design process. To remain physically practical, the range of the degrees of freedom of motion need to be limited to:

$$U_x \leq 2 \text{ meter}, \quad U_z \leq 0.1 \text{ meter}, \quad R_y \leq 5^\circ, \quad R_z \leq 1^\circ$$

Sub questions

- Which load cases need to be taken into account?

Only static loading has been considered in this research. The wave force only has a relatively small influence because of the depth position of the tunnel of 30 m and therefore the wave force is not taken into account in this thesis. The current, due to tides, was modelled as a distributed static load along the tunnel. The load combination of the nett vertical force (i.e. the buoyancy force minus the tunnel weight) and the horizontal current during slack tide is governing. Dynamic loading of the tunnel will also be of influence which was not considered in this study, but must be looked into.

- Which variable parameters are taken into account?

The most significant parameters for the Bjørnafjord crossing are studied to get a better understanding on how these parameters affect the response of structure. The parameters which have been investigated are: the spring stiffness of the vertical supports of the tunnel k_u , the connection stiffness k_ϕ between the tunnel segments and the type of end joint **SC**. Other parameters, for example the structure stiffness EI, have not been considered.

- What is the influence of these parameters on the end joint and on the total structure?

The support spring stiffness k_u only has limited influence on the tunnel structure and the end joint. The Norwegians apparently put a lot of thought into their design, because Bjørnafjord tunnel has the optimal solution regarding the stiffness of the support system.

The segment connections k_ϕ do have an influence on the moment distribution on the total structure, but hardly influences the moments in the end joint. In the Bjørnafjord SFT structure the low connection stiffness has a negative effect on the moment distribution. The segment connections therefore need to be fixed connections.

The types of end joint **SC** applicable in a SFT, have in common that they either have no degrees of freedom or have rotational freedom. Not limiting the rotational degree of freedom in the end joint decreases the moment M_y drastically to a meager 10% of the original design value and therefore can be favourable in respect to the strength requirements of the end joint. Rotational freedom of the end joint allowing rotations during static loading will create physical challenges.

- Which load transfers does the end joint have to absorb?

The value of the loads that need to be transferred in the end joint depend on the degrees of freedom which are allowed in the end joint. All loads remain presents in the end joint; normal forces, shear forces and bending moments in range of respectively 26 MN, 10 MN and 38 till 710 MN.

- Which connections are already available for the end joint?

Only the option of the fixed end joint has been designed in the Bjørnafjord. No other specific type of design for the SFT end joint has been mentioned in literature. Existing connecting elements from other fields of engineering may be incorporated into the end joint design. In chapter 7, proposals are made for other potential solutions. The fixed end joint appears to be most recommendable in view of ease of construction and expected lowest cost of maintenance.

- How to maintain the joint's water tightness?

The Gina-profile is not applicable because of the rotations in the end joint. Initial sketches combining the omega profile and a bellow shaped synthetic profile are the first steps towards flexibility and water tightness.

9. Recommendations

This study resulted in a better understanding in the development of end joint for the SFT. Several aspects were studied but not all aspects were studied in full depth. To gain more, better and/or more detailed insight in the end joint structures the following recommendations are made:

- Only the static loading is considered for the tunnel structure. Considering both the static and dynamic loading gives a better overview of the relevancy these loads play in the force distributions and deformations of the tunnel. The ratio static vs dynamic loading is paramount in accessing lifetime issues such as fatigue and maintenance.
- The load case combining the nett force and the current due to slack tide is governing. This however is based on the assumed direction and distribution of the current along the tunnel. It is advised to examine the current direction and profile in more detail to get a more accurate result on the influence of the current on the tunnel structure.
- The SCIA model has to be improved, starting with the addition of horizontal stiffness. The lack of horizontal stiffness in the SCIA model hampers the parameter study of different types of end joints the most.
- A probabilistic level I approach, in which safety factors are applied, has been used in the analysis of the SCIA model and the parameter study in this research. A full probabilistic analysis however should be performed to consider the influence of the variance of several parameters. Varying multiple parameters at the same time gives a better overview of the effect of the parameters on the structure when the combined unfavourable values of the parameters cause the most undesirable event.
Also, the occurrence of multiple tether support failure needs to be considered. The probability of failure of the full structure is then accounted for.
- The end joints with rotational and translational degree freedom cause physical challenges. Careful considerations need to be made regarding the choice of the type of end joint, finding a compromise between on one hand the large forces in the end joint and on the other hand deformations and rotations which both cause physical challenges.

References

- [1] H. Yan, F. Zhang, J. Yu, The Lectotype Optimization Study on Submerged Floating Tunnel Based Delphi Method, *Procedia Engineering SUFTUS*. 166 (2016) 118–126. doi:10.1016/j.proeng.2016.11.574.
- [2] A.B. Kawade, S.P. Meghe, Submerged Floating Tunnel, *Civil Engineering Portal*. (2014) 1–9. <http://www.engineeringcivil.com/submerged-floating-tunnel.html>.
- [3] F.M. Mazzolani, B. Faggiano, M. Esposto, G. Martire, A new challenge for strait crossings : the immersed inversed cable supported bridge, *Department of Structural Engineering, University of Naples “Federico II”, Italy*. (2009) 138–145.
- [4] E. Wahyuni, Effect of Triangle Cables Configuration on the Behavior of Reinforced Concrete Submerged Floating Tunnel under Hydrodynamic Load, *Procedia Engineering IABSE*. 39 (2017) 3045–3051.
- [5] K. Zhang, Y. Xiang, Y. Du, Research on tubular segment design of submerged floating tunnel, *Procedia Engineering ISAB*. 4 (2010) 199–205. doi:10.1016/j.proeng.2010.08.023.
- [6] M. Eidem, A. Fjeld, T.O. Olsen, Basic design for a Submerged Floating Tube Bridge across the Digernessundet, *Procedia Engineering IABSE*. 39 (2017) 3018–3024.
- [7] K. Li, X. Jiang, Research on Section Form of Submerged Floating Tunnels Considering Structural Internal Force Optimization under Fluid Action, *Procedia Engineering SUFTUS*. 166 (2016) 288–295. doi:10.1016/j.proeng.2016.11.551.
- [8] F.M. Mazzolani, B. Faggiano, G. Martire, Design aspects of the AB prototype in the Qiandao Lake, *Procedia Engineering ISAB*. 4 (2010) 21–33. doi:10.1016/j.proeng.2010.08.005.
- [9] Y. Li, M. Lin, Hydrodynamic coefficients induced by waves and currents for submerged circular cylinder, *Procedia Engineering ISAB*. 4 (2010) 253–261. doi:10.1016/j.proeng.2010.08.029.
- [10] M.S. Dong, G.P. Miao, L.C. Yong, Z.R. Niu, H.P. Pang, C.Q. Hou, Effect of escape device for Submerged Floating Tunnel (SFT) on hydrodynamic loads applied to SFT, *Journal of Hydrodynamics*. 24 (2012) 609–616. doi:10.1016/S1001-6058(11)60284-9.
- [11] A. Mandara, E. Russo, B. Faggiano, F.M. Mazzolani, Analysis of Fluid-structure Interaction for a Submerged Floating Tunnel, *Procedia Engineering SUFTUS*. 166 (2016) 397–404. doi:10.1016/j.proeng.2016.11.572.
- [12] X. Long, F. Ge, Y. Hong, Feasibility study on buoyancy–weight ratios of a submerged floating tunnel prototype subjected to hydrodynamic loads, *Acta Mechanica Sinica/Lixue Xuebao*. 31 (2015) 750–761. doi:10.1007/s10409-015-0428-3.
- [13] W. Chen, Z. Zheng, M. Li, Multi-mode vortex-induced vibration of slender cable experiencing shear flow, *Procedia Engineering ISAB*. 4 (2010) 145–152. doi:10.1016/j.proeng.2010.08.017.
- [14] A.S. Brandtsegg, *Dynamic Modelling and Analysis of Submerged Floating Tunnels*, Norwegian University of Science and Technology, 2012.
- [15] W. Chen, Y. Li, Y. Fu, S. Guo, On Mode Competition during VIVs of Flexible SFT’s Flexible Cylindrical Body Experiencing Lineally Sheared Current, *Procedia Engineering SUFTUS*. 166 (2016) 190–201. doi:10.1016/j.proeng.2016.11.582.
- [16] S. Kim, Hydrodynamic analysis of the submerged floating tunnels under irregular waves, *Procedia Engineering IABSE*. 39 (2017) 3025–3032.
- [17] H. Kunisu, Evaluation of wave force acting on Submerged Floating Tunnels, *Procedia Engineering ISAB*. 4 (2010) 99–105. doi:10.1016/j.proeng.2010.08.012.
- [18] S.N. Sun, Z. Bin Su, Hydrodynamic Pressure on Submerged Floating Tunnel under the P-Wave, *Applied Mechanics and Materials*. 858 (2016) 125–130. doi:10.4028/www.scientific.net/AMM.858.125.
- [19] M.S. Dong, L. Man, The Dynamic Responses of the of the Submerged Floating Tunnel under Seismic effect, *Procedia*

- Engineering SUFTUS. 166 (2016) 152–159. doi:10.1016/j.proeng.2016.11.578.
- [20] G. Martire, B. Faggiano, F.M. Mazzolani, A. Zollo, T.A. Stabile, Seismic analysis of a SFT solution for the Messina Strait crossing, *Procedia Engineering ISAB. 4* (2010) 303–310. doi:10.1016/j.proeng.2010.08.034.
- [21] L. Zhang, W. Chen, Z. Zheng, Controlling parameter for wave types of long flexible cable undergoing vortex-induced vibration, *Procedia Engineering ISAB. 4* (2010) 161–170. doi:10.1016/j.proeng.2010.08.019.
- [22] N. Zhang, H. Xia, W. Guo, J. Zhan, J. Yao, Y. Cao, Vehicle-bridge interaction analysis of heavy load railway, *Procedia Engineering ISAB. 4* (2010) 347–354. doi:10.1016/j.proeng.2010.08.040.
- [23] S. Zhang, L. Wang, Y. Hong, *Procedia Engineering* Vibration behavior and response to an accidental collision of SFT prototype in Qiandao Lake (China), *Procedia Engineering ISAB. 4* (2010) 189–197. doi:10.1016/j.proeng.2010.08.022.
- [24] J. Guo, S. Jiang, Z. Zhang, Fire Thermal Stress and its Damage to Subsea Immersed Tunnel, *Procedia Engineering SUFTUS. 166* (2016) 296–306. doi:10.1016/j.proeng.2016.11.552.
- [25] R. Kovalenko, R.E. Melchers, B. Chernov, Long-term immersion corrosion of steel subject to large annual variations in seawater temperature and nutrient concentration, *Structure and Infrastructure Engineering. 13* (2017) 978–987. doi:10.1080/15732479.2016.1229797.
- [26] H. Yan, Y. Yuan, J. Yu, Fatigue Reliability Analysis of Cable Considering Corrosion, *Procedia Engineering SUFTUS. 166* (2016) 127–135. doi:10.1016/j.proeng.2016.11.575.
- [27] B. Adl-Zarrabi, B. Ebrahimi, M. Hoseini, J. Johnsson, R. Mirzanamadi, M. Taljegard, Safe and Sustainable Coastal Highway Route E39, *Transportation Research Procedia. 14* (2016) 3350–3359. doi:10.1016/j.trpro.2016.05.286.
- [28] Y. Xiang, C. Liu, K. Zhang, Q. Wu, Risk analysis and management of submerged floating tunnel and its application, *Procedia Engineering ISAB. 4* (2010) 107–116. doi:10.1016/j.proeng.2010.08.013.
- [29] Y. Xiang, C. Liu, C. Chao, H. Liu, Risk analysis and assessment of public safety of submerged floating tunnel, *Procedia Engineering ISAB. 4* (2010) 117–125. doi:10.1016/j.proeng.2010.08.014.
- [30] M. Baravalle, J. K??hler, Risk and Reliability Based Calibration of Design Codes for Submerged Floating Tunnels, *Procedia Engineering SUFTUS. 166* (2016) 247–254. doi:10.1016/j.proeng.2016.11.547.
- [31] G. Martire, B. Faggiano, F.M. Mazzolani, Compared cost evaluation among traditional versus innovative strait crossing solutions, *Procedia Engineering ISAB. 4* (2010) 293–301. doi:10.1016/j.proeng.2010.08.033.
- [32] A. Nestegård, S.A. Haugerud, J. Solemsli, K.B. Engebretsen, K. Wåsjø, A. Myhr, K3 / K4 Design Basis Report - Bjornafjord submerged floating tunnel, n.d.
- [33] P. Team, K3 / K4 Technical Report - Bjornafjord submerged floating tunnel, 2016.
- [34] W. Molenaar, M. Voorendt, *Manual Hydraulic Structures*, Faculty of Civil Engineering and Geosciences, Delft, 2018.
- [35] dr. ir. R. van Nes, ir. P.B.L. Wiggenraad, prof. dr. ir. J.W.. van Lint, *Transport & Planning*, Faculty of Civil Engineering and Geosciences, Delft, 2018.
- [36] P. dr. i. J.C. Walraven, *Gewapend Beton*, Faculty of Civil Engineering and Geosciences, Delft, 2011.
- [37] Trelleborg, *Gina Gasket Brochure*, (2015). www.trelleborg.com/engineeredproducts.
- [38] MAURER, *Earthquake Protection Systems, Brochure*. (2017). https://www.maurer.eu/fileadmin/mediapool/01_products/Erdbebenschutzvorrichtungen/Broschueren_TechnischeInfo/MSO_Seismic-Brochure_A4_2017_Online.pdf.
- [39] MAURER, *Expansion Joints*, (2016). https://www.maurer.eu/fileadmin/mediapool/01_products/Dehnfugen/Broschueren_TechnischeInfo/MAU_Expansion_Joints_GB_Online.pdf.

List of Figures

Figure 1 - Continuous methods to cross a water body	1
Figure 2 - Type of SFT support[2]	2
Figure 3 - Location Bjørnafjord.....	9
Figure 4 - General crossing alignments [33]	10
Figure 5 - General SFT configuration [33].....	10
Figure 6 - Cross-section for (a) the general T9.5 profile and (b) the T12.5 lay-by profile [33]	11
Figure 7 - Typical cross tube and horizontal bracing configuration with dog bone [33]	11
Figure 8 - Landfall arrangement prior to installation and in operation [33].....	12
Figure 9 - Plan view of the pontoon-stabilized SFT [33]	12
Figure 10 - Typical sections at (a) mid-span and (b) (c) at support with and without lay-by [33]	13
Figure 11- Typical pontoon support elements [33]	13
Figure 12 - Plan view of the tether-stabilized SFT [33]	14
Figure 13 - Elevation of the tether-stabilized SFT [33]	14
Figure 14 - Typical tether support elements [33]	14
Figure 15 - Typical sections at (a) mid-span and (b) (c) at support with and without lay-by [33]	15
Figure 16 – SCIA basic model of the SFT	18
Figure 17 - Coordinate system SCIA	18
Figure 18 - Pontoon dimensions.....	20
Figure 19 - Truss stiffness parameters	20
Figure 20 – Displacement due to nett buoyance force	22
Figure 21 - Moments in y-direction due to nett buoyance force (SLS).....	22
Figure 22 - Falling and rising tidal current directions, top view	23
Figure 23 - Displacement profile caused by the falling tide, top view.....	24
Figure 24 - Moments in y-direction due to falling tide current (SLS).....	24
Figure 25 – Displacement profile caused by the rising tide, top view	24
Figure 26 – Moments in y-direction due to rising tide current (SLS)	25
Figure 27 - Loading of the tunnel structure during slack tide, top view	25
Figure 28 - Displacement of the tunnel structure due to current during slack tide, top view	25
Figure 29 - Normal forces resulting from slack tide (SLS), side view	26
Figure 30 - Moments in y-direction due to slack tide current (SLS)	26
Figure 31 – Penetration of wave loads (normalized) with water depth [33].....	26
Figure 32 - SCIA model beam identification	28
Figure 33 - Stress-diagram cross-section.....	31
Figure 34 - Analytical model of the tunnel structure.....	37
Figure 35 - Deflection along the tunnel length – Analytical approach	39
Figure 36 - Deflection along the tunnel length - SCIA model with varying spring stiffness, according to the original design ..	39
Figure 37 – Deflection along the tunnel length – SCIA model with mean spring stiffness	39
Figure 38 - Overview of variable parameters	41
Figure 39 - Types of displacement measurements in the parameter study	42
Figure 40 - Displacements due to support spring stiffness	43
Figure 41 - Displacement shape and moment line due to support spring stiffness	44
Figure 42 - Moments due to support spring stiffness	45
Figure 43 - Shear force due to support spring stiffness.....	46
Figure 44 – Moment and shear forces at the end joint due to support spring stiffness	47
Figure 45 - Gina profile before and after full contact.....	49
Figure 46 - Force-compression graph Gina-profile ETS 180/220 (Trelleborg) [37]	50
Figure 47 - Simplified Force-compression graph Gina-profile	50
Figure 48 - Units and directions determining Gina-profile stiffness	51
Figure 49 - Shift rotation axis Gina-profile	53
Figure 50 – Displacements due to segment connection stiffness	54
Figure 51 – Displacement shape and moment lines due to connection stiffness	55

Figure 52 - Moments due to connection stiffness.....	56
Figure 53 - Different systems due to connection stiffness	57
Figure 54 - Shear forces due to connection stiffness	57
Figure 55 - Traffic safety, rotation around x-axis.....	60
Figure 56 - Mechanism of the tether support	60
Figure 57 - Degrees of freedom in the end joint	61
Figure 58 - Local axis system end joint	61
Figure 59 - Displacements and rotations different types of end joints	62
Figure 60 - 3D displacement of the end joint with free translation in x-direction (nr 4).....	63
Figure 61 - 3D displacement of the Fixed end joint (nr 1)	63
Figure 62 - Moments and shear forces due to different types of end joint	64
Figure 63 - Moment line M_y of the Fixed end joint (nr 1)	65
Figure 64 - Moment line M_y of the Hinged end joint (nr 2) and end joint nr 4.....	65
Figure 65 - Minimum distance to overcome height difference	66
Figure 66 - Hollow arch length with rotation R_y	67
Figure 67 - Geometric characters overview for determining the maximum rotation	68
Figure 68 - Variants of the end joint.....	71
Figure 69 - Landfall arrangement prior to installation and in operation [33].....	71
Figure 70 - Cross-section side view fixed end joint [33]	72
Figure 71 - Cross-sections front view fixed end joint [33]	72
Figure 72 - Cantilever finger joint	73
Figure 73 - Seismic lamella joint [38].....	73
Figure 74 - Deformation capabilities [38].....	74
Figure 75 - Examples water tight connection	74
Figure 76 - Concept design for rotations	75
Figure 77 - Concept design for rotations	76
Figure 78 - Concept design for longitudinal displacement	77
Figure 79 - Telescopic expansion joint	78

List of Tables

Table 1 - Cross-sectional properties of the main tube	11
Table 2 - Basic material properties	12
Table 3- Pontoon characteristics [33].....	13
Table 4- Characteristics of the tether mooring [33]	14
Table 5 - Extreme current velocity for given return period [33].....	16
Table 6 - Highest significant wave height values [33].....	16
Table 7 - Primary swell peak values [33]	16
Table 8 - Cross-section values of the main tube as SCIA model	17
Table 9 - Material values of the SFT	17
Table 10 – Force values of the load cases in kN and kNm	28
Table 11 – Maximum displacement values of the load cases in mm	28
Table 12 - Load factors	29
Table 13 - Load combinations	29
Table 14 - SLS values	30
Table 15 - ULS values	30
Table 16 - Displacements in SLS	30
Table 17 - Displacements in ULS.....	30
Table 18 - Values parameter during each individual parameter study.....	42
Table 19 - Maximum rotations due to connection spring stiffness	56
Table 20 - Types of end joint connections	61
Table 21 - Slope lengths necessary regarding displacements Uz	67
Table 22 – Valuable types of End joints.....	69

APPENDIXES

Appendix A – General literature study

Appendix B – SCIA basic model results

Appendix C – IdeaStatica cross-section capacity

Appendix D – Gina-profile properties

Laura Bakker

MSc Hydraulic Engineering – Hydraulic Structures

2018, Delft

APPENDIX A

General Literature Study

Submerged Floating Tunnels

Laura Bakker

MSc Hydraulic Engineering – Hydraulic Structures

2018, Delft

Summary

A general literature study was performed to handpick an interesting and valuable graduation topic. The literature study has been performed using documents limited to publications, papers and reports done specifically for submerged floating tunnels (SFT). The limited resources already resulted in quite the number of documents. The observed “blank spots” are presented per aspect.

Systems

At first glance, multiple alternatives are presented, from free spans to suspension bridges turned upside down. However, many researchers restrict themselves to anchoring using simple tension piles or floating pontoons. Arguments for these preferences are not presented and/or have not been found. Only a basic comparison was made between the alternatives [1], suggesting the tether variants as the most likely winner.

Tunnel tube structure

The same arises for the structural design of the tunnel segments; few alternatives are explored. Some research has been done regarding axial forces in a concrete tunnel lining, the influence of cable configuration on the stress state of the SFT [2][3], the use of different shell materials regarding water tightness and corrosion protection [4]. Only two papers have been found with respect to the layout of the cross-section; a comparison is made between a rectangular and a tubular cross-section[5] and a comparison between an octagon and an elliptical cross-section[6].

There is a mention of the need for appropriate joints [7], but only a small note has been made on the possibility of a spherical hinge and a mechanical device [8]. Another option given is the use of known technologies from immersed tunnels, but without validation. The same holds for tunnel installations as well as the overall construction methods for SFT.

Loading

The load cases of the tunnel structure have been considered on many aspects. The coefficients induced by currents and waves have been investigated and a 2D numerical wave-current tank has been developed, agreeing with experimental data [9]. Research also has been done on the effect of a detachable escape device on the flow and wave loads [10].

Research is done on the dynamic response due to hydraulic loads and the fluid-structure interaction [11]. The structural shape indicated with the BWR is a critical parameter that influences the response of the SFT structure [12]. Considering the hydrodynamics, both currents [13–15] and wave [16,17] vortex induced vibrations have been widely accounted for. Extended research has been done on seismic response such as the individual P-wave [18,19], random excitation and multi-support excitation [20].

Dynamic response and forces have been determined in the tethers [21] as well as for the SFT itself. Dynamic response on traffic moving loads [22] and accidental loads [23] have only been explored lightly.

Other

There have been some researches regarding durability, renewability and safety. Topics which have been encountered are: fire [24], corrosion [25], fatigue [26] and the life cycle of the structure[27]. Research on these topics can be extended, in view of the basic aspects being considered only.

Risk assessment has been lightly investigated. Identifying potential risks and impact factors and developing a risk index system [28]. Researches state that the risks can be minimized to the lowest level [29]. A single research is done regarding the calibration of the design codes for SFT [30].

Only one study has been found on the cost evaluation comparing traditional water crossings and the SFT [31]. In the current design stage, costs are not that relevant in determining whether a SFT is chosen as a valuable alternative.

Conclusion

The general literature study showed a number of ‘blank spots’. The most interesting research topic has been chosen from these blank spots: the shore end joints of the SFT. With this subject, the designer would like to contribute to the development of the SFT in a creative way and hopefully contributing to the process of building the first ever SFT.

Table of Contents

Summary

1.	Introduction.....	1
1.1	Aim.....	2
1.2	Scope	2
2.	Crossing alternatives	3
2.1.	Free	3
2.2.	Pontoons.....	4
2.3.	Tethers	4
2.4.	Columns	5
2.5.	Conclusion.....	5
3.	Tunnel design	6
3.1.	Cross-sectional layout	6
3.2.	Materials	7
3.3.	Joints.....	7
3.4.	Anchoring.....	8
3.5.	Tunnel installations	8
4.	Loads on the SFT structure	9
4.1.	Flow.....	9
4.1.1.	Water pressure	9
4.1.2.	Current: drag and lift forces	9
4.1.3.	Wave loads	9
4.2.	Dynamic response.....	10
4.2.1.	Structural shape	10
4.2.2.	Earthquakes	10
4.2.3.	Hydrodynamics	11
4.3.	Internal loads	12
4.3.1.	Traffic	12
4.3.2.	Impact load	12
5.	Construction methods.....	13
6.	Safety and sustainability.....	13
6.1.	Internal and external collisions	13
6.2.	Fire	14
6.3.	Corrosion and fatigue	14
6.4.	Renewability	14
7.	Risks.....	15
7.1.	System.....	15
7.2.	Main structure	15
7.3.	Operational phase.....	15

8. Costs	15
9. Existing concepts of joints	16
9.1. Immersed tunnels	16
9.1.1. Waterproof	16
9.1.2. Force transfer	16
9.1.3. Displacements	17
9.2. Project Istanbul: Unkapani	17
9.3. Pipelines on large vessels and terminals	19
9.4. Seismic joints	19
Conclusion	20
References	21

1. Introduction

Crossing waters has been done since the beginning of time, starting with the very basics: swimming, sailing and throwing objects across the water. Bridges and later tunnels then were introduced for a more continuous connection between banks. As technology develops in time, more extravagant bridge and tunnel solutions are being constructed.

The Submerged Floating Tunnel (SFT), also called an Archimedes Bridge, is a state of the art solution for crossing deep and large waters. The concept of a SFT has been around for many decades. From just a sketch back in the late 1800s till full worked out designs the last couple of years. However, none has still been build up till today.

The SFT is a tunnel structure which pierces through a water body under the water surface level. Because the buoyancy-weight-ratio is slightly larger or smaller than one, the tunnel tends to float. The position of the tunnel is not fixed by a soil body, but the structure is secured at the shore junctions and/or tethers along the tunnel length.

The main difference of the SFT compared to the conventional tunnels is its position in the water: instead of being located on or under the bed, it passes right through the water. Figure 1 nicely illustrates these differences. The SFT is a desirable solution for locations which are, due to extreme circumstances, difficult to cross using present solutions. The main extreme circumstance which prevents the use of present day solutions is a large water depth. Very large water depths and wide waters, like in the Norwegian fjords, result in tunnels with very long vertical alignments or bridges with a very large span.

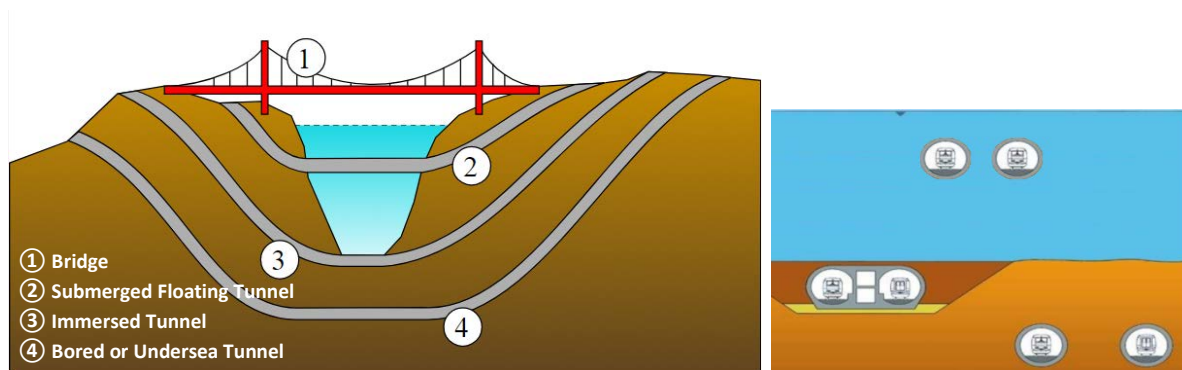


Figure 1 - Continuous methods to cross water¹

The concept of a SFT has been around for many decades. From just a sketch back in the late 1800s till full worked out designs the last couple of years. However, none has still been build up till today. Why? This literature study investigates which aspects need further research and development to be able to build a prototype of the SFT allowing real time measurements.

¹ Modified illustration: https://en.wikipedia.org/wiki/Submerged_floating_tunnel#/media/File:Bridge_types.svg
<https://pt.slideshare.net/Sagnik1/submerged-tunnel-ppt/4?smtNoRedir=1>

1.1 Aim

The aim of this literature study is to find an interesting graduation topic on the submerged floating tunnels. The method used is to document which aspects still need to be researched before building the first ever “test” submerged floating tunnel. The aim is to stay objective and to indicate the “blank spots” in the knowledge about submerged floating tunnels, from which a graduation topic can be formulated.

1.2 Scope

This literature study will be limited to publications, papers and reports done specifically for SFT. The limited resources already result in quite the number of documents. A short overview is given below.

- First SFT conference 1996
- TUST 1997 (ITA report Immersed and Floating Tunnels)
- WTC (ITA) articles relevant to SFT (2014-2016)
- ISAB 2010
- SUFTUS 2016
- IASBE papers from several different years relevant to SFT
- IASBE 2017 (only the related articles)
- Norway projects Reports: Sognefjord, Bjornafjord
- Some Chinese papers (only the ones that are in English)
- Around 30 individual articles and reports

Collecting even more documents has been halted due to the limited time and scope of this study. Hence, the literature collection cannot be seen as complete. For the objective of this study however, determining a graduation topic, the present collection of literature represents a good reflection of the research performed. Gathering even more resources therefore would not have a relevant influence on the result of this study.

2. Crossing alternatives

The exact position and design of the submerged floating tunnel depends on the surroundings of the location, each situation renders different conditions and requirements. For example, the minimal depth of any SFT is determined by the draught of the passing ships. A distinction for SFTs with equal depth positions can be made on the method of support of the SFT.

The SFT can have different types of support structures. Which type is applied mainly depends on the buoyancy to weight ratio. There are many possibilities and combinations. Four main types however can be distinguished:

- free floating
- pontoons suspended
- tension legs
- column supported

A comparison of the main forms of the submerged floating tunnels has been performed [1]: comparing aspects such as main forms, different layouts and anchorage materials using the Delphi method. *“The research paper aims to explain the problems which should be considered in the selection of the submerged floating tunnel alternatives to make a good foundation for the following design of concrete parameters”*

Each concept will be elaborated on and the scope of application of the different support systems will be considered.

2.1. Free

When the buoyancy-weight-ratio is close to one and only in case of small spans, the SFT can have a free support. It is an ideal design shape for it does not need complicated support structures. The tunnel is therefore only anchored at the shore ends.

The length limitation is of structural origin; the maximum moments and shear forces allowed in the cross-section which are caused by the distribution of the loads, are largely influenced by the length of the span. It has to be looked into whether this option could be useful for light traffic loads and certain cross-sectional dimensions, for no research has been done regarding this alternative. The reason for the lack of research on this alternative is because a regular bridge design will probably suffice in these small span cases.

Scope of application: very short distances in the order of several 100 meters.

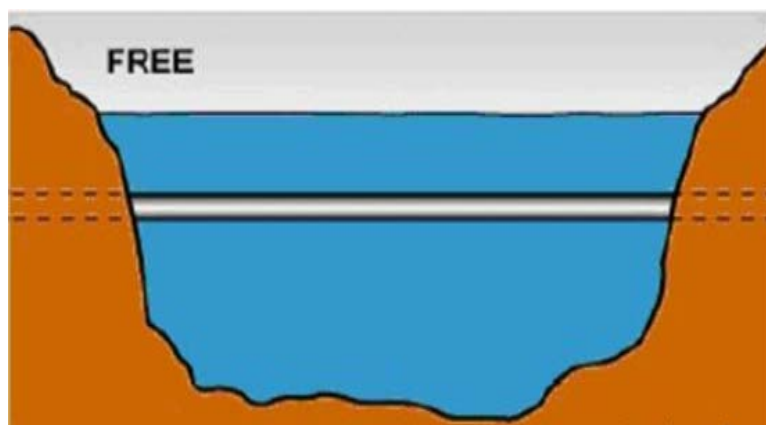


Figure 2 - Anchoring type Free[7]

2.2. Pontoons

At first glance, the pontoon supported SFT seems one of the best options available, for it is independent of the water depth. The pontoons can support fishery and tourism such as overwater facilities. Pontoon suspension however is prone to the influences of wind, waves and currents as well as at risk for collision with ships and floating ice.

The dynamic response and displacements must be looked into with caution, because the pontoons, in view of the vertical cables, can only offer the tunnel vertical restraint.

Scope of application: gentle, non-wave inland rivers and, smaller lakes and non-ice region.

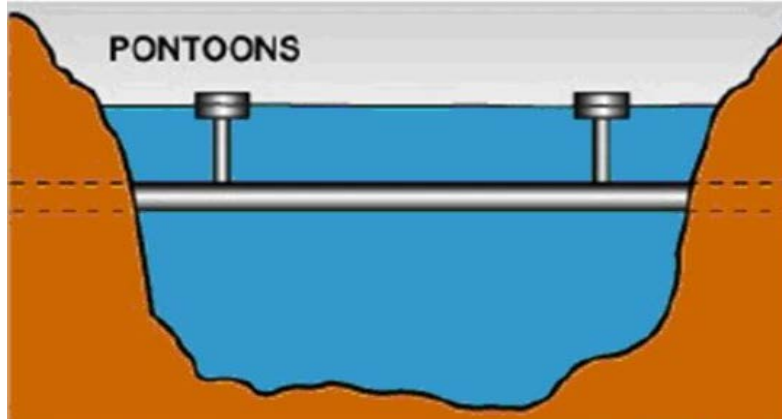


Figure 3 - Anchoring type Pontoons[7]

2.3. Tethers

There are several variants within the tether anchoring as support system for the SFT. The possibilities are endless; from different configurations of tether anchoring to the sea bed, till basically suspended bridges turned upside down. The inversed cable bridge seems convenient with respect to traditional cable bridges, however there has not been made a comparison with other tether configurations [2].

The advantage of the tether suspended tunnel is independent of the water depth and slightly depending on the underwater soil conditions. The structure is not effected by waves or floating ice and does not hinder navigation.

The water current however has quite an effect on the tunnel: fatigue damage may occur in the cables by the effect of vortex induced vibration and wear easily occurs at the upper and the lower ends of joints.

The optimal solution for tether configuration often depends on the project location. Mechanical features are different under different anchor cable arrangement modes. Four types of cable configuration have been comparatively analyzed on the structural displacement, bending moments, strength, distribution of axial tether force, wave load and water flow [32]. Each configuration has (dis)advantages and application largely depends on its location.

Scope of application: widespread use in various ocean environments.

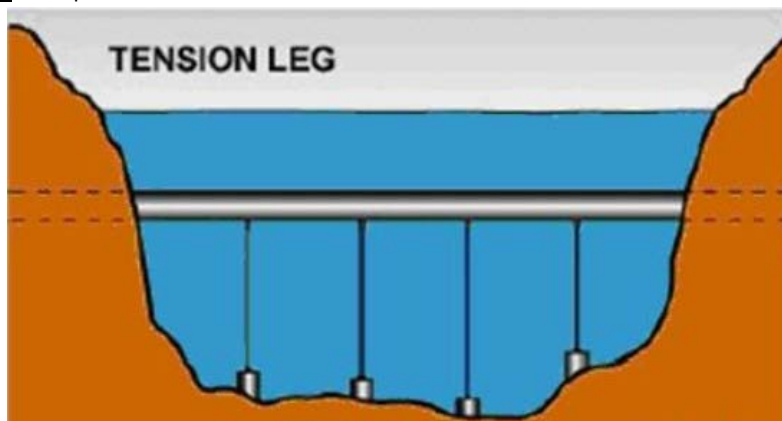


Figure 4 - Anchoring type Tether[7]

2.4. Columns

The SFT supported by columns is in fact an underwater bridge. It has a simple shape which can be substantiated with the mature knowledge of bridge structures. The column support system is limited to shallow waters because the columns cannot become too large. The construction of the columns as well as the maintenance of them under water is costly. Also, the construction has high demands of the soil conditions. This variant is therefore no longer considered as a solution to the objective of the SFT: crossing deep and/or large water bodies.

Scope of application: shallow waters, short tunnel lengths, firm bed.

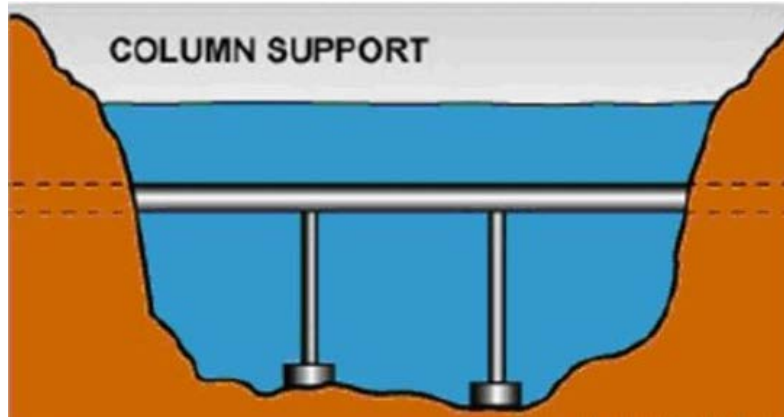


Figure 5 - Anchoring type Tether[7]

2.5. Conclusion

Each type of support has its advantages, disadvantages and scope of application. Which support system will be the best alternative needs to be considered carefully at each specific location. Both the tether and pontoon supported tunnel are suitable for deep water and large crossings, while the free span and column supported SFT are only applicable for small spans or shallow waters.

In respect of deep water crossing, the pontoon concept is considered inferior in many papers to the tether concept. In many publications, the tether concept is the preferred starting point. In general, the concept decision should be made on the geographical circumstances. If a location is agreed, a multi-criteria analysis must be done based on risks and opportunities at that specific location for both concepts.

3. Tunnel design

For basic strength calculations, such as the first estimation of dimensions, the local structural design codes can be used. In the Netherlands and Europe for example, the NEN and EN standards respectively are considered during the design. The same holds for several aspects which can be linked to offshore engineering and other industrial branches. Designing at a more detail level however, will need special attention and careful considerations whilst performing these calculations.

3.1. Cross-sectional layout

The cross-sectional dimensions depend largely on the traffic flow needing to pass through the tunnel. For example, the inner dimensions of the cross-section are determined by whether a single, double or triple lane road is necessary and if both driving directions are combined in one cross-section or kept separate by using multiple tunnel tubes. In case of a SFT, another aspect plays a significant role. Compared to immersed or bored tunnels, the SFT must deal with current and wave loads during the operational phase. Because the shape, size and stiffness of the cross-section influences the dynamic behaviour of the tunnel due to currents, and probably also due to waves, choosing a random cross-section could result in challenges which otherwise could be avoided.

Many papers assume the cross-section to be a circular tube. It can be seen as an obvious selection, considering the advantage of a better force distribution in the lining caused by the water loads. A distinct argumentation for this specific choice of cross-section however has not been given. Other cross-section alternatives therefore could show better results. For example, a rectangular cross-section could provide easier construction or additional fins could be advantageous regarding dynamic responses. The latter has been presented in a research on a side escape device [33]. The device or 'fin' reduces the drag force on a rectangular cross-section.

Expecting such considerations being done in an earlier stage, it is only in 2017 that a small research is done on the possibility of a rectangular cross-section [34]. *"The rectangular shape, compared with the circular one, is subjected to higher drag forces and important vortex shedding and is less efficient for secondary load carrying (for the plate bending)."* The rectangular cross-section however does not have a desirable shape, as was expected.

A cross-section comparison also has been made between two section forms [6]: a polygonal shape (pink) and an elliptical shape (purple), see Figure 6. The elliptical section has a better fluid and structure property than the rectangular section, but the rectangular section is beneficial for processing and transportation. Optimization of the SFT cross-section should be utilized by combining characteristics of the two forms.

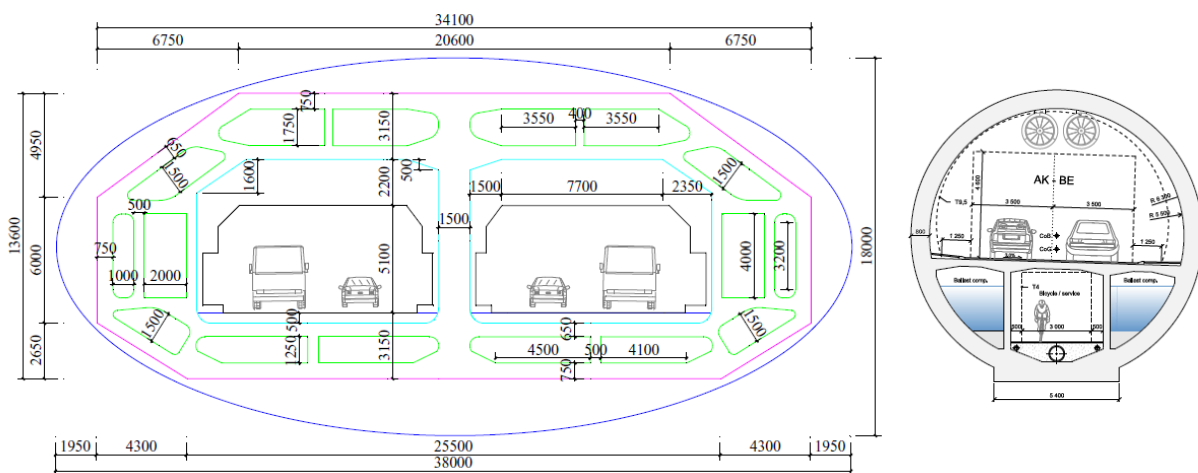


Figure 6 - Cross-section shapes of the tunnel [mm] [6]

3.2. Materials

The materials used for the SFT do not vary much. The majority of the papers consider the basic concrete tube with steel tether or pontoons supports. Researching the material possibilities could lead to a better SFT design. A small amount of papers has considered material application.

A structural property analysis and reliability assessment has been done on the SFT prototype to be built in Qiandao Lake (China) [35]. The cross-section consists of three different material layers, see Figure 7. The strengths of the SFT has been analysed under the actions of wave, current and earthquake loading. The results indicate that for wave and current loading, the SFT has a large allowance of strength. Safety of the prototype (including the joint bolts) however is not guaranteed under seismic loading.

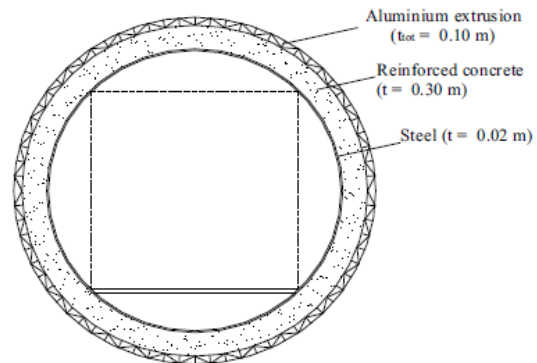


Figure 7 - Cross-section with three material layers[35]

Some suggestions are given on the material used for several aspects of the SFT [4]. Conceptual design of the tunnel elements is considered according to safety, applicability, economy, fine appearance and environmental protection. Meaningful recommendations stem from the conceptual design. The waterproof and corrosion protection is established by the steel shell. If the tube is fabricated out of concrete, self-waterproof roofing is a pivotal issue. The concrete therefore should have a low hydration heat, a high seepage resistance grade and the structural crack and shrinkage crack should be controlled within permissible range. Hydrophobic coating can be applied in crack control of SFT tube. The immersed reinforced concrete is protected from corrosion due to the lack of oxygen. Sulphate cement is not applicable.

A research has been performed on long-term loading of reinforced concrete beams with pre-stressed CFRP (carbon fibre reinforced polymer) [36]. The creep of CFRP is very small on long-term loading and therefore can be used as reinforcement material in concrete.

3.3. Joints

The SFT will most probably consist out of a segmented lining in which joints will be applied. Whether these segment joint are placed to assure flexibility in the longitudinal direction or create a fixed connection depending on the design of the SFT. The Gina and omega profile of immersed tunnels seem to be taken into the design, without further explanation or argumentation. A few papers mention the need for appropriate joints, but no structural details are given.

A clear conceptual definition of the joints and shore connections is given [7]; *“The connections of the tube to the shore require appropriate interface elements to couple the flexible water tube with the much more rigid tunnel bored in the ground. This joint should be able to restrain tube movements, without any unsustainable increase in stresses. On the other hand, the joints must be water tight to be able to prevent entry of water. Additional care in shore connections is required, especially in seismic areas, due to the risk of submarine landslides”*

A small section is dedicated to the shore connection of the Qiandao Lake design [8]. It advised that one of the shore connections must be a spherical hinge which allows both free rotations and axial displacements. The other shore end is connected to a mechanical device behaving in an elastic range which also allows plastic deformation during seismic events.

A second research on the Qiandao Lake design compares two different tunnel end connectors on the aspects of tunnel deflections, axial membrane forces at the tube segment connectors and tunnel end connectors [37]. *“If only one stress relaxation device is used in either tunnel end connector, the maximum axial membrane force occurs at the other end connector. However, if stress relaxation device is used in each tunnel end connector, the axial membrane forces will increase at each tube segment connector.”*

The study investigates only the seismic response of the Submerged Floating Tunnel (SFT) with different types of shore connections[38]. It was found that the dynamic behaviour and seismic response can be significantly changed with the change of the type of shore connections used.

3.4. Anchoring

Almost all the studies regarding the anchoring relate to the pontoons and tethers type crossings. Quite some research has been done regarding the tethers, such as tether configurations, snap forces, foundations and tension force values.

A paper illustrates some construction details of the anchoring connections [8]. Hooks are integrated into the cross-section design to connect the anchoring tethers, see Figure 8. No other papers have been found with such a detailed level regarding the anchoring connections to the tunnel tube.

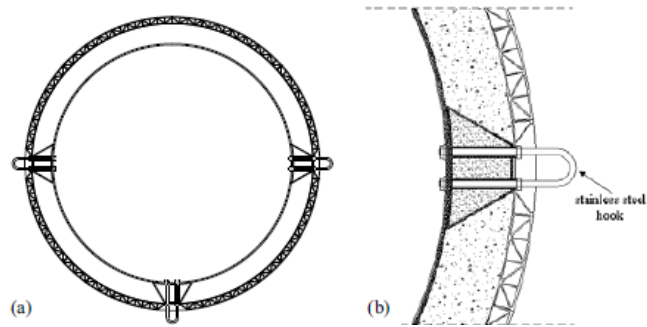


Figure 8 - Anchoring connections [8]

A possible hazard condition for the SFT is that the tethers might undergo slack. Slack phenomena in tethers under large wave heights result in snap forces [39]. Slack will occur in downstream tethers due to the current. A preliminary and fast prediction of the snap forces can be made by the practical procedure stated in the research paper.

A full numerical model of the tether which includes geometric and hydrodynamic nonlinear effects is used to assess the effect of the excitation frequency, amplitude, initial pretension, tether length and inclination angle on the tether's response [40]. The paper states the following result: *"If the design of a tether is based on extreme tension levels, no dynamic analysis is necessary to account for the effects of parametric resonance."*

An analysis has been performed on a reinforced concrete SFT under hydraulic load regarding tether configurations, tether inclination, BWR ratio, deflection and bending stresses [3]. The modeling result showed that the triangle shaped tether configuration with a 36° angle provided the optimal configuration. The SFT is feasible to be applied as an alternative water crossing structure but further investigation is necessary considering other material parameters.

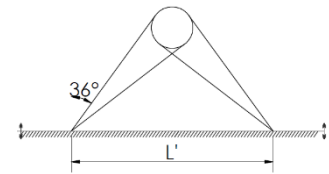


Figure 9 - Optimal tether configuration [3]

The pontoon and tether alternatives for the Bjornafjord crossing have compared on their vertical stiffness [41]. The feasibility study shows the smallest heave acceleration occurs for the tether concept.

A small number of papers investigate the anchoring mechanism of the tethers in the subsoil. A master thesis researches the foundation which uses suction caissons by performing a parametric-study of the static-pile deformation [42]. The study indicates that more refined design method is required to satisfy serviceability limit. *"Although the design for static, primarily horizontally, load cases is well established and presented in this thesis, the application of cyclic loads and its effect on the serviceability limit state is less well developed."* The thesis presents a model setup to test the cyclic response of a model suction caisson in laboratory clay.

A second research paper has been found investigating the bearing capacity of tension piles, used to anchor the tethers [43]. With the use of a two-dimensional axisymmetric finite element model, capable of simulating the shear degradation effects, the bearing capacity of tension piles in various sediments can be predicted efficiently.

3.5. Tunnel installations

The SFT main structure design and its response to the main loading conditions takes precedence over the appliance of auxiliary systems. Researches into the suitability of existing auxiliary systems, such as lighting and ventilation, for SFT therefore probably have not been carried out yet. Existing systems may be used as a template for designing the required systems for the SFT.

A single paper comments, in a small paragraph, on the two existing systems for tunnel ventilation [4]. The horizontal ventilation is reported to have a maximum functionality at a tunnel length of 2.5km. The question remains whether these existing systems are applicable for longer and larger SFTs.

4. Loads on the SFT structure

A large array of loads can be present on the SFT structure and need to be considered during the design phases. The most significant load cases and the main findings in several researches will be elaborated in this chapter.

4.1. Flow

The amount of information available about flow is limited by only considering the simulation and influences of currents and waves which specifically target the response of the SFT. Current and wave loads are often simulated in numerical programs. The dynamic response due to the current and waves is being discussed in the paragraph 4.2.3.

4.1.1. Water pressure

The Submerged Floating Tunnel is located under the water surface. The latter will result in a pressure difference over the tunnel height on the tunnel lining. Pressure variation will be present when the SFT is located in a tidal area. The extent of the relative pressure difference over the height of the tunnel is influenced by the position of the tunnel below the water surface. The influence of this pressure difference would probably be small on the structural strength of the cross-section.

A paper researches the mechanical behaviour of segmental linings with varying water pressures [44]. The paper states that the increased water pressure will result in an increase of thrust force, but a decrease of bending moment and a significant decrease of eccentricity.

4.1.2. Current: drag and lift forces

The SFT is surrounded by flowing water and it is of importance to get a good understanding of how uniform and turbulent flow act around the structure. Research and knowledge from the oil industry as well as basic fluid mechanics can probably supplement to describing the flow behaviour. Not many papers have been found on this topic specifically directed to SFT.

The effect of the escape device on the flow has been studied [10]. The hydrodynamic loads reduce in uniform flow when the escape devices are added to the sides of a box shaped cross-section. The influence of the escape device on the loads in oscillatory flow is very small and can therefore be neglected.

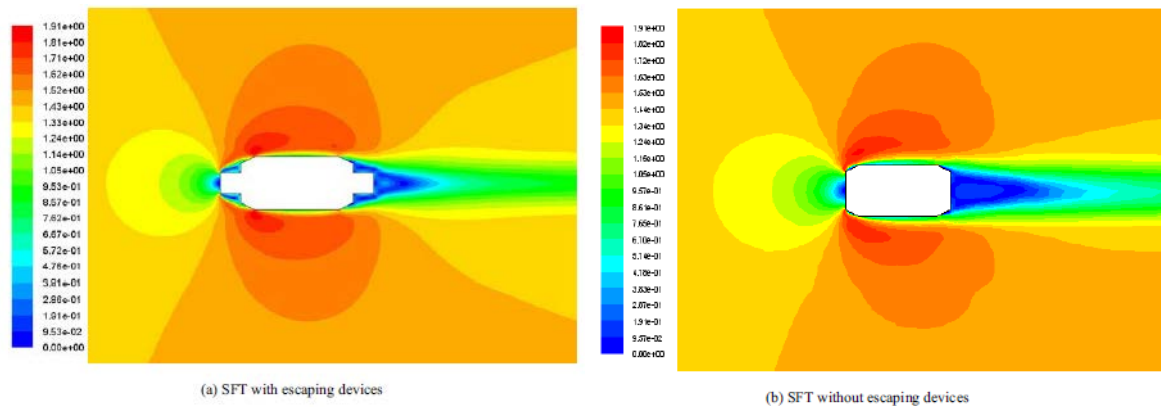


Figure 10 - Contours of velocity magnitude [10]

4.1.3. Wave loads

Wave loads depend on local circumstances. The location, as well as water depth and other marine parameters, are of influence on the wave loads. Determining the wave loads is especially challenging when considering the underwater wave load for a tether anchored SFT. Based on the location, research must be done on the local wave conditions and the resulting load on the structure.

A few papers indicate that for the tether anchored SFT, the tethers are affected by wave excitation and should be carefully analysed. The research on the escape device also considered the wave loads [10]. The horizontal wave load increases to some degree when the escape device is present, but the influence on the vertical wave load is much larger which should be taken into consideration.

A 2D numerical wave-current tank which has been developed, agrees well with experimental data [9]. The simulated wave forces have been used to derive drag and inertia coefficients. *“The drag coefficients decrease significantly with increase in KC (a number indicative for the horizontal velocity) for both directions, while the inertia coefficients decrease slightly with increase of KC. In addition, the coefficients induced by waves and wave-current flows are compared. The results indicate that the currents have a significant influence on the drag coefficients for submerged circular cylinder, while the vertical inertia coefficients induced by wave-current flows are found to be similar to those obtained in waves.”*

4.2. Dynamic response

The SFT is subjected to forces which induce dynamic behaviour. Two limit states must be verified with respect to the dynamic response of the structure: the limit on the serviceability level in terms of accelerations of the structure and the limit on the structural safety level. The dynamic response of the SFT is very important and depends on aspects such as load frequencies, design alternatives and type of supports.

4.2.1. Structural shape

The dimensions and geometric design of the SFT influence the dynamic response. It is crucial to get an understanding of such parameters and what amount of consequence they entail regarding the dynamic response of the structure.

The buoyancy-weight-ratio (BWR) is critical structural parameter that influences the response of the SFT structure and the tether system as well [12]. When the BWR is between 1.25 and 1.4, the SFT response to extremely severe sea states shows impressive improvements for larger BWR [45]. Numerical and physical model studies confirmed that tether slack could diminish when BWR is larger than 1.4 [46]. The slack phenomena however is also related to the inclined mooring angle (IMA) of the tethers and the tether slack diminishes for a IMA larger than 25 degrees. The effect of the BWR and IMA are coupled.

Some suggestions are made about applicable technologies for the SFT based on the value of the BWR [47]. If the BWR is set small and the tunnel is fixed firmly by supporting structure, some of the technologies used for immersed tunnels may be applicable. When a large BWR is adopted and the tunnel is moored by cables, knowledge accumulated for floating bridge might be helpful.

4.2.2. Earthquakes

The effect of seismic loading on the SFT is topic of many research papers which are mainly produced by Chinese graduate students. Multiple models and different types of seismic excitation indicate that earthquakes have an influence on the SFT. Construction strength and structure safety have to be carefully analysed and adjusted withstand earthquakes. Especially the connections to the abutments where the flexible tunnel lining is connected to a solid structure will introduce large internal forces and seismic load is of large influence on the tunnel and the abutment.

A study performed a time domain analyses of the seismic behaviour of the SFT by assuming multi-support excitation [20]. The tunnel displacements and stresses are noticeably larger for the case studies with shorter crossing length. For longer crossing cases, large values of the cables axial force occur in the cable groups located near the shore. The water around the tunnel provides additional damping and inertia.

A simplified model is used to determine the hydrodynamic pressure on the SFT under a seismic P-wave [18]. The paper discusses the effect of shear modulus, Poisson ratio, spring constant of the anchors and anchor spacing. *“The peak value of the amplitude of the hydrodynamic pressure on SFT increases as the Poisson ratio of submarine rock and soil and the spring constant of anchor increases, decreases as the spacing of the anchor increases.”*

A nonlinear dynamic analysis is performed, researching the influence of the P-wave on the SFT as well, regarding tunnel length and stiffness of the anchorage system [19]. The response amplitude of the tube decreases greatly with the increase of the spring stiffness, the length of SFT however has a limited influence on the displacement response. *“the equivalent linear stiffness is recommended no less than 1×10^8 N/m in order to ensure the safety of the SFT operation”*

A single paper researches the dynamic response due to both earthquakes and seaquakes regarding dissipation devices and anchoring bars [48]. The seaquake forces can be an important source of excitation.

A novel method is proposed to obtain the response spectrum compatible to accelerograms [49]. Real life seismic recordings can then be used as input for multi-support excitations.

4.2.3. Hydrodynamics

Hydrodynamics is a complicated mechanism. A lot of research has been performed, in general as well as specific cases for the SFT, but still more complex studies remain to get a better understanding of the full process.

A high quality research performed a complex numerical analyses of fluid-structure interaction [11], based on the Computational Fluid Dynamics (CFD) and the Finite Element Method (FEM) implemented in the ABAQUS code. Even an accurate modelling of turbulent phenomena has been made, based on both Implicit Large Eddy Simulation and RANS-based Spalart-Allmaras model. Both static and dynamic loading has been considered. The main results of the research are; the advantageous hydrodynamic behaviour of the more streamlined elliptical cross section has been confirmed, the less demanding averaged RANS approach provides acceptable results and at least for the tunnel structure, the turbulent water flow should not represent a great issue. The FEM model and the corresponding analysis could be used for future more detailed analysis.

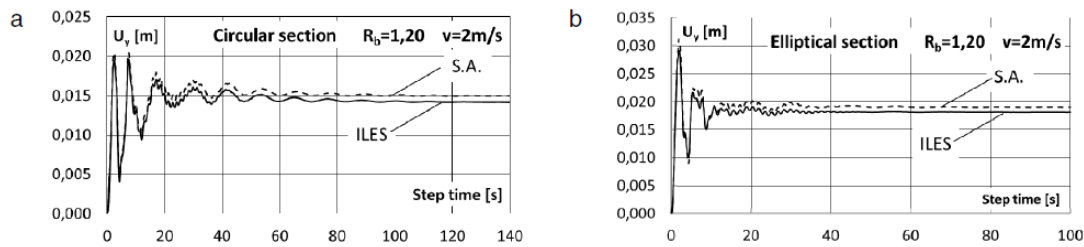


Figure 11 - Horizontal displacement U_y for circular and elliptical section[11]

Vortex-induced vibration

The vortex-induced vibration (VIV) has been studied both for the SFT main body as well as the tethers, though the last has been given the most regard. Multiple models have been developed to predict the effect of VIV such as displacements and stresses. A combination of such models should give a good first estimation of the VIV, however further studies remain to be done on detailing and some non-linear effects.

A modified wake-oscillator model has been created to predict the VIV displacement and stress responses of the cable in non-uniform flow field [13]. *“Both displacement and stress responses become larger as the flow velocity increases; especially higher stress response accompanied with higher frequency vibration should be paid enough attention in practical design of SFT because of its remarkable influence on structure fatigue life.”*

Investigations are performed on the capabilities of dynamic modelling and analysis of the effect of VIV, through a coupling between a 2D CFD simulation and a 3D FEM analysis of the structure trough strip theory [14]. *“The hydrodynamic quantities that are extracted are the time averaged drag coefficient $C_{D,avg}$, the root mean square lift coefficient $C_{L,rms}$, and the non-dimensional shedding frequency St . Compared to experimental data and numerical simulation, the present simulations are able to achieve correct values (first time then for Strouhal)”*

Al lot more research has been performed, combining the VIV and seismic excitation, considering cables under current loading and the vibration control under internal wave and ocean current. These papers state that: reducing the tether spacing reduces the maximum displacement, constraint moment and constraint force while the vibration presents more periodicity [50], that multiple parameters have a great impact on the parametrical excitation frequency [51] and vibration control can be accomplished without any additional devices for the tension legs, but the dynamic response tends to be stronger linear under combined effect of internal wave and ocean current [52].

Mode competition and multi-mode VIV of flexible body in lineally sheared current has been explored [15]. Multi-mode VIV occurs both in non-uniform and uniform fluid profiles and higher order modes occur in sheared current as the towing speed increases and the stress increases as well. *“It is still difficult for the prediction approach to capture all VIV’s, particularly the nonlinear jump or irregularities, and therefore further multi-mode VIV studies remain to be done.”*

Waves

The hydrodynamic influence due to waves is a topic which is challenging, especially for the tether anchored variant of the SFT. The wave load will depend on local circumstances and need to be determined. Not many research are found on this specific topic. Assumed is that there will be more information available about wave dynamics for the pontoon alternative when looking to the floating bridges. A few papers indicate that for the tether anchored SFT, the tethers are affected by wave excitation and should be carefully analysed.

A global performance analysis is suggested on the hydrodynamic characteristics of the tether moored SFTs under irregular waves [16]. An analytical and numerical simulation were made by combining several previous studies for regular waves. Results show that the tethers are clearly effected by wave excitation and the inclined mooring system controls the dynamic motion and should be carefully analysed.

A distinction is made between types of waves, as research has been performed on the effect of the traveling wave in the VIV of the SFT [53]. A modified wake oscillator model is used to simulate response for the SFT: the traveling wave dominates the response of de VIV rather than a standing wave.

The wave force has also been evaluated based on the diffraction theory by Boundary Element Method [17]. Secondly, Morison's equation is used to estimate drag and inertial forces. *“Both methods accurately calculate the wave forces. Drag and inertia force work simultaneously. For SFT, inertia force is dominant when the KC number is less than 15”*

A research investigates the dimensionless parameter controlling the wave types of dynamic response of slender cables undergoing vortex-induced vibration by means of dimensional analysis and finite element numerical simulations [21]. Results show a distinction between three types of VIV responses and that the parameter is related to the system damping including fluid damping and structural damping, order number of the locked-in modes and the aspect ratio of cable.

4.3. Internal loads

4.3.1. Traffic

The dynamic response of the SFT induced by traffic moving loads has only been explored in a handful of papers. Results show that the vertical tether stiffness plays a significant role in the dynamic response.

A research on the dynamic response of a floating bridge due to heavy vehicle loading [22] states that there is no obvious vertical dynamic effect, while the lateral displacement and the vertical and lateral accelerations of the locomotive and cargo vehicles increase with the train speed.

The displacement response due to single moving load has been considered as well [54]. The Galerkin method (kinematic equation) has been used to solve the problem. The results state that the anchor stiffness plays a significant role and the magnitude and velocity of the moving load also has an obvious impact on the dynamic response of the SFT. Increasing the vertical stiffness of the tension legs suppresses the SFT displacements and influences the tube vibration frequency; with a larger vertical stiffness, the influence of moving load becomes more obvious.

A paper puts forward the calculation formula of traffic induced loads, with a comprehensive consideration of different influencing factors [55]. The degree of influence of different factors is obtained by orthogonal experiment method and analytic hierarchy process results in the weights of the influence factors for two judge indexes.

4.3.2. Impact load

Like traffic loads, the dynamic response and structural integrity of impact loads have been explored lightly. The impact load can be internal (traffic) or external (vessel). In both cases the impact load will be a local acting load. Only a few research studies have been found. More research is necessary to represent the effects of impact loads.

The response of SFT to an accidental collision by an object (sinking vessel) has been analysed to assess the deformation and stresses in the tunnel lining [23]. The external aluminium panel lining has a large energy absorption capacity.

One paper presents a suitable model for the global impact response analysis [56]. The analysis takes into consideration the non-linear hydraulic resistance to study the effect of certain parameters and uses several methods; the Hamilton principle, the modal superposition method and the Runge-Kutta method.

The BOEF model is validated to be a suitable simplified method for the global impact response analysis. *“The change of buoyancy-weight ratio has effect on displacement results and the natural frequency of the tube. It suggests the reasonable inclined angle of cable is between 45° and 60°. The hydraulic resistance considered in this paper had an effect of more than 20% on the maximum displacement, so it should not be ignored in analyses.”*

5. Construction methods

Research on construction methods is rarely available. Only limited assumptions are being made regarding the construction of the SFT. Barely anything significant is mentioned in these global statements. The most relevant observations about this subject can be extracted from the design reports from the Norway fjords [57].

One paper validated the suspicion that construction methods used in the immersed tunnels are not suitable for the SFT [58]. An analysis has been performed of the construction environment limits and typical operating diseases of SFT. An estimated 50-87% of these existing construction methods are not suitable for the SFT. A technical breakthrough or innovation is required; a combination of traditional construction method and floating method will be one of the effective options.

A small paragraph in a research paper elaborates on the general fabrication of the tunnel segment consisting of two steel linings and concrete in the middle section [8].

The construction methods clearly contribute to the research question whether a SFT is feasible. More research is necessary about the construction phase of the SFT.

6. Safety and sustainability

There have been some researches regarding durability, renewability and safety of the SFT structure, but for some only the basic conceptual stage has been considered. Extended researches on these topics is crucial, because based on the limited amount of papers, it may be concluded that multiple aspects will threaten the safety and sustainability of the SFT during its lifetime.

Some topics have been investigated, but important topics such as inundation and flood waves have not been considered. Relevant publications and their results have been sorted by topic.

6.1. Internal and external collisions

Impact loads as mentioned previously can be caused by internal (vehicle) and external (Submarine, ship) colliding objects.

A reliability analysis is presented for structures subjected to bullet and the fragment demands [59]. Pseudo fragility curves have been developed for the limit states related to spall and perforation of wall panels, residual velocities of bullets and fragments, and injury to personnel. The proposed analysis method allows designers and owners to determine the probability of spall and perforation, residual velocity, and injury as a function of wall thickness or threat standoff distance.

A collision analysis has been performed by both modelling the SFT and the underwater navigating vessel (UNV) [60]. The overall collision behaviour can be demonstrated when considering a minimum of 2 km range under current collision conditions. The results state that there is a large variation in lateral deformation for BWR and the energy dissipation mostly due to deformation of SFT and UNV.

Ship collision loads on the bridge girder design alternative for the Bjornafjorden has been investigated [61]. Detailed FEM models have been developed for a cruise ship and a steel box girder. The results show that the proposed bridge girder design is generally safe, but research on entire bridge response and safety need to be conducted.

6.2. Fire

Fire resistance is very important because it influence the structural integrity. Three papers have been found which were dedicated to fire damage in SFTs.

A fire resistance study is performed of concrete in the application of tunnel-like structures [62]. The mechanical behaviour of concrete under high temperature in fire has been analysed by performing numerical simulations with a 3D FEM model. The effects of several parameters on the fire resistance time of the SFT exposed to an RABT fire curve have been studied: fire resistance time increases obviously with the increasing of concrete compressive strength and steel strength and the fire resistance time increases when the length of SFT decreases.

Another paper studies the thermal stress redistribution and fire damage of twin-tube structure to achieve a quantitative assessment to thermal stress damage of tunnel linings in fired condition [24]. A modified calculation method is proposed for a building thermal-mechanical coupled method. *"The results show that the temperature inside tube would rise and bring down rapidly, and that tube surface stress induced by heat would exceed concrete compressive strength and lead to disruption. Having or not thermal insulation is a key to tube structure for it can reduce the burst damage depth by 58%"*

The smoke originating from fires need to be considered as well. A full-scale experimental research has been performed on the effect of smoke exhaust strategies [63]. The efficiency of smoke exhaust system was analysed through comparison of the influence of different opening modes of smoke vents. The paper states that the total volume rate of smoke vents when opening two continuous groups of smoke vents downstream is higher, than when two spaced groups of smoke vents are opened downstream. Both options are however higher than the alternative in which only one group of smoke vents is opened.

6.3. Corrosion and fatigue

An important aspect is the corrosion of marine steel, because it is likely that the tether will be fabricated out of steel and in some case studies the SFT has a steel lining. A structure analysis has been applied to predict the corrosion and capacity of marine steel for sheet piles [64]. The results show that ignoring the effects of a changing environment can underestimate structural capacity failure risks, and pollution will have a significant effect on capacity of steel sheet piles. Results from the analysis can be useful, although the research is not intended specifically for the SFT.

The same holds for an analysis of the long-term immersion corrosion of steel. The combined effect is investigated for the case of large variations both in the seawater temperature and in concentration of dissolved nutrients [25]. A new long-term predictive model has been developed which presents acceptable forecasts of corrosion losses.

A second aspect is the fatigue of the tethers because they are exposed to VIV. A tunnel-cable coupling model is considered to obtain a more realistic response [26]. The response of the cable is the largest when the parametric excitation frequency is twice the cable's inherent frequency. During design life of the tethers, the effect of corrosion thinning is significantly greater than randomness of the initial cable diameter.

6.4. Renewability

The life cycle and environmental footprint of structures has become an important aspect of structures the last decade. In the project "Coastal Highway Route 39" in Norway, it is investigated how infrastructure can exploit renewable energy to reduce environmental footprint [27]. Results conclude that: *"(1) Life Cycle Assessment should have a geographical dimension with respect to assumptions and input data, (2) there are substantial potential to reduce the CO2 emissions from the E39, especially when considering an electrification, and (3) the harvested energy from hydronic pavement system can be enough for maintaining ice-free roads in Nordic countries."*

Key factors have been studied which influence the energy consumption of ventilation systems in highway tunnels [65]. CFD and STEPS software are used to simulate operational safety to check whether the ventilation system meet the required evacuation safety. First studies were carried out, with the use of two software programs, how to design long highway tunnel ventilation systems with the design approach of quantitative analysis to achieve energy-saving, environmental protection and safety.

7. Risks

The SFT has not been built yet, because it would contain too many unforeseen risks for investors. The past few years there has been an increase in research regarding risk identification and risk reductions to name a few. More research on several aspects and investigation of more detailed projects is necessary to get a better understanding of the risks concerning the SFT. More than a decade ago, it was already obvious that risk management would play a crucial part [8]: *“In fact, despite the evident advantages of such an innovative solution for waterway crossings, no Submerged Floating Tunnels have been built in the World yet, mainly due to the absence of experimental data, which are fundamental for removing the natural psychological scepticism.”*

Some topics have been investigated, but important topics such as public safety, natural hazards and environmental impact have not been considered. Relevant publications and their results have been sorted by topic.

7.1. System

The first step is to identify the main content of risk analysis of SFT. The risk management has been classified into six stages after which potential risks and impact factors have been identified [28]. The six stages are: planning, feasibility study, design, tendering, construction and operation. Some measures and suggestions in risk control strategy were given.

A more specific research has been performed on deriving the risk index system for public safety of the SFT [29]. The public safety risk is evaluated during construction and operation of SFT. *“The results show that, in spite of facing many technical problems and potential risks, these potential risks of SFT can be controlled or reduced to a minimum level with the help of a reasonable design and certain measures.”*

The hierarchical structure model of risks has been developed for the SFT under the sea conditions in Qiongzhou Strait [66]. The weight values of key factors for the SFT have been determined by an analytic hierarchy process to obtain the risk factors with a relatively large sensitivity. Risk analysis of floating tunnel is a relatively complicated system problem, expert questionnaire survey will be needed in the future.

7.2. Main structure

One paper is leading in investigating whether the existing design codes are applicable to SFT [30]. Results show that the safety code seems to be non-optimal for SFT, as it leads to an over-design. Using the existing codes would result in a conservative design which might be preferable for a first experimental SFT.

A calibration exercise is necessary in order to provide partial safety factors giving homogeneous levels of safety over different SFTs. The reliability level is seen to vary consistently with the cross-section geometry, pre-stressing force and the relative magnitude of different loads. An assessment might lead to typical target safety levels rather than undertaking a full-risk assessment and risk-optimization.

7.3. Operational phase

Especially the operational risks are a primary aspect which need to be considered to give the tunnel's operators a good perspective on the security and risk management of the tunnel.

A single paper performed a risk source analysis and identification which includes a scenario design and simulation analysis, risk loss judgment standards and weight research for structural stability of a long and large immersed tube tunnel in operation period [67]. Risk scores of the structural stability in the operation period are obtained by a quantitative risk calculation method and analysing nine typical scenarios causing structural instability. Transportation of dangerous cargo makes the risk level rise to Level III which is too high. Control measures for risk reduction thus must be implemented.

8. Costs

Costs can easily be estimated for existing tunnel alternatives. The SFT however has no comparative material to make an educated guess about the costs. One paper has tried to make a first estimate of the cost for a SFT structure by evaluating and comparing costs with the Cable Supported Bridge (CSB) [31]. First estimations state that the costs do not deviate much from other water crossing structures.

In the current design stage, costs are not that relevant in determining whether a SFT is chosen as a valuable alternative. Knowledge gaps surrounding the construction and risk assessment are a more prominent discouragement to take the leap.

9. Existing concepts of joints

A few papers mention the need for appropriate joints, see paragraph 3.3, but no structural details are given. Optional end joint solutions from immersed tunnel are considered to be incorporated in the SFT design, as well as solutions from other industrial branches

9.1. Immersed tunnels

Some of the technology from immersed tunnels can probably be used for the SFTs. The elements cannot be applied in the exact same context but with some small alterations it could prove useful. There are some structure elements however that will have to be redesigned completely, because the different functions the joint of the SFT has compared to immersed tunnels, such as axial rotations and larger lateral displacements.

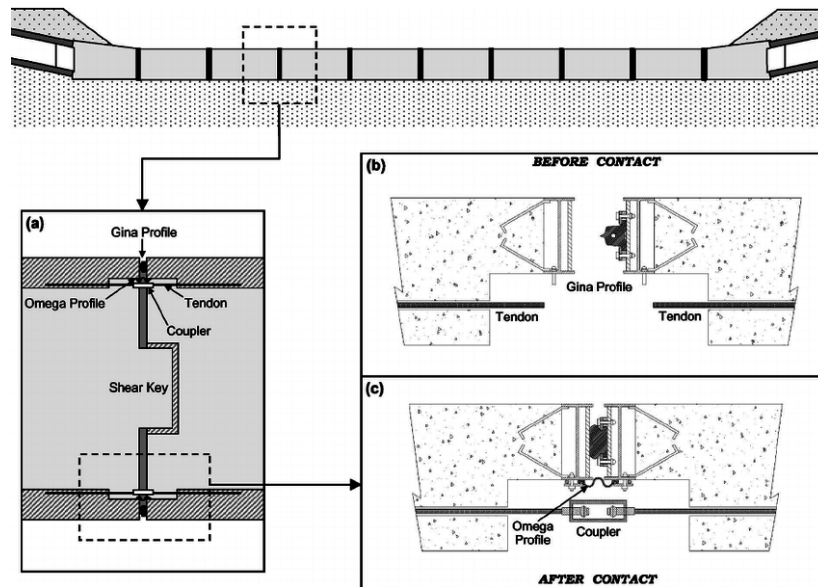


Figure 12 - Standard immersed tunnel²

9.1.1. Waterproof

The Gina gasket and Omega seal are used between the sectional elements of immersed tunnels to prevent water ingress due to external water pressure [68]. These seals are restricted to very small displacements and rotations and cannot transfer shear forces. The Omega seal cannot transfer bending moments either. The limits of these seals need to be observed when considering them for the end joint design of the SFT.

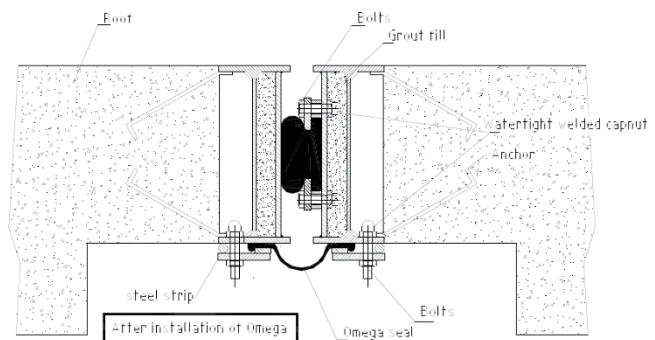


Figure 13 - Gina and omega seal [68]

9.1.2. Force transfer

The immersed tunnel is surrounded by soil, because it is positioned below the bed. The lateral forces therefore can be transferred to the soil and do not have to be fully transferred in the cross-section. The SFT however do not have that privilege because the SFT floats in water. A small part of the lateral forces will be transferred to the supports, but the largest part is taken by the cross-section stiffness. The influence of the water on the response of the SFT mainly is used when the (hydro)dynamics is considered.

² https://www.researchgate.net/profile/Vasileios_Drosos2/publication/234044892/figure/fig5/AS:300078527991811@1448555704432/Aseismic-design-of-the-immersed-section-of-the-proposed-railway-link-a-schematic.png

The same holds for the vertical forces. Immersed tunnels use gravity to hold it into place and are supported continuously by the soil. The SFT is only supported locally and amount of support depends on the buoyancy-weight-ratio and the method of anchoring. In between supports the SFT acts like a beam on two supports.

The essential difference between immersed tunnels and the SFT is the joint system. The immersed tunnel acts like a beam on elastic foundation, while the SFT acts like a beam on multiple supports.

Shear forces are transferred in the segment joint by shear keys. If the end joint for the SFT has to be of the flexible type, careful consideration has to be made regarding the transfer of shear forces. Shear forces and rotations probably will interfere with each others function.

9.1.3. Displacements

Dilatation joints used in immersed tunnels can only adapt to very small displacements. In some cases, these dilatation joints are used to decrease the bending moment in the segments cross-section. Applying these dilatation joints in the SFT should be carefully analysed in respect to their capacity in force and moment transfer.

9.2. Project Istanbul: Unkapani

In Istanbul, an immersed tunnel will be built to connect two sides of the city of Unkapani. The floating bridge with rectangular cross-section will be placed on pile foundation far above the seabed. The tender phase showed a concept for a joint house at one shore connection, allowing large displacements caused by seismic activity [69].

For the extreme seismic event (2475 years), (plastic) hinges are modelled at the original immersion joints. The Gina profile is pre-stressed by tendons to limit the opening of the Gina during a seismic event and securing the water tightness of the joint.

To create and fulfil the plastic hinge conditions at the original immersion joint :

- the hinge conditions are necessary for the horizontal bending moment;
- the prestress cables have to continue through the joint at the outer walls;
- the cables over the joint are anchored in the adjacent elements over a short distance from the joint in a recess of the wall, roof or floor;



Figure 14 - Artist impression SFT in Unkapani³

At one of the shore connections, the traditional immersion joint at the abutments is not possible. The alternative is not to constrain the axial displacement under the seismic loading, which results in major deformations between abutment and the adjacent tunnel element. The rubber seals have to follow this deformation to ensure the water tightness of the tunnel.

³ <https://www.cementonline.nl/library/article/1504776554.9609.jpg>

To accommodate these large displacements (360 mm) a solution is proposed of combining 4 Omega seals of the largest size, see Figure 15.

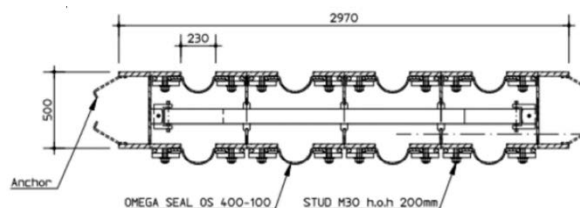
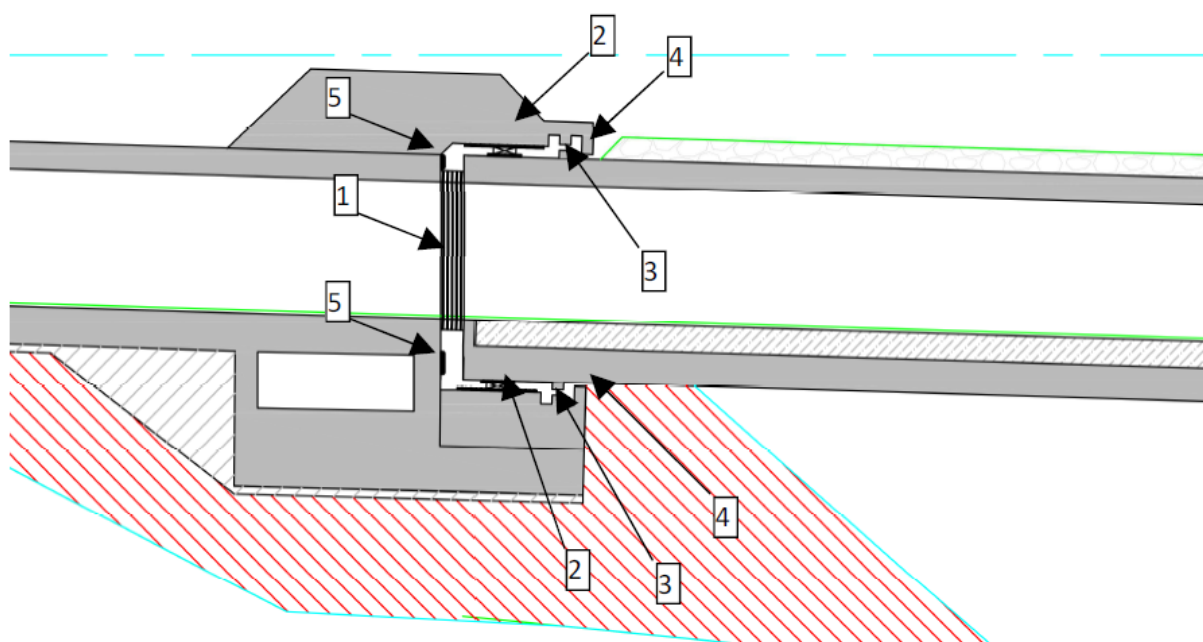


Figure 15 - Proposed flexible water seal[69]



Item	Name	
1	Final water sealing around the tunnels' perimeter.	The water seal will consists out of a number of omega seals in line to accommodate the seismic displacements. At the road a Swivel joists-expansion joint can be used to bear the vehicles loads.
2	Spherical bearings	For fixation in transverse direction, some initial displacement to consider for reduction of the loading.
3	Final water stop (final static)	(Replaceable) omega seal, final water stop but may fail during 2475 years earthquake
4	Temporary water stop (construction and seismic)	Fender used as temporary water stop. Water stop during constructing and after the 2475 years earthquake (in case final water stop fails).
5	Damper (optional)	To protect the concrete of the abutment and the element.

Figure 16 - The transition joint of the Unkapani tunnel[69]

9.3. Pipelines on large vessels and terminals

Pipelines on terminals and vessels have considerable length, requiring compensation for terminal expansion. Axial compensators, like the telescopic expansion joint, can be used to allow axial deformation due to temperature differences. The telescopic expansion joint is illustrated in Figure 17. Whether such a type of joint is useful for the SFT needs to be carefully considered.

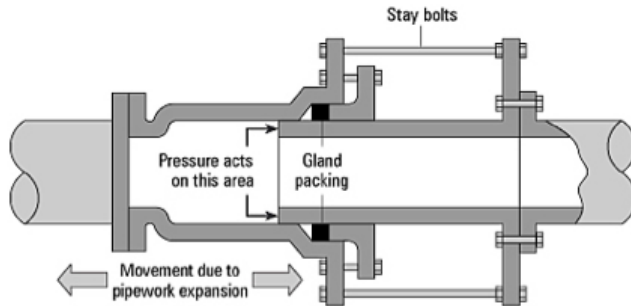


Figure 17 - Telescopic expansion joint⁴



Figure 18 - U shaped pipe connection⁵

Axial deformation can also be compensated by bending with the use of U-shaped connections, see Figure 18. The U-shaped connection cannot be used for the traffic transport function of the SFT.

9.4. Seismic joints

Seismic joints have already been considered and constructed for both the immersed tunnels as well as the bored tunnels.

The seismic joint of the bored tunnel is part of the tunnel under the Bosphorus Strait in Turkey. The project required special design of the lining and the internal structure of the double-deck highway, because Turkey lies in a geological zone of high seismicity and the tunnel runs parallel to the Anatolia plate-boundary. To protect the bored tunnel there are two seismic joints built into the precast concrete segmental lining. These joints allow movement of 75mm in contraction, 75mm in expansion and 50mm shear⁶.

The seismic joint for the bored tunnel (with a diameter of 13.7 m) is promising regarding the applicability on the SFT structure.



Figure 19 - Seismic joint of a circular tunnel⁷

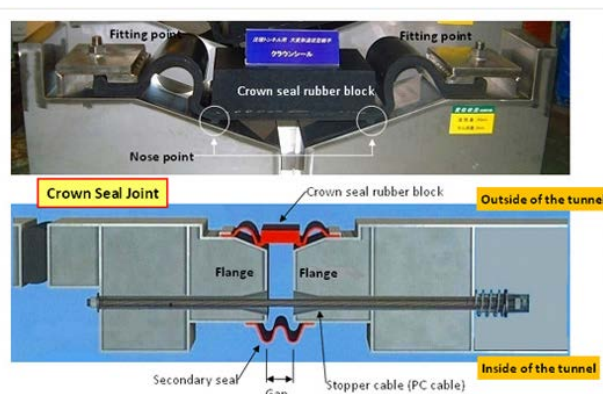


Figure 20 - Crown Seal Joint⁸

The seismic joint for immersed tunnels is a special edition of the immersion joint: the Crown Seal Joint, see Figure 20.

Stress from immersed tube tunnels due to earthquakes can be reduced much more than in the conventional PC-rubber gasket type of flexible joint. Since no resisting members are present, large deformation due to earthquakes or ground settlement can be absorbed. The stopper cables (PC cables) cope with excessive tensile displacement and prevent breaking open of the joint. Applying the crown seal joint for the SFT design has to be considered with caution.

⁴ <http://www.sunnysteel.com/images/What-different-varieties-of-expansion-joints-are-there.jpg>

⁵ <https://static.politifact.com/politifact/photos/460x.jpg>

⁶ <https://www.tunneltalk.com/Turkey-24Sep15-Eurasia-highway-tunnel-crossing-of-the-Bosphorus-in-Istanbul.php>

⁷ http://www.penta-ocean.co.jp/english/business/civil/images/crowncie_il001.jpg

⁸ <https://www.slideshare.net/putikaappa/yumesaki-tunnel>

Conclusion

A general literature study has been performed to investigate which aspects need further research and development, to be able to build a prototype of the SFT allowing real time measurements. The literature study shows that abundant research has been done regarding the hydrodynamic and seismic response of the tunnel structure. Other aspects and parts however have been investigated only on a superficial scale.

Multiple alternative layouts are considered but arguments for one or the other alternative taking preference are not presented. Few alternatives for the structural design of the tunnel segments are looked into and the need for appropriate end joints is frequently mentioned but not explored. Researches regarding safety and risk assessment, durability, renewability and cost evaluation have been performed only on a very basic level.

Through most of the essential parts of the SFT have been researched, some are not. The end joints connecting the tunnel to shore is one of them.

From the aspects found during the literature study, one aspect caught my attention: the design of the end joint of the Submerged Floating Tunnel. As many elements have already been considered, I favour to put my energy into the subject connecting the SFT a step closer to completion.

The end joint, connecting the floating tunnel to the shore, is both a beginning and an end piece which allows others to enter the tunnel to design or inspect their component.

References

- [1] H. Yan, F. Zhang, J. Yu, The Lectotype Optimization Study on Submerged Floating Tunnel Based Delphi Method, *Procedia Engineering SUFTUS*. 166 (2016) 118–126. doi:10.1016/j.proeng.2016.11.574.
- [2] F.M. Mazzolani, B. Faggiano, M. Esposto, G. Martire, A new challenge for strait crossings : the immersed inversed cable supported bridge, Department of Structural Engineering, University of Naples “Federico II”, Italy. (2009) 138–145.
- [3] E. Wahyuni, Effect of Triangle Cables Configuration on the Behavior of Reinforced Concrete Submerged Floating Tunnel under Hydrodynamic Load, *Procedia Engineering IABSE*. 39 (2017) 3045–3051.
- [4] K. Zhang, Y. Xiang, Y. Du, Research on tubular segment design of submerged floating tunnel, *Procedia Engineering ISAB*. 4 (2010) 199–205. doi:10.1016/j.proeng.2010.08.023.
- [5] Mathias Eidem, Arianna Minoretti, Xu Xiang, Anette Fjeld, Design for a Submerged Floating Tube Bridge across the Digernessundet, *Procedia Engineering IABSE* (2017) 3018–3024.
- [6] K. Li, X. Jiang, Research on Section Form of Submerged Floating Tunnels Considering Structural Internal Force Optimization under Fluid Action, *Procedia Engineering SUFTUS*. 166 (2016) 288–295. doi:10.1016/j.proeng.2016.11.551.
- [7] A.B. Kawade, S.P. Meghe, Submerged Floating Tunnel, *Civil Engineering Portal*. (2014) 1–9. <http://www.engineeringcivil.com/submerged-floating-tunnel.html>.
- [8] F.M. Mazzolani, B. Faggiano, G. Martire, Design aspects of the AB prototype in the Qiandao Lake, *Procedia Engineering ISAB*. 4 (2010) 21–33. doi:10.1016/j.proeng.2010.08.005.
- [9] Y. Li, M. Lin, Hydrodynamic coefficients induced by waves and currents for submerged circular cylinder, *Procedia Engineering ISAB*. 4 (2010) 253–261. doi:10.1016/j.proeng.2010.08.029.
- [10] M.S. Dong, G.P. Miao, L.C. Yong, Z.R. Niu, H.P. Pang, C.Q. Hou, Effect of escape device for Submerged Floating Tunnel (SFT) on hydrodynamic loads applied to SFT, *Journal of Hydrodynamics*. 24 (2012) 609–616. doi:10.1016/S1001-6058(11)60284-9.
- [11] A. Mandara, E. Russo, B. Faggiano, F.M. Mazzolani, Analysis of Fluid-structure Interaction for a Submerged Floating Tunnel, *Procedia Engineering SUFTUS*. 166 (2016) 397–404. doi:10.1016/j.proeng.2016.11.572.
- [12] X. Long, F. Ge, Y. Hong, Feasibility study on buoyancy–weight ratios of a submerged floating tunnel prototype subjected to hydrodynamic loads, *Acta Mechanica Sinica/Lixue Xuebao*. 31 (2015) 750–761. doi:10.1007/s10409-015-0428-3.
- [13] W. Chen, Z. Zheng, M. Li, Multi-mode vortex-induced vibration of slender cable experiencing shear flow, *Procedia Engineering ISAB*. 4 (2010) 145–152. doi:10.1016/j.proeng.2010.08.017.
- [14] A.S. Brandtsegg, *Dynamic Modelling and Analysis of Submerged Floating Tunnels*, Norwegian University of Science and Technology, 2012.
- [15] W. Chen, Y. Li, Y. Fu, S. Guo, On Mode Competition during VIVs of Flexible SFT’s Flexible Cylindrical Body Experiencing Lineally Sheared Current, *Procedia Engineering SUFTUS*. 166 (2016) 190–201. doi:10.1016/j.proeng.2016.11.582.
- [16] S. Kim, Hydrodynamic analysis of the submerged floating tunnels under irregular waves, *Procedia Engineering IABSE*. 39 (2017) 3025–3032.
- [17] H. Kunisu, Evaluation of wave force acting on Submerged Floating Tunnels, *Procedia Engineering ISAB*. 4 (2010) 99–105. doi:10.1016/j.proeng.2010.08.012.
- [18] S.N. Sun, Z. Bin Su, Hydrodynamic Pressure on Submerged Floating Tunnel under the P-Wave, *Applied Mechanics and Materials*. 858 (2016) 125–130. doi:10.4028/www.scientific.net/AMM.858.125.
- [19] M.S. Dong, L. Man, The Dynamic Responses of the of the Submerged Floating Tunnel under Seismic effect, *Procedia Engineering SUFTUS*. 166 (2016) 152–159. doi:10.1016/j.proeng.2016.11.578.

- [20] G. Martire, B. Faggiano, F.M. Mazzolani, A. Zollo, T.A. Stabile, Seismic analysis of a SFT solution for the Messina Strait crossing, *Procedia Engineering ISAB. 4* (2010) 303–310. doi:10.1016/j.proeng.2010.08.034.
- [21] L. Zhang, W. Chen, Z. Zheng, Controlling parameter for wave types of long flexible cable undergoing vortex-induced vibration, *Procedia Engineering ISAB. 4* (2010) 161–170. doi:10.1016/j.proeng.2010.08.019.
- [22] N. Zhang, H. Xia, W. Guo, J. Zhan, J. Yao, Y. Cao, Vehicle-bridge interaction analysis of heavy load railway, *Procedia Engineering ISAB. 4* (2010) 347–354. doi:10.1016/j.proeng.2010.08.040.
- [23] S. Zhang, L. Wang, Y. Hong, Procedia Engineering Vibration behavior and response to an accidental collision of SFT prototype in Qiandao Lake (China), *Procedia Engineering ISAB. 4* (2010) 189–197. doi:10.1016/j.proeng.2010.08.022.
- [24] J. Guo, S. Jiang, Z. Zhang, Fire Thermal Stress and its Damage to Subsea Immersed Tunnel, *Procedia Engineering SUFTUS. 166* (2016) 296–306. doi:10.1016/j.proeng.2016.11.552.
- [25] R. Kovalenko, R.E. Melchers, B. Chernov, Long-term immersion corrosion of steel subject to large annual variations in seawater temperature and nutrient concentration, *Structure and Infrastructure Engineering. 13* (2017) 978–987. doi:10.1080/15732479.2016.1229797.
- [26] H. Yan, Y. Yuan, J. Yu, Fatigue Reliability Analysis of Cable Considering Corrosion, *Procedia Engineering SUFTUS. 166* (2016) 127–135. doi:10.1016/j.proeng.2016.11.575.
- [27] B. Adl-Zarrabi, B. Ebrahimi, M. Hoseini, J. Johnsson, R. Mirzananadi, M. Taljegard, Safe and Sustainable Coastal Highway Route E39, *Transportation Research Procedia. 14* (2016) 3350–3359. doi:10.1016/j.trpro.2016.05.286.
- [28] Y. Xiang, C. Liu, K. Zhang, Q. Wu, Risk analysis and management of submerged floating tunnel and its application, *Procedia Engineering ISAB. 4* (2010) 107–116. doi:10.1016/j.proeng.2010.08.013.
- [29] Y. Xiang, C. Liu, C. Chao, H. Liu, Risk analysis and assessment of public safety of submerged floating tunnel, *Procedia Engineering ISAB. 4* (2010) 117–125. doi:10.1016/j.proeng.2010.08.014.
- [30] M. Baravalle, J. K??hler, Risk and Reliability Based Calibration of Design Codes for Submerged Floating Tunnels, *Procedia Engineering SUFTUS. 166* (2016) 247–254. doi:10.1016/j.proeng.2016.11.547.
- [31] G. Martire, B. Faggiano, F.M. Mazzolani, Compared cost evaluation among traditional versus innovative strait crossing solutions, *Procedia Engineering ISAB. 4* (2010) 293–301. doi:10.1016/j.proeng.2010.08.033.
- [32] F. Lin, W. Mengjun, W. Guangdi, C. Peng, Comparative Analysis on Stress State of Submerged Floating Tunnels in Different Anchor Cable Arrangement Modes, *Procedia Engineering SUFTUS. 166* (2016) 279–287. doi:10.1016/j.proeng.2016.11.550.
- [33] M. Dong, G. Miao, R. Zhu, J. Fan, The influence of the escaping device on the hydrodynamics of submerged floating tunnels under flow, *Procedia Engineering ISAB. 4* (2010) 325–331. doi:10.1016/j.proeng.2010.08.037.
- [34] M. Eidem, A. Fjeld, T.O. Olsen, Basic design for a Submerged Floating Tube Bridge across the Digernessundet, *Procedia Engineering IABSE. 39* (2017) 3018–3059.
- [35] S. Zhang, L. Wang, Y. Hong, Structural analysis and safety assessment of submerged floating tunnel prototype in Qiandao Lake (China), *Procedia Engineering ISAB. 4* (2010) 179–187. doi:10.1016/j.proeng.2010.08.021.
- [36] S. Shang, B. Zhang, J. Wu, Long-term performance research on reinforced concreted beams with pre-stressed CFRP, *Procedia Engineering ISAB. 4* (2010) 341–346. doi:10.1016/j.proeng.2010.08.039.
- [37] F. Ge, W. Lu, X. Wu, Y. Hong, Fluid-structure interaction of submerged floating tunnel in wave field, *Procedia Engineering ISAB. 4* (2010) 263–271. doi:10.1016/j.proeng.2010.08.030.
- [38] J. Xiao, G. Huang, Transverse earthquake response and design analysis of submerged floating tunnels with various shore connections, *Procedia Engineering ISAB. 4* (2010) 233–242. doi:10.1016/j.proeng.2010.08.027.
- [39] W. Lu, F. Ge, L. Wang, Y. Hong, Slack phenomena in tethers of submerged floating tunnels under hydrodynamic loads, *Procedia Engineering ISAB. 4* (2010) 243–251. doi:10.1016/j.proeng.2010.08.028.
- [40] D. Cantero, A. Rønnquist, A. Naess, Tension during parametric excitation in submerged vertical taut tethers, *Applied Ocean Research. 65* (2017) 279–289. doi:10.1016/j.apor.2017.05.002.

- [41] M. Reiso, S. Fosbakken, T. Soreide, A. Myhr, V. Kristensen, J. Solemsli, J. Sekse, A. Minorette, Vertical stiffness for tube bridges: Comparing pontoons and tethers, *Procedia Engineering IABSE*. (2015) 2093–2100.
- [42] Y. Duan, Application of Suction Caissons to Submerged Floating Tunnel at Sognefjord in Norway, Chalmers University of Technology, 2014.
- [43] W. Yan, F. Gao, Numerical analysis of interfacial shear degradation effects on axial uplift bearing capacity of a tension pile, *Procedia Engineering ISAB*. 4 (2010) 273–281. doi:10.1016/j.proeng.2010.08.031.
- [44] Y. Fang, H. Wang, J. Guo, Z. Chen, C. Wu, Study on the Mechanical Behavior and the Model Test of Segmental Linings for the Shield Tunnel Undercrossing the Yellow River, *Procedia Engineering SUFTUS*. 166 (2016) 19–31. doi:10.1016/j.proeng.2016.11.532.
- [45] F. Brancaleoni, A. Castellani, P. D’Asdia, Response of Submerged Floating Tunnels to their environment, *Engineering Structures*. 11 (1989) 47–56. doi:10.1016/0141-0296(89)90032-1.
- [46] Y. Hong, F. Ge, W. Lu, On the Two Essential Concepts for SFT: Synergetic Buoyancy-weight Ratio and Slack-taut Map, *Procedia Engineering SUFTUS*. 166 (2016) 221–228. doi:10.1016/j.proeng.2016.11.544.
- [47] S. Kanie, Feasibility studies on various SFT in Japan and their technological evaluation, *Procedia Engineering ISAB*. 4 (2010) 13–20. doi:10.1016/j.proeng.2010.08.004.
- [48] L. Martinelli, M. Domaneschi, C. Shi, Submerged Floating Tunnels under Seismic Motion: Vibration Mitigation and Seaquake effects, *Procedia Engineering SUFTUS*. 166 (2016) 229–246. doi:10.1016/j.proeng.2016.11.546.
- [49] L. Martinelli, G. Barbella, A. Feriani, Modeling of Qiandao lake submerged floating tunnel subject to multi-support seismic input, *Procedia Engineering ISAB*. 4 (2010) 311–318. doi:10.1016/j.proeng.2010.08.035.
- [50] L. Kang, F. Ge, Y. Hong, A Numerical Study on Responses of Submerged Floating structures Undergoing Vortex-induced Vibration and Seismic Excitation, *Procedia Engineering SUFTUS*. 166 (2016) 91–98. doi:10.1016/j.proeng.2016.11.569.
- [51] H. Yan, Y. Luo, J. Yu, Dynamic Response of Submerged Floating Tunnel in the Flow Field, *Procedia Engineering SUFTUS*. 166 (2016) 107–117. doi:10.1016/j.proeng.2016.11.573.
- [52] D. Man-Sheng, T. Xue-Fei, Z. Yuan, T. Fei, Vibration Control of the Submerged Floating Tunnel under Combined effect of Internal Wave and Ocean Current, *Procedia Engineering SUFTUS*. 166 (2016) 160–170. doi:10.1016/j.proeng.2016.11.579.
- [53] X. Wu, F. Ge, Y. Hong, Effect of travelling wave on vortex-induced vibrations of submerged floating tunnel tethers, *Procedia Engineering ISAB*. 4 (2010) 153–160. doi:10.1016/j.proeng.2010.08.018.
- [54] Z. Yuan, D. Man-sheng, D. Hao, Y. Long-chang, Displacement Response of Submerged Floating Tunnel Tube Due to Single Moving Load, *Procedia Engineering SUFTUS*. 166 (2016) 143–151. doi:10.1016/j.proeng.2016.11.577.
- [55] B. Jiang, B. Liang, Study on the Main Influence Factors of Traffic Loads in Dynamic Response of Submerged Floating Tunnels, *Procedia Engineering SUFTUS*. 166 (2016) 171–179. doi:10.1016/j.proeng.2016.11.580.
- [56] Y. Xiang, Y. Yang, Spatial dynamic response of submerged floating tunnel under impact load, *Marine Structures*. 53 (2017) 20–31. doi:10.1016/j.marstruc.2016.12.009.
- [57] P. Team, K3 / K4 Technical Report - Bjornafjord submerged floating tunnel, 2016.
- [58] D. Hao, L. Qinxi, J. Shuping, L. Ke, Enlightenment to Floating Tunnel of Existing Typical Submerged Tunnel, *Procedia Engineering SUFTUS*. 166 (2016) 355–361. doi:10.1016/j.proeng.2016.11.560.
- [59] P. Trasborg, C. Naito, P. Bocchini, P. Olmati, Fragility analysis for ballistic design, *Structure and Infrastructure Engineering*. 13 (2017) 1105–1116. doi:10.1080/15732479.2016.1244209.
- [60] K.-Y. Hong, G.-H. Lee, Collision Analysis of Submerged Floating Tunnel by Underwater Navigating Vessel, *Procedia Engineering IABSE*. (2015) 1–8.
- [61] Y. Sha, J. Amdahl, Design of floating bridge girders against accidental ship collision loads, *Procedia Engineering IABSE*. (2016) 1919–1926.

- [62] X. Long, H. Guo, Fire Resistance Study of Concrete in the Application of Tunnel-like Structures, *Procedia Engineering SUFTUS*. 166 (2016) 13–18. doi:10.1016/j.proeng.2016.11.531.
- [63] S. Liu, Y.Q. Jiang, J.Z. Chen, K. Li, Full-scale Experimental Research on the effect of Smoke Exhaust Strategies on Efficiency of Point Extraction System in an Underwater Tunnel, *Procedia Engineering SUFTUS*. 166 (2016) 362–372. doi:10.1016/j.proeng.2016.11.561.
- [64] L. Peng, M.G. Stewart, R.E. Melchers, Corrosion and capacity prediction of marine steel infrastructure under a changing environment, *Structure and Infrastructure Engineering*. 13 (2017) 988–1001. doi:10.1080/15732479.2016.1229798.
- [65] X. Yang, Design Environmental Protection, Energy Saving and Safety Ventilation System of Long Highway Immersed Tunnel, *Procedia Engineering SUFTUS*. 166 (2016) 32–36. doi:https://doi.org/10.1016/j.proeng.2016.11.533.
- [66] J. Shuping, L. Qinxi, L. Jianjun, C. Gengren, C. Xiang, Research on Risk Sensitivity of Submerged Floating Tunnel Based on Analytic Hierarchy Process, *Procedia Engineering SUFTUS*. 166 (2016) 255–265. doi:10.1016/j.proeng.2016.11.548.
- [67] M. Wu, Q. Zhang, S. Wu, Risk Assessment of Operation Period Structural Stability for Long and Large Immersed Tube Tunnel, *Procedia Engineering SUFTUS*. 166 (2016) 266–278. doi:10.1016/j.proeng.2016.11.549.
- [68] Trelleborg, Gina Gasket Brochure, (2015). www.trelleborg.com/engineeredproducts.
- [69] G.J. Eelco van Putten, Sanne van Aken, Bakker, Golden Horn – Unkapani Submerged Bridge, 2017.

APPENDIX B

SCIA basic model results

Submerged Floating Tunnels

Laura Bakker

MSc Hydraulic Engineering – Hydraulic Structures

2018, Delft

Project SFT MSC Thesis

1. Project

Licence name	Royal HaskoningDHV
Project	SFT MSC Thesis
Part	SFT longitudinal calculation
Description	Tether supported variant
Author	Laura Bakker
Date	19. 10. 2018
Structure	General XYZ
No. of nodes :	274
No. of beams :	410
No. of slabs :	0
No. of solids :	0
No. of used profiles :	4
No. of load cases :	5
No. of used materials :	4
Acceleration of gravity [m/s ²]	9,810
National code	EC - EN

2. Table of contents

1. Project	1
2. Table of contents	1
3. Load cases	2
3.1. Load cases - LC2	2
3.2. Load cases - LC5	2
3.3. Load cases - LC4	3
3.4. Load cases - LC7	3
3.5. Load cases - LC8	4
4. Combinations	4
4.1. Combinations - CO1	4
4.2. Combinations - CO2	5
4.3. Combinations - CO3	6
4.4. Combinations - CO4	6
4.5. Combinations - CO5	7
4.6. Combinations - CO6	7
5. Results	8
5.1. Result cross-sections	8
5.2. Bending moment diagrams	9
5.3. Shearforce diagram	12
5.4. 1D deformations	15

Project SFT MSC Thesis

3. Load cases

3.1. Load cases - LC2

Name	Description	Action type	LoadGroup
	Spec	Load type	
LC2	6% Force	Permanent Standard	LG1

3.1.1. Internal forces on member

Linear calculation, Extreme : Global, System : Principal
Selection : Named selection - buizen
Load cases : LC2

Member	css	dx [m]	Case	N [kN]	Vy [kN]	Vz [kN]	Mx [kNm]	My [kNm]	Mz [kNm]
B220	CS1 - Tube	0,000	LC2	0,00	1257,16	-1348,48	-2261,52	9802,74	-9138,93
B219	CS1 - Tube	0,000	LC2	0,00	-2662,53	2855,92	9887,40	-47994,27	44744,28
B109	CS1 - Tube	76,488	LC2	0,00	-6834,64	7331,07	-10034,85	340464,99	-317410,02
B2	CS1 - Tube	0,000	LC2	0,00	6651,25	-7134,36	9965,12	311629,79	-290527,39
B112	CS1 - Tube	0,000	LC2	0,00	6394,28	-6858,72	-10111,34	299759,30	-279460,80
B114	CS1 - Tube	0,000	LC2	0,00	-425,43	456,33	-4458,05	-125774,40	117257,40

3.1.2. 3D displacement

Linear calculation
Load case: LC2
Selection: Named selection - buizen
Location: In nodes avg. on macro. System: LCS mesh element
Results on 1D member:
Extreme 1D: Global

Name	dx [m]	Fibre	Case	ux [mm]	uy [mm]	uz [mm]	φx [mrad]	φy [mrad]	φz [mrad]	U _{total} [mm]
B112	0,000	1	LC2	0,0	0,0	0,0	0,0	0,0	0,0	0,0
B32	4,940	8	LC2	0,0	-144,8	155,2	-0,1	0,0	0,0	212,3

3.2. Load cases - LC5

Name	Description	Action type	LoadGroup	Duration	Master load case
	Spec	Load type			
LC5	Current F+1	Variable	LG2	Short	None
	Standard	Static			

3.2.1. Internal forces on member

Linear calculation, Extreme : Global, System : Principal
Selection : Named selection - buizen
Load cases : LC5

Member	css	dx [m]	Case	N [kN]	Vy [kN]	Vz [kN]	Mx [kNm]	My [kNm]	Mz [kNm]
B1	CS1 - Tube	40,122	LC5	-13,95	24,18	22,55	0,00	155,62	166,92
B213	CS1 - Tube	49,094	LC5	12839,35	-10,57	-9,85	0,00	-246,56	-264,47
B109	CS1 - Tube	0,000	LC5	10058,63	-218,05	-203,28	0,00	4872,18	5226,07
B2	CS1 - Tube	76,488	LC5	10058,63	218,05	203,28	0,00	4872,18	5226,07
B38	CS1 - Tube	0,000	LC5	11323,72	114,92	107,14	0,00	-5118,90	-5490,71
B127	CS1 - Tube	0,000	LC5	12433,24	-11,50	-10,72	0,00	1115,76	1196,81
B2	CS1 - Tube	0,000	LC5	10110,76	131,23	122,34	0,00	-7581,03	-8131,67

3.2.2. 3D displacement

Linear calculation
Load case: LC5
Selection: Named selection - buizen
Location: In nodes avg. on macro. System: LCS mesh element
Results on 1D member:
Extreme 1D: Global

Project SFT MSC Thesis

Name	dx [m]	Fibre	Case	u _x [mm]	u _y [mm]	u _z [mm]	φ _x [mrad]	φ _y [mrad]	φ _z [mrad]	U _{total} [mm]
B112	0,000	1	LC5	0,0	0,0	0,0	0,0	0,0	0,0	0,0
B165	49,100	1	LC5	0,5	90,0	83,9	0,0	0,0	0,0	123,0

3.3. Load cases - LC4

Name	Description	Action type	LoadGroup	Duration	Master load case
	Spec	Load type			
LC4	Current R-1 Standard	Variable Static	LG2	Short	None

3.3.1. Internal forces on member

Linear calculation, Extreme : Global, System : Principal

Selection : Named selection - buizen

Load cases : LC4

Member	css	dx [m]	Case	N [kN]	V _y [kN]	V _z [kN]	M _x [kNm]	M _y [kNm]	M _z [kNm]
B213	CS1 - Tube	49,094	LC4	-12839,35	10,57	9,85	0,00	246,56	264,47
B1	CS1 - Tube	40,122	LC4	13,95	-24,18	-22,55	0,00	-155,62	-166,92
B2	CS1 - Tube	76,488	LC4	-10058,63	-218,05	-203,28	0,00	-4872,18	-5226,07
B109	CS1 - Tube	0,000	LC4	-10058,63	218,05	203,28	0,00	-4872,18	-5226,07
B127	CS1 - Tube	0,000	LC4	-12433,24	11,50	10,72	0,00	-1115,76	-1196,81
B38	CS1 - Tube	0,000	LC4	-11323,72	-114,92	-107,14	0,00	5118,90	5490,71
B2	CS1 - Tube	0,000	LC4	-10110,76	-131,23	-122,34	0,00	7581,03	8131,67

3.3.2. 3D displacement

Linear calculation

Load case: LC4

Selection: Named selection - buizen

Location: In nodes avg. on macro. System: LCS mesh element

Results on 1D member:

Extreme 1D: Global

Name	dx [m]	Fibre	Case	u _x [mm]	u _y [mm]	u _z [mm]	φ _x [mrad]	φ _y [mrad]	φ _z [mrad]	U _{total} [mm]
B112	0,000	1	LC4	0,0	0,0	0,0	0,0	0,0	0,0	0,0
B165	49,100	1	LC4	-0,5	-90,0	-83,9	0,0	0,0	0,0	123,0

3.4. Load cases - LC7

Name	Description	Action type	LoadGroup
	Spec	Load type	
LC7	6% Force tubes only	Permanent Standard	LG1

3.4.1. Internal forces on member

Linear calculation, Extreme : Global, System : Principal

Selection : Named selection - buizen

Load cases : LC7

Member	css	dx [m]	Case	N [kN]	V _y [kN]	V _z [kN]	M _x [kNm]	M _y [kNm]	M _z [kNm]
B220	CS1 - Tube	0,000	LC7	0,00	1257,51	-1348,85	-6,95	9806,47	-9142,41
B219	CS1 - Tube	0,000	LC7	0,00	-2394,59	2568,52	6323,66	-52826,09	49248,91
B109	CS1 - Tube	76,488	LC7	0,00	-6342,08	6802,73	-4386,26	304455,39	-283838,82
B2	CS1 - Tube	0,000	LC7	0,00	6197,30	-6647,44	4338,17	281789,31	-262707,60
B106	CS1 - Tube	0,000	LC7	0,00	5234,90	-5615,13	-6905,00	171103,41	-159516,90
B5	CS1 - Tube	0,000	LC7	0,00	-2833,38	3039,18	6991,09	-34278,28	31957,09
B3	CS1 - Tube	44,466	LC7	0,00	-34,21	36,69	5314,69	-117956,90	109969,40

3.4.2. 3D displacement

Project SFT MSC Thesis

Linear calculation

Load case: LC7

Selection: Named selection - buizen

Location: In nodes avg. on macro. System: LCS mesh element

Results on 1D member:

Extreme 1D: Global

Name	dx [m]	Fibre	Case	u _x [mm]	u _y [mm]	u _z [mm]	φ _x [mrad]	φ _y [mrad]	φ _z [mrad]	U _{total} [mm]
B112	0,000	1	LC7	0,0	0,0	0,0	0,0	0,0	0,0	0,0
B32	4,940	8	LC7	0,0	-113,9	122,2	-0,1	0,0	0,0	167,1

3.5. Load cases - LC8

Name	Description	Action type	LoadGroup	Duration	Master load case
	Spec	Load type			
LC8	Current RT Standard	Variable Static	LG2	Short	None

3.5.1. Internal forces on member

Linear calculation, Extreme : Global, System : Principal

Selection : Named selection - buizen

Load cases : LC8

Member	css	dx [m]	Case	N [kN]	V _y [kN]	V _z [kN]	M _x [kNm]	M _y [kNm]	M _z [kNm]
B109	CS1 - Tube	0,000	LC8	-16140,47	290,02	270,38	0,00	5276,53	5659,79
B2	CS1 - Tube	76,488	LC8	16140,47	290,02	270,38	0,00	-5276,53	-5659,79
B54	CS1 - Tube	49,403	LC8	-1513,54	-144,63	-134,83	0,00	747,29	801,57
B2	CS1 - Tube	0,000	LC8	16127,43	311,74	290,63	0,00	-26731,86	-28673,52
B153	CS1 - Tube	0,000	LC8	8726,13	-39,46	-36,79	0,00	6788,40	7281,47
B147	CS1 - Tube	0,000	LC8	9990,12	-42,43	-39,55	0,00	6652,44	7135,64
B109	CS1 - Tube	76,488	LC8	-16127,43	311,74	290,63	0,00	26731,86	28673,52

3.5.2. 3D displacement

Linear calculation

Load case: LC8

Selection: Named selection - buizen

Location: In nodes avg. on macro. System: LCS mesh element

Results on 1D member:

Extreme 1D: Global

Name	dx [m]	Fibre	Case	u _x [mm]	u _y [mm]	u _z [mm]	φ _x [mrad]	φ _y [mrad]	φ _z [mrad]	U _{total} [mm]
B112	0,000	1	LC8	0,0	0,0	0,0	0,0	0,0	0,0	0,0
B188	39,276	8	LC8	34,0	184,9	172,4	0,0	0,0	0,0	255,1

4. Combinations

4.1. Combinations - CO1

Name	Description	Type	Load cases	Coeff. [-]
CO1	SLS - Falling tide	Envelope - ultimate	LC2 - 6% Force LC5 - Current F+1	1,00 1,00

4.1.1. Internal forces on member

Linear calculation, Extreme : Global, System : Principal

Selection : Named selection - buizen

Combinations : CO1

Member	css	dx [m]	Case	N [kN]	V _y [kN]	V _z [kN]	M _x [kNm]	M _y [kNm]	M _z [kNm]
B110	CS1 - Tube	0,000	CO1/1	-13,95	1240,08	-1378,63	2235,09	10082,46	-9087,71
B213	CS1 - Tube	49,094	CO1/1	12839,35	310,14	-353,85	-2207,33	-100829,08	93506,98
B109	CS1 - Tube	76,488	CO1/1	10110,76	-6965,87	7208,73	-10034,85	332883,94	-325541,63

Project SFT MSC Thesis

Member	css	dx [m]	Case	N [kN]	Vy [kN]	Vz [kN]	Mx [kNm]	My [kNm]	Mz [kNm]
B2	CS1 - Tube	0,000	CO1/1	10110,76	6782,48	-7012,02	9965,12	304048,74	-298659,07
B2	CS1 - Tube	0,000	CO1/2	0,00	6651,25	-7134,36	9965,12	311629,76	-290527,39
B109	CS1 - Tube	76,488	CO1/2	0,00	-6834,64	7331,07	-10034,85	340464,96	-317409,95
B112	CS1 - Tube	0,000	CO1/1	12401,49	6373,90	-6877,72	-10111,34	298866,34	-280418,56
B114	CS1 - Tube	0,000	CO1/2	0,00	-425,43	456,33	-4458,05	-125774,38	117257,42
B3	CS1 - Tube	44,466	CO1/1	10034,07	-16,32	20,90	6741,17	-120846,51	119595,02

4.1.2. 3D displacement

Linear calculation

Combination: CO1

Selection: Named selection - buizen

Location: In nodes avg. on macro. System: LCS mesh element

Results on 1D member:

Extreme 1D: Global

Name	dx [m]	Fibre	Case	ux [mm]	uy [mm]	uz [mm]	φx [mrad]	φy [mrad]	φz [mrad]	U _{total} [mm]
B112	0,000	1	CO1/1	0,0	0,0	0,0	0,0	0,0	0,0	0,0
B32	9,881	7	CO1/2	7,5	-94,8	201,7	-0,1	0,0	0,1	222,9

Name	Combination key
CO1/1	LC2
CO1/2	LC2 + LC5

4.2. Combinations - CO2

Name	Description	Type	Load cases	Coeff. [-]
CO2	SLS - Rising tide	Envelope - ultimate	LC2 - 6% Force	1,00
			LC4 - Current R-1	1,00

4.2.1. Internal forces on member

Linear calculation, Extreme : Global, System : Principal

Selection : Named selection - buizen

Combinations : CO2

Member	css	dx [m]	Case	N [kN]	Vy [kN]	Vz [kN]	Mx [kNm]	My [kNm]	Mz [kNm]
B213	CS1 - Tube	49,094	CO2/3	-12839,34	331,27	-334,15	-2207,33	-100335,96	94035,93
B110	CS1 - Tube	0,000	CO2/3	13,95	1288,44	-1333,54	2235,09	9771,22	-9421,55
B109	CS1 - Tube	76,488	CO2/2	0,00	-6834,64	7331,07	-10034,85	340464,96	-317409,95
B2	CS1 - Tube	0,000	CO2/2	0,00	6651,25	-7134,36	9965,12	311629,76	-290527,39
B2	CS1 - Tube	0,000	CO2/3	-10110,76	6520,02	-7256,71	9965,12	319210,78	-282395,71
B109	CS1 - Tube	76,488	CO2/3	-10110,76	-6703,41	7453,41	-10034,85	348045,98	-309278,27
B112	CS1 - Tube	0,000	CO2/2	0,00	6394,28	-6858,72	-10111,34	299759,30	-279460,77
B3	CS1 - Tube	44,466	CO2/3	-10034,07	-19,71	17,75	6741,17	-127761,28	112178,02
B114	CS1 - Tube	0,000	CO2/2	0,00	-425,43	456,33	-4458,05	-125774,38	117257,42

4.2.2. 3D displacement

Linear calculation

Combination: CO2

Selection: Named selection - buizen

Location: In nodes avg. on macro. System: LCS mesh element

Results on 1D member:

Extreme 1D: Global

Name	dx [m]	Fibre	Case	ux [mm]	uy [mm]	uz [mm]	φx [mrad]	φy [mrad]	φz [mrad]	U _{total} [mm]
B112	0,000	1	CO2/1	0,0	0,0	0,0	0,0	0,0	0,0	0,0
B32	9,881	9	CO2/2	-7,5	-194,6	108,6	-0,1	0,1	0,0	222,9

Name	Combination key
CO2/1	LC2
CO2/2	LC2 + LC4

Project SFT MSC Thesis

4.3. Combinations - CO3

Name	Description	Type	Load cases	Coeff. [-]
CO3	SLS - Rotary tide	Envelope - ultimate	LC2 - 6% Force	1,00
			LC8 - Current RT	1,00

4.3.1. Internal forces on member

Linear calculation, Extreme : Global, System : Principal
Selection : Named selection - buizen
Combinations : CO3

Member	css	dx [m]	Case	N [kN]	Vy [kN]	Vz [kN]	Mx [kNm]	My [kNm]	Mz [kNm]
B109	CS1 - Tube	0,000	CO3/4	-16140,47	-2602,36	3372,86	-10034,85	-53277,74	60248,99
B2	CS1 - Tube	76,488	CO3/4	16140,47	2999,02	-2635,38	9965,12	-77620,40	61785,24
B109	CS1 - Tube	76,488	CO3/2	0,00	-6834,64	7331,07	-10034,85	340464,96	-317409,95
B2	CS1 - Tube	0,000	CO3/4	16127,43	6962,99	-6843,73	9965,12	284897,92	-319200,90
B2	CS1 - Tube	0,000	CO3/2	0,00	6651,25	-7134,36	9965,12	311629,76	-290527,39
B109	CS1 - Tube	76,488	CO3/4	-16127,43	-6522,90	7621,70	-10034,85	367196,80	-288736,45
B112	CS1 - Tube	0,000	CO3/4	-15266,25	6489,80	-6769,67	-10111,34	281004,70	-299577,60
B114	CS1 - Tube	0,000	CO3/4	-12470,15	-372,20	505,96	-4458,05	-131414,09	111208,07
B217	CS1 - Tube	49,095	CO3/4	12470,15	292,61	-207,14	4458,38	-116048,05	119496,88

4.3.2. 3D displacement

Linear calculation
Combination: CO3
Selection: Named selection - buizen
Location: In nodes avg. on macro. System: LCS mesh element
Results on 1D member:
Extreme 1D: Global

Name	dx [m]	Fibre	Case	ux [mm]	uy [mm]	uz [mm]	Φx [mrad]	Φy [mrad]	Φz [mrad]	U _{total} [mm]
B112	0,000	1	CO3/1	0,0	0,0	0,0	0,0	0,0	0,0	0,0
B32	4,940	10	CO3/2	32,3	-329,5	-17,2	-0,1	0,0	0,0	331,5

Name	Combination key
CO3/1	LC2
CO3/2	LC2 + LC8

4.4. Combinations - CO4

Name	Description	Type	Load cases	Coeff. [-]
CO4	ULS - Falling tide	Envelope - ultimate	LC2 - 6% Force	1,32
			LC5 - Current F+1	1,65

4.4.1. Internal forces on member

Linear calculation, Extreme : Global, System : Principal
Selection : Named selection - buizen
Combinations : CO4

Member	css	dx [m]	Case	N [kN]	Vy [kN]	Vz [kN]	Mx [kNm]	My [kNm]	Mz [kNm]
B110	CS1 - Tube	0,000	CO4/5	-23,01	1628,92	-1827,24	2950,31	13360,20	-11940,69
B213	CS1 - Tube	49,094	CO4/5	21184,92	405,89	-470,33	-2913,68	-133175,76	123341,95
B109	CS1 - Tube	76,488	CO4/5	16682,76	-9238,25	9475,15	-13246,00	436905,06	-432398,40
B2	CS1 - Tube	0,000	CO4/5	16682,76	8996,18	-9215,50	13153,96	398842,59	-396913,41
B2	CS1 - Tube	0,000	CO4/6	0,00	8779,65	-9417,36	13153,96	411351,30	-383496,16
B109	CS1 - Tube	76,488	CO4/6	0,00	-9021,72	9677,01	-13246,00	449413,76	-418981,15
B112	CS1 - Tube	0,000	CO4/5	20462,46	8406,82	-9084,86	-13346,97	394208,90	-370468,61
B114	CS1 - Tube	0,000	CO4/6	0,00	-561,57	602,36	-5884,63	-166022,18	154779,81
B3	CS1 - Tube	44,466	CO4/5	16556,22	-20,99	28,11	8898,35	-158376,48	159089,25

4.4.2. 3D displacement

Project SFT MSC Thesis

Linear calculation

Combination: CO4

Selection: Named selection - buizen

Location: In nodes avg. on macro. System: LCS mesh element

Results on 1D member:

Extreme 1D: Global

Name	dx [m]	Fibre	Case	u _x [mm]	u _y [mm]	u _z [mm]	Φ _x [mrad]	Φ _y [mrad]	Φ _z [mrad]	U _{total} [mm]
B112	0,000	1	CO4/1	0,0	0,0	0,0	0,0	0,0	0,0	0,0
B35	44,463	6	CO4/2	12,3	-87,3	291,6	-0,1	0,0	0,1	304,7

Name	Combination key
CO4/1	1.32*LC2
CO4/2	1.32*LC2 + 1.65*LC5

4.5. Combinations - CO5

Name	Description	Type	Load cases	Coeff. [-]
CO5	ULS - Rising tide	Envelope - ultimate	LC2 - 6% Force	1,32
			LC4 - Current R-1	1,65

4.5.1. Internal forces on member

Linear calculation, Extreme : Global, System : Principal

Selection : Named selection - buizen

Combinations : CO5

Member	css	dx [m]	Case	N [kN]	V _y [kN]	V _z [kN]	M _x [kNm]	M _y [kNm]	M _z [kNm]
B213	CS1 - Tube	49,094	CO5/7	-21184,92	440,76	-437,82	-2913,68	-132362,10	124214,70
B110	CS1 - Tube	0,000	CO5/7	23,01	1708,72	-1752,84	2950,31	12846,65	-12491,54
B109	CS1 - Tube	76,488	CO5/6	0,00	-9021,72	9677,01	-13246,00	449413,76	-418981,15
B2	CS1 - Tube	0,000	CO5/6	0,00	8779,65	-9417,36	13153,96	411351,30	-383496,16
B2	CS1 - Tube	0,000	CO5/7	-16682,76	8563,13	-9619,23	13153,96	423860,00	-370078,91
B109	CS1 - Tube	76,488	CO5/7	-16682,76	-8805,20	9878,88	-13246,00	461922,46	-405563,90
B112	CS1 - Tube	0,000	CO5/6	0,00	8440,44	-9053,51	-13346,97	395682,27	-368888,22
B3	CS1 - Tube	44,466	CO5/7	-16556,22	-26,58	22,91	8898,35	-169785,82	146851,17
B114	CS1 - Tube	0,000	CO5/6	0,00	-561,57	602,36	-5884,63	-166022,18	154779,81

4.5.2. 3D displacement

Linear calculation

Combination: CO5

Selection: Named selection - buizen

Location: In nodes avg. on macro. System: LCS mesh element

Results on 1D member:

Extreme 1D: Global

Name	dx [m]	Fibre	Case	u _x [mm]	u _y [mm]	u _z [mm]	Φ _x [mrad]	Φ _y [mrad]	Φ _z [mrad]	U _{total} [mm]
B112	0,000	1	CO5/1	0,0	0,0	0,0	0,0	0,0	0,0	0,0
B35	44,463	9	CO5/2	-12,3	-284,8	107,7	-0,1	0,1	0,0	304,7

Name	Combination key
CO5/1	1.32*LC2
CO5/2	1.32*LC2 + 1.65*LC4

4.6. Combinations - CO6

Name	Description	Type	Load cases	Coeff. [-]
CO6	ULS - Rotary tide	Envelope - ultimate	LC2 - 6% Force	1,32
			LC8 - Current RT	1,65

4.6.1. Internal forces on member

Linear calculation, Extreme : Global, System : Principal

Selection : Named selection - buizen

Project SFT MSC Thesis

Combinations : CO6

Member	css	dx [m]	Case	N [kN]	Vy [kN]	Vz [kN]	Mx [kNm]	My [kNm]	Mz [kNm]
B109	CS1 - Tube	0,000	CO6/8	-26631,77	-3339,41	4541,40	-13246,00	-68585,37	81396,40
B2	CS1 - Tube	76,488	CO6/8	26631,78	4054,42	-3389,48	13153,96	-104200,18	79688,78
B109	CS1 - Tube	76,488	CO6/6	0,00	-9021,72	9677,01	-13246,00	449413,76	-418981,15
B2	CS1 - Tube	0,000	CO6/8	26610,26	9294,03	-8937,82	13153,96	367243,74	-430807,46
B2	CS1 - Tube	0,000	CO6/6	0,00	8779,65	-9417,36	13153,96	411351,30	-383496,16
B109	CS1 - Tube	76,488	CO6/8	-26610,26	-8507,35	10156,55	-13246,00	493521,31	-371669,86
B112	CS1 - Tube	0,000	CO6/8	-25189,32	8598,06	-8906,57	-13346,97	364737,18	-402080,99
B114	CS1 - Tube	0,000	CO6/8	-20575,74	-473,74	684,24	-5884,63	-175327,70	144798,38
B217	CS1 - Tube	49,095	CO6/8	20575,74	403,81	-257,05	5885,06	-151322,34	159732,16

4.6.2. 3D displacement

Linear calculation

Combination: CO6

Selection: Named selection - buizen

Location: In nodes avg. on macro. System: LCS mesh element

Results on 1D member:

Extreme 1D: Global

Name	dx [m]	Fibre	Case	u _x [mm]	u _y [mm]	u _z [mm]	φ _x [mrad]	φ _y [mrad]	φ _z [mrad]	U _{total} [mm]
B112	0,000	1	CO6/1	0,0	0,0	0,0	0,0	0,0	0,0	0,0
B32	9,881	11	CO6/2	53,1	-495,8	-80,0	-0,1	0,1	0,0	505,0

Name	Combination key
CO6/1	1.32*LC2
CO6/2	1.32*LC2 + 1.65*LC8

5. Results

5.1. Result cross-sections

5.1.1. Result cross-sections - RC1

Name	Description	List
RC1	SLS	CO1 - Envelope - ultimate CO2 - Envelope - ultimate CO3 - Envelope - ultimate

5.1.1.1. Internal forces on member

Linear calculation, Extreme : Global, System : Principal

Selection : Named selection - buizen

Class : RC1

Member	css	dx [m]	Case	N [kN]	Vy [kN]	Vz [kN]	Mx [kNm]	My [kNm]	Mz [kNm]
B109	CS1 - Tube	0,000	CO3/4	-16140,47	-2602,36	3372,86	-10034,85	-53277,74	60248,99
B2	CS1 - Tube	76,488	CO3/4	16140,47	2999,02	-2635,38	9965,12	-77620,40	61785,24
B109	CS1 - Tube	76,488	CO1/1	10110,76	-6965,87	7208,73	-10034,85	332883,94	-325541,63
B2	CS1 - Tube	0,000	CO3/4	16127,43	6962,99	-6843,73	9965,12	284897,92	-319200,90
B2	CS1 - Tube	0,000	CO2/3	-10110,76	6520,02	-7256,71	9965,12	319210,78	-282395,71
B109	CS1 - Tube	76,488	CO3/4	-16127,43	-6522,90	7621,70	-10034,85	367196,80	-288736,45
B112	CS1 - Tube	0,000	CO1/1	12401,49	6373,90	-6877,72	-10111,34	298866,34	-280418,56
B2	CS1 - Tube	0,000	CO1/1	10110,76	6782,48	-7012,02	9965,12	304048,74	-298659,07
B114	CS1 - Tube	0,000	CO3/4	-12470,15	-372,20	505,96	-4458,05	-131414,09	111208,07
B3	CS1 - Tube	44,466	CO1/1	10034,07	-16,32	20,90	6741,17	-120846,51	119595,02

5.1.1.2. 3D displacement

Linear calculation

Class: RC1

Selection: Named selection - buizen

Location: In nodes avg. on macro. System: LCS mesh element

Results on 1D member:

Extreme 1D: Global

Project SFT MSC Thesis

Name	dx [m]	Fibre	Case	u _x [mm]	u _y [mm]	u _z [mm]	φ _x [mrad]	φ _y [mrad]	φ _z [mrad]	U _{total} [mm]
B112	0,000	1	CO1/1	0,0	0,0	0,0	0,0	0,0	0,0	0,0
B32	4,940	10	CO3/2	32,3	-329,5	-17,2	-0,1	0,0	0,0	331,5

Name	Combination key
CO1/1	LC2
CO3/2	LC2 + LC8

5.1.2. Result cross-sections - RC2

Name	Description	List
RC2	ULS	CO4 - Envelope - ultimate CO5 - Envelope - ultimate CO6 - Envelope - ultimate

5.1.2.1. Internal forces on member

Linear calculation, Extreme : Global, System : Principal
Selection : Named selection - buizen
Class : RC2

Member	css	dx [m]	Case	N [kN]	V _y [kN]	V _z [kN]	M _x [kNm]	M _y [kNm]	M _z [kNm]
B109	CS1 - Tube	0,000	CO6/8	-26631,77	-3339,41	4541,40	-13246,00	-68585,37	81396,40
B2	CS1 - Tube	76,488	CO6/8	26631,78	4054,42	-3389,48	13153,96	-104200,18	79688,78
B109	CS1 - Tube	76,488	CO4/5	16682,76	-9238,25	9475,15	-13246,00	436905,06	-432398,40
B2	CS1 - Tube	0,000	CO6/8	26610,26	9294,03	-8937,82	13153,96	367243,74	-430807,46
B2	CS1 - Tube	0,000	CO5/7	-16682,76	8563,13	-9619,23	13153,96	423860,00	-370078,91
B109	CS1 - Tube	76,488	CO6/8	-26610,26	-8507,35	10156,55	-13246,00	493521,31	-371669,86
B112	CS1 - Tube	0,000	CO4/5	20462,46	8406,82	-9084,86	-13346,97	394208,90	-370468,61
B2	CS1 - Tube	0,000	CO4/5	16682,76	8996,18	-9215,50	13153,96	398842,59	-396913,41
B114	CS1 - Tube	0,000	CO6/8	-20575,74	-473,74	684,24	-5884,63	-175327,70	144798,38
B217	CS1 - Tube	49,095	CO6/8	20575,74	403,81	-257,05	5885,06	-151322,34	159732,16

5.1.2.2. 3D displacement

Linear calculation
Class: RC2
Selection: Named selection - buizen
Location: In nodes avg. on macro. System: LCS mesh element

Results on 1D member:

Extreme 1D: Global

Name	dx [m]	Fibre	Case	u _x [mm]	u _y [mm]	u _z [mm]	φ _x [mrad]	φ _y [mrad]	φ _z [mrad]	U _{total} [mm]
B112	0,000	1	CO4/1	0,0	0,0	0,0	0,0	0,0	0,0	0,0
B32	9,881	11	CO6/2	53,1	-495,8	-80,0	-0,1	0,1	0,0	505,0

Name	Combination key
CO4/1	1.32*LC2
CO6/2	1.32*LC2 + 1.65*LC8

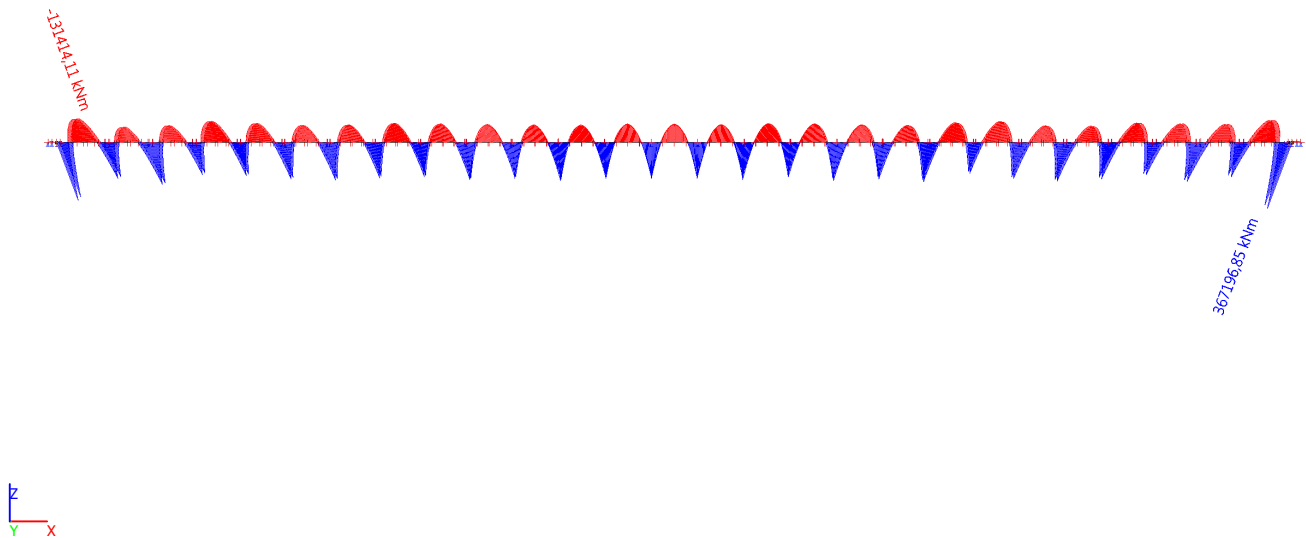
5.2. Bending moment diagrams

5.2.1. Bending moment diagrams - RC1

Name	Description	List
RC1	SLS	CO1 - Envelope - ultimate CO2 - Envelope - ultimate CO3 - Envelope - ultimate

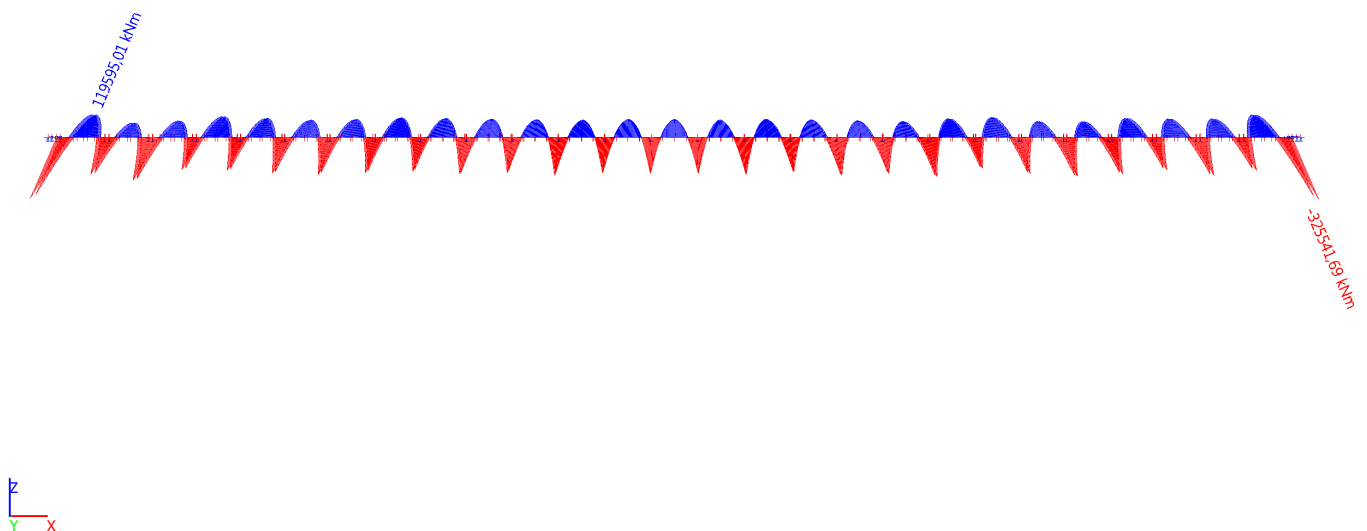
5.2.1.1. 1D internal forces; M_y

Values: M_y
Linear calculation
Class: RC1
Coordinate system: Principal
Extreme 1D: Cross-section
Selection: Named selection - buizen



5.2.1.2. 1D internal forces; M_z

Values: M_z
Linear calculation
Class: RC1
Coordinate system: Principal
Extreme 1D: Cross-section
Selection: Named selection - buizen

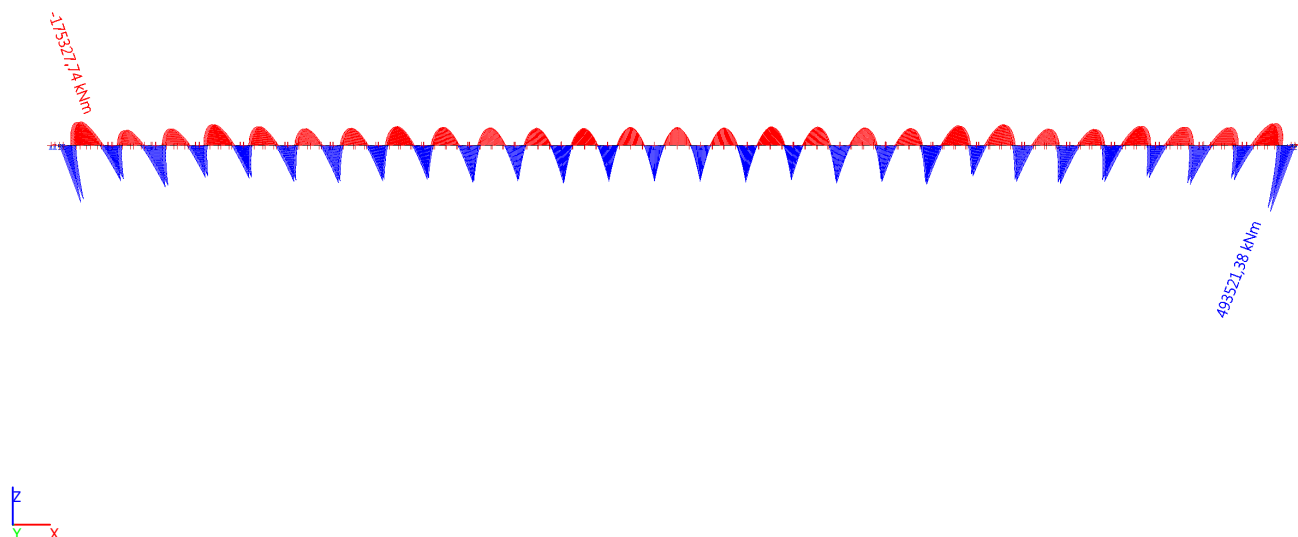


5.2.2. Bending moment diagrams - RC2

Name	Description	List
RC2	ULS	CO4 - Envelope - ultimate
		CO5 - Envelope - ultimate
		CO6 - Envelope - ultimate

5.2.2.1. 1D internal forces; M_y

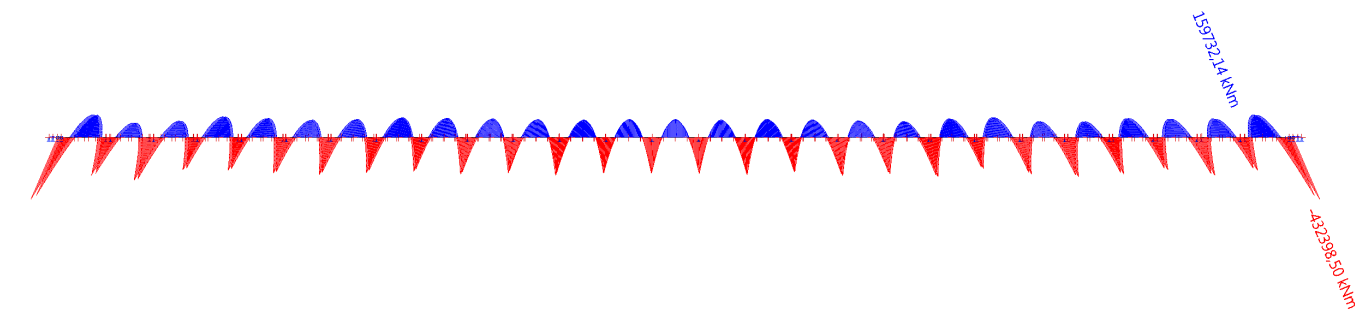
Values: M_y
Linear calculation
Class: RC2
Coordinate system: Principal
Extreme 1D: Cross-section
Selection: Named selection - buizen



Project SFT MSC Thesis

5.2.2.2. 1D internal forces; M_z

Values: **M_z**
Linear calculation
Class: RC2
Coordinate system: Principal
Extreme 1D: Cross-section
Selection: Named selection - buizen



5.3. Shearforce diagram

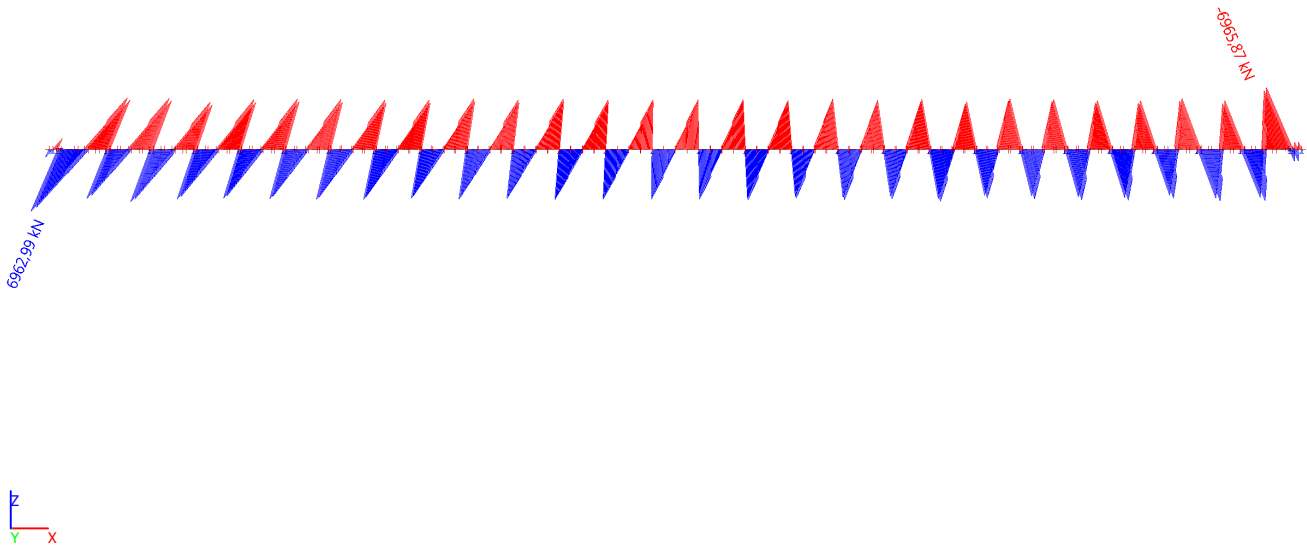
5.3.1. Shearforce diagram - RC1

Name	Description	List
RC1	SLS	CO1 - Envelope - ultimate
		CO2 - Envelope - ultimate
		CO3 - Envelope - ultimate

Project SFT MSC Thesis

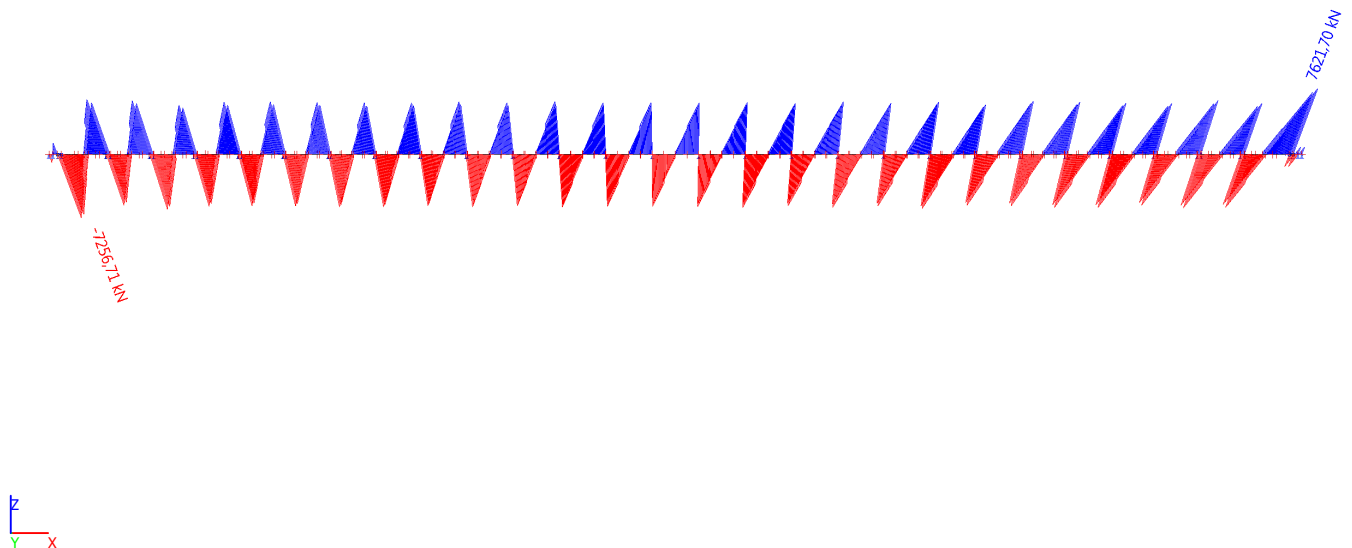
5.3.1.1. 1D internal forces; V_y

Values: V_y
Linear calculation
Class: RC1
Coordinate system: Principal
Extreme 1D: Cross-section
Selection: Named selection - buizen



5.3.1.2. 1D internal forces; V_z

Values: V_z
Linear calculation
Class: RC1
Coordinate system: Principal
Extreme 1D: Cross-section
Selection: Named selection - buizen

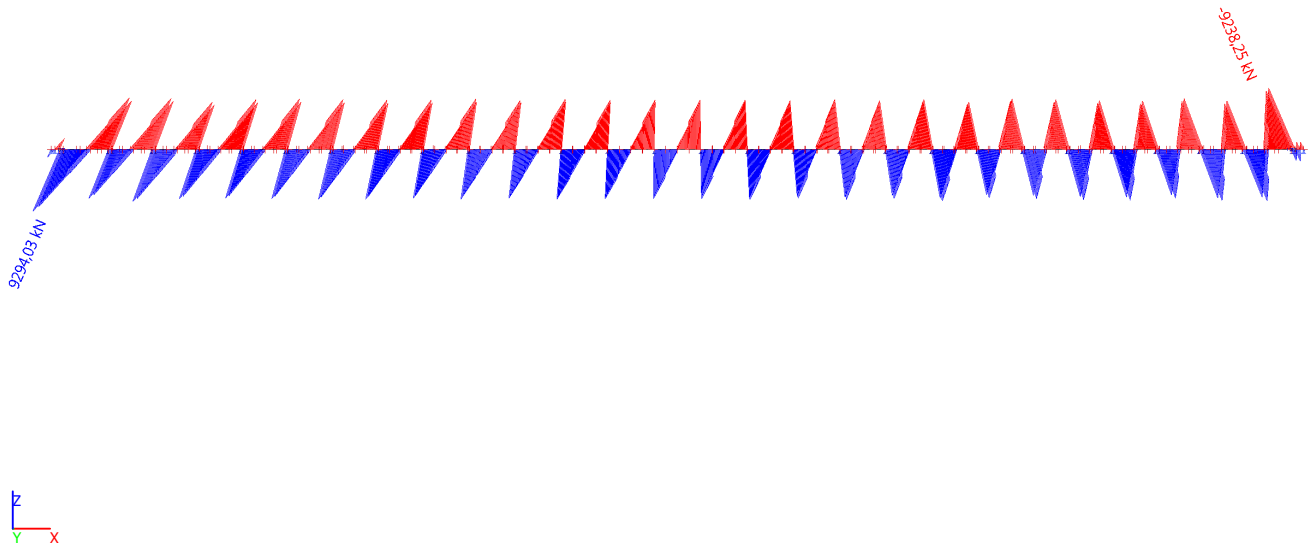


5.3.2. Shearforce diagram - RC2

Name	Description	List
RC2	ULS	CO4 - Envelope - ultimate
		CO5 - Envelope - ultimate
		CO6 - Envelope - ultimate

5.3.2.1. 1D internal forces; V_y

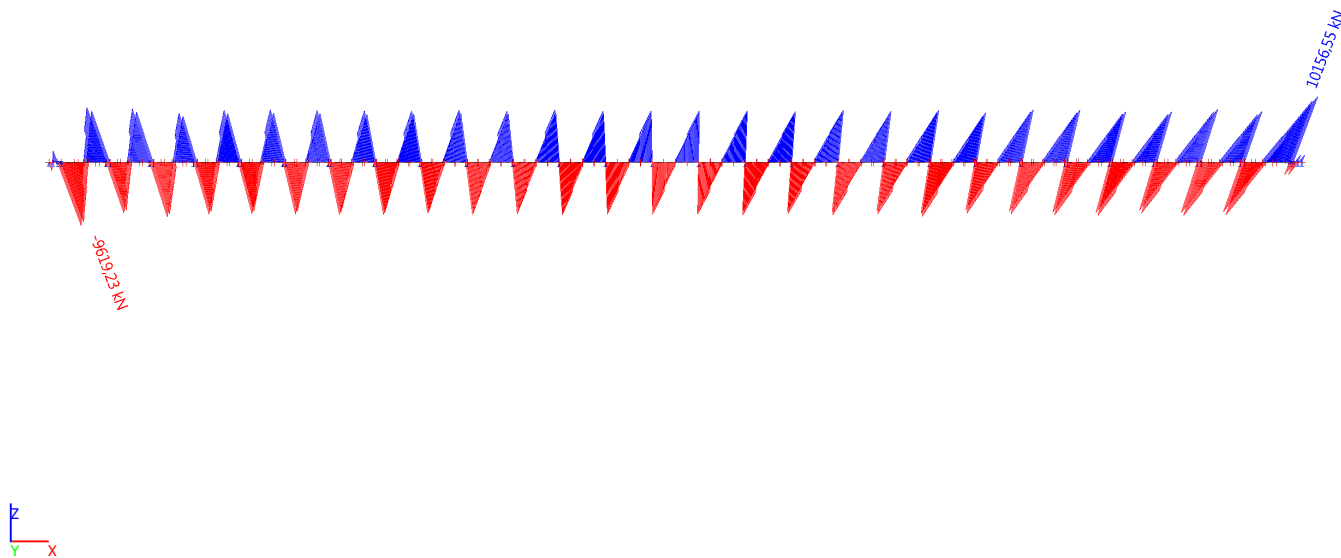
Values: V_y
Linear calculation
Class: RC2
Coordinate system: Principal
Extreme 1D: Cross-section
Selection: Named selection - buizen



Project SFT MSC Thesis

5.3.2.2. 1D internal forces; V_z

Values: V_z
Linear calculation
Class: RC2
Coordinate system: Principal
Extreme 1D: Cross-section
Selection: Named selection - buizen



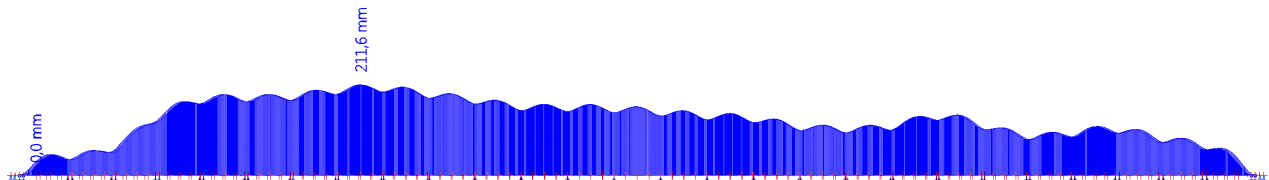
5.4. 1D deformations

5.4.1. 1D deformations - RC1

Name	Description	List
RC1	SLS	CO1 - Envelope - ultimate
		CO2 - Envelope - ultimate
		CO3 - Envelope - ultimate

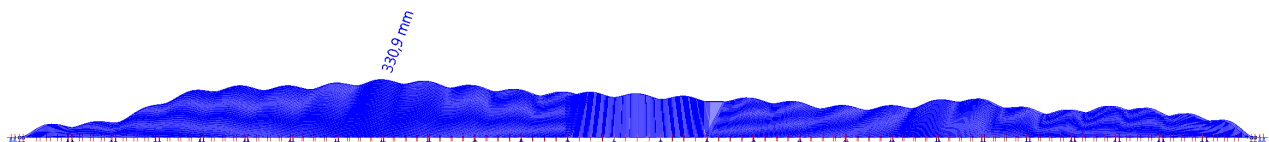
5.4.1.1. 1D deformations; u_z

Values: u_z
Linear calculation
Class: RC1
Coordinate system: Global
Extreme 1D: Global
Selection: Named selection - buizen



5.4.1.2. 1D deformations; U_{total}

Values: U_{total}
Linear calculation
Class: RC1
Coordinate system: Global
Extreme 1D: Global
Selection: Named selection - buizen



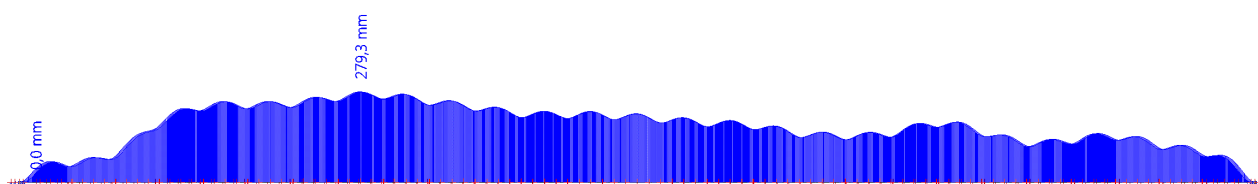
Project SFT MSC Thesis

5.4.2. 1D deformations - RC2

Name	Description	List
RC2	ULS	CO4 - Envelope - ultimate
		CO5 - Envelope - ultimate
		CO6 - Envelope - ultimate

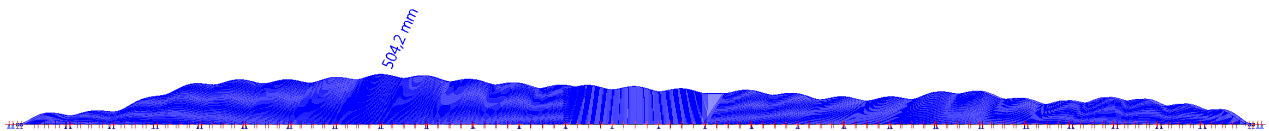
5.4.2.1. 1D deformations; u_z

Values: u_z
Linear calculation
Class: RC2
Coordinate system: Global
Extreme 1D: Global
Selection: Named selection - buizen



5.4.2.2. 1D deformations; U_{total}

Values: U_{total}
Linear calculation
Class: RC2
Coordinate system: Global
Extreme 1D: Global
Selection: Named selection - buizen



APPENDIX C

IdeaStatica cross-section capacity

Submerged Floating Tunnels

Laura Bakker

MSc Hydraulic Engineering – Hydraulic Structures

2018, Delft

Inhoudsopgave

- 1 Projectgegevens
- 2 Snedecontroles
- 2.1 Snede S 1
- 3 Lijst met Staafmacro's
- 4 Lijst met gewapende doorsnedes
- 5 Lijst met gebruikte materialen

1 Projectgegevens

Projectnaam	SFT - design
Auteur	Laura Bakker
Aanmaakdatum	29/10/2018

Nationale Norm

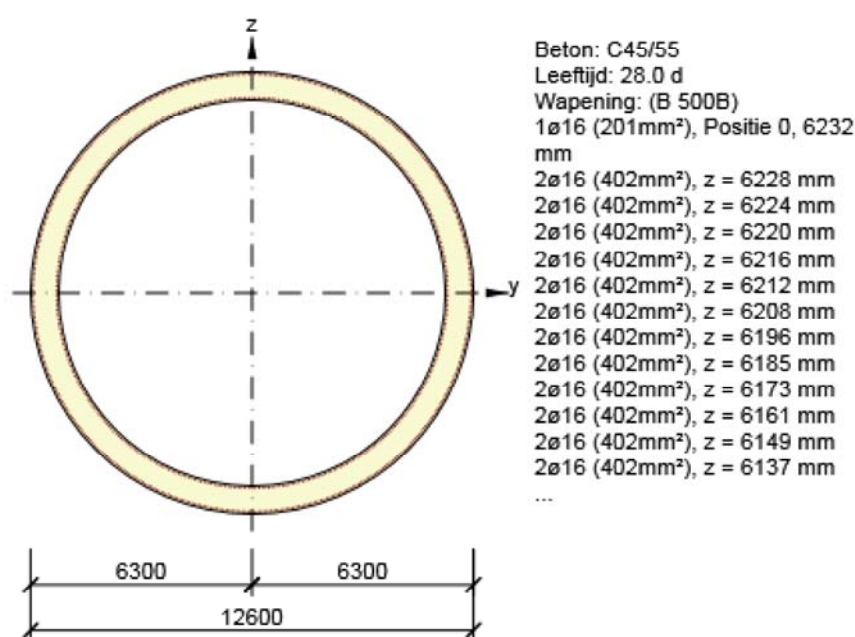
Nationale Norm	EN 1992-1-1:2014-12
Ontwerp levensduur	100 jaar

2 Snedecontroles

2.1 Snede S 1

2.1.1 Extreem S 1 - E 1

Staafmacro	M 1
Gewapende doorsnede	R 1



2.1.1.1 Lasteffecten - snedekrachten








Lasttype	Combinatie type	N [kN]	V _y [kN]	V _z [kN]	T [kNm]	M _y [kNm]	M _z [kNm]
Totaal	Fundamenteel UGT	-280000.0	0.0	13249.0	0.0	617962.0	0.0
Totaal	Karakteristiek	-280000.0	0.0	0.0	0.0	467229.0	0.0
Totaal	Quasi-blijvend	-280000.0	0.0	0.0	0.0	467229.0	0.0

2.1.1.2 Compleet

Maatgevende controle	N _{Ed} [kN]	M _{Ed,y} [kNm]	M _{Ed,z} [kNm]	V _{Ed} [kN]	T _{Ed} [kNm]	Waarde [%]	Controle
Spanningbeperking	-280000.0	467229.0	0.0			73.6	Oké
Type controle	N _{Ed} [kN]	M _{Ed,y} [kNm]	M _{Ed,z} [kNm]	V _{Ed} [kN]	T _{Ed} [kNm]	Waarde [%]	Controle
Weerstand N-My-Mz	-280000.0	617962.0	0.0			43.5	Oké
Dwarskracht	-280000.0			13249.0	0.0	61.7	Oké
Wringing					0.0	0.0	Oké
Interactie	-280000.0	617962.0	0.0	13249.0	0.0	61.7	Oké
Spanningbeperking	-280000.0	467229.0	0.0			73.6	Oké
Scheurwijdte	-280000.0	467229.0	0.0			0.0	Oké

Grenswaarde van de uitnutting van de controle: 100.0 %

Meldingen

Onvolkomenheden	
	Gebruikerswaarde van de effectieve hoogte (volgens de norm) is gebruikt voor de berekening van de dwarskrachtweerstand
	Gebruikerswaarde van de hefboomsarm (volgens de norm) is gebruikt voor de berekening van de dwarskrachtweerstand
	De dwarskracht wordt opgenomen door het beton, beugels zijn enkel nodig volgens detailleringseisen, zie 6.2.2
	Het is niet mogelijk om een equivalente dunwandige doorsnede voor de wringcontrole te maken, maar het is niet noodzakelijk omdat het wringmoment nul is.
	Geen dwarskrachtwapening gevonden in de doorsnede
	Rek in de langwapening veroorzaakt door dwarskracht kan niet worden berekend, omdat het niet mogelijk is om een vakwerkmodel op te zetten vanwege het ontbreken van beugelwapening.
	Scheuren treden er niet op voor korte termijn effect - effectieve betontrekspanning volgens paragraaf 7.1(2) is niet overschreden in de meest getrokken betonvezels

2.1.1.3 Weerstand N-My-Mz

Resultaten weergegeven voor combinatie :Fundamenteel UGT

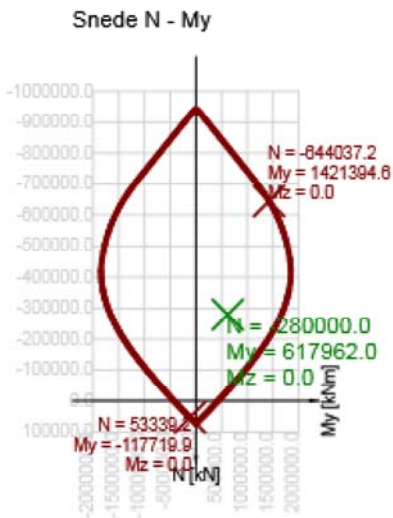
N _{Ed} [kN]	M _{Ed,y} [kNm]	M _{Ed,z} [kNm]	Type	Waarde [%]	Grens [%]	Controle
-280000.0	617962.0	0.0	Nu-Muy-Muz	43.5	100.0	Oké

Rekenwaarde van de weerstand van de doorsnede belast door buiging én normaalkracht

Type	F _{Ed}	F _{Rd1}	F _{Rd2}
N [kN]	-280000.0	-644037.2	53339.2
M _y [kNm]	617962.0	1421394.6	-117719.9
M _z [kNm]	0.0	0.0	0.0

Meldingen

Geen foutmeldingen



Verklaring

Symbol	Verklaring
N_{Ed}	Rekenwaarde van de toegepaste normaalkracht t.g.v. een de blijvende en veranderlijke externe belasting, en de secundaire (parasitaire) effecten van de voorspanning
$M_{Ed,y}$	Rekenwaarde van de toegepaste buigende moment om de y-as t.g.v. een de blijvende en veranderlijke externe belasting, en de secundaire (parasitaire) effecten van de voorspanning
$M_{Ed,z}$	Rekenwaarde van de toegepaste buigende moment om de z-as t.g.v. een de blijvende en veranderlijke externe belasting, en de secundaire (parasitaire) effecten van de voorspanning
Type	Nu-Muy-Muz: Doorsnedeweerstand is bepaald op basis van een aangenomen proportionele verandering van de snedekracht, zodanig dat de excentriciteit gelijk blijft totdat het interactievlak is bereikt. De verandering van de snedekrachten kan worden geïnterpreteerd als de beweging in het vlak langs de lijn tussen de oorsprong (0, 0, 0) en (N_{Ed} , $M_{Ed,y}$, $M_{Ed,z}$). De twee snijpunten vertegenwoordigen de twee extreme waarden van de weerstand. Drie waarden van een extreme worden getoond door het programma: weerstand N_{Rd} en de bijbehorende weerstanden $M_{Rd,y}$ en $M_{Rd,z}$.
Waarde	Berekende waarde van de uitnutting van de doorsnede of een -onderdeel (bv. wapeningstaaf) t.o.v. de grenswaarde
Grens	Grenswaarde van de uitnutting van de controle
Controle	Resultaat van de controle
F_{Ed}	Toegepaste rekenwaarde van de kracht t.g.v. een externe last (zonder effecten van de voorspanning)
F_{Rd1}	Eerste verzameling weerstandskrachten resulterend uit de 1ste snede met het interactievlak
F_{Rd2}	Tweede verzameling weerstandskrachten resulterend uit de 2de snede met het interactievlak

2.1.1.4 Dwarskracht

Resultaten weergegeven voor combinatie :Fundamenteel UGT

V_{Ed} [kN]	N_{Ed} [kN]	V_{Rd} [kN]	Controle zone	Artikel	Waarde [%]	Grens [%]	Controle
13249.0	-280000.0	21465.8	zonder reductie	6.2.2(1)	61.7	100.0	Oké

Rekenwaarde en weerstand van de dwarskracht




V_{Ed} [kN]	$V_{Rd,c}$ [kN]	$V_{Rd,max}$ [kN]	$V_{Rd,r}$ [kN]	$V_{Rd,s}$ [kN]	V_{Rd} [kN]
------------------	--------------------	----------------------	--------------------	--------------------	------------------

V_{Ed} [kN]	$V_{Rd,c}$ [kN]	$V_{Rd,max}$ [kN]	$V_{Rd,r}$ [kN]	$V_{Rd,s}$ [kN]	V_{Rd} [kN]
13249.0	21465.8	183708.0	133902.7	0.0	21465.8

Invoerwaarden en tussenresultaten van de afschuifcontrole

n_c	a_{sw} [mm ² /m]	A_{sl} [mm ²]	b_w [mm]	d [mm]	z [mm]	θ [°]	α [°]	α_{cw} [-]
0	0	0	1600	11340	10206	45.0	90.0	1.25
$C_{Rd,c}$ [-]	k [-]	k_1 [-]	ρ_l [-]	σ_{cp} [MPa]	σ_{wd} [MPa]	v_{min} [MPa]	v [-]	v_1 [-]
0.12	1.13	0.15	0.00	6.0	0.0	0.3	0.49	0.60

Meldingen

Onvolkomenheden	
	Gebruikerswaarde van de effectieve hoogte (volgens de norm) is gebruikt voor de berekening van de dwarskrachtweerstand
	Gebruikerswaarde van de hefboomsarm (volgens de norm) is gebruikt voor de berekening van de dwarskrachtweerstand
	De dwarskracht wordt opgenomen door het beton, beugels zijn enkel nodig volgens detaileringseisen, zie 6.2.2

Verklaring

Symbool	Verklaring
V_{Ed}	Rekenwaarde van de toegepaste dwarskracht
N_{Ed}	Rekenwaarde van de toegepaste normaalkracht
V_{Rd}	De rekenwaarde van de afschuifweerstand
Controle zone	Zonetype waarin de controle is uitgevoerd
Artikel	Artikelnr. (methodetype) gebruikt voor de dwarskrachttoets
Waarde	Berekende waarde van de uitnutting van de doorsnede of een -onderdeel (bv. wapeningstaaf) t.o.v. de grenswaarde
Grens	Grenswaarde van de uitnutting van de controle
Controle	Resultaat van de controle
$V_{Rd,c}$	De afschuifweerstand van de staaf zonder afschuifwapening
$V_{Rd,max}$	Dwarskrachtweerstand van het element berekend op basis van de weerstand van de betondrukdiagonalen
$V_{Rd,r}$	Dwarskrachtweerstand voor de dwarskracht berekend zonder reductie door Beta (6.2.2(6))
$V_{Rd,s}$	De rekenwaarde van de dwarskracht dat kan worden opgenomen door de het vloeien van de beugelwapening
n_c	Aantal snedes van de beugel(s)
a_{sw}	De hoeveelheid beugelwapening
A_{sl}	De hoeveelheid trekwapening
b_w	De breedte van de doorsnede in het hart van de doorsnede
d	Effectieve hoogte van de doorsnede
z	Interne hefboomsarm
θ	Hoek tussen de betondrukdiagonaal en de staafas loodrecht op de dwarskracht
α	De hoek tussen de beugelwapening en de staafas loodrecht op de dwarskracht
α_{cw}	Coëfficiënt die rekening houdt met de spanningstoestand in de drukdiagonaal
$C_{Rd,c}$	Coëfficiënt voor de berekening van de rekenwaarde van de afschuifweerstand van de staaf zonder afschuifwapening
k	Coëfficiënt voor de berekening van de rekenwaarde van de afschuifweerstand van de staaf zonder afschuifwapening

Symbol	Verklaring
k_1	Coëfficiënt voor de berekening van de rekenwaarde van de afschuifweerstand van de staaf zonder afschuifwapening
ρ_l	Wap.verhouding van de getrokken langswapening
σ_{cp}	Normaalspanning in de doorsnede t.g.v. de belasting of voorspanning
σ_{wd}	Reken spanning in de dwarskrachtwapening, zie opmerking 2 van artikel 6.2.3 (3)
v_{min}	Coëfficiënt voor de berekening van de rekenwaarde van de afschuifweerstand van de staaf zonder afschuifwapening
v	Sterkte reductiefactor voor gescheurd beton tijdens de dwarskrachtcontrole
v_1	Sterkte reductiefactor voor gescheurd beton tijdens de dwarskrachtcontrole

2.1.1.5 Wringing

Resultaten weergegeven voor combinatie :Fundamenteel UGT

T_{Ed} [kNm]	T_{Rd} [kNm]	Waarde [%]	Grens [%]	Controle
0.0	309522.5	0.0	100.0	Oké


Rekenwaarde en weerstand van de wringmomenten

T_{Ed} [kNm]	$T_{Rd,c}$ [kNm]	$T_{Rd,max}$ [kNm]	$T_{Rd,s}$ [kNm]	T_{Rd} [kNm]
0.0	309522.5	1612088.5	0.0	309522.5

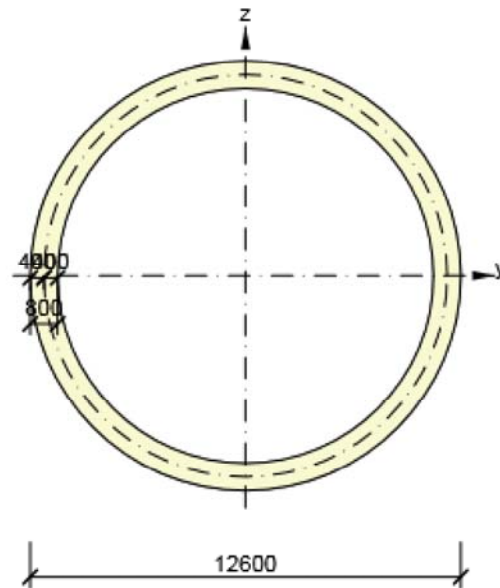
Invoerwaardes en tussenresultaten van de wringcontrole

A_k [mm ²]	u_k [mm]	t_{eff} [mm]	a_{sw} [mm ² /m]	A_{sl} [mm ²]	A_{sp} [mm ²]	θ [°]
109220091	37071	800	0	0	0	45.0

Meldingen

Onvolkomenheden	
	Het is niet mogelijk om een equivalente dunwandige doorsnede voor de wringcontrole te maken, maar het is niet noodzakelijk omdat het wringmoment nul is.

Effectieve dunwandige doorsnede voor wringcontrole



Verklaring

Symbol	Verklaring
T_{Ed}	Rekenwaarde van het toegepaste wringmoment
T_{Rd}	Maatgevende waarde van de wringweerstand
Waarde	Berekende waarde van de uitnutting van de doorsnede of een -onderdeel (bv. wapeningstaaf) t.o.v. de grenswaarde
Grens	Grenswaarde van de uitnutting van de controle
Controle	Resultaat van de controle
$T_{Rd,c}$	Rekenwaarde scheurmoment t.g.v. wringing
$T_{Rd,max}$	De rekenwaarde van de wringweerstand
$T_{Rd,s}$	De rekenwaarde van de wringweerstand, die kan worden geleverd door het vloeien van de wringwapening
A_k	Vlak omsloten door de hartlijnen van de verbonden wanden, inclusief de ingesloten holle delen.
u_k	De perimeter van het oppervlak A_k
t_{eff}	De effectieve wanddikte
a_{sw}	De hoeveelheid beugelwapening dat gebruikt wordt voor de wringcontrole
A_{sl}	De hoeveelheid langswapening binnen de beugel, dat effectief aanwezig is voor de wringweerstand
A_{sp}	Oppervlak van de voorspanwapening binnen de beugel, die effectief weerzaam is voor de wringweerstand
θ	Hoek tussen de betondrukdiagonaal en de staafas loodrecht op de dwarskracht

2.1.1.6 Interactie

Resultaten weergegeven voor combinatie :Fundamenteel UGT

N_{Ed} [kN]	M_{Edy} [kNm]	M_{Edz} [kNm]	V_{Ed} [kN]	T_{Ed} [kNm]	Waarde V+T [%]	Waarde V+T+M [%]	Waarde [%]	Grens [%]	Controle
-280000.0	617962.0	0.0	13249.0	0.0	61.7	27.4	61.7	100.0	Oké

Interactiecontrole voor dwarskracht én wringing (beton)

$V_{Rd,c}$ [kN]	$T_{Rd,c}$ [kNm]	$V_{Rd,max}$ [kN]	$T_{Rd,max}$ [kNm]	Verg. 6.31 [%]	Verg. 6.29 [%]	Waarde [%]	Grens [%]	Controle
--------------------	---------------------	----------------------	-----------------------	-------------------	-------------------	---------------	--------------	----------

$V_{Rd,c}$ [kN]	$T_{Rd,c}$ [kNm]	$V_{Rd,max}$ [kN]	$T_{Rd,max}$ [kNm]	Verg. 6.31 [%]	Verg. 6.29 [%]	Waarde [%]	Grens [%]	Controle
21465.8	309522.5	183708.0	1612088.5	61.7	7.2	61.7	100.0	Oké

Interactiecontrole voor dwarskracht, wrijving én normaalkracht

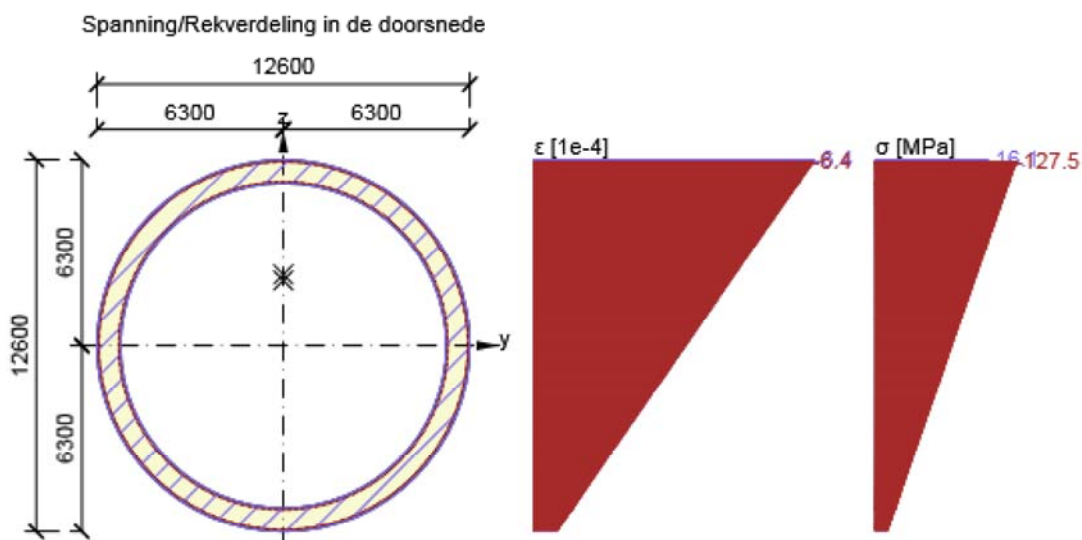
F_b [kN]	$\Delta F_{td,s}$ [kN]	$\Delta F_{td,t}$ [kN]	$\Delta \epsilon_s$ [1e-4]	$\Delta \epsilon_t$ [1e-4]	Extreme in staaf	Waarde [%]	Grens [%]	Controle
-10990.9	13249.0	0.0	0.0	0.0	109	27.4	100.0	Oké

Gedetailleerde staafcontrole

Staaf	y_i [mm]	z_i [mm]	$\Delta \epsilon_{st}$ [1e-4]	ϵ [1e-4]	ϵ_{lim} [1e-4]	$\Delta \sigma_{st}$ [MPa]	σ [MPa]	σ_{lim} [MPa]	Waarde [%]	Controle
109	0	6232	0.0	-6.4	-450.0	0.0	-127.5	-465.9	27.4	Oké

Meldingen

Onvolkomenheden	
!	Geen dwarskrachtwapening gevonden in de doorsnede
!	Rek in de langwapening veroorzaakt door dwarskracht kan niet worden berekend, omdat het niet mogelijk is om een vakwerkmodel op te zetten vanwege het ontbreken van beugelwapening.



Verklaring

Symbool	Verklaring
N_{Ed}	Rekenwaarde van de toegepaste normaalkracht
M_{Edy}	Rekenwaarde van het toegepaste buigend moment om de y-as
M_{Edz}	Rekenwaarde van het toegepaste buigend moment om de z-as
V_{Ed}	Rekenwaarde van de toegepaste dwarskracht
T_{Ed}	Rekenwaarde van het toegepaste wringmoment
Waarde V+T	Berekende U.C.-waarde (uitnutting van de doorsnede) voor interactie tussen dwarskracht en wrijving gerelateerd aan de grenswaarde
Waarde V+T+M	Berekende U.C.-waarde (uitnutting van de doorsnede) voor interactie tussen dwarskracht, wrijving en buiging gerelateerd aan de grenswaarde
Waarde	Berekende waarde van de uitnutting van de doorsnede of een -onderdeel (bv. wapeningstaaf) t.o.v. de grenswaarde
Grens	Grenswaarde van de uitnutting van de controle

Symbol	Verklaring
Controle	Resultaat van de controle
$V_{Rd,c}$	De afschuifweerstand van de staaf zonder afschuifwapening
$T_{Rd,c}$	Rekenwaarde scheurmoment t.g.v. wringing
$V_{Rd,max}$	Dwarskrachtweerstand van het element berekend op basis van de weerstand van de betondrukdiagonalen
$T_{Rd,max}$	De rekenwaarde van de wringweerstand
Verg. 6.31	Het resultaat van de U.C.-waarde van de doorsnede volgens vergelijking (6.31) van EN 1992-1-1
Verg. 6.29	Het resultaat van de U.C.-waarde van de doorsnede volgens vergelijking (6.29) van EN 1992-1-1
F_b	Resulterende kracht in de langswapening t.g.v. buiging en normaalkracht
$\Delta F_{td,s}$	Bijkomende trekkracht in de langswapening t.g.v. dwarskracht berekend als $V_{Ed} \cdot \cot \theta$
$\Delta F_{td,t}$	Bijkomende trekkracht in de langswapening t.g.v. wringing
$\Delta \epsilon_s$	Extra trekrek in de wapening/spanelement t.g.v. dwarskracht
$\Delta \epsilon_t$	Extra trekrek in de wapening/spanelement t.g.v. wringing
Extreme in staaf	Wapeningstaafnr. met de hoogste U.C.-waarde
Staat	Wapeningstaafnr. met de hoogste U.C.-waarde
y_i	y-coördinaat van het drsn. onderdeel(vezel/staaf/spanelement...) gerelateerd aan het zwaartepunt van de doorsnede
z_i	z-coördinaat van het drsn. onderdeel(vezel/staaf/spanelement...) gerelateerd aan het zwaartepunt van de doorsnede
$\Delta \epsilon_{st}$	Bijkomende trekrek in wap.staaf/spanelement t.g.v. de dwarskracht én wringing
ϵ	De rek in de wap.staaf/spanelement t.g.v. dwarskracht, wringing en buiging
ϵ_{lim}	Grenswaarde van de rek in de wap.staaf/spanelement
$\Delta \sigma_{st}$	Bijkomende trekspanning in wap.staaf/spanelement t.g.v. de dwarskracht én wringing
σ	De spanning in de wap.staaf/spanelement t.g.v. de dwarskracht, wringing én buiging
σ_{lim}	Grenswaarde van de spanning in de wap.staaf/spanelement

2.1.1.7 Spanningbeperking

Spanningbeperking - korte termijn effect

Type controle	Type Doorsnedeonderdeel	Index	σ [MPa]	σ_{lim} [MPa]	Waarde [%]	Grens [%]	Controle
7.2(3)-Quasi	Betonvezel	7	-14.9	-20.3	73.6	100.0	Oké

Spanningbeperking - lange termijn effect

Type controle	Type Doorsnedeonderdeel	Index	σ [MPa]	σ_{lim} [MPa]	Waarde [%]	Grens [%]	Controle
7.2(3)-Quasi	Betonvezel	7	-14.4	-20.3	71.1	100.0	Oké

Gedetailleerde controle van het beton - korte termijn effect

Type controle	Vezel	y_i [mm]	z_i [mm]	N [kN]	M_y [kNm]	M_z [kNm]	σ [MPa]	σ_{lim} [MPa]	Waarde [%]	Controle
7.2(2)-Char	7	0	6300	-280000.0	467229.0	0.0	-14.9	-27.0	55.2	Oké
7.2(3)-Quasi	7	0	6300	-280000.0	467229.0	0.0	-14.9	-20.3	73.6	Oké

Gedetailleerde controle van het beton - lange termijn effect

Type controle	Vezel	y_i [mm]	z_i [mm]	N [kN]	M_y [kNm]	M_z [kNm]	σ [MPa]	σ_{lim} [MPa]	Waarde [%]	Controle
---------------	-------	---------------	---------------	-----------	----------------	----------------	-------------------	-------------------------	---------------	----------

Type controle	Vezel	y_i [mm]	z_i [mm]	N [kN]	M_y [kNm]	M_z [kNm]	σ [MPa]	σ_{lim} [MPa]	Waarde [%]	Controle
7.2(2)-Char	7	0	6300	-280000.0	467229.0	0.0	-14.4	-27.0	53.3	Oké
7.2(3)-Quasi	7	0	6300	-280000.0	467229.0	0.0	-14.4	-20.3	71.1	Oké

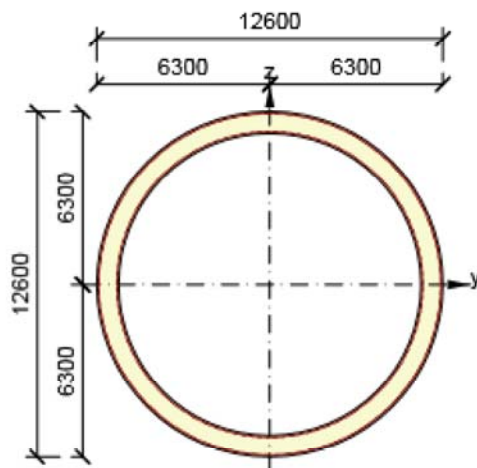
Kruipcoëfficiënt

Bepalingsmethode	h_0 [mm]	A_c [mm ²]	u [mm]	t [d]	t_0 [d]	t_s [d]	RH [%]	Gebruik γ_{lt}	$\phi(t, t_0)$ [-]
Automatisch	1497	29619008	39584	36500.0	28.0	7.0	65	Nee	1.23

Meldingen

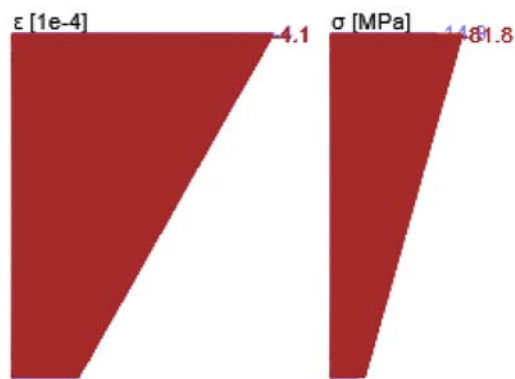
Geen foutmeldingen

Spanning/Rekverdeling in de doorsnede

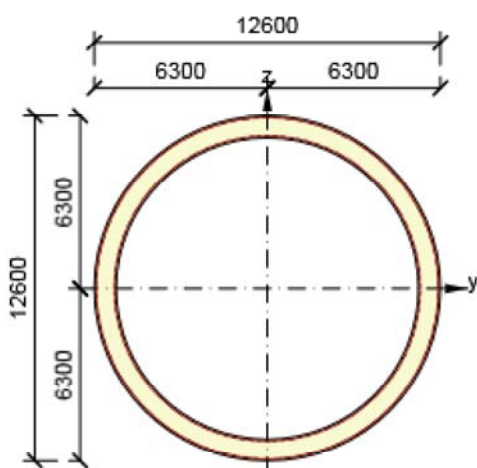


Resultaten weergegeven voor :

- Quasi-blijvende combinatie
- Resultaten voor de korte-termijn stijfheidsberekening

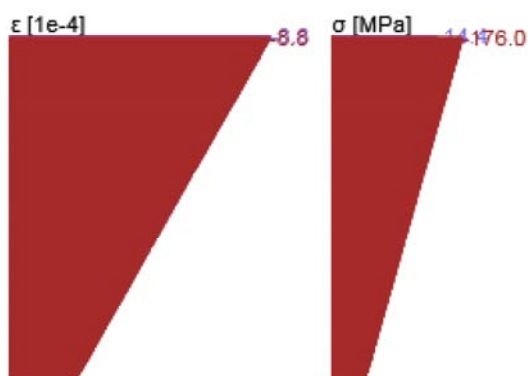


Spanning/Rekverdeling in de doorsnede



Resultaten weergegeven voor :

- Quasi-blijvende combinatie
- Resultaten voor de lange-termijn stijfheidsberekening



Verklaring

Symbol	Verklaring
Type controle	Het nummer van de paragraaf en het type BGT-combinatie, dat gebruikt is voor de berekening van de spanningbeperking.
Type Doorsnedeonderdeel	Opgave van type drsn. onderdeel (betonvezel/wap.staaf/spanelement) met extreme waarde van de controle

Symbool	Verklaring
Index	Betonvezelnr., wap.staafnr. of spanelementnr. met extreme waarde van de controle
σ	De spanning in drsn. onderdeel (vezel/wap.staaf/spanelement...) berekend voor de toegepaste BGT-combinatie
σ_{lim}	Grenswaarde van de spanning in drsn. onderdeel (vezel/wap.staaf/spanelement...) berekend voor de toegepaste BGT-combinatie
Waarde	Berekende waarde van de uitnutting van de doorsnede of een -onderdeel (bv. wapeningstaaf) t.o.v. de grenswaarde
Grens	Grenswaarde van de uitnutting van de controle
Controle	Resultaat van de controle
Vezel	Betonvezelnr. met hoogste U.C.-waarde
y_i	y-coördinaat van het drsn. onderdeel(vezel/staaf/spanelement...) gerelateerd aan het zwaartepunt van de doorsnede
z_i	z-coördinaat van het drsn. onderdeel(vezel/staaf/spanelement...) gerelateerd aan het zwaartepunt van de doorsnede
N	Normaalkracht voor toegepaste BGT-combinatie
M_y	Buigend moment om de y-as voor de toegepaste BGT-combinatie
M_z	Buigend moment om de z-as voor de toegepaste BGT-combinatie
h_0	De grootte = $2A_c / u$, waar A_c het betonoppervlak is en u de omtrek dat wordt blootgesteld aan uitdroging
A_c	Het doorsnede oppervlak van beton
u	De perimeter van het gedeelte dat blootgesteld wordt aan uitdroging
t	De betonleeftijd in dagen op het beschouwde tijdstip
t_0	De betonleeftijd in dagen bij het aanbrengen van de belasting
t_s	De betonleeftijd (in dagen) bij het begin van de krimp (of zwellen). Normaal gesproken is dit nadat de curing (behandeling) is beëindigd
Gebruik γ_{lt}	Gebruik lange-termijn uitgesteld rek inschattingsfactor volgens bijlage B, artikel B.105 (103)
$\phi(t, t_0)$	Berekende waarde van de kruipcoëfficiënt

2.1.1.8 Scheurwijdte

Scheurwijdte - korte termijn effect

Combinatie	N [kN]	M_y [kNm]	M_z [kNm]	w_k [mm]	w_{lim} [mm]	Waarde [%]	Grens [%]	Controle
Quasi	-280000.0	467229.0	0.0	0.000	0.300	0.0	100.0	Oké


Scheurwijdte - lange termijn effect

Combinatie	N [kN]	M_y [kNm]	M_z [kNm]	w_k [mm]	w_{lim} [mm]	Waarde [%]	Grens [%]	Controle
Quasi	-280000.0	467229.0	0.0	0.000	0.300	0.0	100.0	Oké

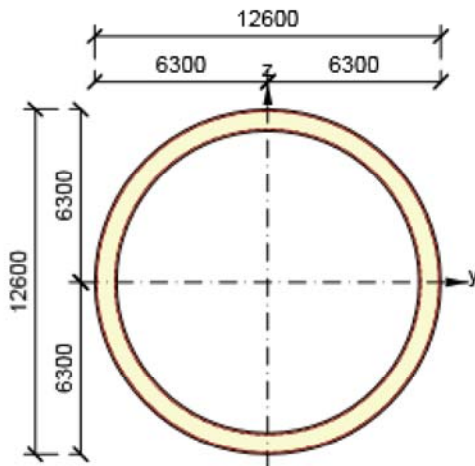
Kruipcoëfficiënt

Bepalingmethode	h_0 [mm]	A_c [mm ²]	u [mm]	t [d]	t_0 [d]	t_s [d]	RH [%]	Gebruik γ_{lt}	$\phi(t, t_0)$ [-]
Automatisch	1497	29619008	39584	36500.0	28.0	7.0	65	Nee	1.23

Meldingen

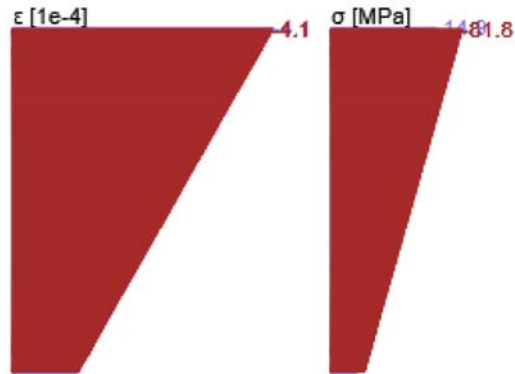
Onvolkomenheden	
	Scheuren treden er niet op voor korte termijn effect - effectieve betontrekspanning volgens paragraaf 7.1(2) is niet overschreden in de meest getrokken betonvezels

Spanning/Rekverdeling in de doorsnede

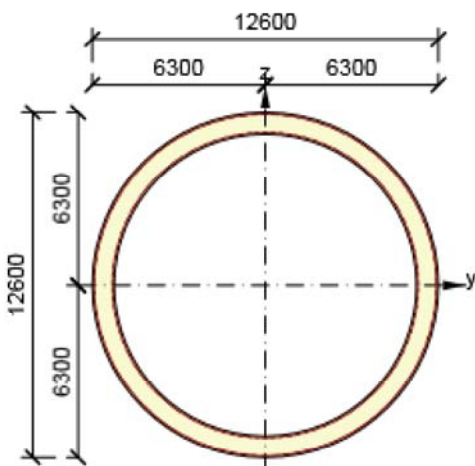


Resultaten weergegeven voor :

- Quasi-blijvende combinatie
- Resultaten voor de korte-termijn stijfheidsberekening

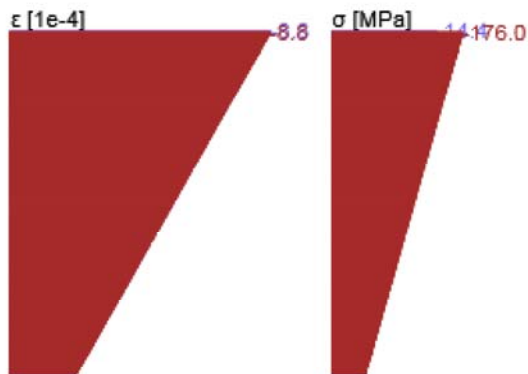


Spanning/Rekverdeling in de doorsnede



Resultaten weergegeven voor :

- Quasi-blijvende combinatie
- Resultaten voor de lange-termijn stijfheidsberekening



Verklaring

Symbol	Verklaring
Combinatie	Gebruikte combinatie voor de berekening inclusief r_{sup} of rinf coëfficiënt volgens 5.10.9
N	Normaalkracht voor de BGT-combinatie
M_y	Buigend moment om de y-as voor de BGT-combinatie
M_z	Buigend moment om de z-as voor de BGT-combinatie
w_k	De scheurwijdte berekend volgens 7.3.4
w_{lim}	Grenswaarde van de scheurwijdte volgens tabel 7.1N
Waarde	Berekende waarde van de uitnutting van de doorsnede of een -onderdeel (bv. wapeningstaaf) t.o.v. de grenswaarde
Grens	Grenswaarde van de uitnutting van de controle
Controle	Resultaat van de controle
h_0	De grootte = $2A_c / u$, waar A_c het betonoppervlak is en u de omtrek dat wordt blootgesteld aan uitdroging
A_c	Het doorsnede oppervlak van beton
u	De perimeter van het gedeelte dat blootgesteld wordt aan uitdroging
t	De betonleeftijd in dagen op het beschouwde tijdstip

Symbool	Verklaring
t_0	De betonleeftijd in dagen bij het aanbrengen van de belasting
t_s	De betonleeftijd (in dagen) bij het begin van de krimp (of zwellen). Normaal gesproken is dit nadat de curing (behandeling) is beëindigd
Gebruik γ_{it}	Gebruik lange-termijn uitgesteld rek inschattingsfactor volgens bijlage B, artikel B.105 (103)
$\phi(t, t_0)$	Berekende waarde van de kruipcoëfficiënt

2.1.1.9 Detailleringseisen

Resultaten weergegeven voor combinatie :Fundamenteel UGT

N_{Ed} [kN]	$M_{Ed,y}$ [kNm]	$M_{Ed,z}$ [kNm]	Verh.-lang [%]	Verh.-Dwarskracht [%]	Maatgevend [%]	Grens [%]	Controle
-280000.0	617962.0	0.0	13.4	0.0	13.4	100.0	Oké

Controle van de detailleringseisen van de langswapening

Type	Waarde _{ber}	Waarde _{lim}	Verh. [%]	Controle
Minimale wap.perct. van de langswapening (9.2.1.1 (1)) [%]	0.00	0.20	0.0	Oké
Maximale wap.perc. van de langswapening (9.2.1.1(3)) [%]	0.54	4.00	13.4	Oké
Minimale afstand van de langswapening (8.2 (2)) [mm]	0	0	0.0	Uit
Maximale afstand van de langswapening (9.2.3 (4)) [mm]	0	350	0.0	Oké





Controle van de detailleringseisen voor de beugels

Type	Waarde _{ber}	Waarde _{lim}	Verh. [%]	Controle
Minimum wap.perc. voor de dwarskrachtwapening (9.2.2 (5)) [%]	0.00	0.00	0.0	Uit
Maximale h.o.h. afstand van de beugels (9.2.2 (6)) [mm]	0	0	0.0	Uit
Maximale beugelbeenafstand (9.2.2 (8)) [mm]	0	0	0.0	Uit
Minimale doorndiameter van een beugel (8.3 (2)) [-]	0.00	0.00	0.0	Uit

Invoerwaarden en tussenresultaten voor detailleringcontrole

b_w [mm]	d [mm]	A_c [mm ²]	$b_t * d$ [mm ²]	f_{yk} [MPa]	f_{yd} [MPa]	f_{ck} [MPa]	f_{ctm} [MPa]	f_{cd} [MPa]
1600	11340	29619008	29319021	500.0	434.8	45.0	3.8	30.0

Meldingen

	Onvolkomenheden
	Gebruikerswaarde van de effectieve hoogte (volgens de norm) is gebruikt voor de berekening van de dwarskrachtweerstand
	Gebruikerswaarde van de hefboomsarm (volgens de norm) is gebruikt voor de berekening van de dwarskrachtweerstand
	Interne fout in de berekening van de maximale afstand van de wapeningsstaven
	Geen dwarskrachtwapening gevonden in de doorsnede

Verklaring

Symbool	Verklaring
N_{Ed}	Rekenwaarde van de toegepaste normaalkracht
$M_{Ed,y}$	Rekenwaarde van het toegepaste buigend moment om de y-as
$M_{Ed,z}$	Rekenwaarde van het toegepaste buigend moment om de z-as
Verh.-lang	U.C.-waarde voor de detailleringseisen van de langswapening

Symbol	Verklaring
Verh. _{Dwarskracht}	U.C.-waarde voor de detailleringseisen van de beugels
Maatgevend	U.C.-waarde voor de detailleringseisen van alle onderdelen
Grens	Grenswaarde voor de detailleringseisen
Controle	Resultaat van de controle
Type	Type van gecontroleerde detailleringseis
Waarde _{ber}	Reken- of toegepaste hoeveelheid, die uiting geeft aan de detailleringseis
Waarde _{lim}	Grenswaarde van de hoeveelheid, die uiting geeft aan de detailleringseis
Verh.	Verhouding van de toelaatbare en de toegepaste hoeveelheid, die uiting geeft aan de detailleringseis in verhouding tot de grenswaarde

3 Lijst met Staafmacro's

Staafmacro M 1

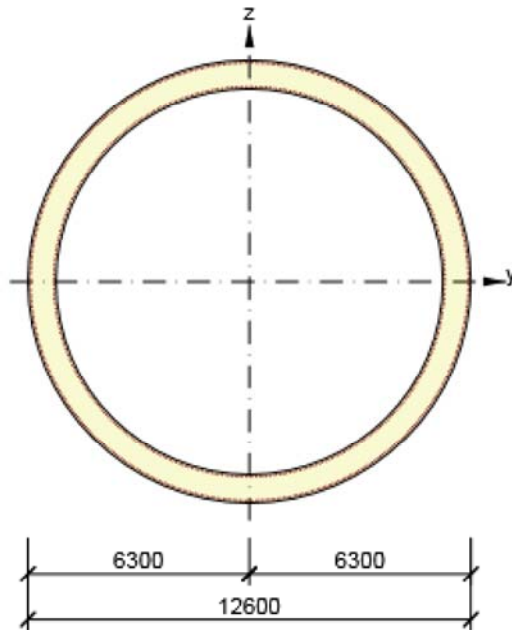
Staaftype	Ligger
Milieuklasse	XC4, XD3, XS3
Relatieve vochtigheid	65 %
Φ_{inf}	Berekend
Belangrijkheid van rekenstaaf	Belangrijk

Buig slankheid gegevens

Vrije ruimte tussen de dagzijdes van de steunpunten (5.3.2.2 (1)) m	Breedte van het steunpunt (5.3.2.2 (1))		Ondersteuningsomstandigheid	
	Links mm	Rechts mm	Links	Rechts
1.00	400	400	Niet-doorgaande ligger	Niet-doorgaande ligger

4 Lijst met gewapende doorsneden

Gewapende doorsnede R 1



Doorsnede-onderdelen

Buisvormige doorsnede (12600 / 11000mm), Materiaal: C45/55	
Punt 1	6300; 0 mm
Punt 2	5820; 2411 mm
Punt 3	4455; 4455 mm
Punt 4	2411; 5820 mm
Punt 5	0; 6300 mm
Punt 6	-2411; 5820 mm
Punt 7	-4455; 4455 mm
Punt 8	-5820; 2411 mm
Punt 9	-6300; 0 mm
Punt 10	-5820; -2411 mm
Punt 11	-4455; -4455 mm
Punt 12	-2411; -5820 mm
Punt 13	0; -6300 mm
Punt 14	2411; -5820 mm
Punt 15	4455; -4455 mm
Punt 16	5820; -2411 mm
Punt 17	6300; 0 mm

Openingen

Opening 1, vertex 1	5500; 0 mm
Opening 1, vertex 2	5081; 2105 mm
Opening 1, vertex 3	3889; 3889 mm
Opening 1, vertex 4	2105; 5081 mm
Opening 1, vertex 5	0; 5500 mm
Opening 1, vertex 6	-2105; 5081 mm

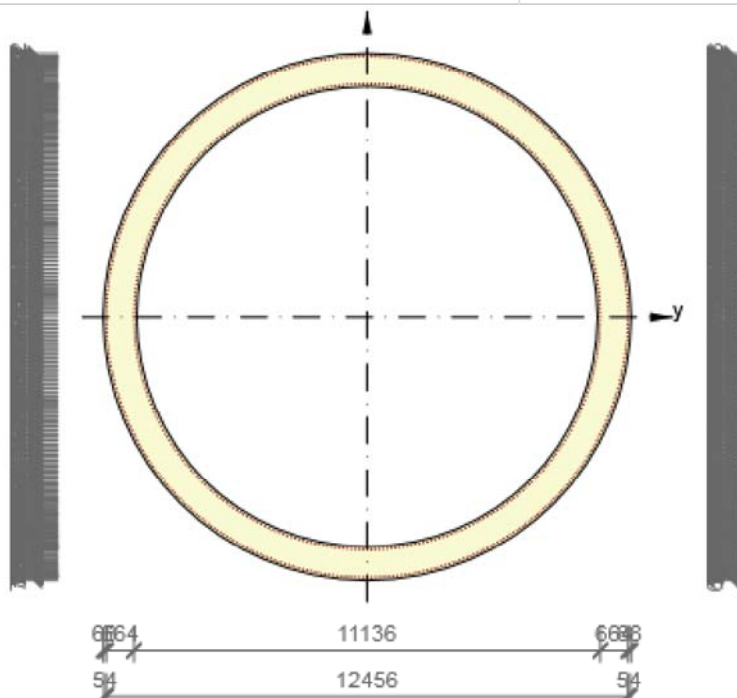
Opening 1, vertex 7	-3889; 3889 mm
Opening 1, vertex 8	-5081; 2105 mm
Opening 1, vertex 9	-5500; 0 mm
Opening 1, vertex 10	-5081; -2105 mm
Opening 1, vertex 11	-3889; -3889 mm
Opening 1, vertex 12	-2105; -5081 mm
Opening 1, vertex 13	0; -5500 mm
Opening 1, vertex 14	2105; -5081 mm
Opening 1, vertex 15	3889; -3889 mm
Opening 1, vertex 16	5081; -2105 mm
Opening 1, vertex 17	5500; 0 mm

Doorsnede-eigenschappen

A [mm ²]	S _y [mm ³]	S _z [mm ³]	I _y [mm ⁴]	I _z [mm ⁴]	C _{gy} [mm]	C _{gz} [mm]	i _y [mm]	i _z [mm]
29619008	0	0	517231440981477	517231440981478	0	0	4179	4179

Betondekking gerelateerd aan de doorsnederanden

Opening 1, rand 1	60 mm
Opening 1, rand 2	60 mm



Langswapening [kg/m]	Beugels [kg/m]	Totale massa [kg/m]	Wapening / m3 beton [kg/m ³]
1250	0	1250	42

Langswapening

Staaf	Ø [mm]	Materiaal	Y [mm]	Z [mm]
1	16	B 500B	6232	0
2	16	B 500B	6228	91
3	16	B 500B	6224	181

Project: SFT - design
 Projectnr.:
 Auteur: Laura Bakker

Staaf	Ø [mm]	Materiaal	Y [mm]	Z [mm]
4	16	B 500B	6220	272
5	16	B 500B	6216	362
6	16	B 500B	6212	453
7	16	B 500B	6208	543
8	16	B 500B	6196	633
9	16	B 500B	6185	723
10	16	B 500B	6173	813
11	16	B 500B	6161	902
12	16	B 500B	6149	992
13	16	B 500B	6137	1082
14	16	B 500B	6118	1171
15	16	B 500B	6098	1259
16	16	B 500B	6078	1348
17	16	B 500B	6059	1436
18	16	B 500B	6039	1524
19	16	B 500B	6020	1613
20	16	B 500B	5992	1699
21	16	B 500B	5965	1786
22	16	B 500B	5938	1872
23	16	B 500B	5911	1959
24	16	B 500B	5883	2045
25	16	B 500B	5856	2131
26	16	B 500B	5821	2215
27	16	B 500B	5787	2299
28	16	B 500B	5752	2383
29	16	B 500B	5717	2466
30	16	B 500B	5683	2550
31	16	B 500B	5648	2634
32	16	B 500B	5606	2714
33	16	B 500B	5564	2794
34	16	B 500B	5523	2875
35	16	B 500B	5481	2955
36	16	B 500B	5439	3036
37	16	B 500B	5397	3116
38	16	B 500B	5348	3192
39	16	B 500B	5300	3269
40	16	B 500B	5251	3345
41	16	B 500B	5202	3422
42	16	B 500B	5154	3498
43	16	B 500B	5105	3574
44	16	B 500B	5050	3646
45	16	B 500B	4995	3718
46	16	B 500B	4939	3790

Project: SFT - design
 Projectnr.:
 Auteur: Laura Bakker

Staaf	Ø [mm]	Materiaal	Y [mm]	Z [mm]
47	16	B 500B	4884	3862
48	16	B 500B	4829	3934
49	16	B 500B	4774	4006
50	16	B 500B	4713	4073
51	16	B 500B	4652	4139
52	16	B 500B	4590	4206
53	16	B 500B	4529	4273
54	16	B 500B	4468	4340
55	16	B 500B	4407	4407
56	16	B 500B	4340	4468
57	16	B 500B	4273	4529
58	16	B 500B	4206	4590
59	16	B 500B	4139	4652
60	16	B 500B	4073	4713
61	16	B 500B	4006	4774
62	16	B 500B	3934	4829
63	16	B 500B	3862	4884
64	16	B 500B	3790	4939
65	16	B 500B	3718	4995
66	16	B 500B	3646	5050
67	16	B 500B	3574	5105
68	16	B 500B	3498	5154
69	16	B 500B	3422	5202
70	16	B 500B	3345	5251
71	16	B 500B	3269	5300
72	16	B 500B	3192	5348
73	16	B 500B	3116	5397
74	16	B 500B	3036	5439
75	16	B 500B	2955	5481
76	16	B 500B	2875	5523
77	16	B 500B	2794	5564
78	16	B 500B	2714	5606
79	16	B 500B	2634	5648
80	16	B 500B	2550	5683
81	16	B 500B	2466	5717
82	16	B 500B	2383	5752
83	16	B 500B	2299	5787
84	16	B 500B	2215	5821
85	16	B 500B	2131	5856
86	16	B 500B	2045	5883
87	16	B 500B	1959	5911
88	16	B 500B	1872	5938
89	16	B 500B	1786	5965

Project: SFT - design
 Projectnr.:
 Auteur: Laura Bakker

Staaf	Ø [mm]	Materiaal	Y [mm]	Z [mm]
90	16	B 500B	1699	5992
91	16	B 500B	1613	6020
92	16	B 500B	1524	6039
93	16	B 500B	1436	6059
94	16	B 500B	1348	6078
95	16	B 500B	1259	6098
96	16	B 500B	1171	6118
97	16	B 500B	1082	6137
98	16	B 500B	992	6149
99	16	B 500B	902	6161
100	16	B 500B	813	6173
101	16	B 500B	723	6185
102	16	B 500B	633	6196
103	16	B 500B	543	6208
104	16	B 500B	453	6212
105	16	B 500B	362	6216
106	16	B 500B	272	6220
107	16	B 500B	181	6224
108	16	B 500B	91	6228
109	16	B 500B	0	6232
110	16	B 500B	-91	6228
111	16	B 500B	-181	6224
112	16	B 500B	-272	6220
113	16	B 500B	-362	6216
114	16	B 500B	-453	6212
115	16	B 500B	-543	6208
116	16	B 500B	-633	6196
117	16	B 500B	-723	6185
118	16	B 500B	-813	6173
119	16	B 500B	-902	6161
120	16	B 500B	-992	6149
121	16	B 500B	-1082	6137
122	16	B 500B	-1171	6118
123	16	B 500B	-1259	6098
124	16	B 500B	-1348	6078
125	16	B 500B	-1436	6059
126	16	B 500B	-1524	6039
127	16	B 500B	-1613	6020
128	16	B 500B	-1699	5992
129	16	B 500B	-1786	5965
130	16	B 500B	-1872	5938
131	16	B 500B	-1959	5911
132	16	B 500B	-2045	5883

Project: SFT - design
 Projectnr.:
 Auteur: Laura Bakker

Staaf	Ø [mm]	Materiaal	Y [mm]	Z [mm]
133	16	B 500B	-2131	5856
134	16	B 500B	-2215	5821
135	16	B 500B	-2299	5787
136	16	B 500B	-2383	5752
137	16	B 500B	-2466	5717
138	16	B 500B	-2550	5683
139	16	B 500B	-2634	5648
140	16	B 500B	-2714	5606
141	16	B 500B	-2794	5564
142	16	B 500B	-2875	5523
143	16	B 500B	-2955	5481
144	16	B 500B	-3036	5439
145	16	B 500B	-3116	5397
146	16	B 500B	-3192	5348
147	16	B 500B	-3269	5300
148	16	B 500B	-3345	5251
149	16	B 500B	-3422	5202
150	16	B 500B	-3498	5154
151	16	B 500B	-3574	5105
152	16	B 500B	-3646	5050
153	16	B 500B	-3718	4995
154	16	B 500B	-3790	4939
155	16	B 500B	-3862	4884
156	16	B 500B	-3934	4829
157	16	B 500B	-4006	4774
158	16	B 500B	-4073	4713
159	16	B 500B	-4139	4652
160	16	B 500B	-4206	4590
161	16	B 500B	-4273	4529
162	16	B 500B	-4340	4468
163	16	B 500B	-4407	4407
164	16	B 500B	-4468	4340
165	16	B 500B	-4529	4273
166	16	B 500B	-4590	4206
167	16	B 500B	-4652	4139
168	16	B 500B	-4713	4073
169	16	B 500B	-4774	4006
170	16	B 500B	-4829	3934
171	16	B 500B	-4884	3862
172	16	B 500B	-4939	3790
173	16	B 500B	-4995	3718
174	16	B 500B	-5050	3646
175	16	B 500B	-5105	3574

Project: SFT - design
 Projectnr.:
 Auteur: Laura Bakker

Staaf	Ø [mm]	Materiaal	Y [mm]	Z [mm]
176	16	B 500B	-5154	3498
177	16	B 500B	-5202	3422
178	16	B 500B	-5251	3345
179	16	B 500B	-5300	3269
180	16	B 500B	-5348	3192
181	16	B 500B	-5397	3116
182	16	B 500B	-5439	3036
183	16	B 500B	-5481	2955
184	16	B 500B	-5523	2875
185	16	B 500B	-5564	2794
186	16	B 500B	-5606	2714
187	16	B 500B	-5648	2634
188	16	B 500B	-5683	2550
189	16	B 500B	-5717	2466
190	16	B 500B	-5752	2383
191	16	B 500B	-5787	2299
192	16	B 500B	-5821	2215
193	16	B 500B	-5856	2131
194	16	B 500B	-5883	2045
195	16	B 500B	-5911	1959
196	16	B 500B	-5938	1872
197	16	B 500B	-5965	1786
198	16	B 500B	-5992	1699
199	16	B 500B	-6020	1613
200	16	B 500B	-6039	1524
201	16	B 500B	-6059	1436
202	16	B 500B	-6078	1348
203	16	B 500B	-6098	1259
204	16	B 500B	-6118	1171
205	16	B 500B	-6137	1082
206	16	B 500B	-6149	992
207	16	B 500B	-6161	902
208	16	B 500B	-6173	813
209	16	B 500B	-6185	723
210	16	B 500B	-6196	633
211	16	B 500B	-6208	543
212	16	B 500B	-6212	453
213	16	B 500B	-6216	362
214	16	B 500B	-6220	272
215	16	B 500B	-6224	181
216	16	B 500B	-6228	91
217	16	B 500B	-6232	0
218	16	B 500B	-6228	-91

Staaf	Ø [mm]	Materiaal	Y [mm]	Z [mm]
219	16	B 500B	-6224	-181
220	16	B 500B	-6220	-272
221	16	B 500B	-6216	-362
222	16	B 500B	-6212	-453
223	16	B 500B	-6208	-543
224	16	B 500B	-6196	-633
225	16	B 500B	-6185	-723
226	16	B 500B	-6173	-813
227	16	B 500B	-6161	-902
228	16	B 500B	-6149	-992
229	16	B 500B	-6137	-1082
230	16	B 500B	-6118	-1171
231	16	B 500B	-6098	-1259
232	16	B 500B	-6078	-1348
233	16	B 500B	-6059	-1436
234	16	B 500B	-6039	-1524
235	16	B 500B	-6020	-1613
236	16	B 500B	-5992	-1699
237	16	B 500B	-5965	-1786
238	16	B 500B	-5938	-1872
239	16	B 500B	-5911	-1959
240	16	B 500B	-5883	-2045
241	16	B 500B	-5856	-2131
242	16	B 500B	-5821	-2215
243	16	B 500B	-5787	-2299
244	16	B 500B	-5752	-2383
245	16	B 500B	-5717	-2466
246	16	B 500B	-5683	-2550
247	16	B 500B	-5648	-2634
248	16	B 500B	-5606	-2714
249	16	B 500B	-5564	-2794
250	16	B 500B	-5523	-2875
251	16	B 500B	-5481	-2955
252	16	B 500B	-5439	-3036
253	16	B 500B	-5397	-3116
254	16	B 500B	-5348	-3192
255	16	B 500B	-5300	-3269
256	16	B 500B	-5251	-3345
257	16	B 500B	-5202	-3422
258	16	B 500B	-5154	-3498
259	16	B 500B	-5105	-3574
260	16	B 500B	-5050	-3646
261	16	B 500B	-4995	-3718

Project: SFT - design
 Projectnr.:
 Auteur: Laura Bakker

Staaf	Ø [mm]	Materiaal	Y [mm]	Z [mm]
262	16	B 500B	-4939	-3790
263	16	B 500B	-4884	-3862
264	16	B 500B	-4829	-3934
265	16	B 500B	-4774	-4006
266	16	B 500B	-4713	-4073
267	16	B 500B	-4652	-4139
268	16	B 500B	-4590	-4206
269	16	B 500B	-4529	-4273
270	16	B 500B	-4468	-4340
271	16	B 500B	-4407	-4407
272	16	B 500B	-4340	-4468
273	16	B 500B	-4273	-4529
274	16	B 500B	-4206	-4590
275	16	B 500B	-4139	-4652
276	16	B 500B	-4073	-4713
277	16	B 500B	-4006	-4774
278	16	B 500B	-3934	-4829
279	16	B 500B	-3862	-4884
280	16	B 500B	-3790	-4939
281	16	B 500B	-3718	-4995
282	16	B 500B	-3646	-5050
283	16	B 500B	-3574	-5105
284	16	B 500B	-3498	-5154
285	16	B 500B	-3422	-5202
286	16	B 500B	-3345	-5251
287	16	B 500B	-3269	-5300
288	16	B 500B	-3192	-5348
289	16	B 500B	-3116	-5397
290	16	B 500B	-3036	-5439
291	16	B 500B	-2955	-5481
292	16	B 500B	-2875	-5523
293	16	B 500B	-2794	-5564
294	16	B 500B	-2714	-5606
295	16	B 500B	-2634	-5648
296	16	B 500B	-2550	-5683
297	16	B 500B	-2466	-5717
298	16	B 500B	-2383	-5752
299	16	B 500B	-2299	-5787
300	16	B 500B	-2215	-5821
301	16	B 500B	-2131	-5856
302	16	B 500B	-2045	-5883
303	16	B 500B	-1959	-5911
304	16	B 500B	-1872	-5938

Staaf	Ø [mm]	Materiaal	Y [mm]	Z [mm]
305	16	B 500B	-1786	-5965
306	16	B 500B	-1699	-5992
307	16	B 500B	-1613	-6020
308	16	B 500B	-1524	-6039
309	16	B 500B	-1436	-6059
310	16	B 500B	-1348	-6078
311	16	B 500B	-1259	-6098
312	16	B 500B	-1171	-6118
313	16	B 500B	-1082	-6137
314	16	B 500B	-992	-6149
315	16	B 500B	-902	-6161
316	16	B 500B	-813	-6173
317	16	B 500B	-723	-6185
318	16	B 500B	-633	-6196
319	16	B 500B	-543	-6208
320	16	B 500B	-453	-6212
321	16	B 500B	-362	-6216
322	16	B 500B	-272	-6220
323	16	B 500B	-181	-6224
324	16	B 500B	-91	-6228
325	16	B 500B	0	-6232
326	16	B 500B	91	-6228
327	16	B 500B	181	-6224
328	16	B 500B	272	-6220
329	16	B 500B	362	-6216
330	16	B 500B	453	-6212
331	16	B 500B	543	-6208
332	16	B 500B	633	-6196
333	16	B 500B	723	-6185
334	16	B 500B	813	-6173
335	16	B 500B	902	-6161
336	16	B 500B	992	-6149
337	16	B 500B	1082	-6137
338	16	B 500B	1171	-6118
339	16	B 500B	1259	-6098
340	16	B 500B	1348	-6078
341	16	B 500B	1436	-6059
342	16	B 500B	1524	-6039
343	16	B 500B	1613	-6020
344	16	B 500B	1699	-5992
345	16	B 500B	1786	-5965
346	16	B 500B	1872	-5938
347	16	B 500B	1959	-5911

Project: SFT - design
 Projectnr.:
 Auteur: Laura Bakker

Staaf	Ø [mm]	Materiaal	Y [mm]	Z [mm]
348	16	B 500B	2045	-5883
349	16	B 500B	2131	-5856
350	16	B 500B	2215	-5821
351	16	B 500B	2299	-5787
352	16	B 500B	2383	-5752
353	16	B 500B	2466	-5717
354	16	B 500B	2550	-5683
355	16	B 500B	2634	-5648
356	16	B 500B	2714	-5606
357	16	B 500B	2794	-5564
358	16	B 500B	2875	-5523
359	16	B 500B	2955	-5481
360	16	B 500B	3036	-5439
361	16	B 500B	3116	-5397
362	16	B 500B	3192	-5348
363	16	B 500B	3269	-5300
364	16	B 500B	3345	-5251
365	16	B 500B	3422	-5202
366	16	B 500B	3498	-5154
367	16	B 500B	3574	-5105
368	16	B 500B	3646	-5050
369	16	B 500B	3718	-4995
370	16	B 500B	3790	-4939
371	16	B 500B	3862	-4884
372	16	B 500B	3934	-4829
373	16	B 500B	4006	-4774
374	16	B 500B	4073	-4713
375	16	B 500B	4139	-4652
376	16	B 500B	4206	-4590
377	16	B 500B	4273	-4529
378	16	B 500B	4340	-4468
379	16	B 500B	4407	-4407
380	16	B 500B	4468	-4340
381	16	B 500B	4529	-4273
382	16	B 500B	4590	-4206
383	16	B 500B	4652	-4139
384	16	B 500B	4713	-4073
385	16	B 500B	4774	-4006
386	16	B 500B	4829	-3934
387	16	B 500B	4884	-3862
388	16	B 500B	4939	-3790
389	16	B 500B	4995	-3718
390	16	B 500B	5050	-3646

Project: SFT - design
 Projectnr.:
 Auteur: Laura Bakker

Staaf	Ø [mm]	Materiaal	Y [mm]	Z [mm]
391	16	B 500B	5105	-3574
392	16	B 500B	5154	-3498
393	16	B 500B	5202	-3422
394	16	B 500B	5251	-3345
395	16	B 500B	5300	-3269
396	16	B 500B	5348	-3192
397	16	B 500B	5397	-3116
398	16	B 500B	5439	-3036
399	16	B 500B	5481	-2955
400	16	B 500B	5523	-2875
401	16	B 500B	5564	-2794
402	16	B 500B	5606	-2714
403	16	B 500B	5648	-2634
404	16	B 500B	5683	-2550
405	16	B 500B	5717	-2466
406	16	B 500B	5752	-2383
407	16	B 500B	5787	-2299
408	16	B 500B	5821	-2215
409	16	B 500B	5856	-2131
410	16	B 500B	5883	-2045
411	16	B 500B	5911	-1959
412	16	B 500B	5938	-1872
413	16	B 500B	5965	-1786
414	16	B 500B	5992	-1699
415	16	B 500B	6020	-1613
416	16	B 500B	6039	-1524
417	16	B 500B	6059	-1436
418	16	B 500B	6078	-1348
419	16	B 500B	6098	-1259
420	16	B 500B	6118	-1171
421	16	B 500B	6137	-1082
422	16	B 500B	6149	-992
423	16	B 500B	6161	-902
424	16	B 500B	6173	-813
425	16	B 500B	6185	-723
426	16	B 500B	6196	-633
427	16	B 500B	6208	-543
428	16	B 500B	6212	-453
429	16	B 500B	6216	-362
430	16	B 500B	6220	-272
431	16	B 500B	6224	-181
432	16	B 500B	6228	-91
433	16	B 500B	5568	0

Project: SFT - design
 Projectnr.:
 Auteur: Laura Bakker

Staaf	Ø [mm]	Materiaal	Y [mm]	Z [mm]
434	16	B 500B	5564	97
435	16	B 500B	5560	194
436	16	B 500B	5555	291
437	16	B 500B	5551	388
438	16	B 500B	5547	485
439	16	B 500B	5534	582
440	16	B 500B	5522	678
441	16	B 500B	5509	774
442	16	B 500B	5496	871
443	16	B 500B	5483	967
444	16	B 500B	5462	1062
445	16	B 500B	5441	1157
446	16	B 500B	5420	1251
447	16	B 500B	5399	1346
448	16	B 500B	5378	1441
449	16	B 500B	5349	1534
450	16	B 500B	5320	1626
451	16	B 500B	5291	1719
452	16	B 500B	5261	1812
453	16	B 500B	5232	1904
454	16	B 500B	5195	1994
455	16	B 500B	5158	2084
456	16	B 500B	5121	2174
457	16	B 500B	5084	2263
458	16	B 500B	5046	2353
459	16	B 500B	5002	2439
460	16	B 500B	4957	2526
461	16	B 500B	4912	2612
462	16	B 500B	4867	2698
463	16	B 500B	4822	2784
464	16	B 500B	4770	2866
465	16	B 500B	4718	2948
466	16	B 500B	4665	3030
467	16	B 500B	4613	3112
468	16	B 500B	4561	3194
469	16	B 500B	4502	3271
470	16	B 500B	4443	3348
471	16	B 500B	4384	3425
472	16	B 500B	4325	3502
473	16	B 500B	4265	3579
474	16	B 500B	4200	3651
475	16	B 500B	4134	3722
476	16	B 500B	4068	3794

Project: SFT - design
 Projectnr.:
 Auteur: Laura Bakker

Staaf	Ø [mm]	Materiaal	Y [mm]	Z [mm]
477	16	B 500B	4003	3866
478	16	B 500B	3937	3937
479	16	B 500B	3866	4003
480	16	B 500B	3794	4068
481	16	B 500B	3722	4134
482	16	B 500B	3651	4200
483	16	B 500B	3579	4265
484	16	B 500B	3502	4325
485	16	B 500B	3425	4384
486	16	B 500B	3348	4443
487	16	B 500B	3271	4502
488	16	B 500B	3194	4561
489	16	B 500B	3112	4613
490	16	B 500B	3030	4665
491	16	B 500B	2948	4718
492	16	B 500B	2866	4770
493	16	B 500B	2784	4822
494	16	B 500B	2698	4867
495	16	B 500B	2612	4912
496	16	B 500B	2526	4957
497	16	B 500B	2439	5002
498	16	B 500B	2353	5046
499	16	B 500B	2263	5084
500	16	B 500B	2174	5121
501	16	B 500B	2084	5158
502	16	B 500B	1994	5195
503	16	B 500B	1904	5232
504	16	B 500B	1812	5261
505	16	B 500B	1719	5291
506	16	B 500B	1626	5320
507	16	B 500B	1534	5349
508	16	B 500B	1441	5378
509	16	B 500B	1346	5399
510	16	B 500B	1251	5420
511	16	B 500B	1157	5441
512	16	B 500B	1062	5462
513	16	B 500B	967	5483
514	16	B 500B	871	5496
515	16	B 500B	774	5509
516	16	B 500B	678	5522
517	16	B 500B	582	5534
518	16	B 500B	485	5547
519	16	B 500B	388	5551

Project: SFT - design
 Projectnr.:
 Auteur: Laura Bakker

Staaf	Ø [mm]	Materiaal	Y [mm]	Z [mm]
520	16	B 500B	291	5555
521	16	B 500B	194	5560
522	16	B 500B	97	5564
523	16	B 500B	0	5568
524	16	B 500B	-97	5564
525	16	B 500B	-194	5560
526	16	B 500B	-291	5555
527	16	B 500B	-388	5551
528	16	B 500B	-485	5547
529	16	B 500B	-582	5534
530	16	B 500B	-678	5522
531	16	B 500B	-774	5509
532	16	B 500B	-871	5496
533	16	B 500B	-967	5483
534	16	B 500B	-1062	5462
535	16	B 500B	-1157	5441
536	16	B 500B	-1251	5420
537	16	B 500B	-1346	5399
538	16	B 500B	-1441	5378
539	16	B 500B	-1534	5349
540	16	B 500B	-1626	5320
541	16	B 500B	-1719	5291
542	16	B 500B	-1812	5261
543	16	B 500B	-1904	5232
544	16	B 500B	-1994	5195
545	16	B 500B	-2084	5158
546	16	B 500B	-2174	5121
547	16	B 500B	-2263	5084
548	16	B 500B	-2353	5046
549	16	B 500B	-2439	5002
550	16	B 500B	-2526	4957
551	16	B 500B	-2612	4912
552	16	B 500B	-2698	4867
553	16	B 500B	-2784	4822
554	16	B 500B	-2866	4770
555	16	B 500B	-2948	4718
556	16	B 500B	-3030	4665
557	16	B 500B	-3112	4613
558	16	B 500B	-3194	4561
559	16	B 500B	-3271	4502
560	16	B 500B	-3348	4443
561	16	B 500B	-3425	4384
562	16	B 500B	-3502	4325

Project: SFT - design
 Projectnr.:
 Auteur: Laura Bakker

Staaf	Ø [mm]	Materiaal	Y [mm]	Z [mm]
563	16	B 500B	-3579	4265
564	16	B 500B	-3651	4200
565	16	B 500B	-3722	4134
566	16	B 500B	-3794	4068
567	16	B 500B	-3866	4003
568	16	B 500B	-3937	3937
569	16	B 500B	-4003	3866
570	16	B 500B	-4068	3794
571	16	B 500B	-4134	3722
572	16	B 500B	-4200	3651
573	16	B 500B	-4265	3579
574	16	B 500B	-4325	3502
575	16	B 500B	-4384	3425
576	16	B 500B	-4443	3348
577	16	B 500B	-4502	3271
578	16	B 500B	-4561	3194
579	16	B 500B	-4613	3112
580	16	B 500B	-4665	3030
581	16	B 500B	-4718	2948
582	16	B 500B	-4770	2866
583	16	B 500B	-4822	2784
584	16	B 500B	-4867	2698
585	16	B 500B	-4912	2612
586	16	B 500B	-4957	2526
587	16	B 500B	-5002	2439
588	16	B 500B	-5046	2353
589	16	B 500B	-5084	2263
590	16	B 500B	-5121	2174
591	16	B 500B	-5158	2084
592	16	B 500B	-5195	1994
593	16	B 500B	-5232	1904
594	16	B 500B	-5261	1812
595	16	B 500B	-5291	1719
596	16	B 500B	-5320	1626
597	16	B 500B	-5349	1534
598	16	B 500B	-5378	1441
599	16	B 500B	-5399	1346
600	16	B 500B	-5420	1251
601	16	B 500B	-5441	1157
602	16	B 500B	-5462	1062
603	16	B 500B	-5483	967
604	16	B 500B	-5496	871
605	16	B 500B	-5509	774

Project: SFT - design
 Projectnr.:
 Auteur: Laura Bakker

Staaf	Ø [mm]	Materiaal	Y [mm]	Z [mm]
606	16	B 500B	-5522	678
607	16	B 500B	-5534	582
608	16	B 500B	-5547	485
609	16	B 500B	-5551	388
610	16	B 500B	-5555	291
611	16	B 500B	-5560	194
612	16	B 500B	-5564	97
613	16	B 500B	-5568	0
614	16	B 500B	-5564	-97
615	16	B 500B	-5560	-194
616	16	B 500B	-5555	-291
617	16	B 500B	-5551	-388
618	16	B 500B	-5547	-485
619	16	B 500B	-5534	-582
620	16	B 500B	-5522	-678
621	16	B 500B	-5509	-774
622	16	B 500B	-5496	-871
623	16	B 500B	-5483	-967
624	16	B 500B	-5462	-1062
625	16	B 500B	-5441	-1157
626	16	B 500B	-5420	-1251
627	16	B 500B	-5399	-1346
628	16	B 500B	-5378	-1441
629	16	B 500B	-5349	-1534
630	16	B 500B	-5320	-1626
631	16	B 500B	-5291	-1719
632	16	B 500B	-5261	-1812
633	16	B 500B	-5232	-1904
634	16	B 500B	-5195	-1994
635	16	B 500B	-5158	-2084
636	16	B 500B	-5121	-2174
637	16	B 500B	-5084	-2263
638	16	B 500B	-5046	-2353
639	16	B 500B	-5002	-2439
640	16	B 500B	-4957	-2526
641	16	B 500B	-4912	-2612
642	16	B 500B	-4867	-2698
643	16	B 500B	-4822	-2784
644	16	B 500B	-4770	-2866
645	16	B 500B	-4718	-2948
646	16	B 500B	-4665	-3030
647	16	B 500B	-4613	-3112
648	16	B 500B	-4561	-3194

Project: SFT - design
 Projectnr.:
 Auteur: Laura Bakker

Staaf	Ø [mm]	Materiaal	Y [mm]	Z [mm]
649	16	B 500B	-4502	-3271
650	16	B 500B	-4443	-3348
651	16	B 500B	-4384	-3425
652	16	B 500B	-4325	-3502
653	16	B 500B	-4265	-3579
654	16	B 500B	-4200	-3651
655	16	B 500B	-4134	-3722
656	16	B 500B	-4068	-3794
657	16	B 500B	-4003	-3866
658	16	B 500B	-3937	-3937
659	16	B 500B	-3866	-4003
660	16	B 500B	-3794	-4068
661	16	B 500B	-3722	-4134
662	16	B 500B	-3651	-4200
663	16	B 500B	-3579	-4265
664	16	B 500B	-3502	-4325
665	16	B 500B	-3425	-4384
666	16	B 500B	-3348	-4443
667	16	B 500B	-3271	-4502
668	16	B 500B	-3194	-4561
669	16	B 500B	-3112	-4613
670	16	B 500B	-3030	-4665
671	16	B 500B	-2948	-4718
672	16	B 500B	-2866	-4770
673	16	B 500B	-2784	-4822
674	16	B 500B	-2698	-4867
675	16	B 500B	-2612	-4912
676	16	B 500B	-2526	-4957
677	16	B 500B	-2439	-5002
678	16	B 500B	-2353	-5046
679	16	B 500B	-2263	-5084
680	16	B 500B	-2174	-5121
681	16	B 500B	-2084	-5158
682	16	B 500B	-1994	-5195
683	16	B 500B	-1904	-5232
684	16	B 500B	-1812	-5261
685	16	B 500B	-1719	-5291
686	16	B 500B	-1626	-5320
687	16	B 500B	-1534	-5349
688	16	B 500B	-1441	-5378
689	16	B 500B	-1346	-5399
690	16	B 500B	-1251	-5420
691	16	B 500B	-1157	-5441

Project: SFT - design
 Projectnr.:
 Auteur: Laura Bakker

Staaf	Ø [mm]	Materiaal	Y [mm]	Z [mm]
692	16	B 500B	-1062	-5462
693	16	B 500B	-967	-5483
694	16	B 500B	-871	-5496
695	16	B 500B	-774	-5509
696	16	B 500B	-678	-5522
697	16	B 500B	-582	-5534
698	16	B 500B	-485	-5547
699	16	B 500B	-388	-5551
700	16	B 500B	-291	-5555
701	16	B 500B	-194	-5560
702	16	B 500B	-97	-5564
703	16	B 500B	0	-5568
704	16	B 500B	97	-5564
705	16	B 500B	194	-5560
706	16	B 500B	291	-5555
707	16	B 500B	388	-5551
708	16	B 500B	485	-5547
709	16	B 500B	582	-5534
710	16	B 500B	678	-5522
711	16	B 500B	774	-5509
712	16	B 500B	871	-5496
713	16	B 500B	967	-5483
714	16	B 500B	1062	-5462
715	16	B 500B	1157	-5441
716	16	B 500B	1251	-5420
717	16	B 500B	1346	-5399
718	16	B 500B	1441	-5378
719	16	B 500B	1534	-5349
720	16	B 500B	1626	-5320
721	16	B 500B	1719	-5291
722	16	B 500B	1812	-5261
723	16	B 500B	1904	-5232
724	16	B 500B	1994	-5195
725	16	B 500B	2084	-5158
726	16	B 500B	2174	-5121
727	16	B 500B	2263	-5084
728	16	B 500B	2353	-5046
729	16	B 500B	2439	-5002
730	16	B 500B	2526	-4957
731	16	B 500B	2612	-4912
732	16	B 500B	2698	-4867
733	16	B 500B	2784	-4822
734	16	B 500B	2866	-4770

Project: SFT - design
 Projectnr.:
 Auteur: Laura Bakker

Staaf	Ø [mm]	Materiaal	Y [mm]	Z [mm]
735	16	B 500B	2948	-4718
736	16	B 500B	3030	-4665
737	16	B 500B	3112	-4613
738	16	B 500B	3194	-4561
739	16	B 500B	3271	-4502
740	16	B 500B	3348	-4443
741	16	B 500B	3425	-4384
742	16	B 500B	3502	-4325
743	16	B 500B	3579	-4265
744	16	B 500B	3651	-4200
745	16	B 500B	3722	-4134
746	16	B 500B	3794	-4068
747	16	B 500B	3866	-4003
748	16	B 500B	3937	-3937
749	16	B 500B	4003	-3866
750	16	B 500B	4068	-3794
751	16	B 500B	4134	-3722
752	16	B 500B	4200	-3651
753	16	B 500B	4265	-3579
754	16	B 500B	4325	-3502
755	16	B 500B	4384	-3425
756	16	B 500B	4443	-3348
757	16	B 500B	4502	-3271
758	16	B 500B	4561	-3194
759	16	B 500B	4613	-3112
760	16	B 500B	4665	-3030
761	16	B 500B	4718	-2948
762	16	B 500B	4770	-2866
763	16	B 500B	4822	-2784
764	16	B 500B	4867	-2698
765	16	B 500B	4912	-2612
766	16	B 500B	4957	-2526
767	16	B 500B	5002	-2439
768	16	B 500B	5046	-2353
769	16	B 500B	5084	-2263
770	16	B 500B	5121	-2174
771	16	B 500B	5158	-2084
772	16	B 500B	5195	-1994
773	16	B 500B	5232	-1904
774	16	B 500B	5261	-1812
775	16	B 500B	5291	-1719
776	16	B 500B	5320	-1626
777	16	B 500B	5349	-1534

Staaft	Ø [mm]	Materiaal	Y [mm]	Z [mm]
778	16	B 500B	5378	-1441
779	16	B 500B	5399	-1346
780	16	B 500B	5420	-1251
781	16	B 500B	5441	-1157
782	16	B 500B	5462	-1062
783	16	B 500B	5483	-967
784	16	B 500B	5496	-871
785	16	B 500B	5509	-774
786	16	B 500B	5522	-678
787	16	B 500B	5534	-582
788	16	B 500B	5547	-485
789	16	B 500B	5551	-388
790	16	B 500B	5555	-291
791	16	B 500B	5560	-194
792	16	B 500B	5564	-97

5 Lijst met gebruikte materialen

Beton

Naam	f_{ck} [MPa]	f_{cm} [MPa]	f_{ctm} [MPa]	E_{cm} [MPa]	μ [-]	Eenheidsmassa [kg/m ³]
C45/55	45.0	53.0	3.8	36283.2	0.20	2500
$\epsilon_{c2} = 20.0 \cdot 10^{-4}$, $\epsilon_{cu2} = 35.0 \cdot 10^{-4}$, $\epsilon_{c3} = 17.5 \cdot 10^{-4}$, $\epsilon_{cu3} = 35.0 \cdot 10^{-4}$, Exponent - n: 2.00, Korrelgrootte toelagmateriaal = 16 mm, Cementklasse: R (s = 0.20), Type diagram: Parabolisch						

Verklaring

Symbol	Verklaring
f_{ck}	Karakteristieke cilindrische betondruksterkte bij 28 dagen
f_{cm}	Gemiddelde waarde van de cilindrische druksterkte van beton
f_{ctm}	Gemiddelde axiale treksterkte van beton
E_{cm}	Secant elasticiteitsmodulus van beton
ϵ_c	Betondrukrek bij piekspanning f_c
ϵ_{cu}	Uiterste drukrek in het beton

Wapeningstaal

Naam	f_{yk} [MPa]	f_{tk} [MPa]	E [MPa]	μ [-]	Eenheidsmassa [kg/m ³]
B 500B	500.0	540.0	200000.0	0.20	7850
$f_{tk}/f_{yk} = 1.08$, $\epsilon_{uk} = 500.0 \cdot 10^{-4}$, Type: Staven, Staafooppervlak: Geribb, Klasse: B, Vervaardiging: Warmgewalst, Type diagram: Bi-lineair met oplopende tak					

Verklaring

Symbol	Verklaring
f_{yk}	Karakteristieke vloeisterkte van de wapening
f_{tk}	Karakteristieke treksterkte van de wapening

Project: SFT - design
Projectnr.:
Auteur: Laura Bakker



Symbool	Verklaring
E	Elasticiteitsmodulus van wapeningsstaal
ϵ_{uk}	Karakteristieke rek van de wapening of voorspanstaal bij de maximale belasting

APPENDIX D

GINA-profile Properties

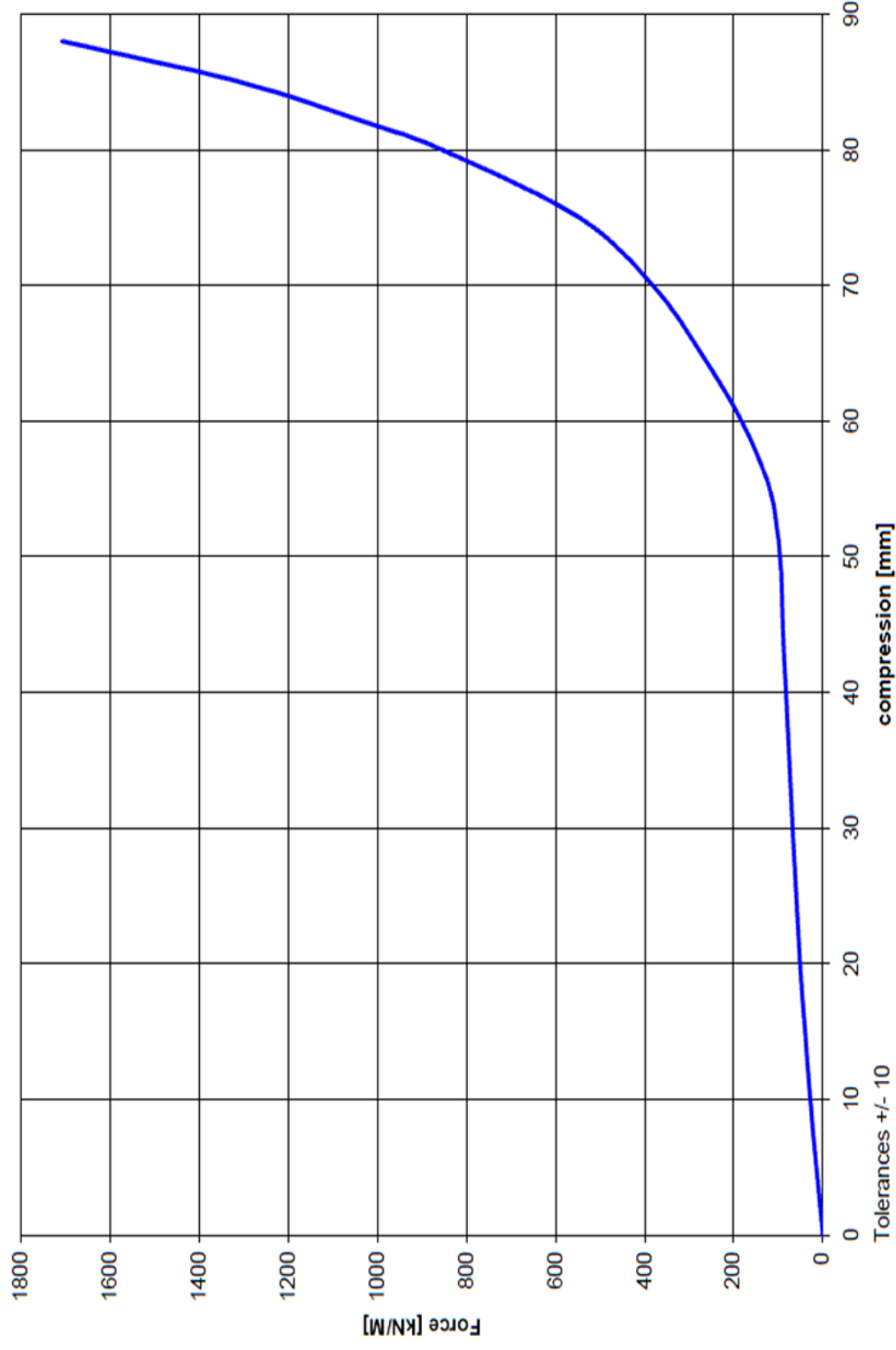
Submerged Floating Tunnels

Laura Bakker

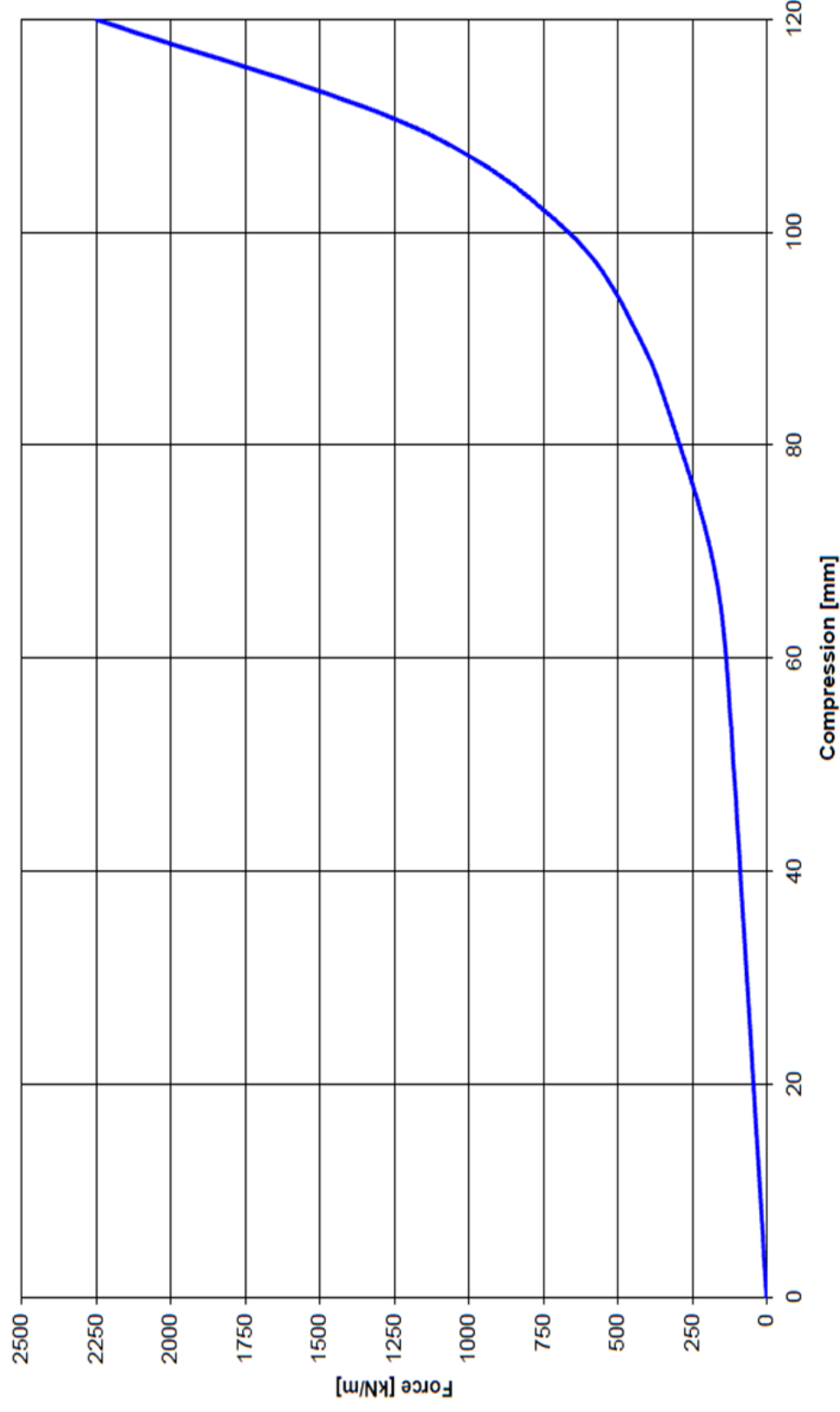
MSc Hydraulic Engineering – Hydraulic Structures

2018, Delft

Force-compression graph Gina ETS-130-160



Force-compression graph Gina ETS 180-220



Tolerance on compression $\pm 10\%$

Gina 180-220 f-c np

**Force-compression graph
Gina gasket ETS 200-260 SN**

